약학박사 학위논문

Characterization of chemical constituents from *Sicyos angulatus* and *Ambrosia artemisiifolia* using molecular networking and mass defect filtering

Molecular networking과 mass defect filtering을 적용한 가시박과 돼지풀 유래 화학 성분 연구

2019 년 8 월

서울대학교 대학원

약학과 생약학 전공

안 진 표

Characterization of chemical constituents from *Sicyos angulatus* and *Ambrosia artemisiifolia* using molecular networking and mass defect filtering

Molecular networking과 mass defect filtering을 적용한

가시박과 돼지풀 유래 화학 성분 연구

지도교수 오 원 근

이 논문을 약학박사 학위논문으로 제출함

2019 년 8 월

서울대학교 대학원

약학과 생약학전공

안 진 표

안진표의 약학박사 학위논문을 인준함

2019 년 8 월

위 원 장 _____ (인)

부위원장 _____ (인)

위 원 _____ (인)

위 원 _____ (인)

위 원 _____ (인)

Abstract

Characterization of chemical constituents from *Sicyos angulatus* and *Ambrosia artemisiifolia* using molecular networking and mass defect filtering

Part 1

A library of extracted natural materials (Korea Bioactive Natural Material Bank) have been screened to discover candidates for the treatment of non-alcoholic liver disease (NAFLD), and the 70% ethanol extract of *Sicyos angulatus* was found to inhibit hepatic lipid accumulation. Bioassay–guided fractionation of this bioactive extract yielded five previously undescribed flavonoid glycosides (**1**, **8**, **9**, **11**, and **12**) and one previously undescribed flavonolignan glycoside (**13**) along with seven known flavonoid glycosides (**2-7**, and **10**). The chemical structures of these compounds were elucidated by a combination of extensive spectroscopic analysis, including MS, NMR, and UV techniques. Compounds **1-4**, **6**, and **11-13** showed inhibitory effects on the lipid accumulation induced by high concentrations of palmitic acid and glucose in HepG2 cells. Four selected compounds (**1**, **3**, **4**, and **13**) were tested for lipid content in a dose-dependent manner (10, 20, and 40 μM), and among those compounds, kaempferol 3-*O*-*β*-D-glucopyranosyl-7-*O*-α-L-rhamnopyranoside (**4**) showed the strongest inhibition of hepatic lipid production in HepG2 cells. In an oil-red O staining assay, five compounds (**1**, **3**, **4**, **11**, and **13**) were shown to reduce hepatic lipid accumulation better than what was observed in

the vehicle control group. The present study suggests a new class of chemical entities for developing bioactive agents for the treatment of diseases caused by fat accumulation in the liver.

Part 2

In Alzheimer's disease (AD), amyloid-β (Aβ) accumulation in the brain results in neuronal cell death and is one of the major causes of dementia. Since the current therapeutic agents are not yet sufficiently effective or safe, there have been attempts to find new neuroprotective chemicals against Aβ-induced cytotoxicity. A 70% EtOH extract of the whole plants of *Ambroisa artemisiifolia* (common ragweed) was selected after the screening of a natural extract library. Seven new eudesmane-type glycosides (**1**-**7**) and seven known compounds (**8**-**14**) were obtained through bioactivity-guided fractionation from the aerial parts of this plant. Their structures were determined on the basis of their NMR spectra, HRESIMS analysis, and ECD calculations. Among them, compounds **1**, **2**, **4**-**6**, **8**-**9**, **11**, and **13**-**14** showed protective effects against Aβ-induced cytotoxicity in Aβ_{42}-transfected HT22 cells. The most active compounds, **5** and **6**, exhibited moderate protective activity dose-dependently (10, 20, and 40 μM).

Keywords: *Sicyos angulatus*, molecular networking, NAFLD, *Ambrosia artemisiifolia*, mass defect filtering, neuroprotection

Student Number: 2014-31251

Table of Contents

List of Schemes

List of Tables

List of Figures

Part 1.

List of Abbreviations

$[\alpha]_D$: specific rotation

br s: broad singlet

n-BuOH: *n*-buthanol

CC: column chromatography

CH_3CN: acetonitrile

d: doublet

dd: double of doublet

DMEM: Dulbecco's modified Eagle's medium

DMSO: dimethyl sulfoxide

EtOAc: ethyl acetate

EtOH: ethanol

FBS: fetal bovine serum

HMBC: heteronuclear multiple bond correlation

HPLC: high performance liquid chromatography

HRESIMS: high-resolution electrospray ionization mass spectrometry

HSQC: heteronuclear single quantum coherence

Hx: hexane

Hz: hertz

IHD: indices of hydrogen deficiency

IR: infrared radiation

KBNMB: Korea Bioactive Natural Material Bank

LC3: light chain 3

m: multiplet

MeOH: methanol

MTT: 3-(4,5-dimethyl-2-thiazolyl)-2,5-diphenyl-2*H*-tetrazolium bromide

m/z: mass to charge ratio

NMR: nuclear magnetic resonance

NOESY: nuclear overhauser effect spectroscopy

NP: normal-phase (silica gel)

PBS: phosphate buffered saline

RP-C_{18}: C_{18}-reversed phase silica gel

s: singlet

t: triplet

T1DM: type 1 diabetes mellitus

TLC: thin-layer chromatography

Part 1. Flavone glycosides from *Sicyos angulatus* and their inhibitory effects on hepatic accumulation

1. Introduction

1.1. Non alcoholic fatty liver disease (NAFLD)

Non-alcoholic fatty liver disease (NAFLD) is the starting point for the progression of several liver diseases such as simple steatosis, non-alcoholic steatohepatitis (NASH), and liver cirrhosis. Accumulation of triglycerides in the liver is a characteristic marker of NAFLD and an important stage in the pathogenesis of NAFLD, and more severe NASH is indicated by inflammation, steatosis, and fibrosis (Trauner et al., 2010). To date, several mechanisms have been known to be involved in lipid accumulation in liver, but *de novo* hepatic lipogenesis (DNL) and elevated peripheral fatty acids are considered to be the most dominant contributors to hepatic lipid accumulation in NAFLD (Tilg and Moschen, 2008). Approximately 20-40% of patients with NAFLD or NASH eventually develop fibrosis and cirrhosis (Assy et al., 2009). NAFLD is the second most common reason for liver transplantation in the US and the most rapidly increasing indication for requiring liver transplantation in patients with hepatocellular carcinoma (HCC) (Younossi et al., 2016).

The pathogenesis of NAFLD is strongly associated with the metabolic syndrome. The liver plays a critical role in carbohydrate metabolism as it is responsible for blood glucose balance through glycogenesis and glycogenolysis. Approximately 96% of patients with cirrhosis have glucose tolerance and 30% have been clinically diagnosed as diabetic, which explains the importance of controlling fat accumulation in the liver (Garcia-Compean et al., 2009). Even an increased risk of HCC has been reported to be related to metabolic factors including obesity and

diabetes. Fatty liver disease is usually associated with insulin resistance because soluble mediators from immune cells and free fatty acids are involved in the insulin regulation system and NAFLD manifestation (Reddy and Rao, 2006). Several inflammatory cytokines, including TNFα and IL-6, which are produced in a series of steps, are crucial triggers of a series of liver diseases such as NAFLD, NASH and liver cirrhosis. Several drugs are available for treat NAFLD including statin, metformin, and fibrates. However, these drugs are associated with adverse effects or contraindications (Collier., 2007). A few natural products were reported for their anti-NAFLD effects and few side effects were expected from natural products sources (Zhang et al., 2013; Xu et al., 2014). Since NAFLD has rapidly increased with the spread of metabolic syndrome and also with population ageing, attempts have been made to isolate NAFLD inhibitory materials from natural products.

1.2. *Sicyos angulatus*

The genus *Sicyos*, which contains approximately 40 species, is one of the most diverse genus within the family Cucurbitaceae. A *Sicyos angulatus* L. (www.theplantlist.org) (synonym *Elaterium trifoliatum* L.) is a vine plant that grows along wet areas and river banks (Figure 1). This plant is considered a troublesome weed because of its rapid growth, which allows it to quickly cover land and push out other plants (Lara-Núñez et al., 2009). *S. angulatus* has been introduced in Korea for the purpose of crossbreeding with other fruit plants, but the rapid growth of this plant has made it harmful to Korean wetlands. However, before the flowering, the young leaf of this plant is listed as an edible raw material in the Korean Food Standards Codex (KFSC), and thus the possibility of it being used as a source of functional foods has been suggested (MFDS, 2018). To date, studies on *S. angulatus* have mostly focused on ecological aspects based on the environmental hazards associated with this plant, and little has been reported on the chemical constituents of *S. angulatus*. Several flavonoid glycosides and sterols have been identified as chemical constituents of this plant, but no biological activities have been reported (Na et al., 2013; Akihisa et al., 1987) (Figure 2).

Recently, we orally administered the 70% EtOH extract of the leaves and stems of *S. angulatus* to apolipoprotein E-deficient (apoE$^{-/-}$) mice with an atherogenic diet for 8 weeks, and a significant reduction in atherosclerotic plaque area in the whole aorta and aortic sinus was observed compared with vehicle-treated mice. In addition, gene expression levels of proatherogenic cytokines such as interleukin-6 (IL6) and tumour necrosis factor α (TNFα) were significantly decreased in the aorta of apoE$^{-/-}$ mice treated with the 70% EtOH extract of *S. angulatus* (Kim et al., 2017).

Figure 1. Stem and leaf of *S. angulatus*

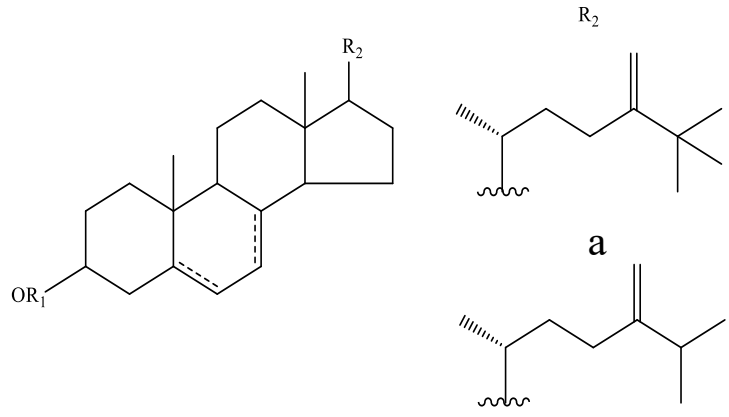

1 5α-H, Δ^7, R_1 = H,

2 5α-H, Δ^7, R_1 = Ac,

3 Δ^5, R_1 = H

4 Δ^5, R_1 = Ac

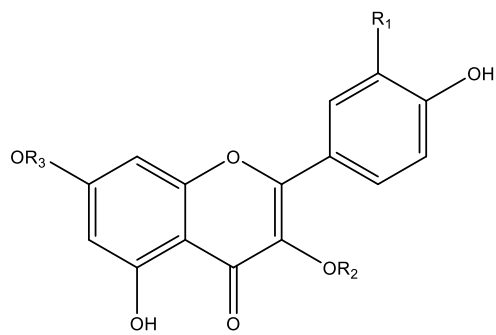

1 R_1 = OH, R_2 = galactosyl, R_3 = rhamnosyl

2 R_1 = OH, R_2 = rutinosyl, R_3 = rhamnosyl

3 R_1 = OH, R_2 = glucosyl, R_3 = rhamnosyl

4 R_1 = H, R_2 = robinobiosyl, R_3 = rhamnosyl

5 R_1 = H, R_2 = rhamnosyl, R_3 = glucosyl

6 R_1 = H, R_2 = rutinosyl, R_3 = rhamnosyl

Figure 2. Structures of chemical constituents reported in *S. angulatus.*

1.3. Molecular networking

Mass based metabolomics has been increasingly used in natural product research. Molecular networking was introduced in the metabolomics field recently and this cutting-edge technology has led to the advance in natural product (NP) research. This emerging computer-based approach has been settled well because of the advance in mass instrumentation and data processing. Significant progression of mass instrumentation allows accurate detection of exact mass and chemical formula of large or complex dataset (Grauso et al., 2019). In addition, mass instrument manufactures developed advanced data analysis tool such as MassHunter, MZmine, Markerllynx and so on. To analysis natural products, data process is crucial and essential step impacting upon the quality of data output. During the process, data becomes more accurate and reliable. It distinguishes the metabolites from analytical interferences. Raw mass data contains not only metabolites but also back ground noises such as solvent impurities, adducts and dimers. Furthermore, the data process program detects the overlapping chromatographic peaks to distinguish two peak of very similar retention time or align the retention time between different samples.

Combining the preprocessing efficiency and simplicity of MZmine with the molecular network visualization via the GNPS platform (http://gnps.ucsd.edu) allows rapid tentative identification as well as clustering components. Structurally similar compounds generate similar mass fragment. So the similarities of fragment pattern between two compounds can be used for grouping components (Allard et al., 2016) (Figure 3). For example, kaempferol glycoside and quercetin glycoside generate different product ion fragment since their aglycone is different. Kaempferol glycosides share product ion of *m/z* 269.0450 ($C_{15}H_9O_5$), however, at the same time,

quercetin glycosides share product ion of 285.0399 ($C_{15}H_9O_6$) since quercetin has one more oxygen at B ring compared to kaempferol. Therefore, within a kaempferol glycoside group, compounds possessing same aglycone connected strongly with high cosine score. Likewise, based on mass fragment pattern, molecular families cluster together with in a network (Fox Ramos et al., 2019). There are several algorithms to mark similarities of each compounds such as probability-based matching system, normalized Euclidean distance, absolute value distance, cosine correlation and so on. In this research cosine correlation method was used.

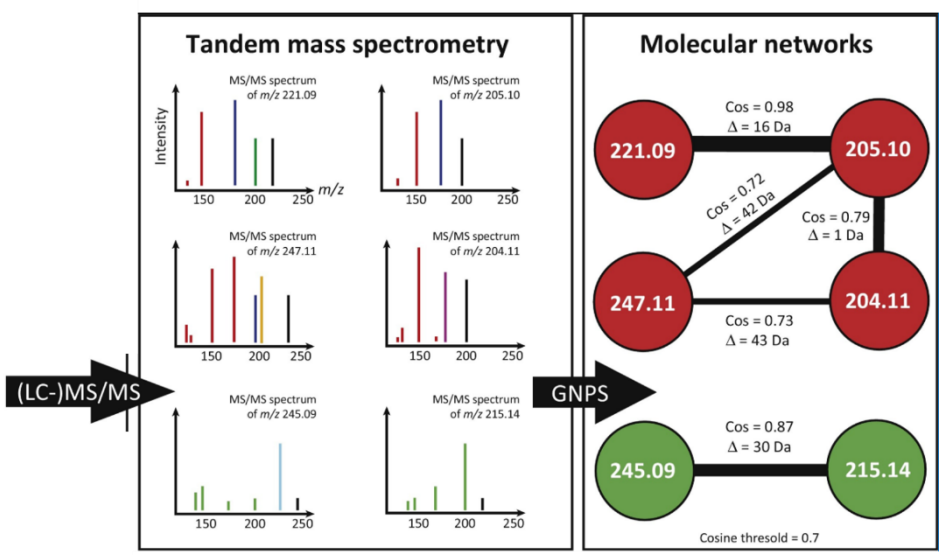

Figure 3. The concept of molecular network (Quinn et al., 2016)

This algorithm is more reliable than just matching the precursor based on database including Scifinder or Beilstein Dictionary of Natural Products. The MS fragment provides more detail and clear information such as sugar [162 (hexose), 132 (pentose)] or acyl groups [104 (benzoyl), 82 (tigloyl) and 42 (acetyl)]. Furthermore, as mentioned above, the major daughter ion gives strong evidence for the chemical structure of the aglycone. Since the molecular networking enables researchers to identify compounds rapidly, many researchers have applied this method to dereplicate known compounds from complex mixtures. Some researchers use "seed" spectra to precisely dereplicate in the mixture (Yang et al., 2013). Since the fragment pattern of isolated compound was clearly elucidated, it enables researchers to predict the chemical structure of its analogues in a high level of confidence (Figure 4). Molecular networking also used to find the bioactive components from the fraction. In classical bioassay-guided fractionation, although the researcher find bioactivity at total extract level, subsequent fractionation may lead to miss the bioactive compounds or isolate previously reported well-known compounds such as quercetin and apigenin. However, by using the molecular networking, bioactivity score of each peak was predicted based on its structure. By using this method, bioactive compounds were properly isolated without being lost. For example, Nothias et al developed a bioinformatic workflow to able to map bioactivity score in molecular network.

Although there are shortcomings of molecular networking due to limiting information on natural compounds, GNPS has collected numerous spectral libraries sets such as NIH, MassBank and NIST. Furthermore, the number of MS/MS spectra data are updated continuously by other libraries and researchers.

And this emerging recent analysis tool can exhibit strong synergistic effect when combined with conventional chemical analysis method such as UV spectrum analysis especially for phenolic compounds like flavonoid. Since phenolic compound presents strong UV spectrum, the UV information enables researchers to precisely confirm the peaks according to their retention time together with the results from molecular networking.

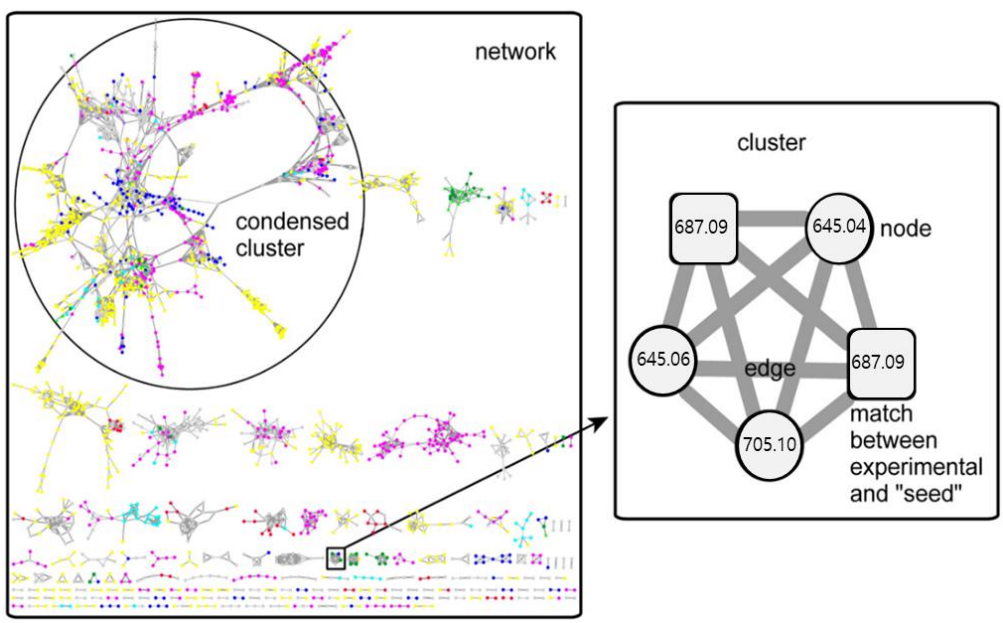

Figure 4. “Seed” compound to identify the analogues (Yang et al., 2013)

1.4. UV spectrum

Molecules possessing bonding or non-bonding electrons absorb energy as ultraviolet to excite electrons to higher anti-bonding molecular orbitals. An electron is excited from a full orbital into an empty anti-bonding orbital (Figure 5). The easier the electrons excited, the longer the wavelength was absorbed and there are four types of transitions; π–π*, n–π*, σ–σ*, and n–σ*. In practice, the absorption frequencies for C-C, C-H and isolated C=C is difficult to differentiate (Vansco et al., 2018). However, flavonoid structure consists of conjugated chromophoric system and displays characteristic UV spectrum. Thus UV spectrum present strong evidence for flavonoid structure and this analysis tool exhibit synergistic effect when combined with molecular networking.

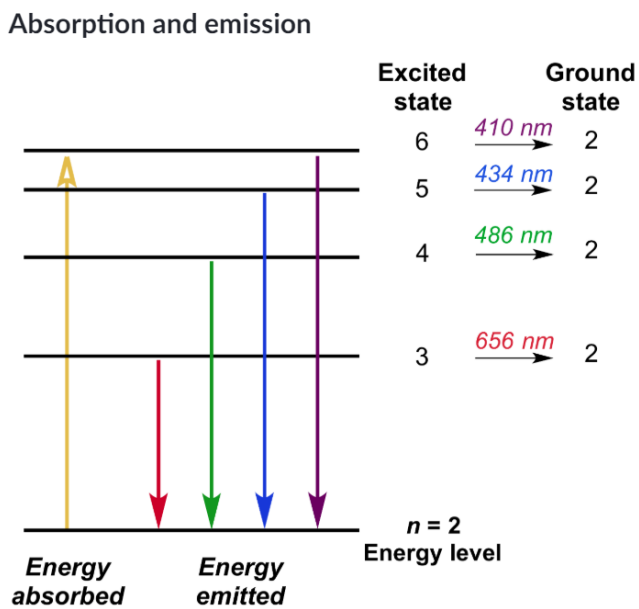

Figure 5. The excitation of electron and its relationship with UV wavelength.

1.5. Purpose of research

In the screening programme for identifying anti-NAFLD agents in medicinal plants, the 70% ethanol extract of the leaf and stem of *S. angulatus* showed a potential inhibitory effect on hepatic lipid accumulation (Scheme 1). Thus, the purification and structural determination of biologically active compounds from *S. angulatus* was undertaken.

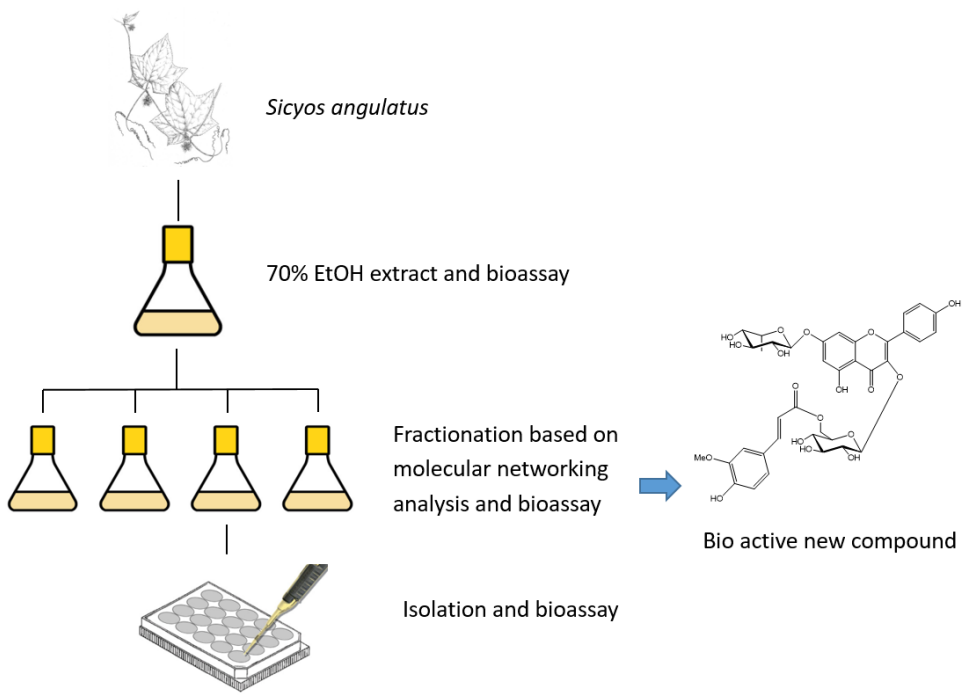

Scheme 1. The bio-guided isolation strategy of *S. angulatus*.

2. Materials and methods

2.1. Plant materials

S. angulatus was collected in August, 2015 in Gangwon province in Korea, and the sample was authenticated by Professor W. K. Oh at Seoul National University. A voucher specimen (SNU2015-0008) was deposited at the Medicinal Plant Garden of Seoul National University, Seoul, Korea.

2.2. Chemicals, reagents and chromatography

2.2.1. Chemistry reagents

- Normal-phase silica gel (ZEOprep 60 40-63 μm) and Reversed-phase silica gel (Cosmosil 75C_{18}-PREP) were purchased from Merck (Darmstadt, Germany).

- Sephadex^{TM} LH-20 (a bead-formed dextran medium for gel filtration) from Sigma-Aldrich (St. Louis, MO, USA) was used for column chromatography (CC).

- TLC Silica gel 60 F_{254} (20 × 20 cm plate) and TLC Silica gel 60 RP-18 F_{254S} (20 × 20 cm plate) from Merck (Darmstadt, Germany).

- Solvents for extraction and isolation were purchased from Dae Jung Pure Chemical Engineering Co. Ltd. (Siheung, Korea).

- Solvents (ACN, MeOH) for HPLC chromatography were bought from HoneyWell Burdick & Jackson®, USA.

- NMR solvents were purchased from Cambridge Isotope Laboratories, Inc., USA.

2.1.2 Reagents for *in vitro* assay

- 2-NBDG (Invitrogen, Eugene, OR, USA)

- BCA protein assay kit (Bio-Rad Laboratories, Inc., Hercules, CA, USA)

- Chemiluminescence Western blot detection kit (Thermo sci., Rockford, IL, USA)

- Dexamethasone, 3-isobutyl-1-methyl-xanthine, MTT (Sigma, St. Louis, MO, USA)

- DMEM, FBS, Trypsin (Hyclone, Logan, UT, USA)

- Dimethyl sulfoxide (DMSO) (Junsei Chemical Co. Ltd., Tokyo, Japan)

- Insulin (Roche, Mannheim, Germany)

- Na^+/K^+ ATPase α1 antibody (Cell signaling Technology, Inc., Beverly, MA, USA)

- Penicillin (100 U/mL), and streptomycin (100 μg/mL), calf serum, horse serum (Gibco, NY, USA)

- Phosphate-buffered saline (PBS) (Takara, Shiga, Japan)

- Polyvinylidene fluoride (PVDF) membranes (PVDF 0.45 μm, Immobilon-P., USA)

2.2.2. Experimental instruments

- Clean bench: Class II Biological Safety Cabinet, ESCO®

- CO_2 incubator: Forma Series II water jacketed CO_2 incubator, THERMO

- Evaporator: EYELA KSB-202, Japan

- ESIMS spectrometer: Agilent Technologies 6130 Quadrupole LC/MS spectrometer equipped with an Agilent Technologies 1260 Infinity LC system (Agilent Technologies, Inc., Santa Clara, CA, USA)

- Fluorescence microplate reader: Spectra Max Gemini XPS, Molecular Devices, San Jose, CA, USA

- Fluorescence microscope: Olympus ix70 Fluorescence Microscope, Olympus Corporation, Tokyo, Japan

- HPLC system: Gilson 321 pump and Gilson UV/VIS 151 detector, USA.

- IR spectrometer: JASCO, FT/IR-4200, USA

- Microscope: Promo vert, China

- NMR spectrometers:

    Bruker 500 MHz spectrometer (Bruker, Billerica, MA USA)

    JNM-ECA 600 MHz spectrometer (JEOL Ltd., Tokyo, Japan)

- Optical rotations: JASCO P-2000 polarimeter (JASCO International Co. Ltd., Tokyo, Japan).

2.3. Molecular networking

Tandem mass spectrometry molecular networks were generated using the GNPS platform. The data were converted into mzXML format and imported to MZmine 2.27. The mass detection was applied with the noise level at 1000 (for MS) and 100 (for MS/MS). The chromatogram was convoluted with ions presenting a minimum height of 2000, minimum time span of 0.01 min, and *m/z* tolerance of 5.0 ppm. The parameter for deconvolution was as follows; peak duration range of 0.02-0.10 min, minimum peak height of 1500 and baseline level of 300. Chromatograms were isotope with isotopic peak grouper algorithm with a *m/z* tolerance of 5.0 ppm. The cosine score of each vector ranges from 0 to 1. To lower the complexity of the network, the comparison is applied between pairs of spectra that have at least three matched ions and at least over 0.5 of cosine score. Data were open and visualized using Cytoscape 3.5.0 software.

2.4. Extraction and isolation schemes

The dried leaves and stems of *S. angulatus* (1 kg) were extracted with 70% EtOH at room temperature three times for one week. The extract was concentrated under reduced pressure to yield a dried sample (115 g). The concentrated extract was then suspended in H_2O and successively partitioned with *n*-hexane, EtOAc, and *n*-BuOH. The EtOAc fraction, which exhibited the strongest inhibitory activity against hepatic lipid accumulation in the HepG2 cell. The active fraction, EA part was chromatographed over silica gel (7 × 50 cm; 63-200 μm particle size) and eluted with gradient mixtures of *n*-hexane/EtOAc/MeOH (10:1:0 → 0:0:1, each 2 L) to afford five sub-fractions (F1–5). Fraction F4 was purified by reversed-phase silica gel CC (eluted with MeOH/H_2O, 4:6, v/v) to give 8 fractions (F4.1–4.8). Fraction F4.2 (500 mg) was subsequently separated on a silica gel column (4 × 40 cm; 63-200 μm particle size) with gradient mixtures of EtOAc/MeOH (9:1 → 0:1, each 2 L) to afford six sub-fractions (F4.2.1–4.2.6). Fraction 4.2.2 (120 mg) was further purified by HPLC (Gilson system using an Optima Pak C_{18} column [10 × 250 mm, 10 μm particle size, mobile phase CH_3CN/H_2O (18:82, v/v), flow rate 2 mL/min; UV detector wavelengths at 205 and 254 nm) to yield compounds **3** (7.0 mg; t_R = 33.4 min), **4** (3.0 mg; t_R = 37.0 min), **5** (2.0 mg; t_R = 43.4 min), **6** (1.2 mg; t_R = 38.0 min), **8** (2.2 mg; t_R = 31.5 min), **11** (2.3 mg; t_R = 32.3 min), **12** (2.2 mg; t_R = 36.3 min) and **13** (1.7 mg; t_R = 38.3 min). Fraction 4.2.3 (220 mg) was subjected to Sephadex LH-20 column chromatography with a MeOH/H_2O system (7:3) and afforded 4 subfractions (F4.2.3.1–4.2.3.4). Further purification of fraction 4.2.3.2. by HPLC (eluted with CH_3CN/H_2O, 4:1, v/v)

gave compounds **1** (5.0 mg; t_R = 55.0 min), **2** (9.0 mg; t_R = 60.0 min), **9** (1.9 mg; t_R = 50.0 min) and **10** (1.7 mg; t_R = 48.0 min). Subfraction F4.2.6 was further purified by HPLC (CH_3CN/H_2O, 4:21, v/v) to yield compound **7** (1.0 mg; t_R = 32.5 min). (Scheme 2)

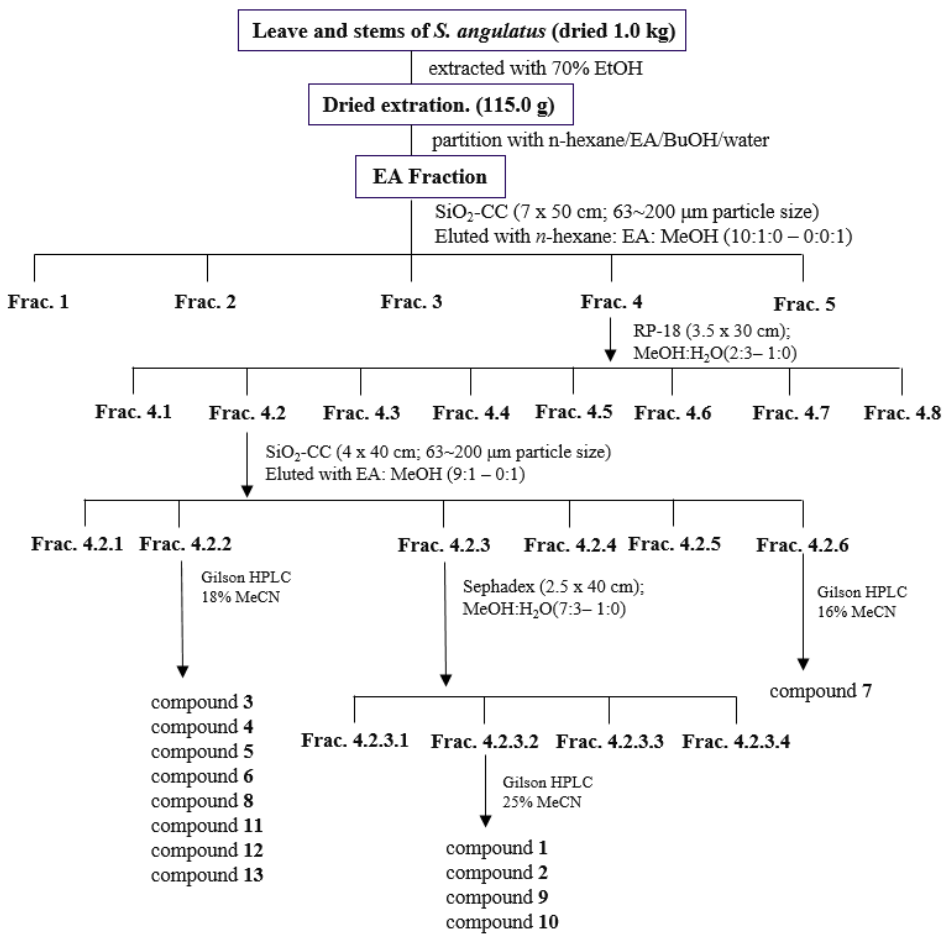

Scheme 2. Isolation scheme of 70% EtOH fraction of *S. angulatus.*

2.5. Chemical and spectral properties of isolated compounds

Kaempferol 3-*O*-(6-*O*-*E*-feruloyl)-*β*-D-glucopyranosyl-7-*O*-*α*-L-rhamnopyranoside (**1**)

Yellowish powder

$C_{37}H_{38}O_{18}$

$[\alpha]_D^{25}$ -92.2 (*c* 0.5, MeOH)

HRESIMS: *m/z* 769.2006 $[M - H]^-$ (calcd for 769.1985)

UV (MeOH) λ_{max} (log ε) 265 (3.75), 328 (3.41) nm

IR ν_{max} 3299, 1656, 1588, 1291, 1181, 1085 cm^{-1}

^1H NMR data (500 MHz, DMSO-d_6): See table 1

^{13}C NMR data (125 MHz, DMSO-d_6): See table 2

Kaempferol 3-*O*-(6-*O*-*E*-coumaroyl)-*β*-D-glucopyranosyl-7-*O*-*α*-L-rhamnopyranoside (**2**)

Yellow powder

$C_{36}H_{36}O_{17}$

$[\alpha]_D^{25}$ -67.8 (*c* 0.2, MeOH)

HRESIMS *m*/*z* 739.1880 $[M - H]^-$ (calcd for 739.1874)

UV (MeOH) λ_{max} (log ε) 266 (3.62), 319 (3.20) nm

IR (KBr) ν_{max} 3398, 2972, 2361, 1701 cm^{-1}

^{1}H NMR (500 MHz, DMSO-d_6): δ_H 8.02 (2H, d, J = 8.0 Hz, H-2', 6'), 7.38 (2H, d, J = 8.0 Hz, H-2''', 6'''), 7.32 (1H, d, J = 15.5 Hz, H-7'''), 6.85 (2H, d, J = 8.0 Hz, H-3', 5'), 6.77 (2H, d, J = 8.0 Hz, H-3''', 5'''), 6.32 (1H, br s, H-6), 6.12 (1H, d, J = 15.5 Hz, H-8'''), 5.48 (1H, br s, H-1''''), 5.45 (1H, d, J = 7.5 Hz, H-1''), 4.24 (1H, d, J = 11.6 Hz, H-6''a), 4.10 (1H, dd, J = 11.6, 6.0 Hz, H-6''b), 3.84 (1H, br s, H-2''''), 3.62 (1H, dd, J = 9.0, 2.6 Hz, H-3''''), 3.40 (1H, m, H-4''''), 3.32 (1H, m, H-5''), 3.29 (1H, m, H-3''), 3.25 (1H, m, H-2''), 3.22 (1H, m, H-5''''), 3.19 (1H, m, H-4''), 1.10 (3H, d, J = 6.0 Hz, H-6'''').

^{13}C NMR (125 MHz, DMSO-d_6): δ_C 155.9 (C-2), 133.3 (C-3), 177.6 (C-4), 160.7 (C-5), 99.3 (C-6), 161.5 (C-7), 94.6 (C-8), 156.9 (C-9), 105.5 (C-10), 120.6 (C-1'), 130.2 (C-2'), 115.1 (C-3'), 160.2 (C-4'), 115.1 (C-5'), 130.2 (C-6'), 100.9 (C-1''), 74.3 (C-2''), 76.2 (C-3''), 70.0 (C-4''), 74.1 (C-5''), 62.8 (C-6''), 124.9 (C-1'''), 130.9 (C-2'''), 115.7 (C-3'''), 159.9 (C-4'''), 115.7 (C-5'''), 130.9 (C-6'''), 144.6 (C-7'''), 113.6 (C-8'''), 166.2 (C-9'''), 98.3 (C-1''''), 69.8 (C-2''''), 70.2 (C-3''''), 71.6 (C-4''''), 69.7 (C-5''''), 17.9 (C-6'''').

Kaempferol-3-*O*-(6-*O*-*α*-L-rhamnopyranosyl)-*β*-D-glucopyranosyl-7-*O*-*α*-L-rhamnoside. (**3**)

White amorphous powder

$C_{33}H_{40}O_{19}$

$[\alpha]_D^{25}$ -80.5 (*c* 0.2, MeOH)

HRESIMS *m*/*z* 739.2079 $[M - H]^-$ (calcd for 739.2085).

UV (MeOH) λ_{max} (log ε) 266 (3.80), 345 (3.10) nm

IR (KBr) ν_{max} 3400, 2970, 2938, 1698, 1617 cm^{-1};

^{1}H NMR (500 MHz, DMSO-d_6): δ_H 8.01 (2H, d, J = 8.7 Hz, H-2', 6'), 6.88 (2H, d, J = 8.7 Hz, H-3', 5'), 6.77 (1H, br s, H-8), 6.44 (1H, br s, H-6), 5.54 (1H, s, H-1''''), 5.35 (1H, d, J = 7.4 Hz, H-1''), 4.38 (1H, br s, H-1'''), 3.84 (1H, br s, H-2''''), 3.67 (1H, d, J = 10.6 Hz, H-6''a), 3.64 (1H, dd, J = 9.6, 2.4 Hz, H-3''''), 3.48 (1H, m, H-4''), 3.47 (1H, m, H-3'''), 3.46 (1H, m, H-2''), 3.45 (1H, m, H-5''''), 3.44 (1H, m, H-5'''), 3.40 (1H, m, H-2'''), 3.34 (1H, m, H-3''), 3.22 (1H, m, H-6''b), 3.20 (1H, m, H-4''), 3.19 (1H, m, H-4''''), 3.11 (1H, m, H-4'''), 3.10 (1H, m, H-5''), 1.11 (3H, d, J = 6.0 Hz, H-6''''), 0.97 (3H, d, J = 6.0 Hz, H-6''').

^{13}C NMR (125 MHz, DMSO-d_6): δ_C 156.0 (C-2), 133.5 (C-3), 177.6 (C-4), 160.8 (C-5), 99.3 (C-6), 161.6 (C-7), 94.6 (C-8), 157.2 (C-9), 105.6 (C-10), 120.6 (C-1'), 130.9 (C-2'), 115.1 (C-3'), 160.2 (C-4'), 115.1 (C-5'), 130.9 (C-6'), 101.2 (C-1''), 74.1 (C-2''), 76.3 (C-3''), 70.3 (C-4''), 75.8 (C-5''), 66.7 (C-6''), 100.7 (C-1'''), 70.2 (C-2'''), 70.5 (C-3'''), 71.8 (C-4'''), 68.2 (C-5'''), 17.7 (C-6'''), 98.3 (C-1''''), 69.8 (C-2''''), 70.0 (C-3''''), 71.6 (C-4''''), 69.8 (C-5''''), 17.9 (C-6'''').

Kaempferol-3-*O*-β-D-glucopyranosyl-7-*O*-α-L-rhamnoside. (**4**)

White amorphous powder

$C_{27}H_{30}O_{15}$

$[\alpha]_D^{25}$ 50.6 (*c* 0.2, MeOH)

HRESIMS *m/z* 593.1502 $[M - H]^-$ (calcd for 593.1506).

UV (MeOH) λ_{max} (log ε) 266 (3.30), 343 (3.05) nm

IR (KBr) ν_{max} 3709, 2971, 2870, 1698 cm^{-1}

^1H NMR (400 MHz, DMSO-d_6): δ_H 8.07 (2H, d, *J* = 8.8 Hz, H-2', 6'), 6.88 (2H, d, *J* = 8.8 Hz, H-3', 5'), 6.82 (1H, br s, H-8), 6.44 (1H, br s, H-6), 5.54 (1H, s, H-1'''), 5.47 (1H, d, *J* = 7.3 Hz, H-1''), 3.83 (1H, br s, H-2'''), 3.64 (1H, dd, *J* = 9.3, 2.4 Hz, H-3'''), 3.53 (1H, d, *J* = 11.6 Hz, H-6''a), 3.48 (1H, m, H-5''), 3.45 (1H, m, H-5'''), 3.34 (1H, m, H-3''), 3.32 (1H, m, H-6''b), 3.27 (1H, m, H-2''), 3.46 (1H, m, H-3''), 3.19 (1H, m, H-4'''), 1.11 (3H, d, *J* = 6.0 Hz, H-6''').

^{13}C NMR (100 MHz, DMSO-d_6): δ_C 156.0 (C-2), 133.4 (C-3), 177.5 (C-4), 160.9 (C-5), 99.4 (C-6), 161.5 (C-7), 94.9 (C-8), 156.6 (C-9), 105.6 (C-10), 120.6 (C-1'), 130.9 (C-2'), 115.1 (C-3'), 160.2 (C-4'), 115.1 (C-5'), 130.9 (C-6'), 100.6 (C-1''), 74.1 (C-2''), 76.4 (C-3''), 70.2 (C-4''), 74.5 (C-5''), 60.8 (C-6''), 98.3 (C-1'''), 69.9 (C-2'''), 70.5 (C-3'''), 71.5 (C-4'''), 69.8 (C-5'''), 17.9 (C-6''').

Kaempferol-7-*O*-β-D-glucopyranoside (**5**)

White amorphous powder

$C_{21}H_{20}O_{10}$

$[\alpha]_D^{25}$ 60.8 (*c* 0.2, MeOH)

HRESIMS *m/z* 431.0985 $[M - H]^-$ (calcd for 431.0978).

IR (KBr) ν_{max} 3403, 2935, 1704, 1388, 1134 cm^{-1};

^{1}H NMR (800 MHz, DMSO-d_6): δ_H 7.95 (2H, d, *J* = 8.0 Hz, H-2', 6'), 6.94 (2H, d, *J* = 8.0 Hz, H-3', 5'), 6.87 (1H, s, H-3), 6.82 (1H, br s, H-8), 6.44 (1H, br s, H-6), 5.06 (1H, d, *J* = 7.3 Hz, H-1"), 3.70 (1H, d, *J* = 11.3 Hz, H-6"a), 3.48 (1H, dd, *J* = 11.0, 5.6 Hz, H-6"b), 3.46 (1H, m, H-5"), 3.31 (1H, m, H-3"), 3.28 (1H, m, H-2"), 3.19 (1H, m, H-4");

^{13}C NMR (200 MHz, DMSO-d_6): δ_C 164.2 (C-2), 103.0 (C-3), 182.0 (C-4), 161.4 (C-5), 99.5 (C-6), 162.9 (C-7), 94.8 (C-8), 156.9 (C-9), 105.3 (C-10), 120.9 (C-1'), 128.6 (C-2'), 116.0 (C-3'), 161.1 (C-4'), 116.0 (C-5'), 128.6 (C-6'), 99.8 (C-1"), 73.0 (C-2"), 76.4 (C-3"), 69.5 (C-4"), 77.1 (C-5"), 60.5 (C-6").

Kaempferol-3-*O*-β-D-glucopyranoside (**6**)

White amorphous powder

$C_{21}H_{20}O_{11}$

$[\alpha]_D^{25}$ -64.2 (*c* 0.2, MeOH)

IR (KBr) ν_{max} 3401, 2971, 2923, 2371, 2320 cm^{-1}

^{1}H NMR (600 MHz, DMSO-d_6): δ_H 8.10 (2H, d, *J* = 8.6 Hz, H-2', 6'), 6.90 (2H, d, *J* = 8.6 Hz, H-3', 5'), 6.80 (1H, d, *J* = 1.6 Hz, H-8), 6.20 (1H, d, *J* = 1.6 Hz, H-6), 5.40 (1H, d, *J* = 7.6 Hz, H-1"), 3.56 (1H, d, *J* = 11.0 Hz, H-6"a), 3.34 (1H, m, H-3"), 3.23 (1H, m, H-4"), 3.22 (1H, m, H-6"b), 3.15 (1H, m, H-5"), 3.11 (1H, m, H-2").

^{13}C NMR (150 MHz, DMSO-d_6): δ_C 156.0 (C-2), 133.4 (C-3), 177.5 (C-4), 160.9 (C-5), 99.4 (C-6), 161.5 (C-7), 94.9 (C-8), 156.6 (C-9), 105.6 (C-10), 120.6 (C-1'), 130.9 (C-2'), 115.1 (C-3'), 160.2 (C-4'), 115.1 (C-5'), 130.9 (C-6'), 100.6 (C-1"), 74.1 (C-2"), 76.4 (C-3"), 70.2 (C-4"), 74.5 (C-5"), 60.8 (C-6").

Kaempferol 3-*O*-*α*-L-rhamnopyranosyl-(1→6)-*β*-D-glucopyranoside (**7**)

White amorphous powder

$C_{27}H_{30}O_{15}$

$[\alpha]_D^{25}$ 56.7. (*c* 0.2, MeOH)

UV (MeOH): λ_{max} (log ε) 280 (3.7), 250 (3.8) nm

IR (KBr) ν_{max} 3400, 2972, 2942, 2371 cm^{-1}

^{1}H NMR (400 MHz, DMSO-d_6): δ_H 7.97 (2H, d, *J* = 8.8 Hz, H-2', 6'), 6.87 (2H, d, *J* = 8.8 Hz, H-3', 5'), 6.34 (1H, br s, H-8), 6.14 (1H, br s, H-6), 5.28 (1H, d, *J* = 7.7 Hz, H-1"), 4.37 (1H, s, H-1'"), 3.64 (1H, d, *J* = 11.0 Hz, H-6"a), 3.40 (1H, br s, H-2'"), 3.24 (1H, m, H-3'"), 3.48 (1H, m, H-5"), 3.45 (1H, m, H-5'"), 3.34 (1H, m, H-3"), 3.32 (1H, m, H-6"b), 3.27 (1H, m, H-2"), 3.46 (1H, m, H-3"), 3.19 (1H, m, H-4'"), 0.98 (3H, d, *J* = 6.0 Hz, H-6'").

^{13}C NMR (100 MHz, DMSO-d_6): δ_C 156.9 (C-2), 133.2 (C-3), 177.4 (C-4), 161.2 (C-5), 98.8 (C-6), 164.2 (C-7), 93.8 (C-8), 159.9 (C-9), 103.9 (C-10), 120.9 (C-1'), 130.9 (C-2'), 115.1 (C-3'), 159.9 (C-4'), 115.1 (C-5'), 130.9 (C-6'), 101.3 (C-1"), 74.2

(C-2"), 76.3 (C-3"), 69.9 (C-4"), 75.7 (C-5"), 66.9 (C-6"), 100.8 (C-1'"), 70.3 (C-2'"), 70.6 (C-3'"), 71.8 (C-4'"), 68.2 (C-5'"), 17.7 (C-6'").

Kaempferol 3-*O*-*β*-D-apiofuranosyl-7-*O*-*β*-D-glucopyranosyl-(1→3)-*α*-L-rhamnopyranoside (**8**)

Reddish gum

$C_{32}H_{38}O_{19}$

$[\alpha]_D^{25}$ -60.3 (*c* 0.5, MeOH)

HRESIMS *m/z* 725.1961 $[M - H]^-$ (calcd for 725.1935).

UV (MeOH) λ_{max} (log ε) 271 (3.80), 348 (3.30) nm

IR ν_{max} 3345, 1657, 1603, 1348, 1175, 1077 cm^{-1}

^1H NMR data (800 MHz, DMSO-d_6): See table 3

^{13}C NMR data (200 MHz, DMSO-d_6): See table 4

Quercetin 3-*O*-(6-*O*-*E*-feruloyl)-*β*-D-glucopyranosyl-7-*O*-*α*-L-rhamnopyranoside (**9**)

Yellowish powder

$C_{37}H_{38}O_{19}$

$[\alpha]_D^{25}$ -115.0 (*c* 0.5, MeOH)

HRESIMS *m/z* 785.1964 $[M - H]^-$ (calcd for 785.1935).

UV (MeOH) λ_{max} (log ε) 265 (3.71), 326 (3.40) nm

IR ν_{max} 3304, 1656, 1598, 1446, 1286, 1181, 1085 cm^{-1}

^1H NMR data (800 MHz, DMSO-d_6): See table 1

^{13}C NMR data (200 MHz, DMSO-d_6): See table 2

Quercetin 3-*O*-(6-*O*-*E*-coumaroyl)-*β*-D-glucopyranosyl-7-*O*-*α*-L-rhamnopyranoside (**10**)

White amorphous powder

$C_{36}H_{36}O_{18}$

$[\alpha]_D^{25}$ -100.5 (*c* 0.2, MeOH)

HRESIMS *m*/*z* 755.1830 $[M - H]^-$ (calcd for 755.1823).

UV (MeOH): λ_{max} (log ε) 266 (2.8), 326 (3.0) nm

IR (KBr) ν_{max} 3390, 2971, 1057, 1013 cm^{-1}

^{1}H NMR (600 MHz, DMSO-d_6): δ_H 7.59 (1H, d, *J* = 2.0 Hz, H-2'), 7.56 (1H, dd, *J* = 8.4, 2.1 Hz, H-6'), 7.38 (2H, d, *J* = 8.6 Hz, H-2''', 6'''), 7.33 (1H, d, *J* = 15.5 Hz, H-7'''), 6.83 (1H, d, *J* = 8.4 Hz, H-5'), 6.77 (2H, d, *J* = 8.5 Hz, H-3''', 5'''), 6.69 (1H, d, *J* = 2.0 Hz, H-8), 6.30 (1H, d, *J* = 2.0 Hz, H-6), 6.11 (1H, d, *J* = 15.5 Hz, H-8'''), 5.49 (1H, d, *J* = 7.6 Hz, H-1''), 5.48 (1H, br s, H-1''''), 4.23 (1H, d, *J* = 10.3 Hz, H-6''a), 4.11 (1H, dd, *J* = 11.0, 6.2 Hz, H-6''b), 3.84 (1H, br s, H-2''''), 3.61 (1H, m, H-3''''), 3.40 (1H, m, H-2''), 3.38 (1H, m, H-4''), 3.30 (1H, m, H-5''), 3.28 (1H, m, H-3''), 3.28 (1H, m, H-4''''), 3.28 (1H, m, H-3''), 3.22 (1H, m, H-5''''), 1.10 (3H, d, *J* = 6.1 Hz, H-6'''').

^{13}C NMR (150 MHz, DMSO-d_6): δ_C 156.7 (C-2), 133.3 (C-3), 177.5 (C-4), 160.7 (C-5), 99.2 (C-6), 161.5 (C-7), 94.3 (C-8), 155.8 (C-9), 105.4 (C-10), 120.8 (C-1'),

116.2 (C-2'), 144.5 (C-3'), 148.7 (C-4'), 115.1 (C-5'), 121.6 (C-6'), 100.7 (C-1''), 74.3 (C-2''), 76.2 (C-3''), 70.0 (C-4''), 73.9 (C-5''), 62.8 (C-6''), 124.9 (C-1'''), 130.1 (C-2'''), 115.6 (C-3'''), 159.7 (C-4'''), 115.6 (C-5'''), 130.1 (C-6'''), 144.8 (C-7'''), 113.6 (C-8'''), 166.2 (C-9'''), 98.3 (C-1''''), 70.0 (C-2''''), 70.2 (C-3''''), 71.5 (C-4''''), 69.8 (C-5''''), 17.8 (C-6'''').

Kaempferol 3-*O*-(6-*O*-*E*-feruloyl)-*β*-D-glucopyranosyl-7-*O*-*α*-L-rhamnopyranosyl-(1→6)-*β*-D-glucopyranosyl-(1→3)-*α*-L-rhamnopyranoside (**11**).

Yellowish gum

$C_{49}H_{58}O_{27}$

$[\alpha]_D^{25}$ -78.5 (*c* 0.5, MeOH)

HRESIMS *m/z* 1077.3108 $[M - H]^-$ (calcd for 1077.3093).

UV (MeOH) λ_{max} 265 (3.50), 327 (3.38) nm

IR ν_{max} 3304, 1656, 1596, 1275, 1190, 1075, 1040 cm^{-1}

^1H NMR data (800 MHz, DMSO-d_6): See table 1

^{13}C NMR data (200 MHz, DMSO-d_6): See table 2

Kaempferol 3-*O*-(6-*O*-*E*-feruloyl)-*β*-D-glucopyranosyl-7-*O*-*β*-D-glucopyranosyl-(1→3)-*α*-L-rhamnopyranoside (**12**)

Yellowish powder

$C_{43}H_{48}O_{23}$

$[\alpha]_D^{25}$ -64.9 (*c* 0.5, MeOH)

HRESIMS *m*/*z* 931.2523 $[M - H]^-$ (calcd for 931.2514).

UV (MeOH) λ_{max} (log ε) 265 (3.65), 328 (3.58) nm

IR ν_{max} 3339, 1656, 1596, 1280, 1175, 1085 cm^{-1}

^1H NMR data (800 MHz, DMSO-d_6): See table 1

^{13}C NMR data (200 MHz, DMSO-d_6): See table 2

Tricin 4′-*O*-(7′′*R*,8′′*R*-guaiacylglyceryl)ether-7-*O*-α-L-rhamnopyranosyl-(1→4)-*O*-β-D-glucopyranoside (**13**)

Amorphous powder

$[\alpha]_D^{25}$ -39.8 (*c* 0.5, MeOH)

$C_{39}H_{46}O_{20}$

HRESIMS *m*/*z* 833.2513 $[M - H]^-$ (calcd for 833.2510).

UV (MeOH) λ_{max} (log ε) 223 (5.17), 269 (3.45), 340 (2.78) nm

IR ν_{max} 3424, 1658, 1613, 1495, 1459, 1352, 1256, 1133 cm^{-1}

^1H NMR data (800 MHz, DMSO-d_6): See table 3

^{13}C NMR data (200 MHz, DMSO-d_6): See table 4

Table 1. ^{1}H NMR spectroscopic data for compounds **1**, **9**, and **11**-**12** (in DMSO-d_6).

position	**1**[a]	**9**[b]	**11**[b]	**12**[b]
6	6.33 (d, 2.0)	6.30 (d, 2.1)	6.32 (d, 2.0)	6.32 (d, 2.0)
8	6.73 (d, 2.0)	6.69 (d, 2.0)	6.59 (d, 2.0)	6.76 (d, 2.0)
2'	8.02 (d, 8.0)	7.58 (d, 2.1)	8.14 (d, 8.8)	8.09 (d, 8.9)
3'	6.86 (d, 8.0)		6.87 (d, 8.8)	6.86 (d, 8.9)
5'	6.86 (d, 8.0)	6.93 (d, 8.4)	6.87 (d, 8.8)	6.86 (d, 8.9)
6'	8.02 (d, 8.0)	7.56 (dd, 8.4, 2.1)	8.14 (d, 8.8)	8.09 (d, 8.9)
β-D-glc Ⅰ				
1"	5.45 (d, 7.5)	5.49 (d, 7.6)	5.33 (d, 7.6)	5.41 (d, 7.6)
2"	3.25 (m)	3.39 (m)	3.26 (m)	3.26 (m)
3"	3.28 (m)	3.27 (m)	3.23 (m)	3.28 (m)
4"	3.23 (m)	3.39 (m)	3.15 (m)	3.23 (m)
5"	3.30 (m)	3.30 (m)	3.50 (m)	3.30 (m)
6"	4.24 (dd, 11.5, 2.0) 4.12 (m)	4.24 (d, 10.1) 4.13 (dd, 11.9, 6.2)	4.41 (dd, 11.8, 1.8) 4.23 (dd, 11.9, 7.0)	4.18 (dd, 11.2, 3.7) 4.07 (dd, 11.3, 7.5)
ferulic acid				
2'''	7.20 (d, 1.2)	7.20 (d, 1.8)	7.10 (d, 1.8)	7.18 (d, 1.8)
5'''	6.78 (d, 8.0)	6.77 (d, 8.1)	6.60 (d, 8.1)	6.77 (d, 8.1)
6'''	6.95 (dd, 8.0, 1.2)	6.94 (dd, 8.2, 1.8)	6.92 (dd, 8.1, 1.8)	6.95 (dd, 8.2, 1.8)
7'''	7.35 (d, 15.5)	7.34 (d, 15.8)	7.49 (d, 15.8)	7.35 (d, 15.8)
8'''	6.25 (d, 15.5)	6.24 (d, 15.8)	6.39 (d, 15.8)	6.24 (d, 15.8)
OMe	3.81 (s, 3H)	3.81 (s, 3H)	3.68 (s, 3H)	3.79 (s, 3H)
α-L- rha Ⅰ				
1''''	5.47 (br s)	5.46 (br s)	5.44 (d, 1.2)	5.48 (br s)
2''''	3.84 (br s)	3.84 (br s)	4.08 (br s)	4.11 (br s)
3''''	3.62 (dd, 9.0, 2.6)	3.61 (dd, 8.2, 3.2)	3.72 (dd, 9.0, 2.5)	3.75 (dd, 9.1, 3.1)
4''''	3.40 (m)	3.28 (m)	3.51 (m)	3.52 (m)
5''''	3.24 (m)	3.23 (m)	3.45 (m)	3.51 (m)
6''''	1.09 (d, 6.0, 3H)	1.09 (d, 6.2, 3H)	1.10 (d, 6.0, 3H)	1.11 (d, 6.1, 3H)
β-D-glc Ⅱ				
1'''''			4.48 (d, 7.7)	4.48 (d, 7.6)
2'''''			3.14 (m)	3.09 (m)
3'''''			3.24 (m)	3.18 (m)
4'''''			3.26 (m)	3.09 (m)
5'''''			3.17 (m)	3.16 (m)
6'''''			3.71 (d, 10.0) 3.25 (overlapped)	3.70 (d, 11.0) 3.45 (m)
α-L- rha Ⅱ				
1''''''			4.38 (d, 1.2)	
2''''''			3.25 (br s)	
3''''''			3.41 (m)	
4''''''			3.06 (m)	
5''''''			3.09 (m)	
6''''''			0.97 (d, 6.0, 3H)	

[a] NMR 500 MHz; [b] NMR 800 MHz.

Table 2. ^{13}C NMR spectroscopic data for compounds **1**, **9**, and **11-12** (in DMSO-d_6).

position	**1**[a]	**9**[b]	**11**[b]	**12**[b]
2	156.9	156.8	155.8	155.8
3	133.4	133.4	133.6	133.5
4	177.6	177.5	177.5	177.6
5	160.8	160.8	160.7	160.7
6	99.2	99.2	99.1	99.2
7	161.5	161.5	161.1	161.2
8	94.6	94.4	94.6	94.8
9	155.9	155.8	157.3	156.9
10	105.5	105.5	105.5	105.5
1'	120.8	120.8	120.8	120.6
2'	130.9	116.3	131.0	131.1
3'	115.1	144.8	115.0	115.0
4'	160.2	148.2	160.0	160.1
5'	115.1	115.2	115.0	115.0
6'	130.9	121.7	131.0	131.1
β-D-glc Ⅰ				
1"	101.0	100.8	101.5	101.6
2"	74.3	74.4	75.6	74.0
3"	76.2	76.3	76.0	76.2
4"	70.1	70.0	70.2	69.8
5"	74.1	74.0	74.1	74.1
6"	62.8	62.9	63.4	62.9
ferulic acid				
1"'	125.5	125.5	125.3	125.5
2"'	110.9	110.9	110.5	110.9
3"'	147.8	147.8	147.6	147.8
4"'	149.3	149.3	149.2	149.3
5"'	115.4	115.4	115.1	115.4
6"'	123.2	123.1	123.0	123.1
7"'	144.9	144.9	145.2	145.0
8"'	113.9	113.9	113.9	113.9
9"'	166.3	166.3	166.6	166.2
OMe	55.6	55.6	55.4	55.6
α-L-rha Ⅰ				
1""	98.3	98.4	97.9	98.1
2""	69.8	69.8	69.2	68.2
3""	70.2	70.2	81.2	80.7
4""	71.6	71.6	70.1	70.5
5""	69.8	69.8	69.6	68.9
6""	17.9	17.8	17.8	17.8
β-D-glc Ⅱ				
1""'			105.0	104.6
2""'			73.8	72.9
3""'			76.4	76.2
4""'			70.5	69.5
5""'			74.2	76.7
6""'			66.7	60.9
α-L-rha Ⅱ				
1"""			100.6	
2"""			68.1	
3"""			70.2	
4"""			71.8	
5"""			69.8	
6"""			17.7	

[a] NMR 125 MHz; [b] NMR 200 MHz.

Table 3. ^{1}H NMR spectroscopic data for compounds **8** and **13** (in DMSO-d_6).

position	**8**[a]	position	**13**[a]
3		3	7.14 (s)
6	6.48 (d, 2.0)	6	6.39 (d, 2.0)
8	6.86 (d, 2.0)	8	6.90 (d, 2.0)
2'	7.98 (d, 8.0)	2'	7.32 (s)
3'	6.91 (d, 8.0)	3'	
5'	6.91 (d, 8.0)	5'	
6'	7.98 (d, 8.0)	6'	7.32 (s)
β-D-api		OMe	3.87 (s, 6H)
1"	5.74 (d, 2.1)	Guaiacyl	
2"	4.19 (d, 2.4)	1"	
3"		2"	6.93 (br s)
4"	3.60 (d, 9.3) 3.49 (d, 9.3)	3"	
5"	3.31 (d, 11.0) 3.30 (d, 11.0)	4"	
α-L- rha		5"	6.69 (d, 8.1)
1'"	5.59 (br s)	6"	6.75 (dd, 8.0, 1.6)
2'"	4.10 (br s)	7"	4.79 (m)
3'"	3.7 (dd, 8.7, 3.2)	8"	4.37 (m)
4'"	3.52 (m)	9"	3.70 (m), 3.49 (m)
5'"	3.51 (m)	OMe	3.74 (s, 3H)
6'"	1.14 (d, 6.0, 3H)	β-D-glc	
β-D-glc		1'"	5.21 (d, 7.7)
1""	4.48 (d, 7.7)	2'"	3.48 (m)
2""	3.09 (m)	3'"	3.48 (m)
3""	3.18 (m)	4'"	3.51 (m)
4""	3.09 (m)	5'"	3.18 (m)
5""	3.16 (m)	6'"	3.47 (m) 3.46 (m)
6""	3.68 (dd, 11.7, 1.9) 3.43 (dd, 11.7, 5.7)	α-L- rha	
		1""	5.12 (br s)
		2""	3.69 (br s)
		3""	3.34 (m)
		4""	3.21 (m)
		5""	3.77 (m)
		6""	1.18 (d, 6.0, 3H)

[a] NMR 800 MHz

Table 4. ^{13}C NMR spectroscopic data for compounds **8** and **13** (in DMSO-d_6).

position	**8**[a]	position	**13**[a]
2	157.3	2	163.9
3	133.7	3	105.1
4	177.0	4	182.2
5	160.9	5	161.0
6	99.5	6	99.6
7	161.4	7	162.8
8	94.8	8	95.0
9	155.9	9	157.0
10	105.7	10	105.6
1'	120.5	1'	124.9
2'	130.7	2'	104.3
3'	115.5	3'	152.9
4'	160.1	4'	139.7
5'	115.5	5'	152.9
6'	130.7	6'	104.3
β-D-api		OMe	56.3
1"	109.2	Guaiacyl	
2"	77.1	1"	133.2
3"	79.4	2"	110.9
4"	75.1	3"	146.9
5"	62.7	4"	145.4
α-L- rha		5"	114.7
1"'	98.2	6"	119.7
2"'	68.9	7"	72.1
3"'	80.7	8"	86.5
4"'	70.5	9"	60.3
5"'	69.6	OMe	55.5
6"'	17.8	β-D-glc	
β-D-glc		1"'	98.2
1""	104.6	2"'	77.3
2""	73.9	3"'	77.2
3""	76.2	4"'	76.4
4""	69.9	5"'	69.8
5""	76.7	6"'	60.5
6""	60.9	α-L- rha	
		1""	100.5
		2""	70.4
		3""	70.5
		4""	71.8
		5""	68.4
		6""	18.0

[a] NMR 200 MHz

2.6. Computational chemistry for ECD calculation

Turbomole at the def-SV(P) basis set for all atoms and the B3LYP functional was used to optimize the ground-state geometries with density functional theory (DFT) calculations. Harmonic frequency calculations were used to further confirm the ground states. The calculated ECD data corresponding to the optimized structures were obtained with TDDFT at the B3LYP functional. The ECD spectra were simulated by overlapping Gaussian functions for each transition (σ is the width of the band at *1/e* height). ΔE_i and R_i are the excitation energies and rotatory strengths for transition i, respectively. For this report, the value of σ was 0.10 eV.

$$\Delta\varepsilon(E) = \frac{1}{2.297 \times 10^{-39}} \frac{1}{\sqrt{2\pi\sigma}} \sum_{i}^{A} \Delta E_i R_i e^{\left[-(E-\Delta E_i)^2/(2\sigma)^2\right]}$$

The Boltzmann-averaged computed ECD spectrum of the 5 representative conformers, corresponding 99% of the total Boltzmann distribution, was in good agreement with the experimental ECD spectrum of **13**, which exhibited two strong positive cotton effects at 250 nm and 286 nm. These results suggested the absolute configuration of **13** was 7′′*R*,8′′*R*.

2.7. Cell viability and triglyceride quantification in HepG2 cells

To determine the cell viability, the 3-(4,5-dimethylthiazol-2-yl)-2,5-diphenyltetrazolium bromide (MTT, Sigma, MO, USA) assay was performed. HepG2 cells were grown in 96-well plates with 5×10^3 cells per well for 1 day. Then, the isolated compounds were tested for their cytotoxicity against the HepG2 cell line using serum-free media. After 24 hours of incubation, 20 µL of the MTT solution (2

mg/mL) was added to each well, and the cultures were further incubated for 4 hours at 37℃. After removing the liquid, the formazan crystals were dissolved in 100 μL of dimethyl sulfoxide (DMSO). The absorbance of the purple formazan was measured at 550 nm using a microplate reader (VersaMax, PA, USA). Error bars were calculated as the mean ± SD of three independent experiments. HepG2 cells were grown in 12-well plates until 70-80% confluence and then the cells were induced into *in vitro* insulin-resistance models with high concentrations of glucose, free fatty acid, and insulin. Briefly, the cells were treated with various test compounds in the presence of a mixture of 0.2 mM palmitic acid (Sigma, MO, USA), 30 mM glucose, 50 nM insulin and 0.1% bovine serum albumin (BSA) (Sigma, MO, USA) for 24 hours. Then, the cells were washed with phosphate-buffered saline (PBS), and the total intracellular lipids were extracted using cold 1% Triton X-100 solution (Sigma, MO, USA) in PBS. The triglyceride levels were measured using a fluorometric triglyceride quantification kit (Cell Biolabs, Inc, CA, USA). Analyses were conducted following the manufacturer's protocol with slight modifications. The fluorescence intensity was measured at ex/em = 530/585 nm using a fluorescence microplate reader (Spectra Max Gemini XPS, Molecular Devices, San Jose, CA, USA). Error bars were presented as the mean ± SD (n = 3).

2.8. Oil-red O staining in HepG2 cells

HepG2 cells were plated in 12-well plates until reaching 70-80% confluence. The cells were then treated with glucose, free fatty acid and insulin as above described. The insulin-resistant cells were exposed to the strong candidates and fenofibrate (Sigma, MO, USA) as a positive control. After 24 hours of incubation,

the cells were fixed with 5% formalin solution for 30 minutes and then incubated with oil-red O (Sigma, MO, USA) working solution for 15 minutes at room temperature. After that, the cells were washed once with 60% isopropanol, and three times with water. The nuclei were stained with hematoxylin solution (Sigma, Mo, USA) for 2 minutes at room temperature. In addition, another experiment was performed by staining the nuclei with 500 nM DAPI solution (Molecular Probes, OR, USA). The red oil droplets were visualized using fluorescence microscopy (Olympus ix70 Fluorescence Microscope, Olympus Corporation, Tokyo, Japan).

2.9. Statistical analysis

Data are presented by the mean ± SD of three independent experiments. For quantitative analysis of Western blotting, ImageJ software was applied. The one-way analysis of variance (ANOVA) was used to determine the significant differences between groups following Tukey's or Duncan's post hoc test as appropriate, which conducted in SPSS Statistics 23 (SPSS, Inc., Chicago, IL, USA). Statistical significance was accepted at * $p < 0.05$, ** $p < 0.01$, and *** $p < 0.001$.

3. Results and discussion

3.1. Molecular networking based grouping and identifying of chemical constituents

Most major cluster consists of flavonoid glycosides and they are divided into two groups (Figure 6). In the first group, flavonoids were identified to possess only sugar moieties based on database analysis. However, in the second group, flavonoids were identified to contain not only sugar but also “prop-2-enoate” moiety. Based on this result, one group of flavonoid glycoside has potential to possess cinamoyl moiety. And this explains the inhibitory effects on lipid accumulation of *S. angulatus* since large numbers of researches have demonstrated the hepatic protective effect of cinamoyl group. Regarding the exact mass, the first decimal place was “2” in the first group and “1” in the second group since the mass defect of cinnamoyl group is greater than that of sugar moiety. For example, the mass defect of coumaric acid ($C_9H_8O_3$;164.0473) is 0473, whereas, that of rhamnose ($C_6H_{12}O_5$;164.0685) is 0685. The whole process of molecular networking was performed within a day and yielded information about compounds at a higher level of confidence.

Library based identification was confirmed by UV spectrum analysis that the second flavonoid group contain cinnamoyl functional group. Molecular networking method not only dereplicates known molecules from complex compounds, it also clusters related analogues.

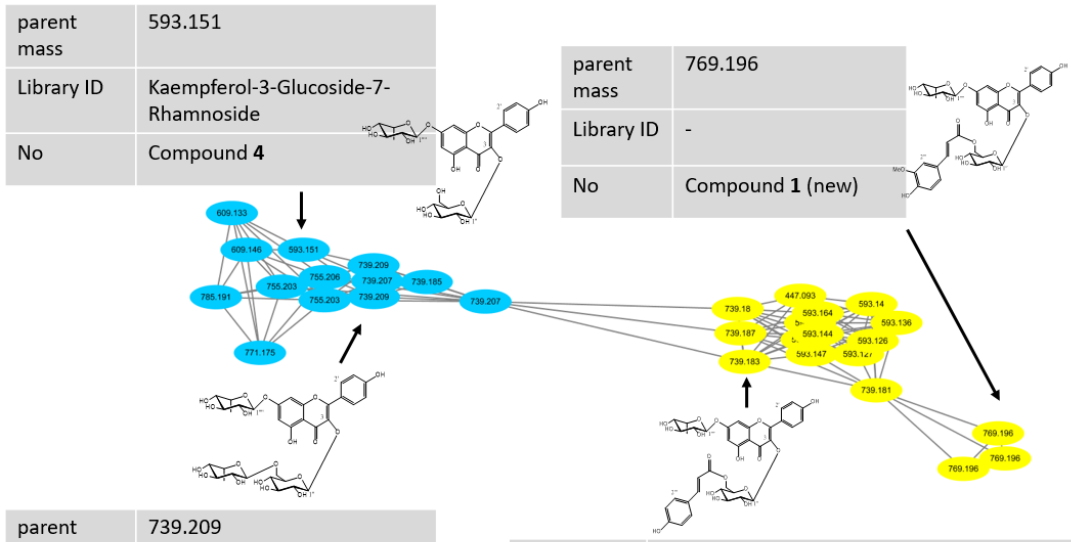

Figure 6. Flavonoid cluster of *S. angulatus* and library based identification

3.2. UV spectrum analysis

The 70% ethanol extract of *S. angulatus* was analyzed by UV spectrum. As shown in figure 7, some flavonoid glycosides present their UV maxima at 350 nm, however, on the other hand, others present UV maxima at around 325 nm. This suggested that some flavonoid glycosides contain cinnamoyl group such as ferulic acid, coumaric acid or caffeic acid because the UV maxima at 325 nm is the indicative of ferulic acid. The UV maxima was shifted upfield among flavonoid glycosides with cinnamoyl group. This result was consistent with molecular networking data.

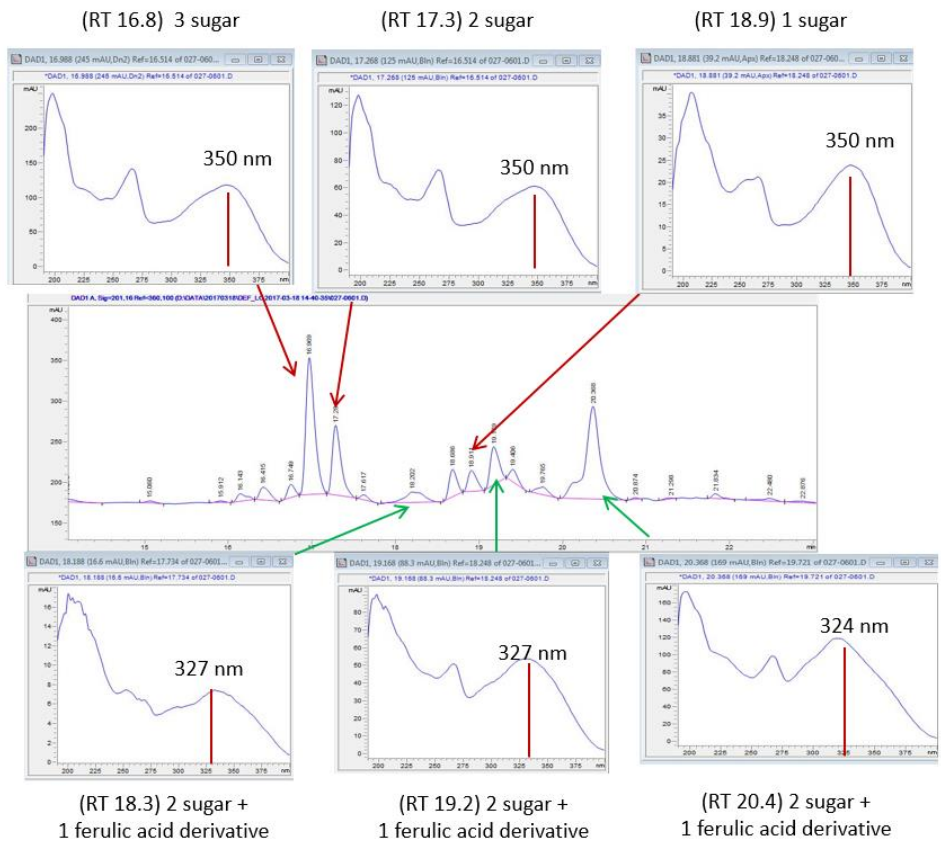

Figure 7. UV spectrum of 70% ethanol extracted *S. angulatus*.

3.3. Elucidation of chemical structures of isolated compounds from *S. angulatus* (**1**–**13**)

3.3.1. Compound **1**

Compound **1** was obtained as a yellowish powder with $[\alpha]_D^{25}$ –92.2 (*c* 0.5, MeOH). The molecular formula $C_{37}H_{38}O_{18}$ was determined from the HRESIMS ion peak at *m*/*z* 769.2006 $[M - H]^-$ (calcd for $C_{37}H_{37}O_{18}$, 769.1985). The IR spectrum of compound **1** suggested the presence of hydroxyl (3299 cm^{-1}) and *α*,*β*-unsaturated carbonyl groups (1656 cm^{-1}). The ^1H and ^{13}C NMR spectra of compound **1** displayed the presence of an A_2B_2 aromatic spin system at δ_H 8.02 (2H, d, *J* = 8.0 Hz, H-2', 6') and 6.86 (2H, d, *J* = 8.0 Hz, H-3', 5'), with corresponding carbons at δ_C 130.9 and 115.1, respectively, which is indicative of the B ring of a flavonoid (Figures 8 and 9). The meta-coupled protons of ring A resonated at δ_H 6.33 (1H, d, *J* = 2.0 Hz, H-6) and 6.73 (1H, d, *J* = 2.0 Hz, H-8). Two olefinic protons with a large coupling constant at δ_H 7.35 (1H, d, *J* = 15.5 Hz) and 6.25 (1H, d, *J* = 15.5 Hz) indicated a ferulic acid moiety in a trans-configuration. The ^{13}C NMR spectrum presented signals for 37 carbons, including two *α*,*β*-unsaturated carbonyl groups (δ_C 177.6 and 166.3), four olefinic carbon signals (δ_C 156.9-113.9), 18 aromatic carbon signals (δ_C 94.6-161.5), 11 oxygenated carbons (δ_C 101.0-62.8), one methoxy carbon (δ_C 55.6) and one methyl carbon signal (δ_C 17.9). The above data suggested that compound **1** is a flavonoid glycoside with a ferulic acid moiety. Proton signals at δ_H 5.45 (1H, d, *J* = 7.5 Hz) and 5.47 (1H, br s) were clearly indicative of anomeric protons, and the coupling constants suggested that a glucose is present as the *β*-isomer, and the other sugar, a rhamnose, is present as the *α*-isomer. Their presence was supported by the positive mass fragment ions at 625 [M – 146 (rhamnopyranosyl) + H]$^+$ and 433 [M

– 176 (ferulic acid) – 162 (glucopyranosyl) + H]$^+$. The HMBC correlation from an anomeric proton at δ_H 5.45 (1H, d, J = 7.5 Hz) to C-3 (δ_C 133.4) established the linkage of a glucopyranosyl moiety at C-3 of the aglycone. The anomeric proton of rhamnose (δ_H 5.47, 1H, br s) showed a HMBC correlation with C-7 (δ_C 161.5) of the aglycone (Figure 11). All the NMR data of compound **1** were similar to those of kaempferol 3-*O*-*β*-D-glucopyranosyl-7-*O*-*α*-L-rhamnopyranoside, which was isolated from *Chenopodium murale* (Gohar et al., 2000), except for the attachment of the ferulic acid moiety to C-6" of the glucose in compound **1**. The chemical shift of C-6" in the glucose (δ_C 62.8) in compound **1** was shifted downfield compared to the C-6" of the glucose (δ_C 61.0) in kaempferol 3-*O*-*β*-D-glucopyranosyl-7-*O*-*α*-L-rhamnopyranoside. This was further confirmed by the HMBC correlation from H-6" of the glucose (δ_H 4.24 and 4.12) to C-9"' of the ferulic acid moiety (δ_C 166.3) (Figure 10). The position of methoxy and hydroxyl at ferulic acid was confirmed by ROE correlation between methoxy at δ_H 3.81 and ferulosy H-2 at δ_H 7.20 (d, J = 1.2 Hz). Therefore, compound **1** was characterized as kaempferol 3-*O*-(6-*O*-*E*-feruloyl)-*β*-D-glucopyranosyl-7-*O*-*α*-L-rhamnopyranoside.

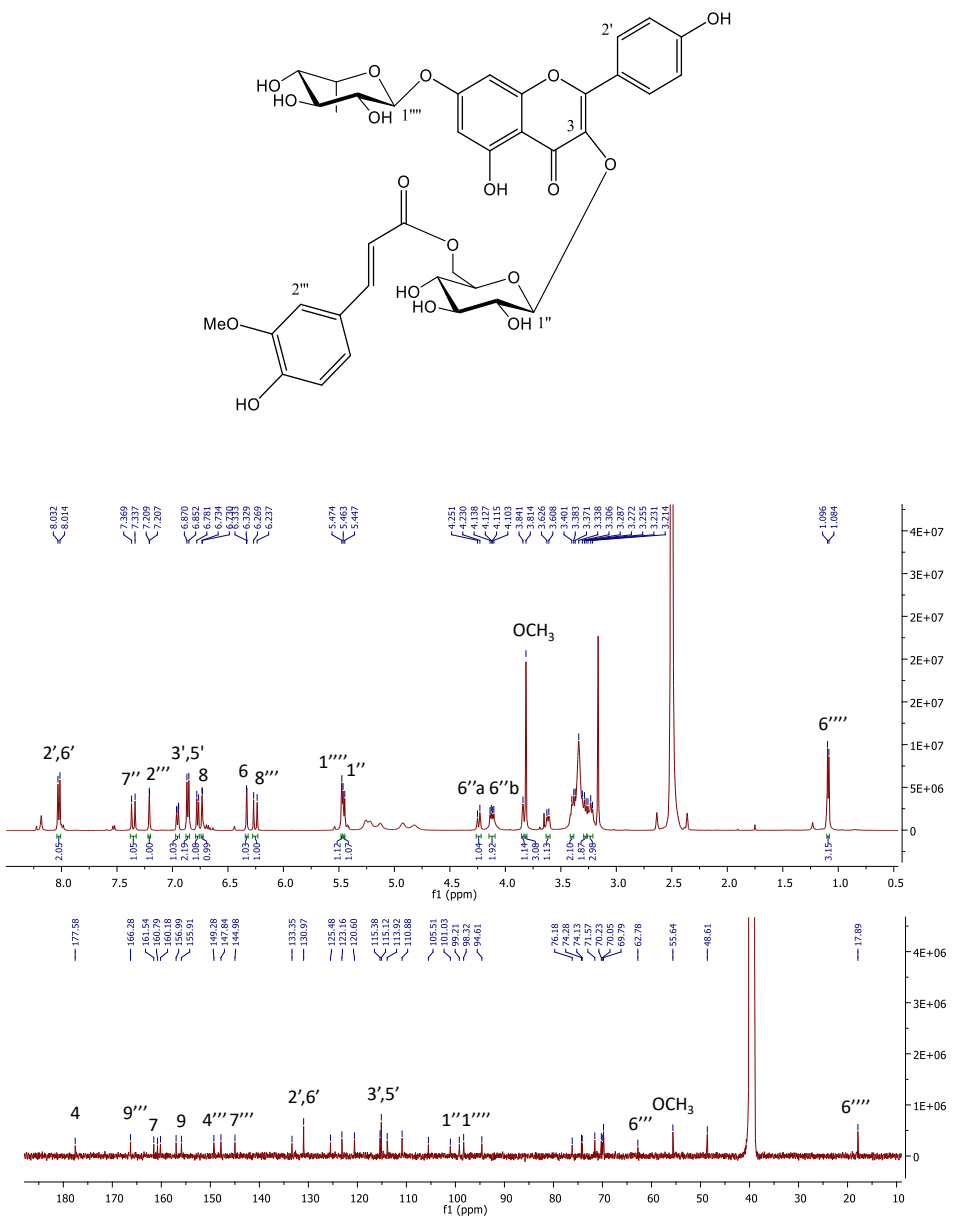

Figure 8. ^{1}H and ^{13}C NMR spectra (DMSO-d_6, 500/125 MHz) of compound **1**

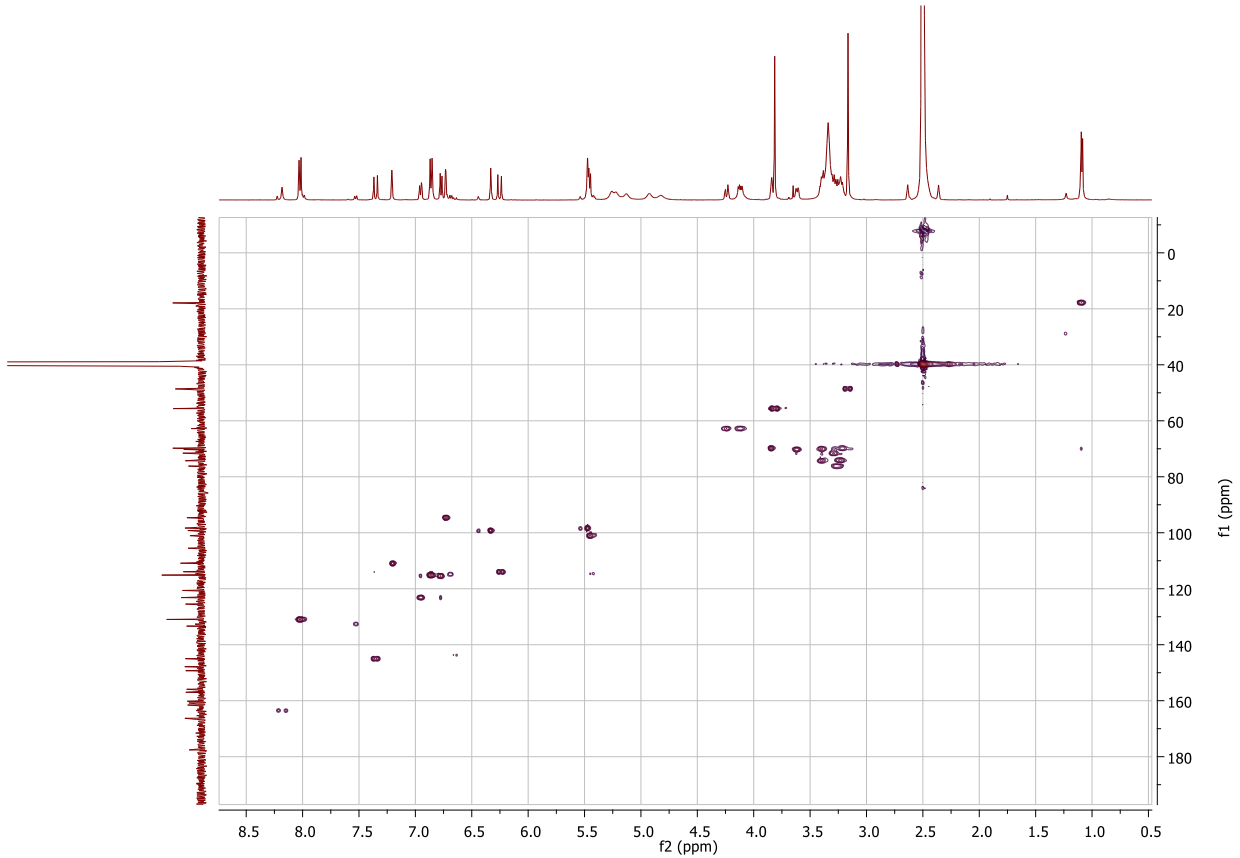

Figure 9. HSQC spectrum (DMSO-d_6, 500 MHz) of compound **1**

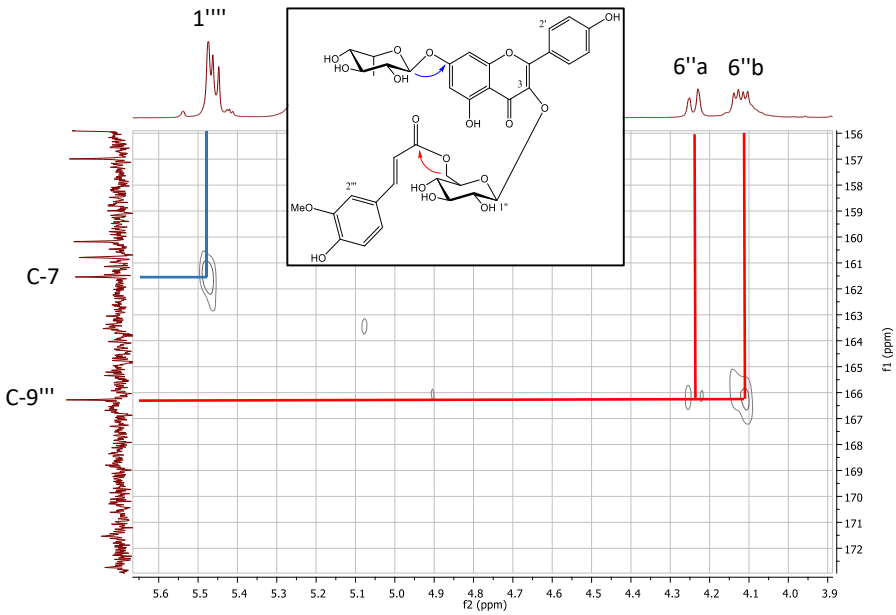

Figure 10. Key HMBC correlations (DMSO-d_6, 500 MHz) of compound **1**

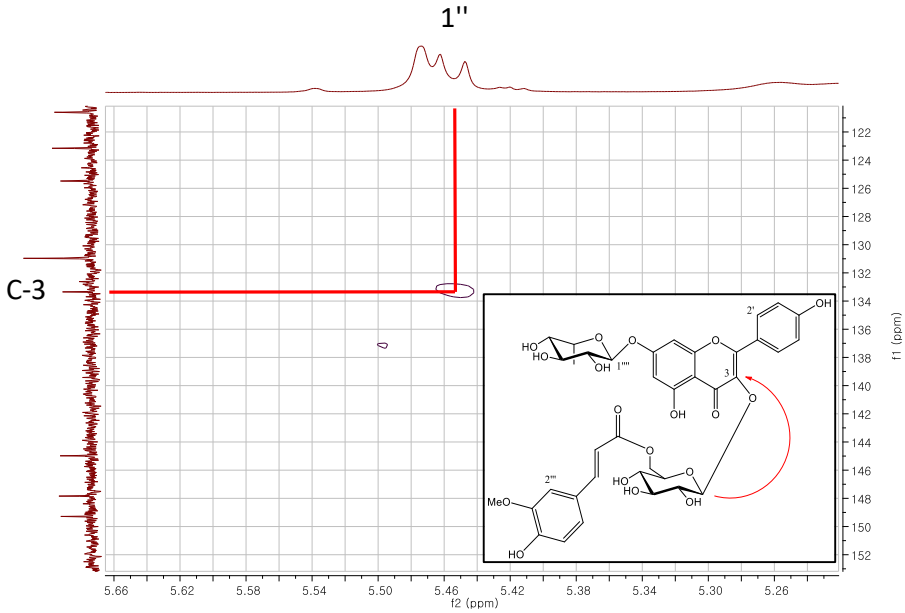

Figure 11. Key HMBC correlations (DMSO-d_6, 500 MHz) of compound **1**

3.3.2. Compound **2**

Compound **2** was isolated as an amorphous powder with $[\alpha]_D^{25}$ -67.8 (*c* 0.2, MeOH). Its molecular formula of **2** was identified as $C_{36}H_{36}O_{17}$ based on an ion peak at *m*/*z* 739.1880 $[M - H]^-$ HRESIMS (calcd for $C_{36}H_{35}O_{17}$, 739.1874). The calculation of IHD for this compound was recorded as nineteen indices. The characteristic difference is the replacement of the ferulic acid group in **1** [(δ_H 7.20, d, *J* = 1.2 Hz), (δ_H 6.95, dd, *J* = 8.0, 1.2 Hz), (δ_H 6.78, d, *J* = 8.0 Hz)] by the coumaric acid group in **2** [(δ_H 7.38, 2H, d, *J* = 8.0 Hz), (δ_H 6.77, 2H, d, *J* = 8.0 Hz)]. Two olefinic protons with a large coupling constant at δ_H 7.32 (1H, d, *J* = 15.5 Hz) and 6.12 (1H, d, *J* = 15.5 Hz) indicated a ferulic acid moiety in a trans-configuration (Figure 12). With above observed spectroscopic data, compound **2** was determined to be kaempferol 3-*O*-(6-*O*-*E*-coumaroyl)-*β*-D-glucopyranosyl-7-*O*-*α*-L-rhamnopyranoside.

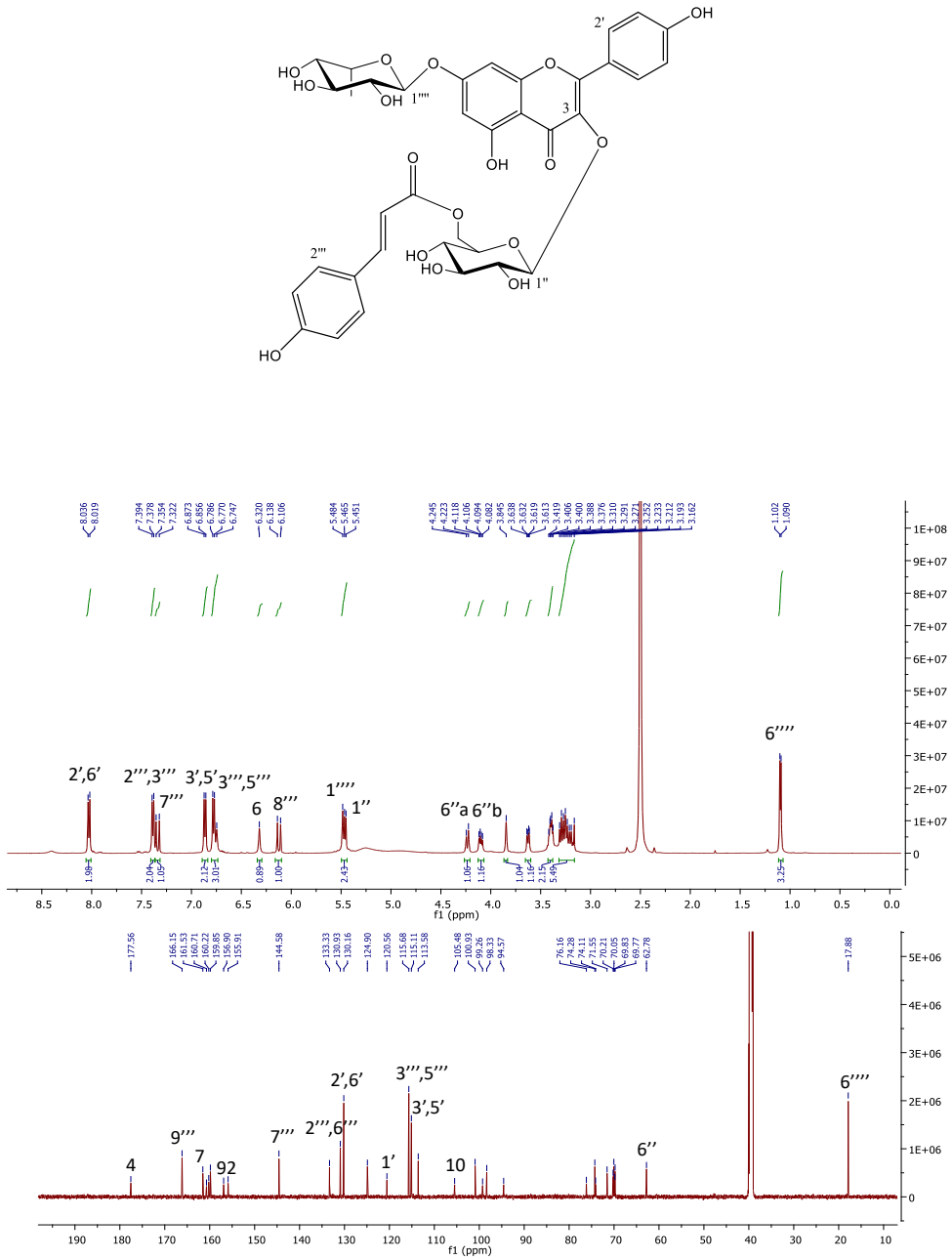

Figure 12. ^{1}H and ^{13}C NMR spectra (DMSO-d_6, 500/125 MHz) of compound **2**

3.3.3. Compound **3**

Compound **3**, an amorphous powder with $[\alpha]_D^{25}$ -80.5 (*c* 0.2, MeOH), was formulated as $C_{33}H_{40}O_{19}$ based on the HRESIMS (*m/z* 739.2079 $[M-H]^-$;calcd for $C_{33}H_{39}O_{19}$, 739.2085). The IHD of this compound was calculated as fourteen indices. The ^1H and ^{13}C NMR spectra of compound **3** presented an A_2B_2 aromatic spin system at δ_H 8.01 (2H, d, *J* = 8.7 Hz, H-2', 6') and 6.88 (2H, d, *J* = 8.7 Hz, H-3', 5'), with corresponding carbons at δ_C 130.9 and 115.1, respectively (Figure 13). Three anomeric protons were shown at δ_H 5.54 (s, H-1''''), 5.35 (d, *J* = 7.4 Hz, H-1'') and 4.38 (br s, H-1''') indicating the presence of two rhamnose and one glucose in combination with the mass fragment. The major ion of compound **3** was m/z 739.2 [M - H]-, and the ion produced by the loss of 292 Da (2 rhamnose) and 162 Da (glucose) suggested the existence of sugars. On the basis of above information, compound **3** was characterized to be kaempferol-3-*O*-(6-*O*-*α*-L-rhamnopyranosyl)-*β*-D-glucopyranosyl-7-*O*-*α*-L-rhamnoside (Refaat et al., 2015).

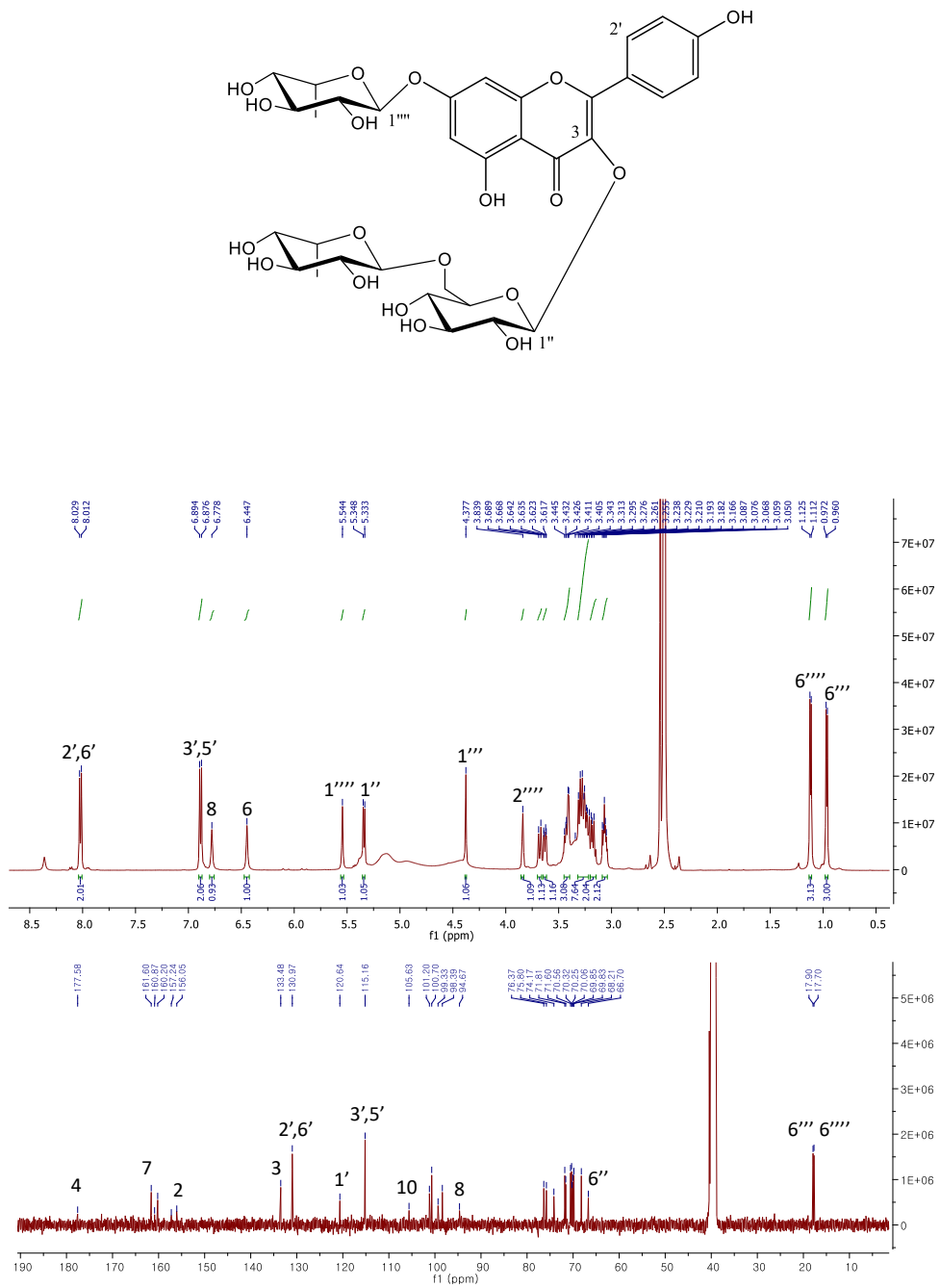

Figure 13. ^{1}H and ^{13}C NMR spectra (DMSO-d_6, 500/125 MHz) of compound **3**

3.3.4. Compound **4**

Compound **4**, an amorphous powder with $[\alpha]_D^{25}$ 50.6 (*c* 0.5, MeOH) gave a molecular formula of $C_{27}H_{30}O_{15}$ from the HRESIMS ion peak at *m*/*z* 593.1502 $[M - H]^-$ (calcd for $C_{27}H_{29}O_{15}$, 593.1506). All NMR data of compound **4** showed similar chemical shifts with compound **3** (Figure 14). The difference was the absence of rhamnose unit at C-6 of glucose, which was suggested by a upfield chemical shift of C-6 of glucose (δ_C 60.8; +5.9 ppm) compared to that of compound **3** (δ_C 66.7). The anomeric proton signal at δ_H 5.54 (1H, s) and δ_H 5.47 (1H, d, *J* = 7.3 Hz) suggested the existence of rhamnose and glucose, respectively. With above mentioned spectroscopic data, compound **4** was determined as kaempferol-3-*O*-*β*-D-glucopyranosyl-7-*O*-*α*-L-rhamnoside (Lee et al., 2017).

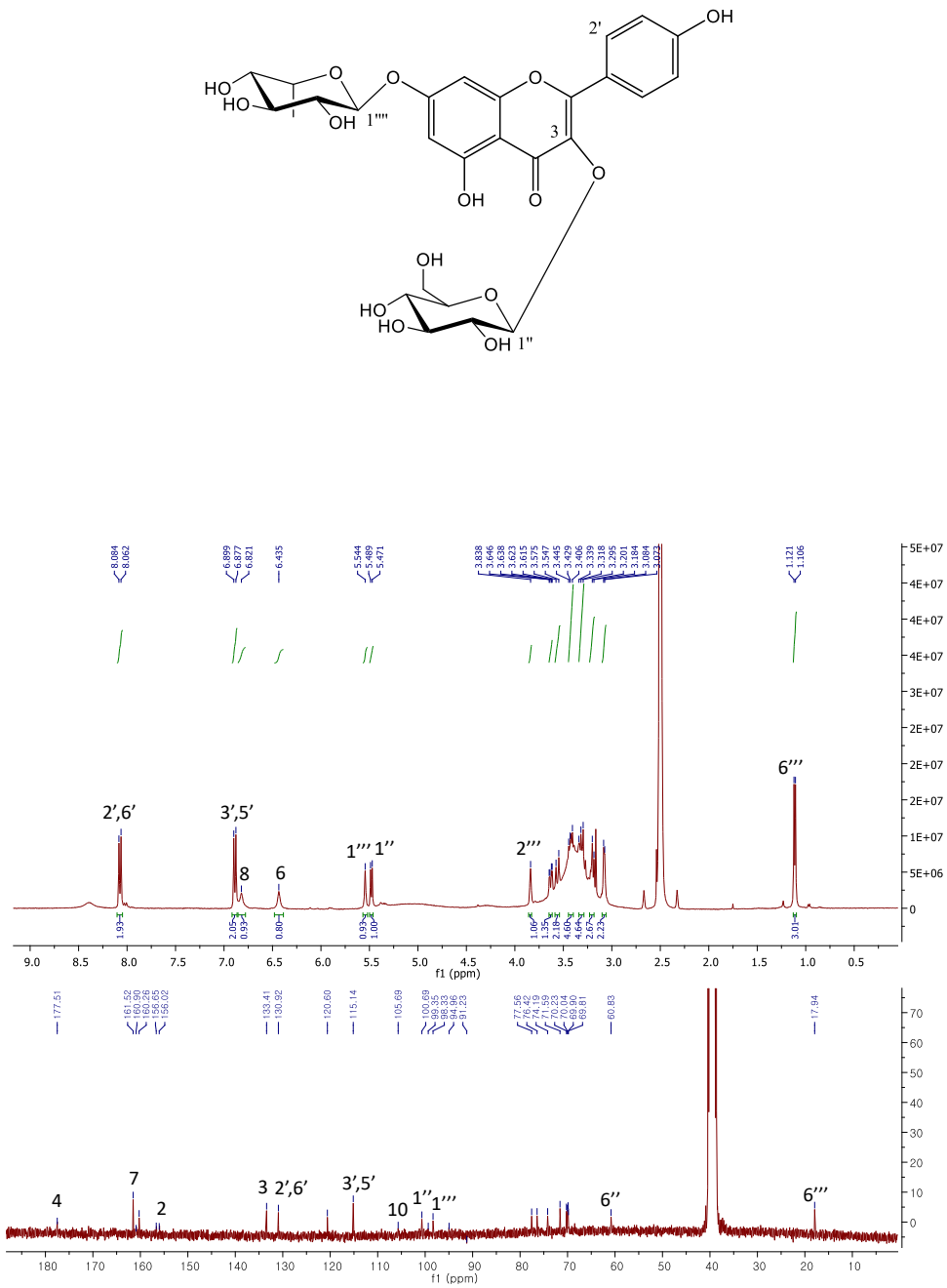

Figure 14. ^{1}H and ^{13}C NMR spectra (DMSO-d_6, 400/100 MHz) of compound **4**

3.3.5. Compound **5**

Compound **5** was obtained as an amorphous powder with $[\alpha]_D^{25}$ 60.8 (*c* 0.2, MeOH). The HRESIMS of this compound revealed an ion peak at *m*/*z* 431.0985 [M – H]$^-$ (calcd for $C_{21}H_{19}O_{10}$, 431.0978). It suggested a molecular formula $C_{21}H_{20}O_{10}$ and indicated the presence of twelve IHD. The ^{1}H NMR spectrum presented a singlet olefinic proton at δ_H 6.87 (1H, s, H-3). An A_2B_2 aromatic spin system at δ_H 7.95 (2H, d, *J* = 8.0 Hz, H-2', 6') and 6.94 (2H, d, *J* = 8.0 Hz, H-3', 5') were observed with corresponding carbons at δ_C 128.6 and 116.0, respectively (Figure 15). The H-6 (δ_H 6.44, br s) was meta coupled with H-8 (δ_H 6.82, br s). The anomeric proton of glucose was observed at δ_H 5.06 (1H, d, *J* = 7.3 Hz). The chemical shift of C-7 in aglycone (δ_C 162.9) in compound **5** was shifted upfield compared to that of apigenin (δ_C 165.0) suggesting the attachment of glucose at C-7 of aglycone (Xu et al., 2009). The above spectroscopic data revealed that compound **5** was apigenin-7-*O*-*β*-D-glucopyranoside (Lee et al., 2017).

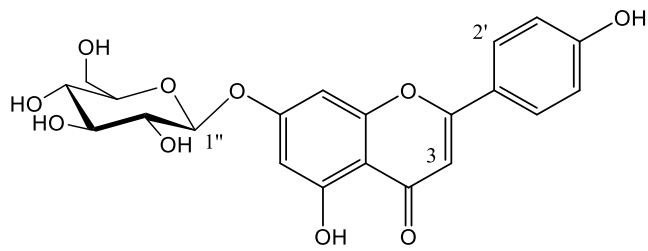

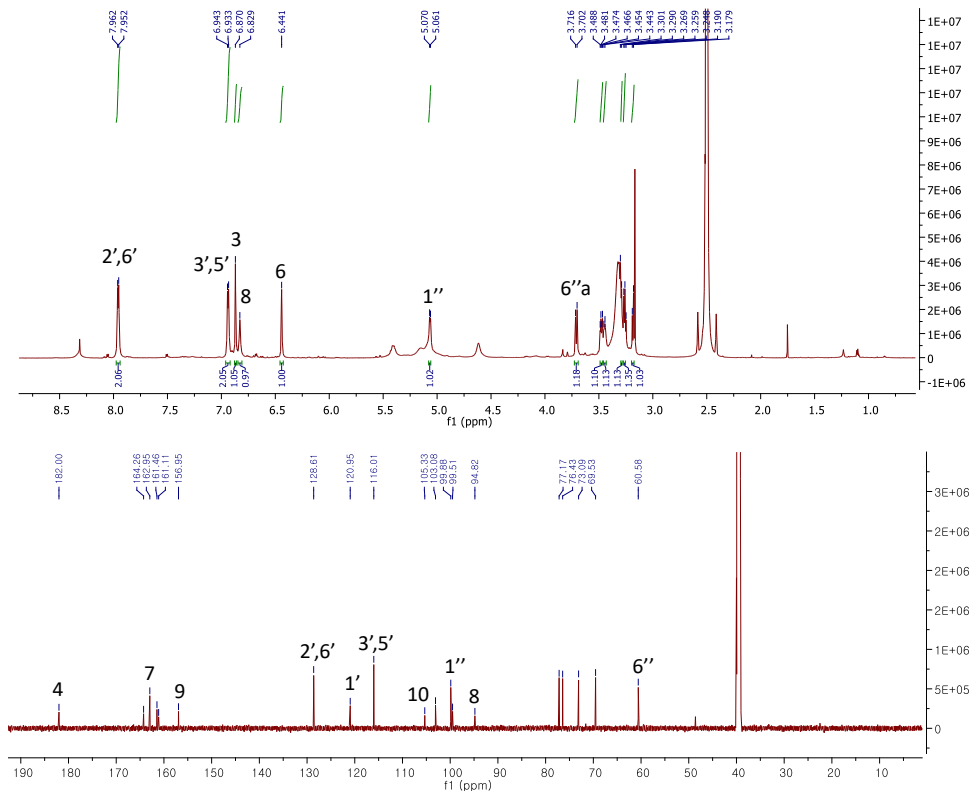

Figure 15. ^{1}H and ^{13}C NMR spectra (DMSO-d_6, 800/200 MHz) of compound **5**

3.3.6. Compound **6**

Compound **6**, an amorphous powder with $[\alpha]_D^{25}$ -64.2 (*c* 0.3, MeOH), was determined to have a molecular formula of $C_{21}H_{20}O_{11}$, as suggested by the HRESIMS peaks at *m/z* 447.0932 $[M - H]^-$ (calcd for $C_{21}H_{19}O_{11}$, 447.0927). According to NMR experiment, compound **6** clearly demonstrated a similar skeleton with compound **5** except the glycosidic position. In compound **6**, the olefinic proton of H-3 was not shown, indicating that C-3 was substituted by glucose (Figure 16). Thus, compound **6** was characterized as astragalin (Kang et al., 2012).

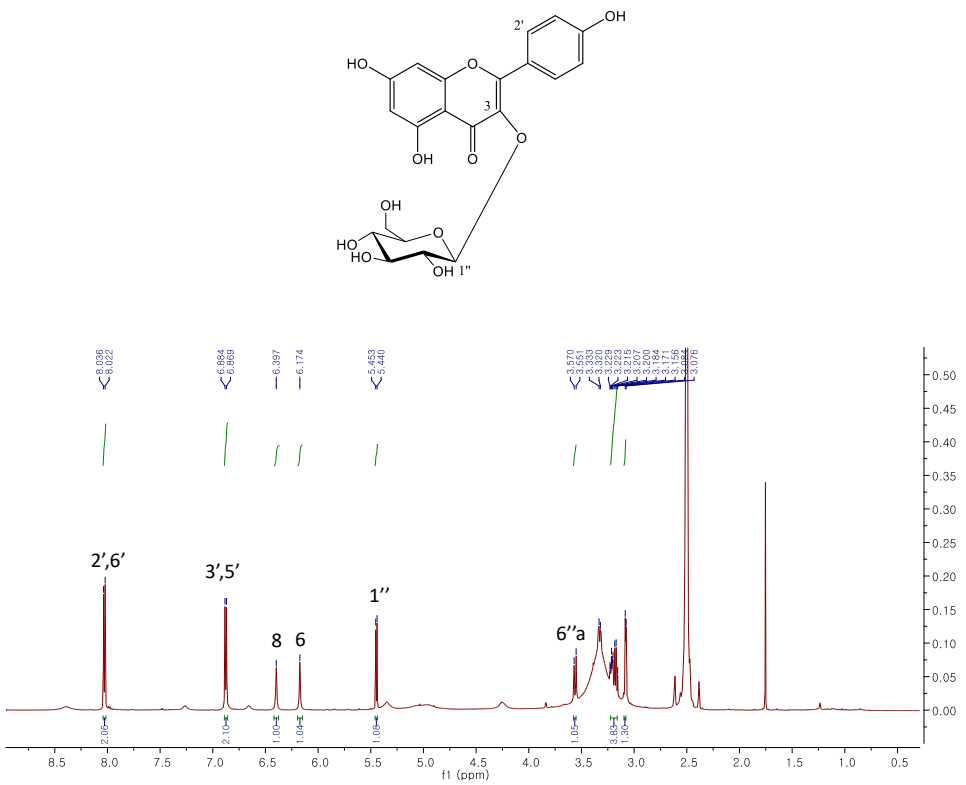

Figure 16. ^{1}H NMR spectrum (DMSO-d_6, 600 MHz) of compound **6**

3.3.7. Compound **7**

Compound **7** was isolated as an amorphous powder with $[\alpha]_D^{25}$ 56.7 (*c* 0.3, MeOH) and its molecular formula of $C_{27}H_{30}O_{15}$ was analyzed based on the HRESIMS (*m*/*z* 593.1511 $[M - H]^-$, calcd for $C_{27}H_{29}O_{15}$, 593.1506). The IDH for this compound was recorded as thirteen. Different to compound **6**, one rhmanose was attached to H-6 of glucose. Two anomeric protons were shown at δ_H 5.28 (1H, d, J = 7.7 Hz) and δ_H 4.37 (1H, s) with corresponding carbon signals at δ_C 101.3 and 100.8, respectively (Figure 17). The methyl group of rhamnose was indicated based on proton signal at δ_H 0.98 (3H, d, J = 6.0 Hz). With above mentioned spectroscopic data, compound **7** was determined as kaempferol-3-*O*-rutinoside (Xu et al., 2012).

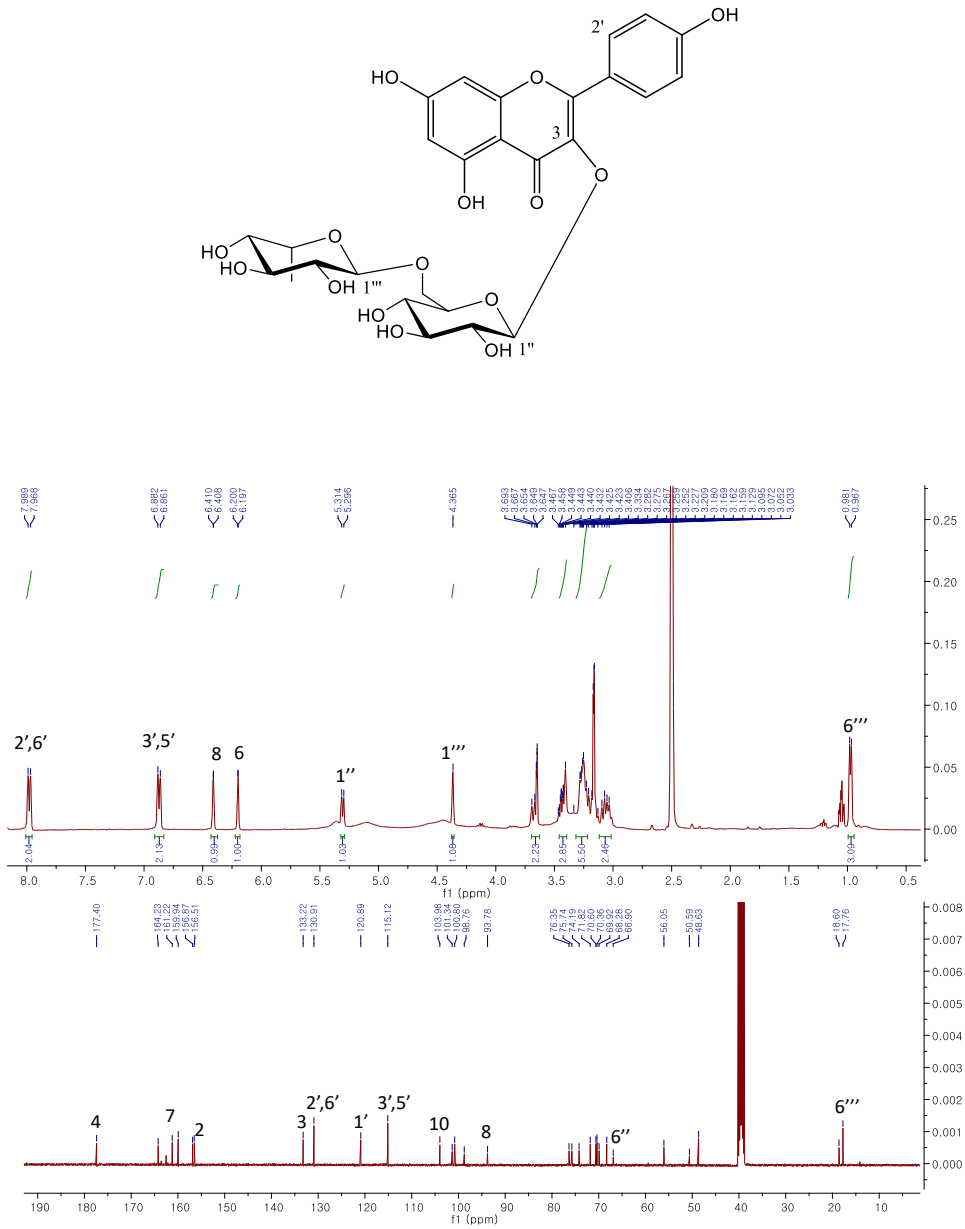

Figure 17. ^{1}H and ^{13}C NMR spectra (DMSO-d_6, 400/100 MHz) of compound **7**

3.3.8. Compound **8**

Compound **8**, a reddish gum with $[\alpha]_D^{25}$ –60.3 (*c* 0.5, MeOH), possessed the molecular formula $C_{32}H_{38}O_{19}$ based on a HRESIMS peak at *m*/*z* 725.1961 $[M - H]^-$ (calcd for $C_{32}H_{37}O_{19}$, 725.1935), which corresponds to 14 degrees of hydrogen deficiency. The IR spectrum of **8** showed characteristic peaks of hydroxyl (3345 cm^{-1}) and *α*,*β*-unsaturated carbonyl groups (1657 cm^{-1}). The ^1H and ^{13}C NMR data for the aglycone of **8** revealed signals identical to those of **1** (Figure 18). Considering the proton NMR signals of the sugar moieties, three anomeric protons were observed at δ_H 5.74 (d, *J* = 2.1 Hz), 5.59 (br s) and 4.48 (d, *J* = 7.7 Hz). The anomeric proton signal at δ_H 5.74 (d, *J* = 2.1 Hz) was assigned to an apiose moiety by a series of pentose proton signals containing two methylene groups based on the COSY spectrum. The rhamnose anomeric proton at δ_H 5.59 (br s) and the glucose anomeric proton at δ_H 4.48 (d, *J* = 7.7 Hz) revealed *α* and *β* configurations, respectively. The identities of these fragments were supported by the positive mass fragment ions at 595 $[M - 132 \text{ (apiofuranosyl)} + H]^+$, 565 $[M - 162 \text{ (glucopyranosyl)} + H]^+$, 433 $[M - 162 \text{ (glucopyranosyl)} - 132 \text{ (apiofuranosyl)} + H]^+$. All the NMR data of compound **8** were similar to those of kaempferol 3-*O*-*β*-D-apiofuranosyl-7-*O*-*α*-L-rhamnopyranoside, which has been isolated from *Lotus edulis* (Spanou et al., 2008), except for the attachment of the glucopyranosyl unit to C-3''' of the rhamnose in compound **8**, based on the HMBC correlation from H-3''' of rhamnose (δ_H 3.70) to C-1'''' of glucose (δ_C 104.6) (Figures 19-21). These results were further confirmed by the deshielding of the signal corresponding to C-3''' of rhamnose, which was shifted downfield by approximately 10 ppm compared to that of compound **1**. Therefore,

compound **8** was determined to be kaempferol 3-*O*-*β*-D-apiofuranosyl-7-*O*-*β*-D-glucopyranosyl-(1→3)-*α*-L-rhamnopyranoside.

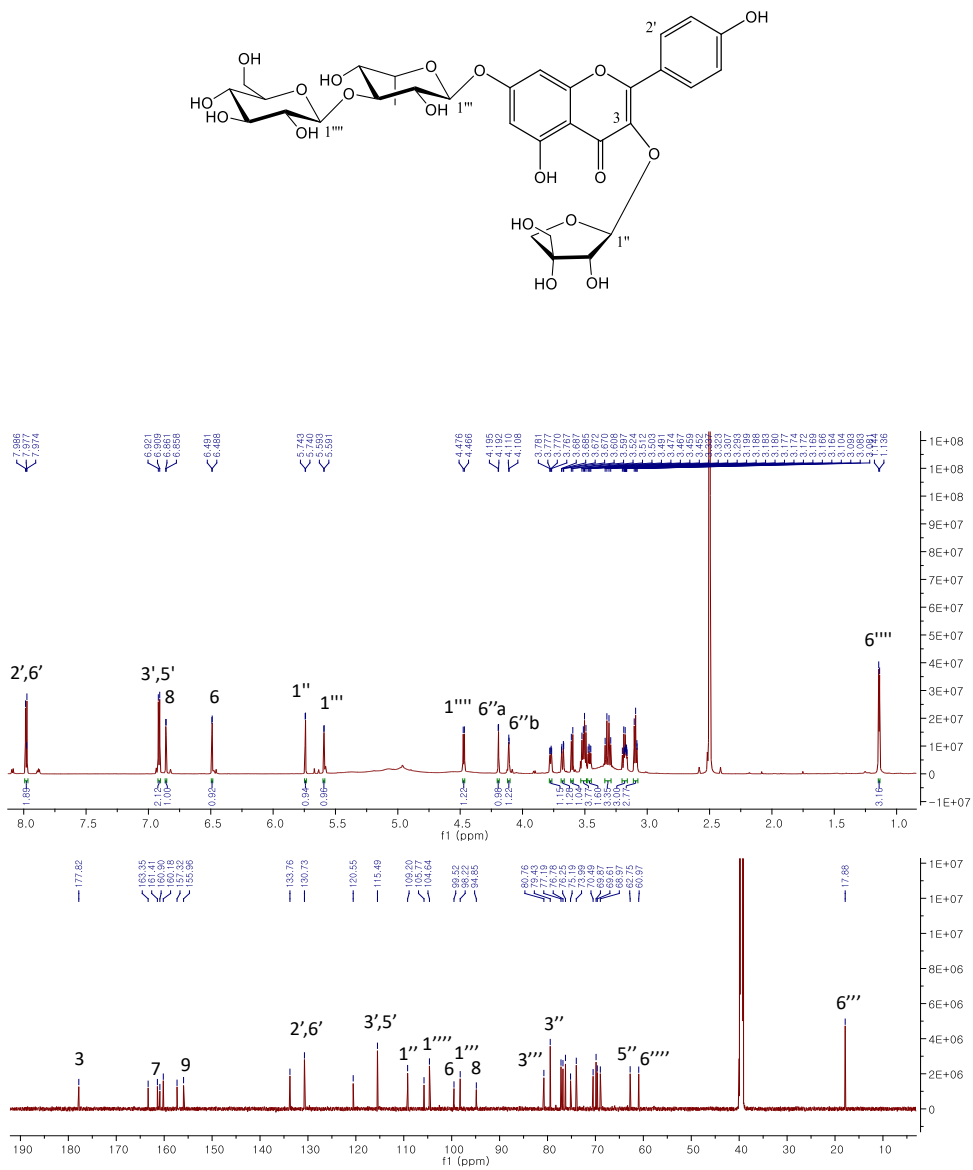

Figure 18. ^{1}H and ^{13}C NMR spectra (DMSO-d_6, 800/200 MHz) of compound **8**

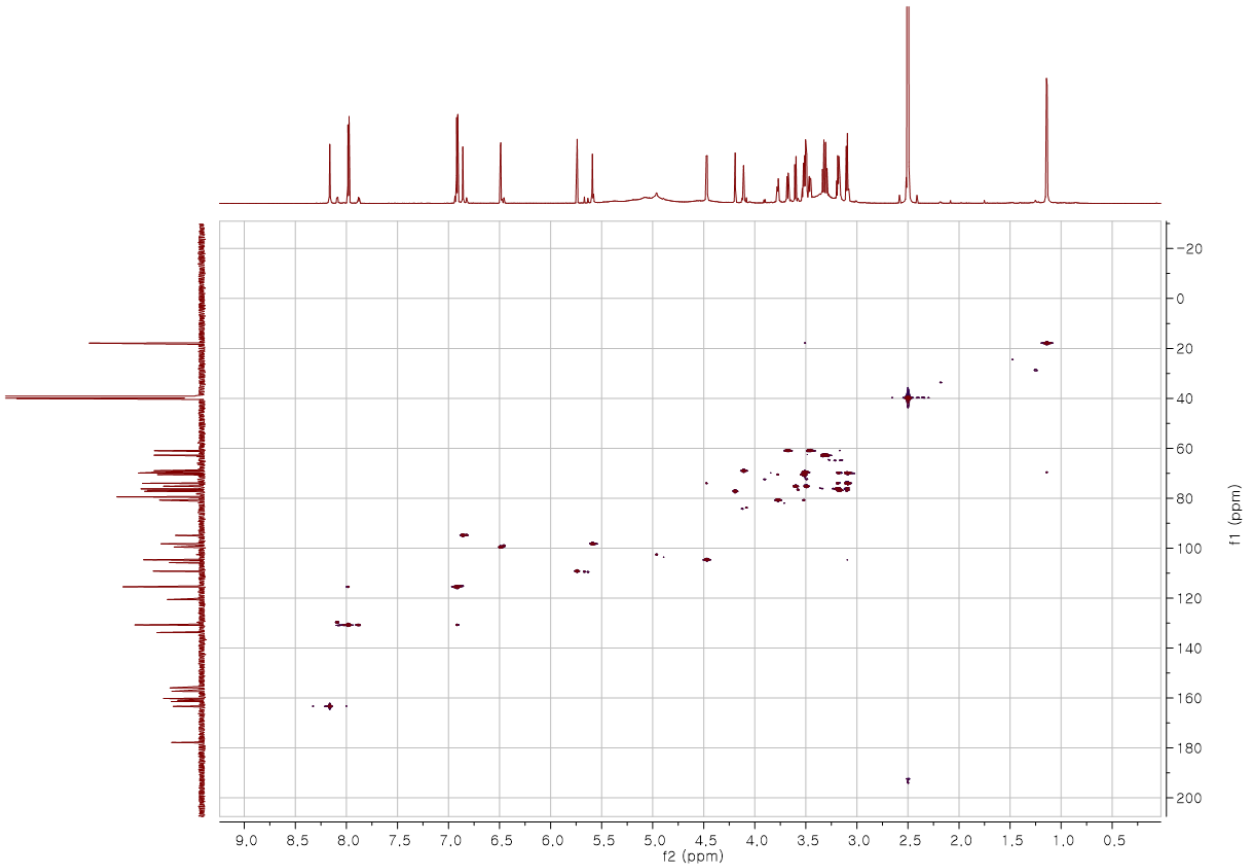

Figure 19. HSQC spectrum (DMSO-d_6, 800 MHz) of compound **8**

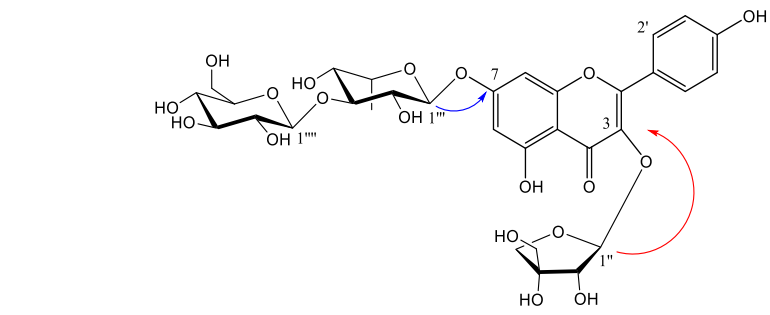

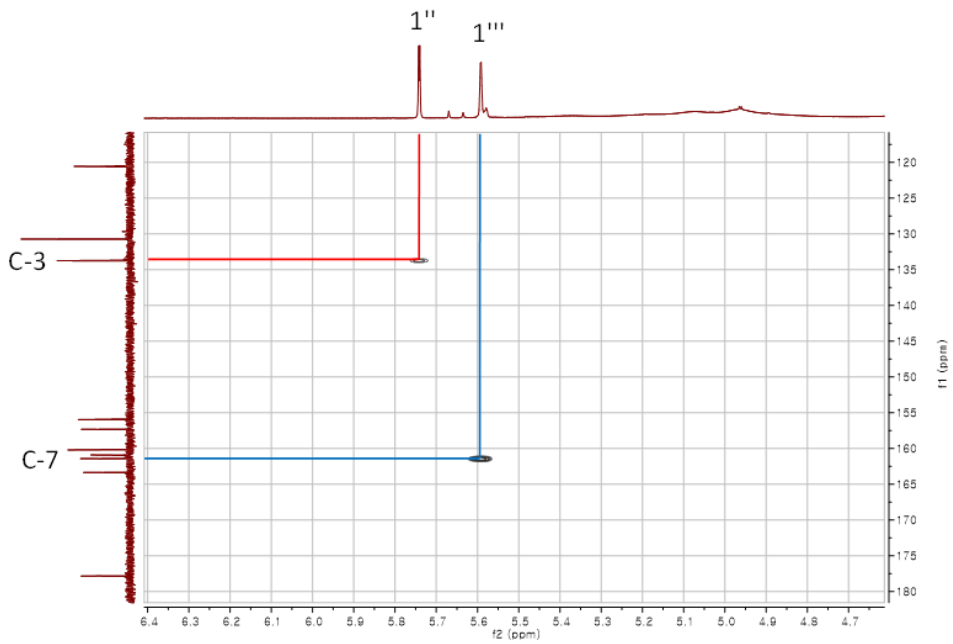

Figure 20. Key HMBC correlations (DMSO-d_6, 800 MHz) of compound **8**

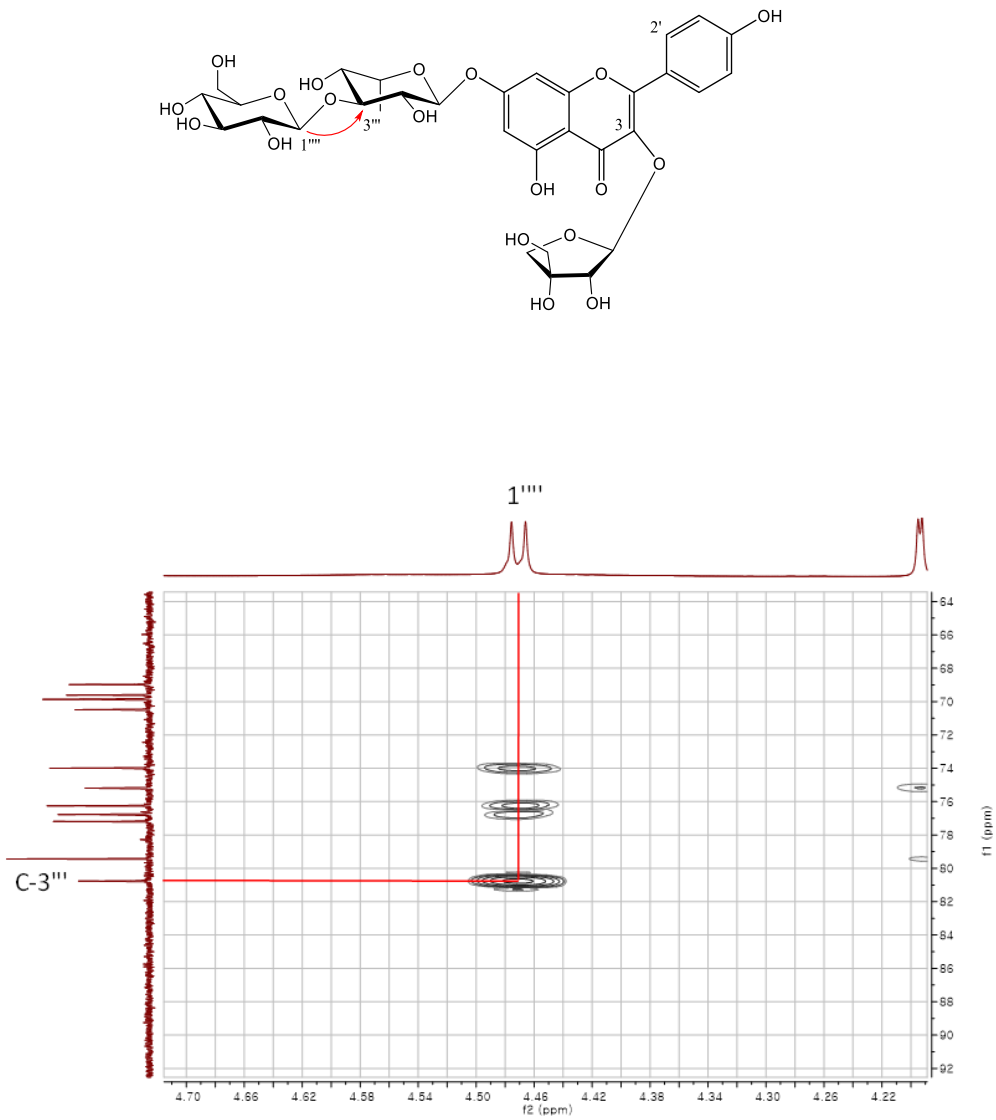

Figure 21. Key HMBC correlations (DMSO-d_6, 800 MHz) of compound **8**

3.3.9. Compound **9**

Compound **9** was isolated as a yellowish powder with a negative optical rotation ($[\alpha]_D^{25}$−115.0 (*c* 0.5, MeOH)). Its molecular formula was assigned as $C_{37}H_{38}O_{19}$ based on the $[M - H]^-$ ion peak at *m*/*z* 785.1964 (calcd for $C_{37}H_{37}O_{19}$, 785.1935) in the HRESIMS. Its IR spectrum showed bands indicative of a hydroxyl group (3304 cm^{-1}) and an *α*,*β*-unsaturated carbonyl group (1656 cm^{-1}). The NMR spectra of compound **9** were similar to those of compound **1** except for the additional hydroxyl group on the B ring, indicating compound **9** possessed a quercetin aglycone instead of a kaempferol (Figure 22). The ^1H and ^{13}C NMR spectra of compound **9** displayed the presence of an ABX aromatic spin system at δ_H 7.58 (1H, d, *J* = 2.1 Hz, H-2'), 6.93 (1H, d, *J* = 8.4 Hz, H-5') and 7.56 (1H, dd, *J* = 8.4, 2.1 Hz, H-6') with the corresponding carbons at δ_C 116.3 (C-2'), 115.2 (C-5') and 121.7 (C-6'), respectively, for the B ring of the flavonoid. Therefore, compound **9** was characterized as quercetin 3-*O*-(6-*O*-*E*-feruloyl)-*β*-D-glucopyranosyl-7-*O*-*α*-L-rhamnopyranoside.

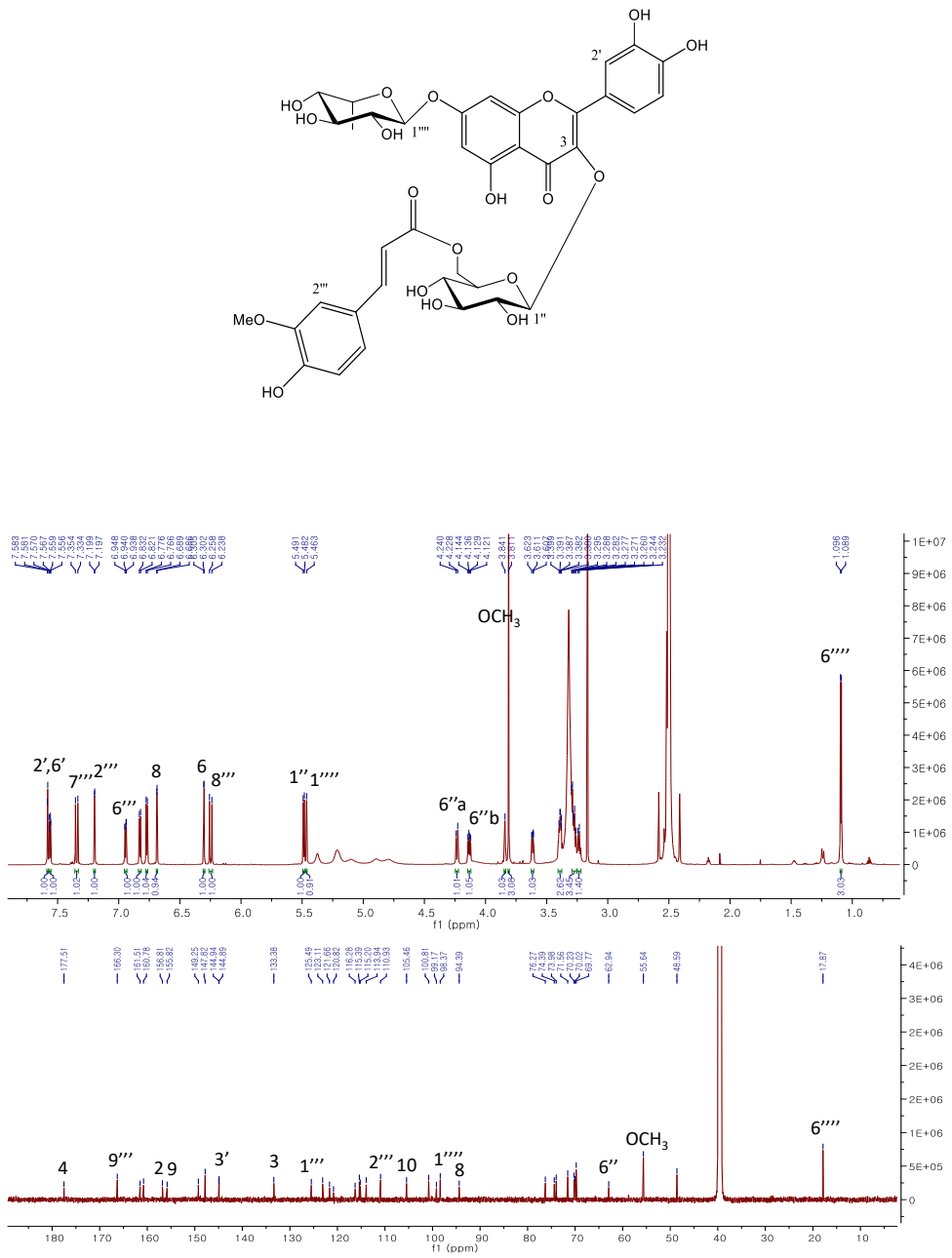

Figure 22. ^{1}H and ^{13}C NMR spectra (DMSO-d_6, 800/200 MHz) of compound **9**

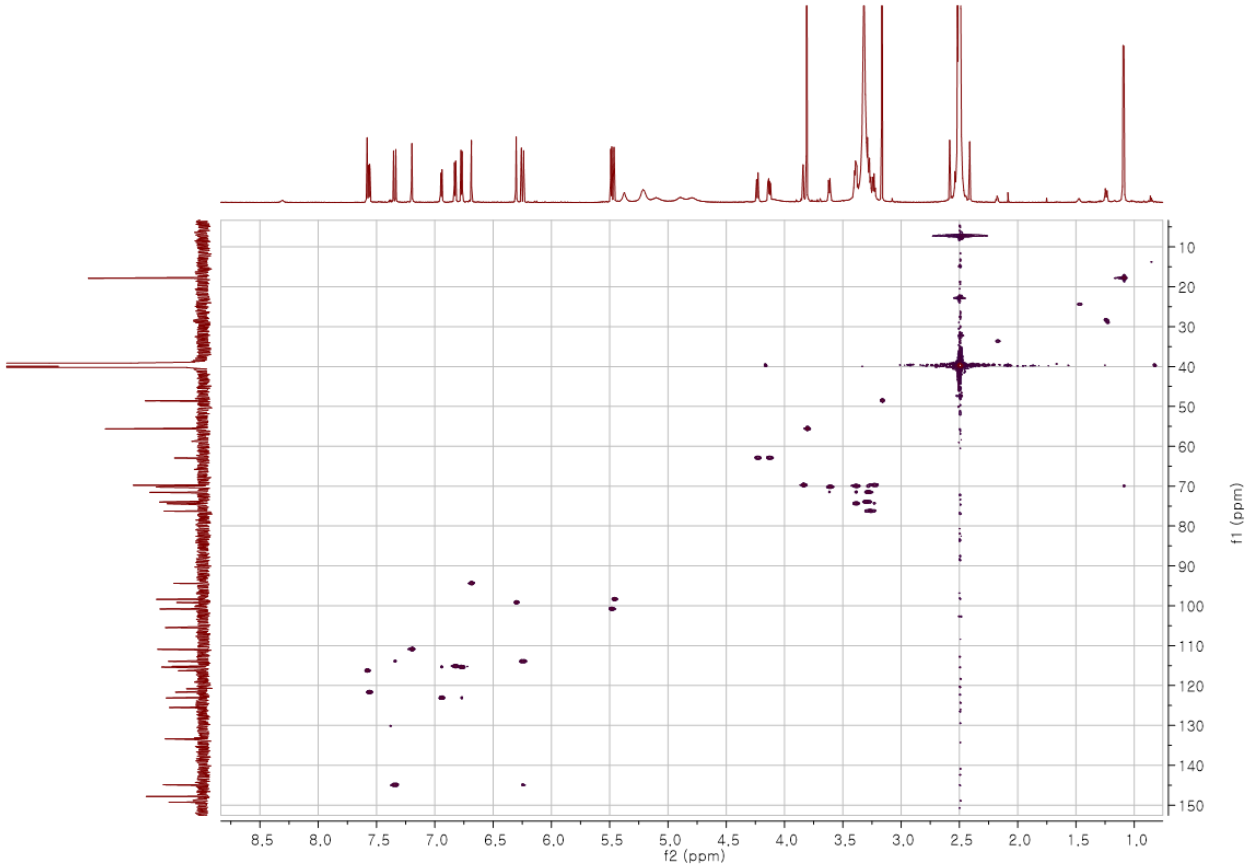

Figure 23. HSQC spectrum (DMSO-d_6, 800 MHz) of compound **9**

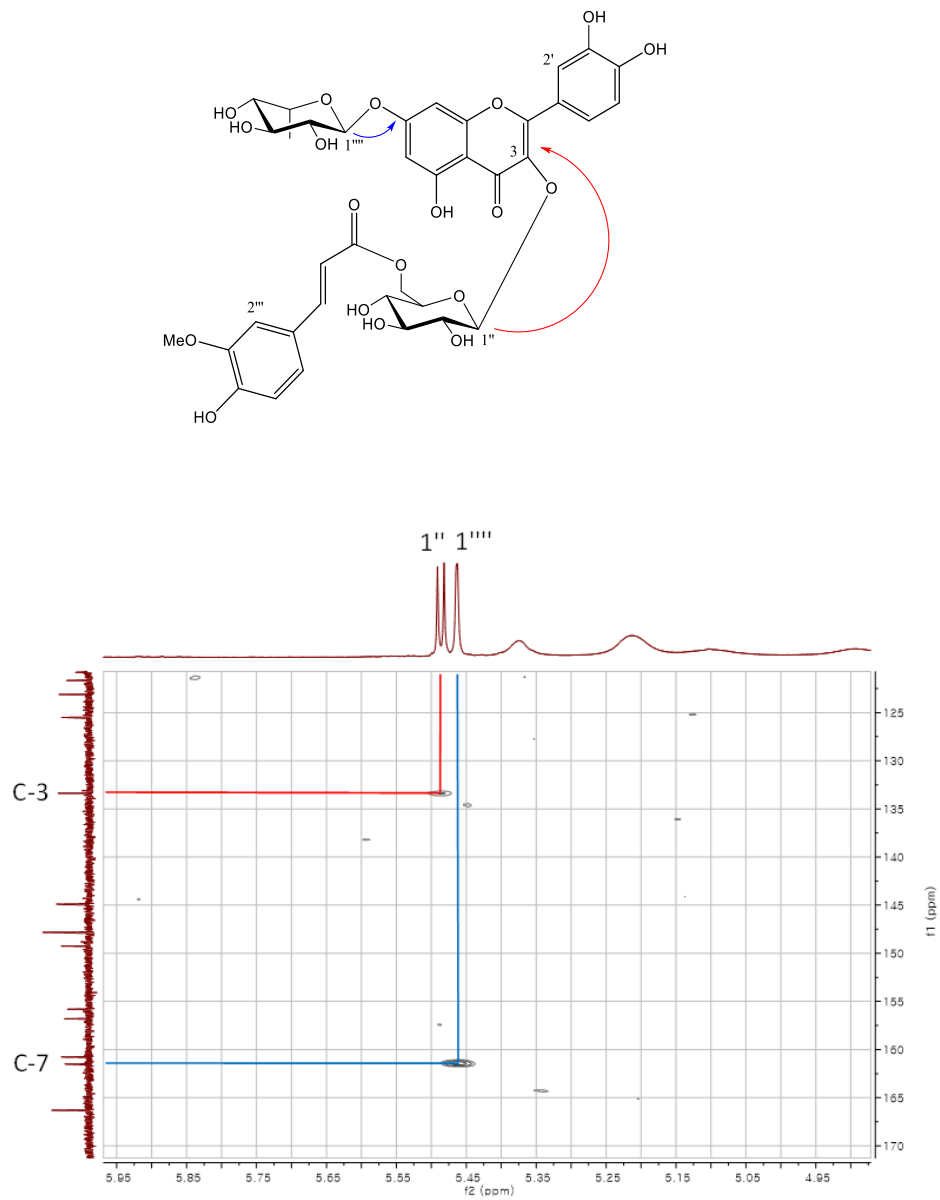

Figure 24. Key HMBC correlations (DMSO-d_6, 800 MHz) of compound **9**

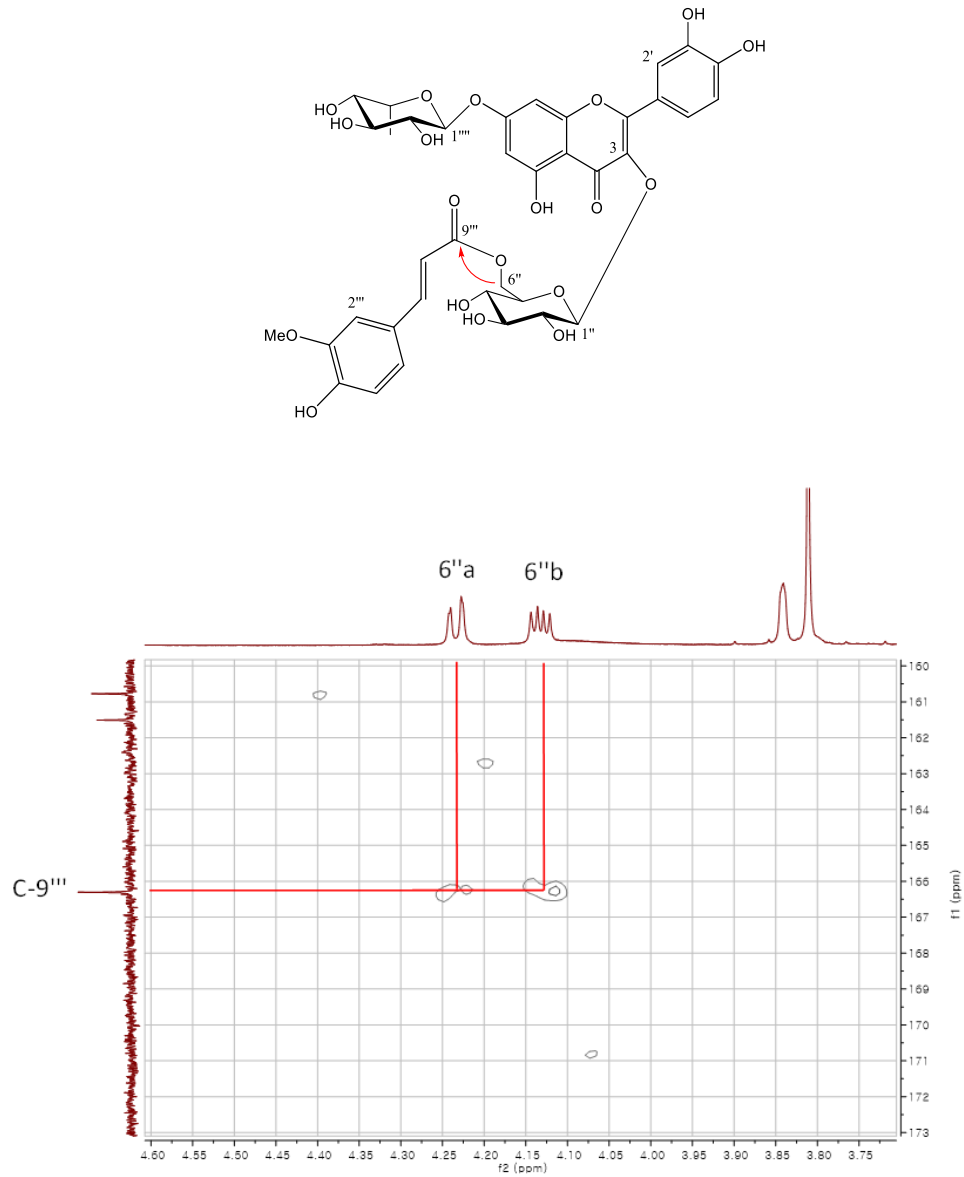

Figure 25. Key HMBC correlations (DMSO-d_6, 800 MHz) of compound **9**

3.3.10. Compound **10**

Compound **10**, an amorphous powder with $[\alpha]_D^{25}$ -100.5 (*c* 0.3, MeOH), was determined to have a molecular formula of $C_{36}H_{36}O_{18}$, as suggested by the HRESIMS peaks at *m/z* 755.1830 $[M - H]^-$ (calcd for $C_{36}H_{35}O_{18}$, 755.1823). The calculation of IHD for this compound was recorded as nineteen indices. The characteristic difference is the replacement of the ferulic acid group in **9** [(δ_H 7.20, d, *J* = 1.2 Hz), (δ_H 6.94, dd, *J* = 8.2, 1.8 Hz), (δ_H 6.77, d, *J* = 8.1 Hz)] by the coumaric acid group in **10** [(δ_H 7.38, 2H, d, *J* = 8.6 Hz), (δ_H 6.77, 2H, d, *J* = 8.5 Hz)] (Figure 26). Two olefinic protons with a large coupling constant at δ_H 7.33 (1H, d, *J* = 15.5 Hz) and 6.11 (1H, d, *J* = 15.5 Hz) indicated a ferulic acid moiety in a trans-configuration. With above observed spectroscopic data, compound **10** was determined to be quercetin 3-*O*-(6-*O*-*E*-coumaroyl)-*β*-D-glucopyranosyl-7-*O*-*α*-L-rhamnopyranoside (Gohar et al., 2000).

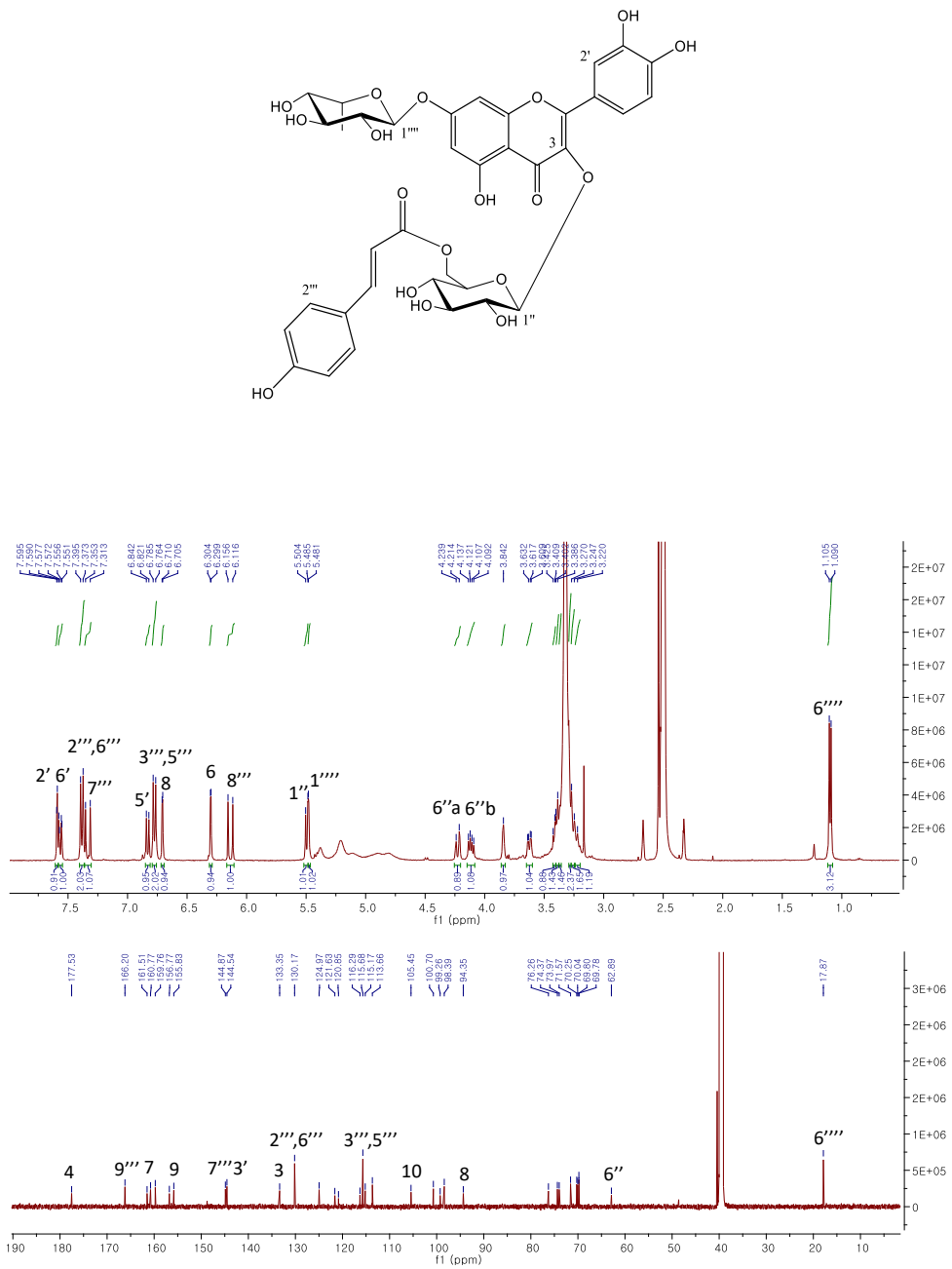

Figure 26. ^{1}H and ^{13}C NMR spectra (DMSO-d_6, 600/150 MHz) of compound **10**

3.3.11. Compound **11**

Compound **11**, a yellowish gum with $[\alpha]_D^{25}$ –78.5 (*c* 0.5, MeOH), possessed a molecular formula of $C_{49}H_{58}O_{27}$ based on its HRESIMS peaks at *m/z* 1077.3108 [M – H]$^-$ (calcd for $C_{49}H_{57}O_{27}$, 1077.3093). The IR spectrum of compound **11** indicated the presence of hydroxyl (3304 cm^{-1}) and *α*,*β*-unsaturated carbonyl groups (1656 cm^{-1}). The spectroscopic data of **11** suggested that the structure of **11** was similar to that of **1**. The difference was the attachment of a *α*-rhamnopyranosyl-(1→6)-*O*-*β*-D-glucopyranosyl fragment to C-3'''' of the rhamnose (Rha I) (δ_C 81.2). The glucopyranosyl unit (Glc II) was suggested to attach to C-3'''' of the rhamnose (Rha I) based on the HMBC correlation from H-1'''' (δ_H 4.48) to C-3'''' (δ_C 81.2). The HMBC correlation from H-1''''' (δ_H 4.38) to C-6'''' (δ_C 66.7) suggested the linkage of the rhamnopyranosyl fragment (Rha II) to the glucopyranosyl (Glc II) (Figures 27-30). Therefore, compound **11** was determined to be kaempferol 3-*O*-(6-*O*-*E*-feruloyl)-*β*-D-glucopyranosyl-7-*O*-*α*-L-rhamnopyranosyl-(1→6)-*β*-D-glucopyranosyl-(1→3)-*α*-L-rhamnopyranoside.

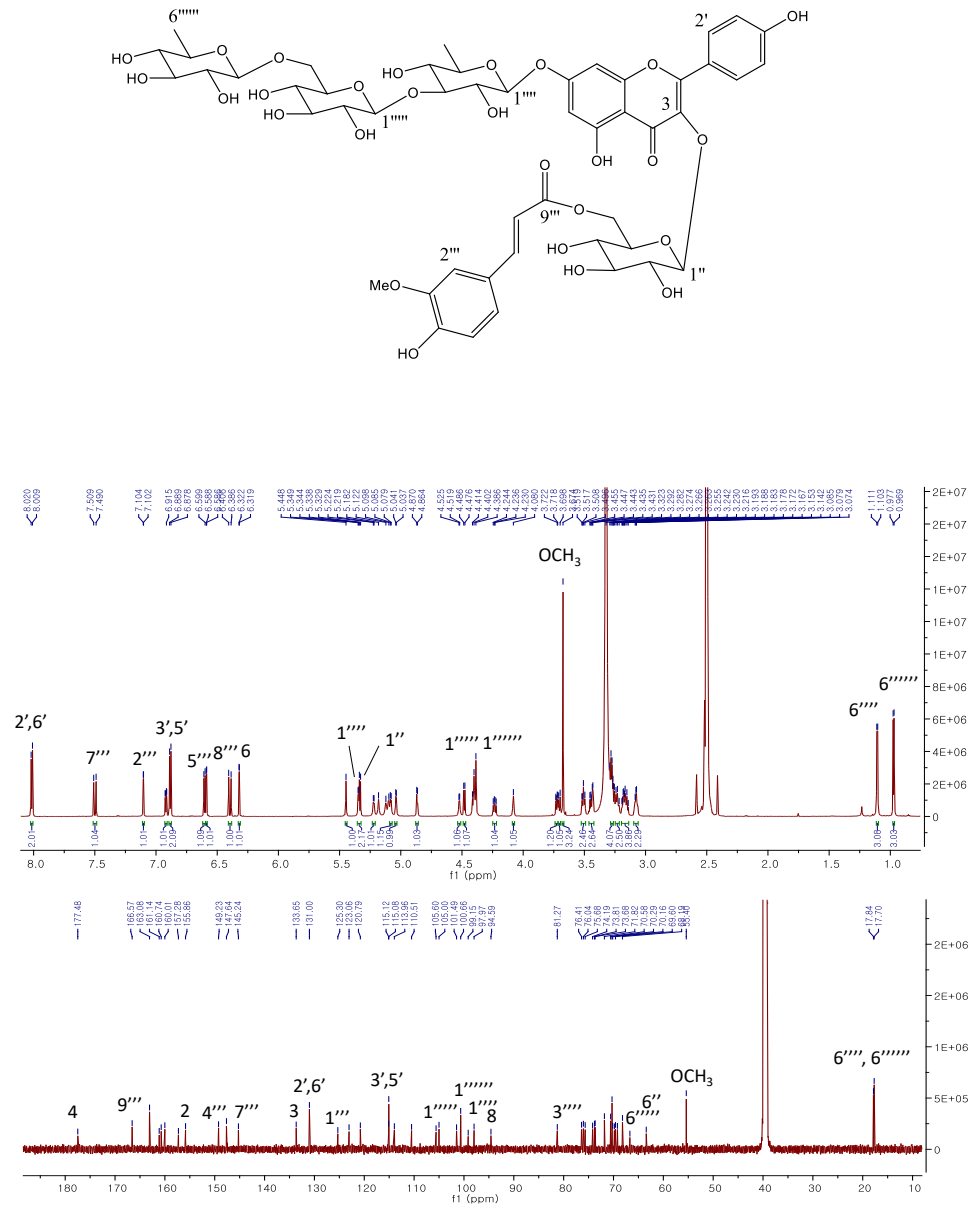

Figure 27. ^{1}H and ^{13}C NMR spectra (DMSO-d_6, 800/200 MHz) of compound **11**

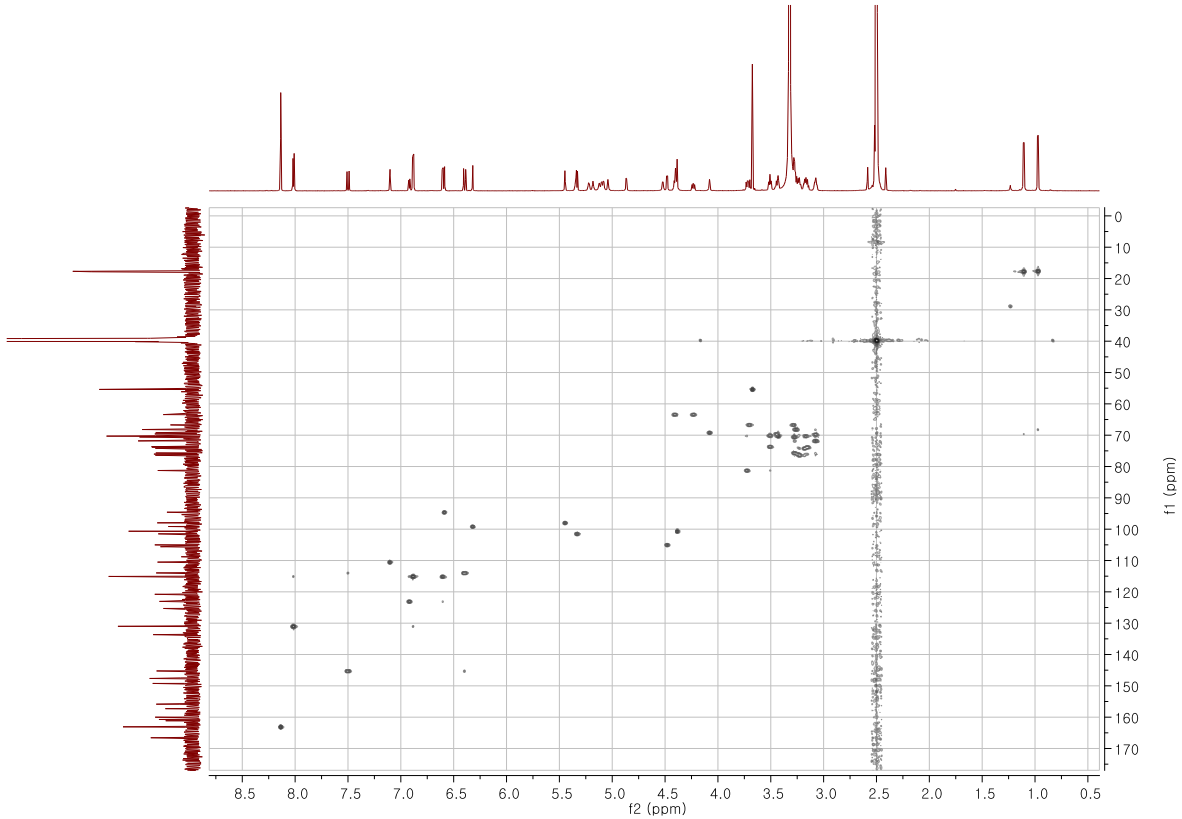

Figure 28. HSQC spectrum (DMSO-d_6, 800 MHz) of compound **11**

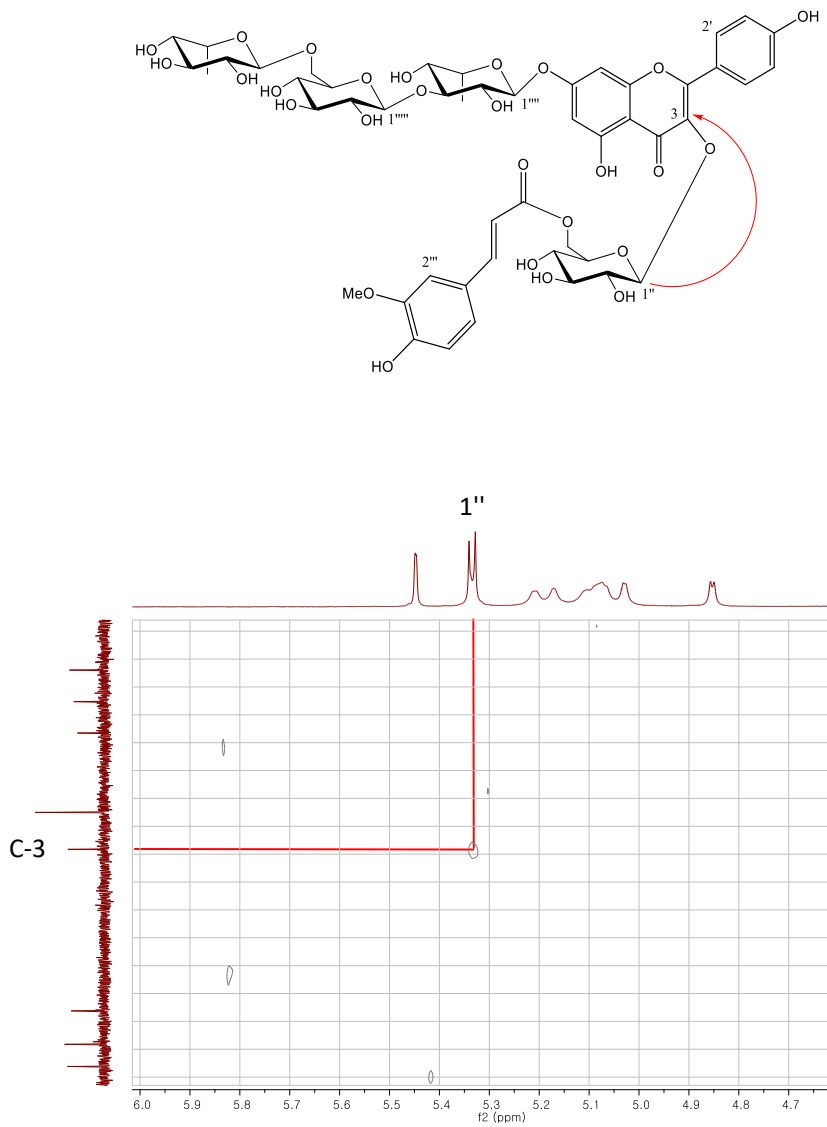

Figure 29. Key HMBC correlations (DMSO-d_6, 800 MHz) of compound **11**

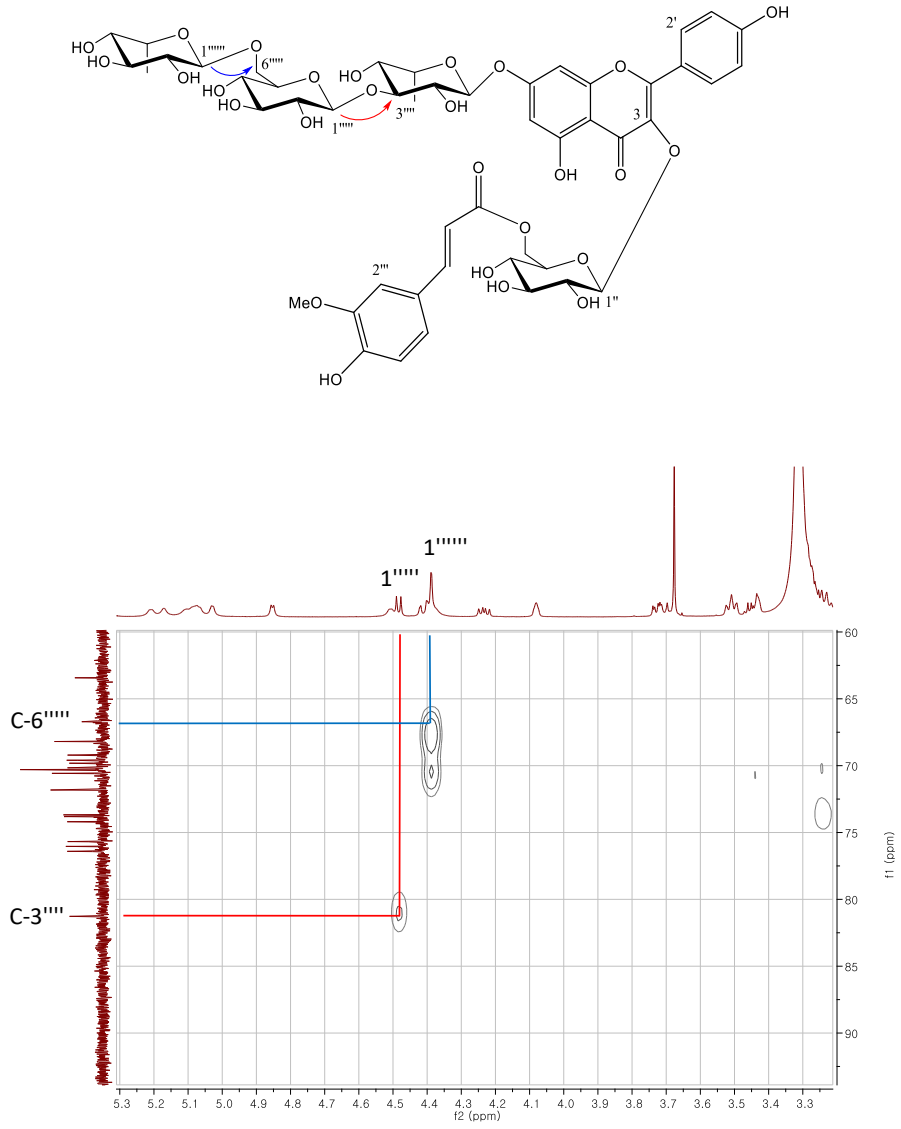

Figure 30. Key HMBC correlations (DMSO-d_6, 800 MHz) of compound **11**

3.3.12. Compound **12**

Compound **12** was obtained as a yellowish powder with a negative optical rotation ($[\alpha]_D^{25}$ −64.9 (*c* 0.5, MeOH)). The molecular formula $C_{43}H_{48}O_{23}$ was suggested by the HRESIMS peak at *m*/*z* 931.2523 $[M - H]^-$ (calcd for $C_{43}H_{47}O_{23}$, 931.2514). The IR spectrum of compound **12** indicated the presence of hydroxyl (3339 cm^{-1}) and *α*,*β*-unsaturated carbonyl groups (1656 cm^{-1}). The NMR spectra of compound **12** were similar to those of compound **1** except for a glucose attached to C-3"" of the rhamnose (Figures 31 and 33). The glucopyranosyl unit (Glc II) was found to be linked to C-3"" of the rhamnose based on the HMBC correlation from H-1"""" (δ_H 4.48) to C-3"" (δ_C 80.7), and this was confirmed by the deshielding of the signal corresponding to C-3"" of the rhamnose, which was shifted downfield by approximately 10 ppm compared to that of compound **1** (Figure 32). Therefore, compound **12** was characterized as kaempferol 3-*O*-(6-*O*-*E*-feruloyl)-*β*-D-glucopyranosyl-7-*O*-*β*-D-glucopyranosyl-(1→3)-*α*-L-rhamnopyranoside.

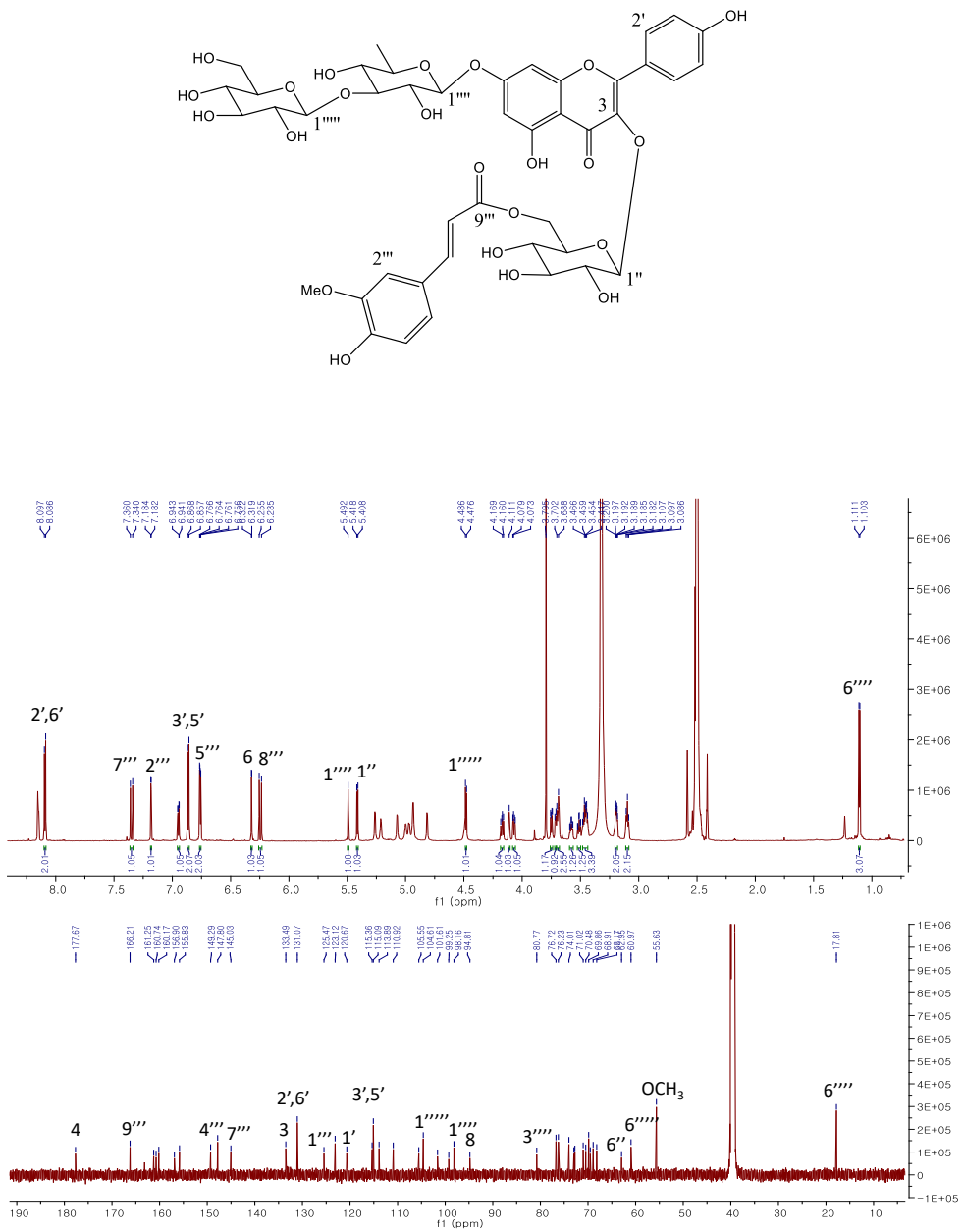

Figure 31. ^{1}H and ^{13}C NMR spectra (DMSO-d_6, 800/200 MHz) of compound **12**

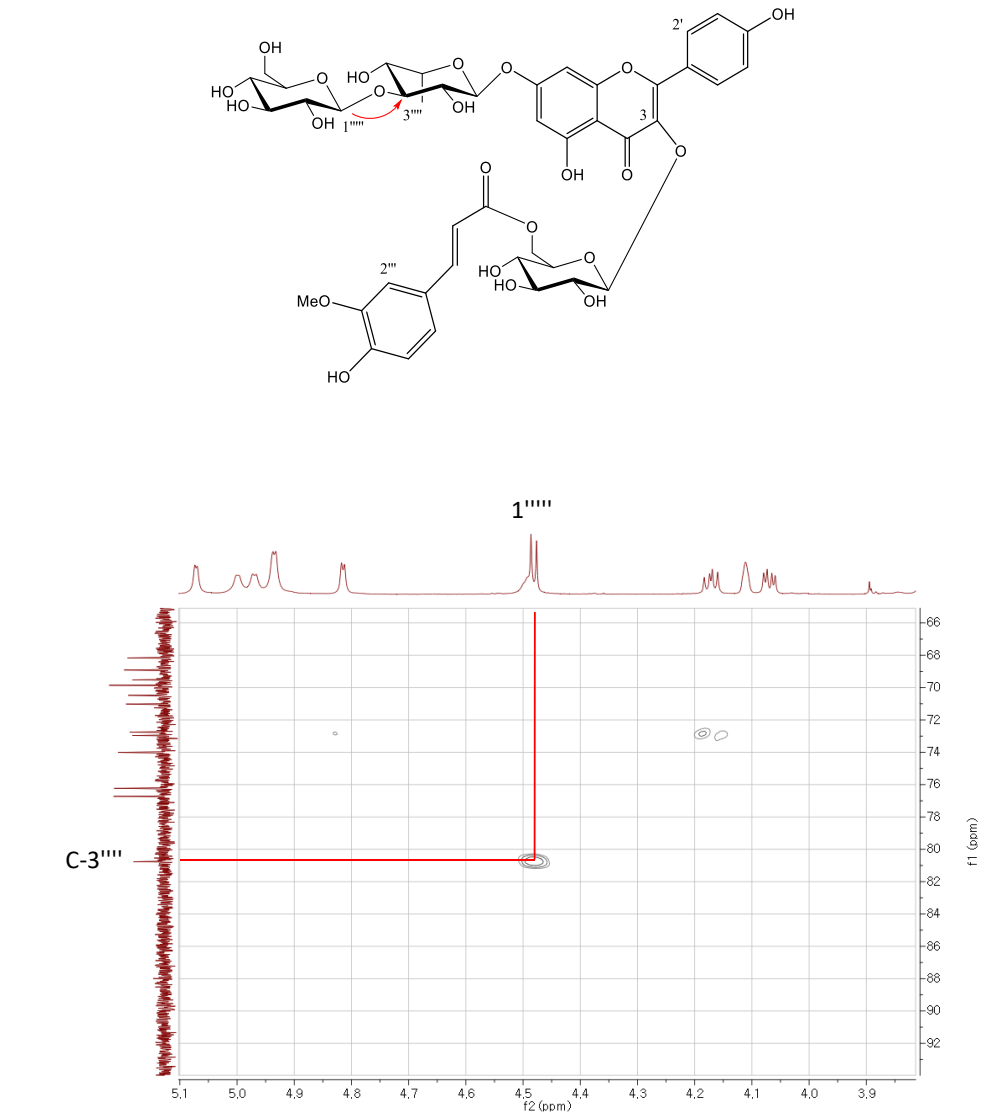

Figure 32. Key HMBC correlations (DMSO-d_6, 800 MHz) of compound **12**

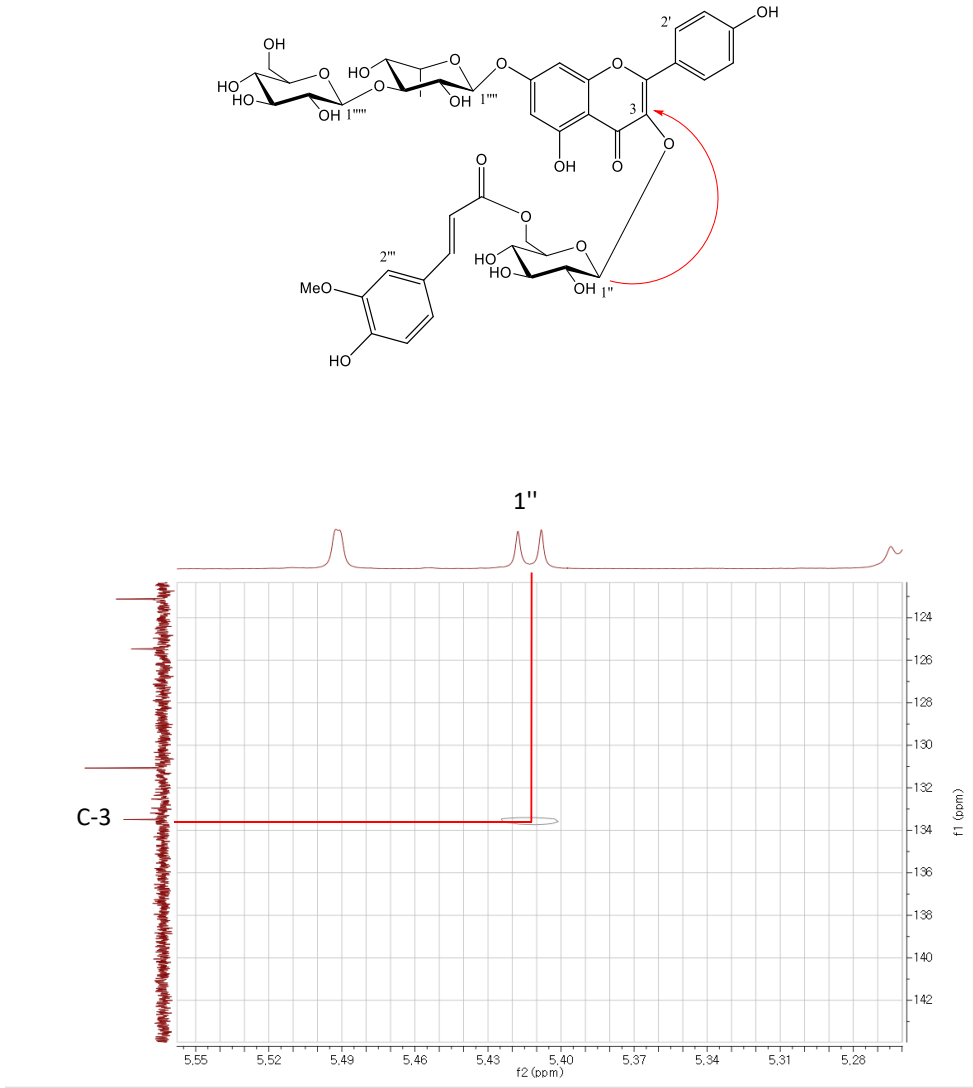

Figure 33. Key HMBC correlations (DMSO-d_6, 800 MHz) of compound **12**

3.3.13. Compound **13**

Compound **13** was isolated as an amorphous powder with a negative optical rotation $[\alpha]_D^{25}$ −39.8 (*c* 0.5, MeOH). Its molecular formula was assigned as $C_{39}H_{46}O_{20}$ based on the $[M - H]^-$ ion peak at *m*/*z* 833.2513 (calcd for $C_{39}H_{45}O_{20}$, 833.2510) in its HRESIMS. The IR spectrum showed the bands of a hydroxyl group (3424 cm^{-1}) and *α*,*β*-unsaturated carbonyl groups (1658 cm^{-1}). The ^1H NMR spectrum of **13** showed signals at δ_H 7.32 (2H, s), 7.14 (1H, s), 6.90 (1H, d, *J* = 2.0 Hz), 6.39 (1H, d, *J* = 2.0 Hz) and 3.87 (6H, s), indicating the presence of a tricin fragment with carbon signals at C-1' (δ_C 124.9), C-3' (δ_C 152.9) and C-5' (δ_C 152.9) (Figure 34). The other proton signals at δ_H 6.93 (1H, br s), 6.75 (1H, dd, *J* = 8.0, 1.6 Hz), 6.69 (1H, d, *J* = 8.1 Hz), 4.79 (1H, m), 4.37 (1H, m), 3.74 (3H, s), 3.70 (1H, m) and 3.49 (1H, m) were predicted to be from a guaiacylglyceryl moiety. Two methoxy groups on the B ring resonated at δ_H 3.87, and this was confirmed by the HMBC correlations from δ_H 3.87 to C-3' and 5' (δ_C 152.9). The guaiacylglyceryl moiety was confirmed to be attached to C-4' based on the HMBC correlation from H-8'' (δ_C 4.37) to C-4' (δ_C 139.7) (Figure 35). The HMBC correlation from the anomeric proton at δ_H 5.21 (1H, d, *J* = 7.7 Hz) to C-7 (δ_C 162.8) suggested a glucopyranosyl moiety was attached at C-7. The other anomeric proton of the rhamnose (δ_H 5.12) showed an HMBC correlation to C-4''' of the glucose (δ_C 76.4). The NMR spectra of compound **13** were similar to those of tricin 4'-*O*-(*threo*-*β*-guaiacylglyceryl)ether-7-*O*-*β*-glucopyranoside except for the attachment of the rhamnose to C-4''' of the glucose (Lee et al., 2015) (Figures 35-37). The relative configuration of compound **13** was determined based on the ROESY correlation between H-7'' (δ_H 4.79) and H-8'' (δ_H 4.37), which suggested H-7'' and H-8'' were on the same face of the compound

(Figures 38 and 39). To determine the absolute configuration of compound **13**, the ECD spectra for (7"*R*,8"*R*)-**13** and (7"*S*,8"*S*)-**13** were calculated using TDDFT at the B3LYP/def-SV(P) level. The conformational search of 7"*R*,8"*R*-**13** using the molecular mechanics force field (MMFF) was performed, and the five lowest energy conformers corresponded to 99% of the total Boltzmann distribution (Table 5). The calculated ECD spectrum of 7"*R*,8"*R*-**13** was in good agreement with the experimental ECD spectrum for compound **13** (Figure 40). Therefore, compound **13** was characterized as tricin 4'-*O*-(7"*R*,8"*R*-guaiacylglyceryl)ether-7-*O*-*α*-L-rhamnopyranosyl-(1→4)-*O*-*β*-D-glucopyranoside.

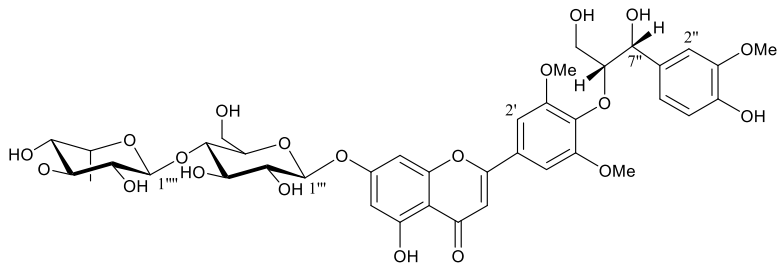

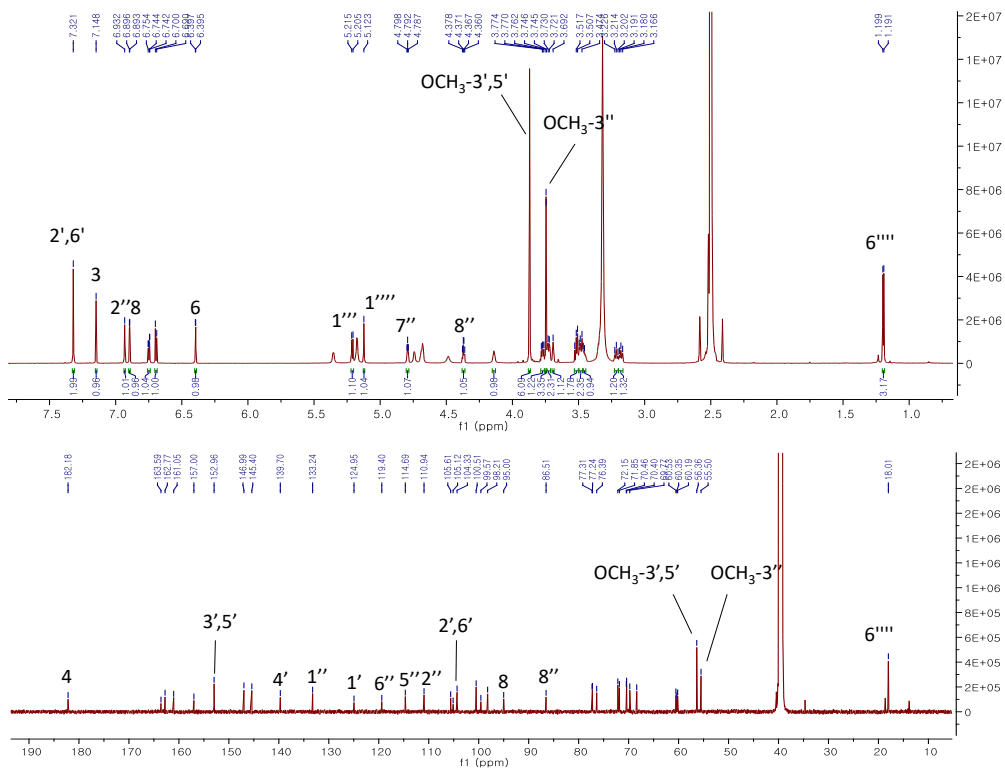

Figure 34. ^{1}H and ^{13}C NMR spectra (DMSO-d_6, 800/200 MHz) of compound **13**

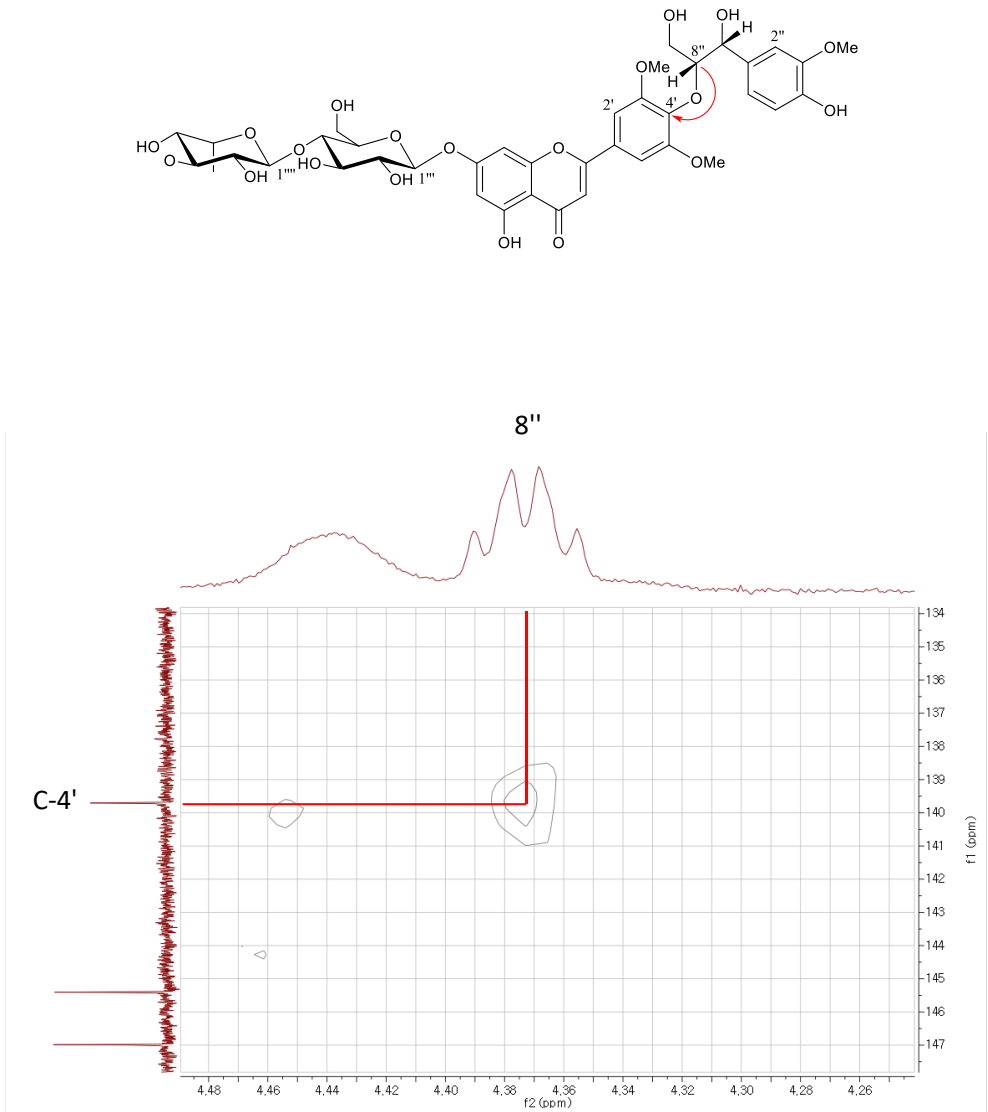

Figure 35. Key HMBC correlations (DMSO-d_6, 800 MHz) of compound **13**

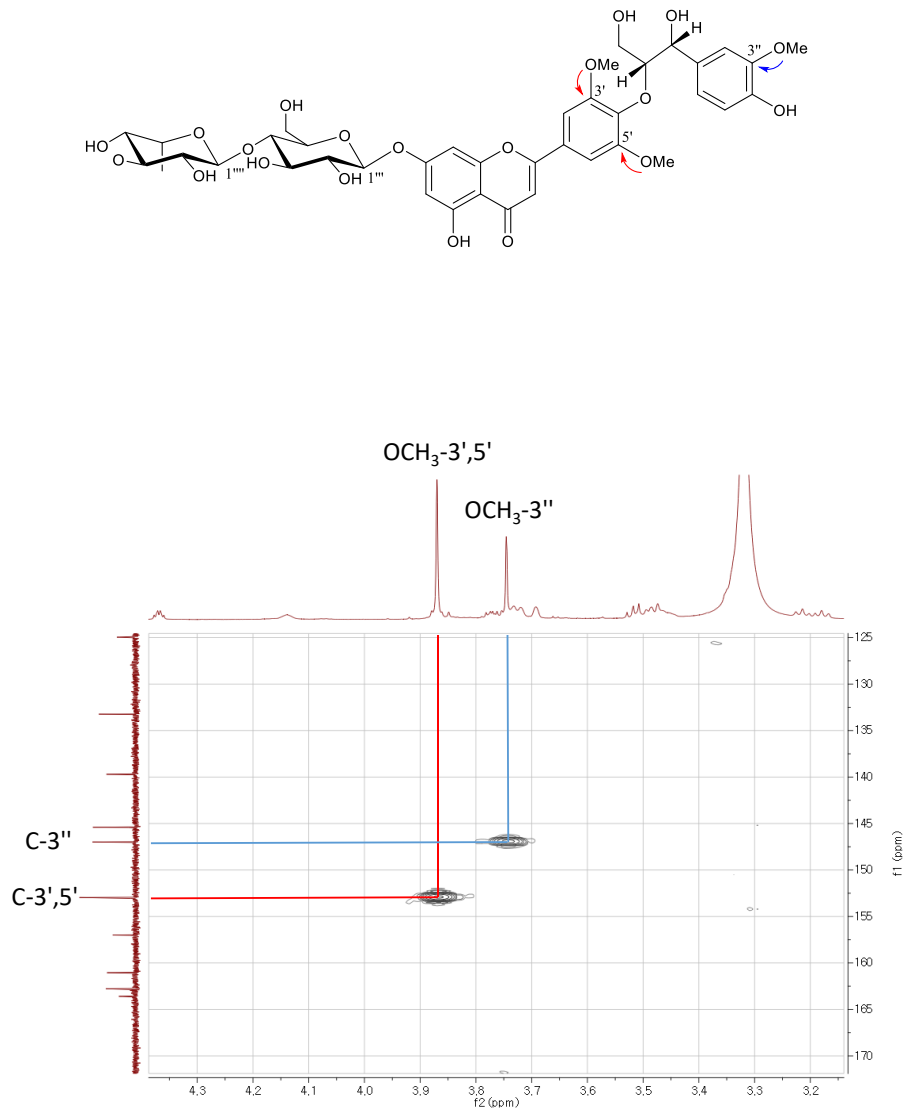

Figure 36. Key HMBC correlations (DMSO-d_6, 800 MHz) of compound **13**

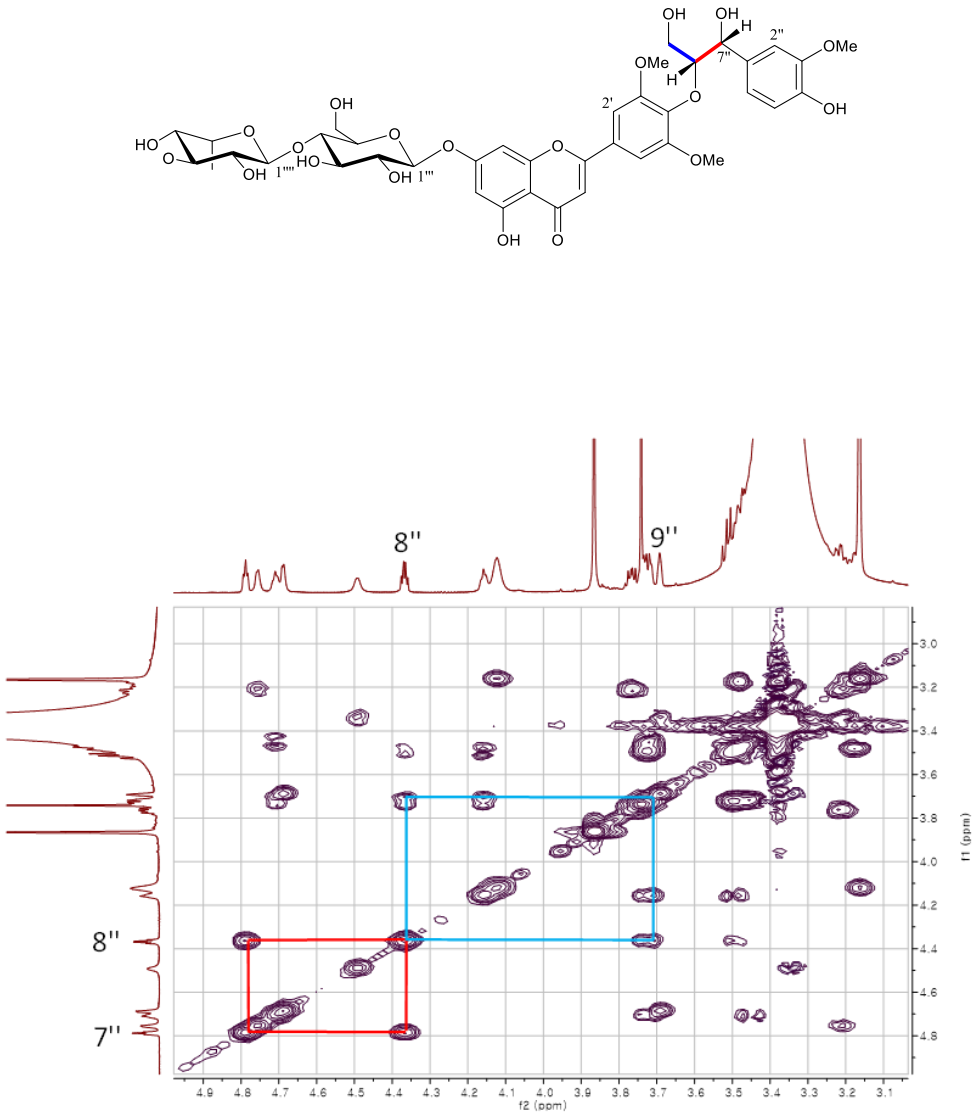

Figure 37. Key COSY correlations (DMSO-d_6, 800 MHz) of compound **13**

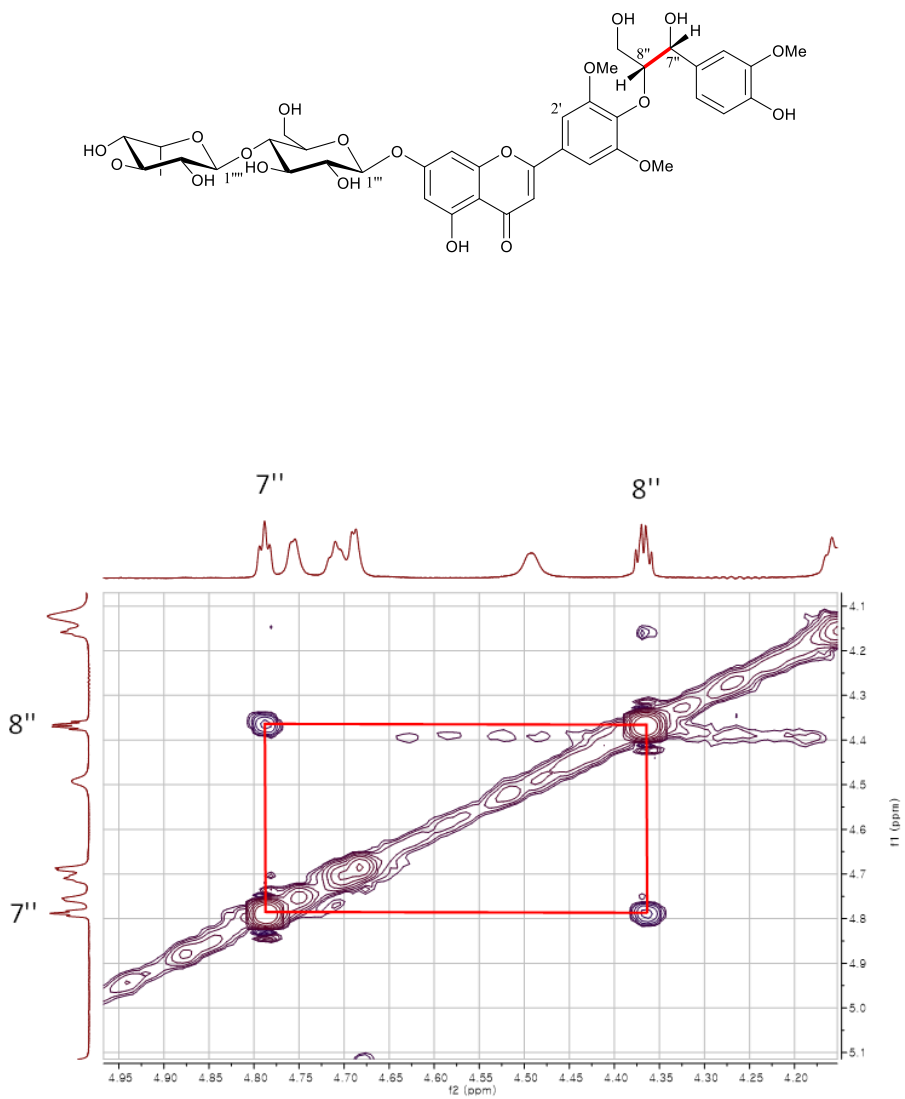

Figure 38. Key ROESY correlations (DMSO-d_6, 800 MHz) of compound **13**

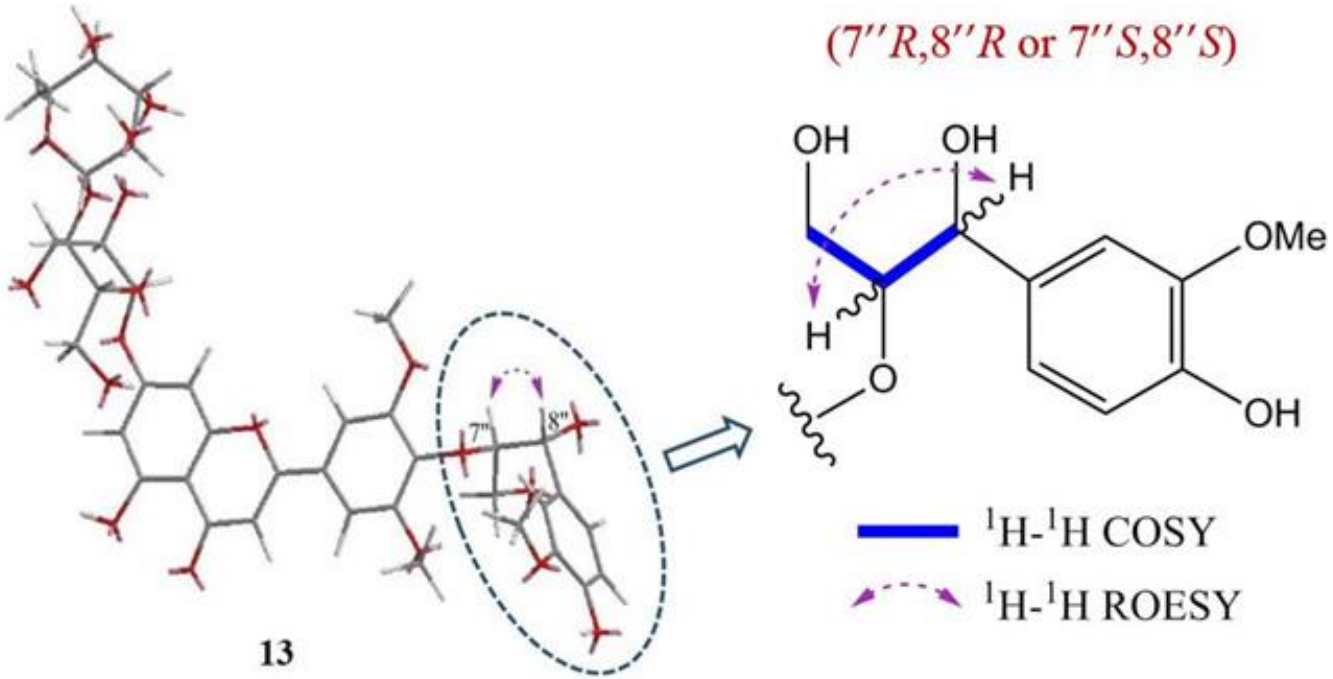

Figure 39. Key ^{1}H-^{1}H COSY and ROESY correlations of the guaiacylglyceryl moiety of compound **13**

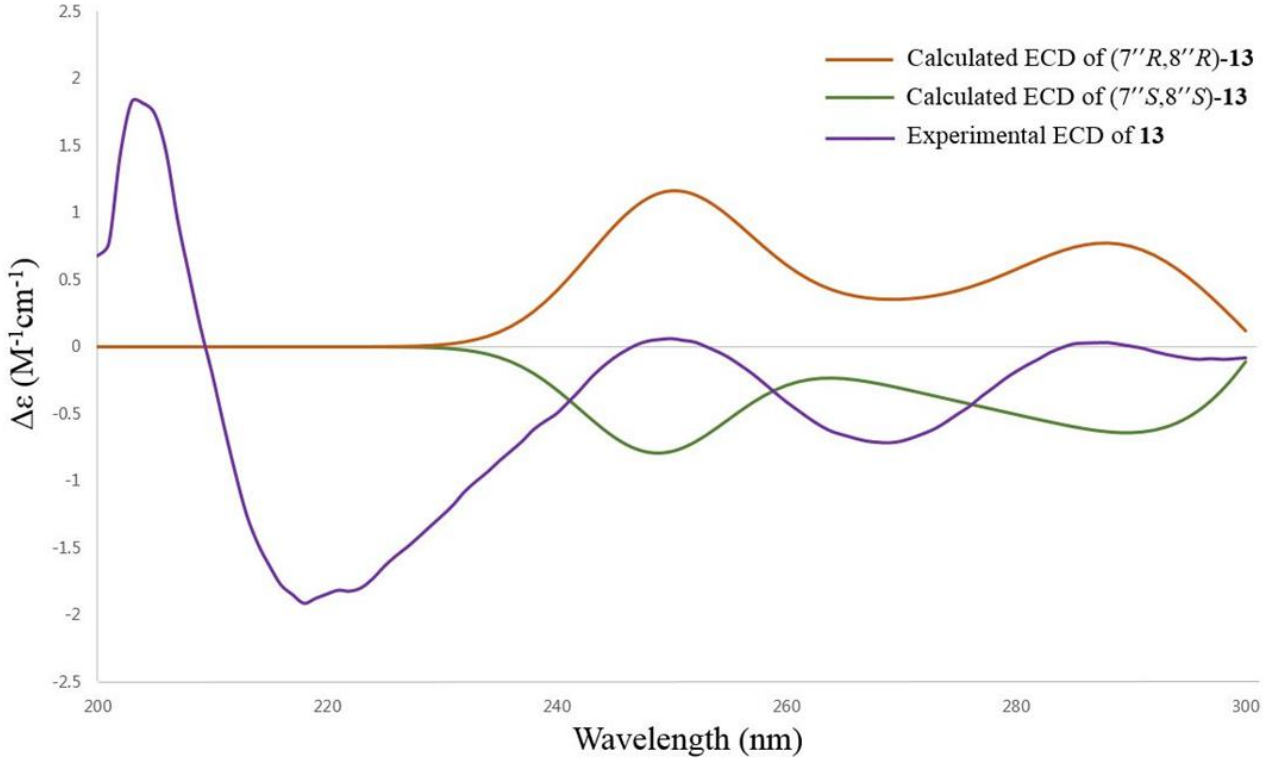

Figure 40. Comparison of experimental and calculated ECD spectra of **13**

Table 5. Calculated DFT B3LYP/def-SV(P) free energies, population and theoretical averaged rotary strength values for the major conformers of 7′′*R*,8′′*R* of compound **13**.

conformer	ΔG[a]	p_i [b]	*n* states[c]													
			1	**2**	**3**	**4**	**5**	**6**	**7**	**8**	**9**	**10**	**11**	**12**	**13**	**14**	**15**
1	0	50.347	0.4	3.5	3.8	9.7	26.8	-0.4	0.3	-0.7	9.5	36.4	-9.7	6.7	-20.1	-15.1	4.2
2	0.025	48.250	0.8	4.7	4.3	9.7	25.5	-0.4	0.3	-0.5	9.9	36.8	-9.3	4.2	-20.5	-14.9	4.2
3	2.123	1.397	1.8	-42.7	-0.1	-31.1	-1.7	-0.3	-19.8	7.9	-22.7	-9.1	-5.2	-30.3	73.2	9.6	-6.3
4	5.772	0.002	16.1	5.8	12.3	8.8	-0.1	14.2	-0.1	-8.4	4.7	37.1	-20.4	20.4	-41.0	-3.3	4.1
5	6.048	0.001	-9.7	0.5	15.0	13.1	22.0	-16.4	11.7	6.3	-0.9	-3.4	-0.2	87.5	-79.4	3.1	4.4
Weighted value			0.6	3.4	4.0	9.1	25.8	-0.4	0.0	-0.5	9.2	36.0	-9.4	5.0	-19.0	-14.7	4.1
Average wavelength (nm)			242.2	245.5	249.3	251.2	252.5	263.5	265.4	269.3	270.2	292.1	299.3	305.1	312.8	332.3	358.7

[a]DFT B3LYP/def-SV(P) Gibbs free energies in kcal/mol relative to the absolute G value for the global minimum -720295,4490 kcal/mol. [b]In percent from ΔG values at 298 K and 1 atm. $p_i = \frac{e^{-\varepsilon_i/kT}}{\sum_{i=1}^{M} e^{-\varepsilon_i/kT}}$ (K=Boltzmann constant, T = temperature, ε = Energy). [c]DFT B3LYP/def-TZVP rotary strength values.

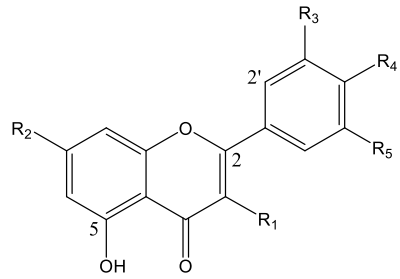

	R_1	R_2	R_3	R_4	R_5
1	*O*-S_1	*α*-rha	H	OH	H
2	*O*-S_2	*α*-rha	H	OH	H
3	α-rha(1→6)*β*-glc	*α*-rha	H	OH	H
4	*β*-glc	*α*-rha	H	OH	H
5	H	*β*-glc	H	OH	H
6	*β*-glc	OH	H	OH	H
7	α-rha(1→6)*β*-glc	OH	H	OH	H
8	*β*-api	*β*-glc(1→3)*α*-rha	H	OH	H
9	*O*-S_1	*α*-rha	OH	OH	H
10	*O*-S_2	*α*-rha	OH	OH	H
11	*O*-S_1	*α*-rha(1→6)*β*-glc(1→3)*α*-rha	H	OH	H
12	*O*-S_1	*β*-glc(1→3)*α*-rha	H	OH	H
13	H	*α*-rha(1→4)*β*-glc	OMe	S_3	OMe

S_1 =

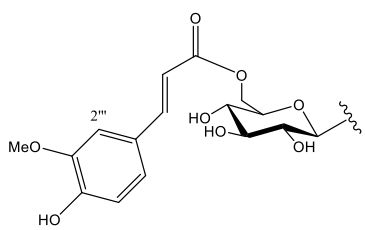

S_2 =

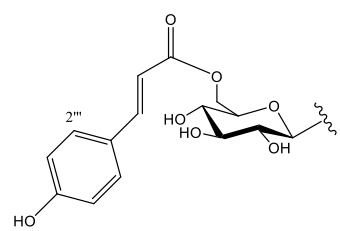

S_3 =

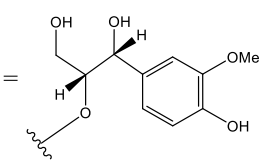

Figure 41. Structures of isolated compounds from *S. angulatus.*

3.4. Inhibitory effects on hepatic lipid accumulation

The reduction of hepatic lipid accumulation in this study was measured using HepG2 cells, which can be applied as a cell model for NAFLD. In the present study, we established a fatty liver cell model by incubating HepG2 cells in a high-glucose (30 mM glucose) and high-palmitic acid (0.2 mM palmitate) medium (Kuo et al., 2012; Ding et al., 2014). To determine if the test concentrations of the isolated compounds were toxic, HepG2 cells were treated with 100 μM of compounds **1-13**, and the cell viability was measured by the MTT assay. Since none of the compounds showed significant cytotoxicity at 100 μM, compounds **1-13** were tested at a concentration of 40 μM to determine their inhibitory effects on hepatic TG accumulation (Figure 42).

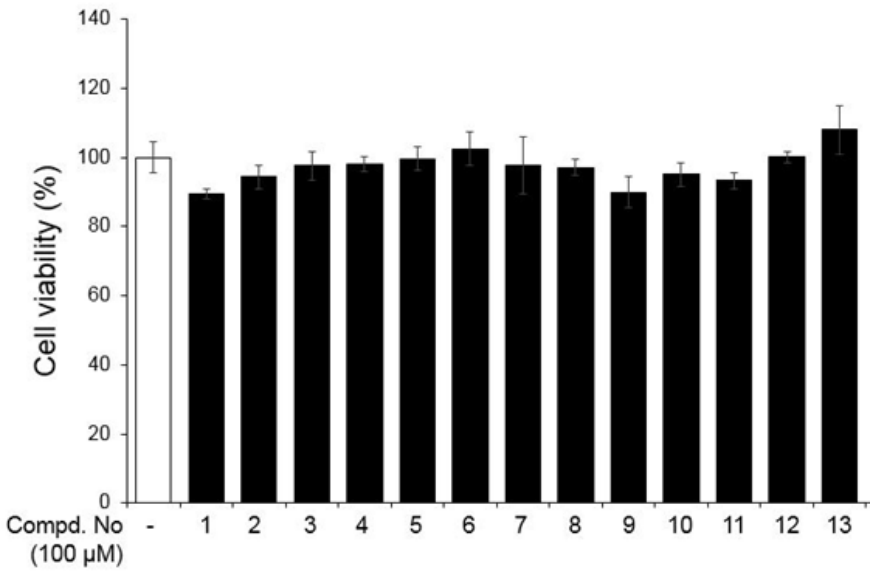

Figure 42**.** Cytotoxicity effects of isolated compounds (**1-13**) on the HepG2 cells

Compounds **1-4**, **6**, and **11-13** inhibited the lipid accumulation induced by high concentrations of palmitic acid and glucose in HepG2 cells. Among the 13 tested compounds, compound **4** exhibited the greatest effect on TG accumulation in the cell (Figure 43). In addition, compounds **1**, **3**, **4**, and **13** showed dose-dependent inhibition (10, 20 and 40 μM) of hepatic TG accumulation (Figure 44).

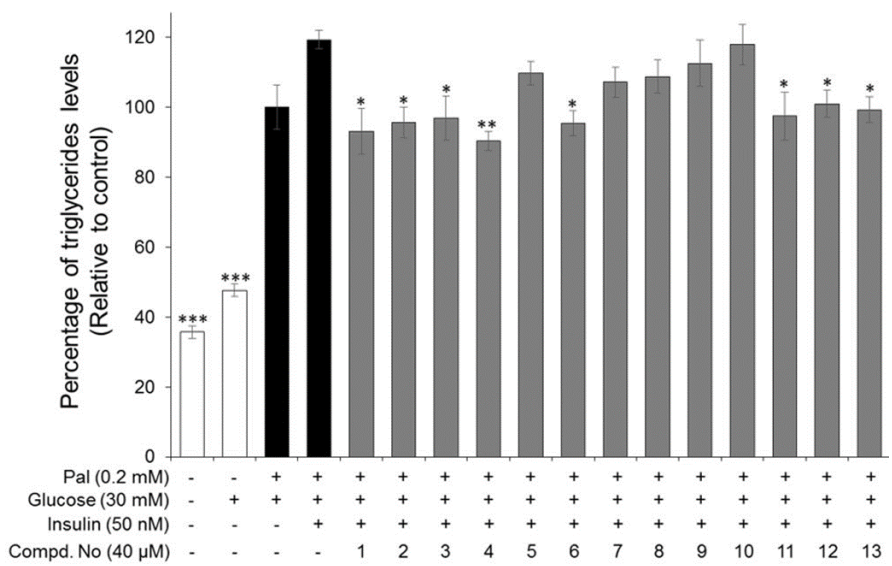

Figure 43**.** Inhibitory effects of the isolated compounds from *S. angulatus* on the high-glucose and high-palmitic acid induced lipid accumulation. HepG2 cells were treated with a mixture of palmitate (0.2 mM), glucose (30 mM), BSA (0.1%, w/v) and insulin (50 nM) in the absence or presence of compounds (**1-13**) at a concentration of 40 μM. Data are calculated as the mean ± SD (*n*=3) at * $p < 0.05$, ** $p < 0.01$, and *** $p < 0.001$ compared with the mixture of palmitate, glucose and insulin group.

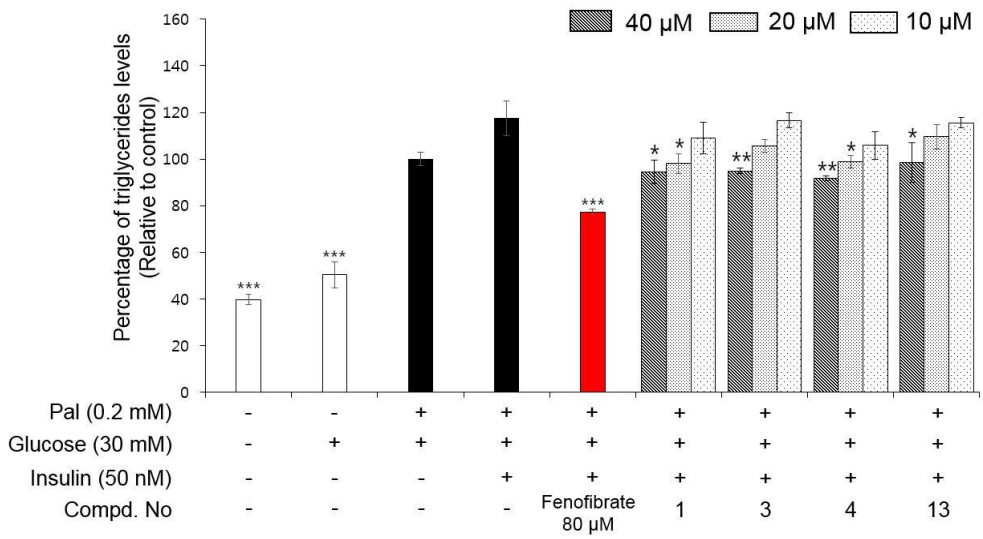

Figure 44**.** HepG2 cells were treated with a mixture of palmitate (0.2 mM), glucose (30 mM), BSA (0.1%, w/v) and insulin (50 nM) in the absence or presence of several compounds (**1**, **3**, **4**, and **13)** at various concentrations (10, 20, and 40 µM). After 24 hours of incubation, the intracellular triglyceride levels were evaluated using a fluorometric triglyceride quantification kit. The results are expressed as the mean ± SD of three independent experiments; *$p < 0.05$, **$p < 0.01$, and ***$p < 0.01$ compared with the mixture of palmitate, glucose and insulin group

The test compounds treated in HepG2 cells were analysed with an oil-red O staining assay using 40 μM fenofibrate, a drug clinically used to treat NAFLD, as a positive control. The cells were fixed and stained with the oil-red O solution after 1 day of incubation and observed with a microscope to capture the image. Compounds **1**, **3**, **4**, **11**, and **13** were found to significantly reduce lipid accumulation in HepG2 cells compared to the mixture of palmitate, glucose and insulin group.

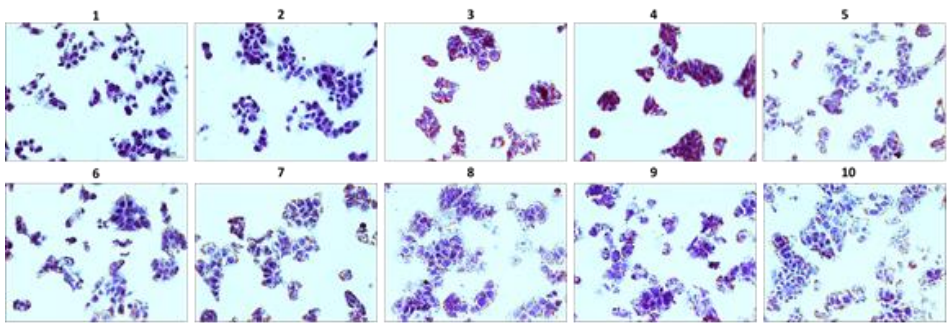

Figure 45**.** Effects of strong candidates (**1**, **3**, **4**, **11**, and **13**) on the reduction of lipid accumulation in the insulin-resistance model using oil red O and hematoxylin staining method, original uncropped images. The images (1-10) are as follows; (1) ctrl without glucose; (2) ctrl with glucose (30 mM) only; (3) palmitate (0.2 mM) and glucose (30 mM); (4) mixture of palmitate (0.2 mM), glucose (30 mM) and insulin (50 nM); (5-10) mixture of palmitate (0.2 mM), glucose (30 mM) and insulin (50 nM) with fenofibrate and compounds **1**, **3**, **4**, **11**, and **13** (40 μM), respectively.

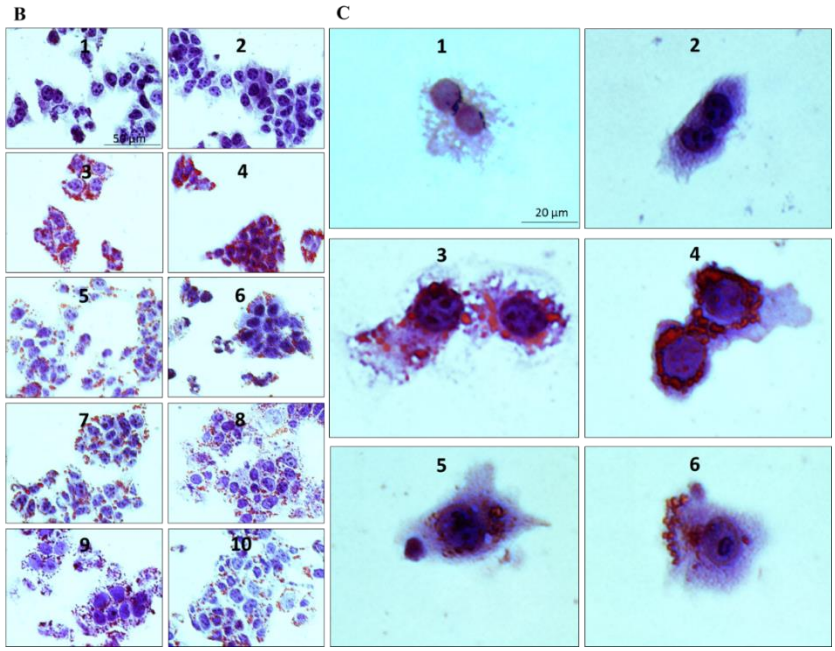

Figure 46. Effects of compounds **1**, **3**, **4**, **11**, and **13** on reduction of lipid accumulation in the insulin-resistance model using the oil-red O staining method. HepG2 cells were exposed to the test compounds (40 µM), which dissolved in the media containing the palmitate and insulin as described in the experimental section. After 1 day of incubation, the cells were fixed and stained with the oil-red O and hematoxylin solution. Images were captured using an Olympus microscope. The images (1-10) are as follows; (1) ctrl without glucose; (2) ctrl with glucose (30 mM); (3) palmitate (0.2 mM) and glucose (30 mM); (4) mixture of palmitate (0.2 mM), glucose (30 mM) and insulin (50 nM); (5-10) mixture of palmitate (0.2 mM), glucose (30 mM) and insulin (50 nM) with fenofibrate (positive control) and tested compounds **1**, **3**, **4**, **11**, and **13** (40 µM), respectively. (**C**) The image on the right (1-6) were magnified to see oil droplets in the cells. Treatment of compound **4** from *S. angulatus* in the HepG2 cell model shows the shape of the reduced oil droplets.

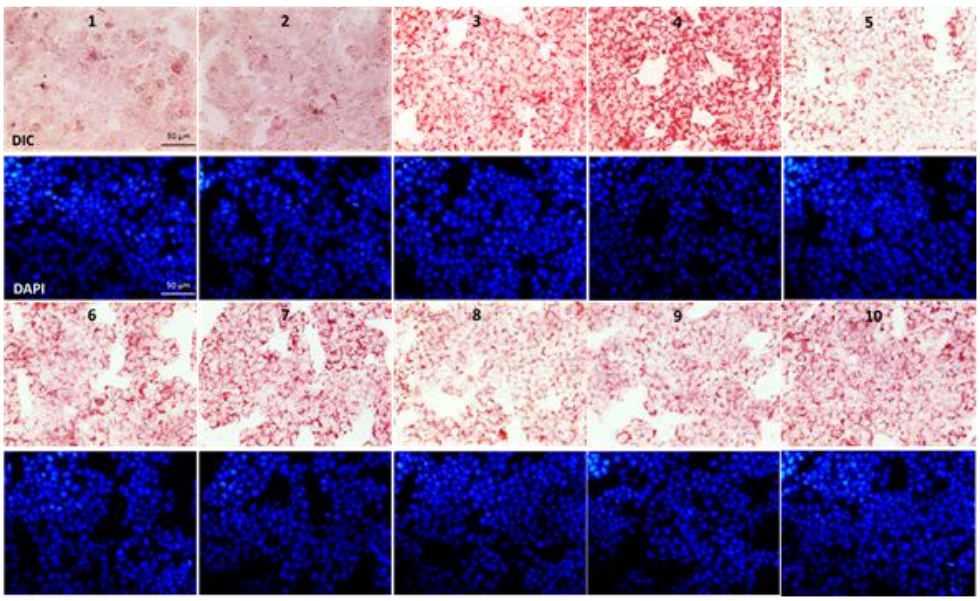

Figure 47**.** Inhibitory effects of compounds **1**, **3**, **4**, **11**, and **13** on the palmitate and glucose-induced lipid accumulation using oil red O and DAPI staining method. Images were observed the red oil droplets and the nucleus using a fluorescence microscope. Each images (1-10) are as follows:(1) ctrl without glucose; (2) ctrl with glucose (30 mM) only; (3) palmitate (0.2 mM) and glucose (30 mM); (4) mixture of palmitate (0.2 mM), glucose (30 mM), and insulin (50 nM); (5-10) mixture of palmitate (0.2 mM), glucose (30 mM), and insulin (50 nM) with Fenofibrate, compounds **1**, **3**, **4**, **11**, and **13** (40 μM), respectively.

Among the eight bioactive compounds, seven compounds (**1**-**4**, **6**, **11**, and **12**) are kaempferol glycosides and compound **13** is flavonolignan glycoside. These data are consistent with previously reported studies in which kaempferol glycoside decreased hepatic lipid content. Dietary kaempferol showed inhibitory effect on hepatic lipid content (Chang et al., 2011), and the kaempferol glycoside-rich fraction of soy bean leaves reduced lipid accumulation in liver by decreasing the expression of proliferator activated receptor (PPAR-γ) and sterol regulatory element binding protein (SREBP-1c) in animal test (Zang et al., 2015). PPAR-γ and SREBP-1c are important regulators of lipid metabolism in liver, and their levels are decreased when AMPK is activated (Ahmed and Byrne, 2007). Structure-activity relationship (SAR) analysis revealed that the presence of a cinnamoyl group enhanced the bioactivity. Kaempferol 3-*O*-β-D-glucopyranoside derivatives possessing either a coumaroyl or feruloyl group at C-6″ of the glucose showed significant inhibitory activities (**1**, **2**, **11**, and **12**). These results are in good agreement with previous studies that kaempferol 3-*O*-(6-*O*-*E*-coumaroyl)-β-D-glucopyranoside showed strong anti-diabetic activity (Ikechukwu and Ifeanyi, 2016; Zhang et al., 2014). However, few studies were reported on compounds with feruloyl moieties. In this research, we report their strong inhibitory effects on hepatic lipid accumulation. In addition, concerning their chemical structures, the structure of compound **13** is similar to that of silymarin flavonolignan glycosides, indicating its hepatoprotective effect (Cui et al., 2017).

4. Conclusions

A library of extracted natural materials (Korea Bioactive Natural Material Bank) have been screened to discover candidates for the treatment of non-alcoholic liver disease (NAFLD), and the 70% ethanol extract of *S. angulatus* was found to inhibit hepatic lipid accumulation. Herein, five previously undescribed flavonoid glycosides (**1**, **8, 9**, **11**, and **12**) and one previously undescribed flavonolignan glycoside (**13**) along with seven known flavonoid glycosides (**2-7**, and **10**) were isolated. To determine their inhibitory effects on hepatic lipid accumulation, we established a fatty liver cell model by incubating HepG2 cells with a high-glucose and high-palmitic acid medium. Compounds **1-4**, **6**, and **11-13** were found to inhibit hepatic lipid accumulation. Especially compounds **1**, **3**, **4**, and **13** showed strong inhibitory effects (10, 20, and 40 μM) on hepatic lipid accumulation in a dose-dependent manner. Compounds **1**, **3**, **4**, **11**, and **13** were also analysed for their inhibitory activities using oil-red O staining. These data demonstrated that kaempferol glycosides have inhibitory effects on fatty liver disease. Notably, kaempferol 3-*O*-*β*-D-glucopyranoside derivatives possessing a cinnamoyl moiety showed significant inhibitory activities (**1**, **2**, **11**, and **12**). This study suggests that the 70% EtOH extract of *S. angulatus* and flavonoid glycosides (**1**, **8, 9**, **11**, and **12**) from this plant can reduce the fat accumulation in HepG2 cells without cytotoxicity.

Part 2. Eudesmane glycosides from *Ambrosia artemisiifolia* (Common Ragweed) as potential neuroprotective agents

1. Introduction

1.1. Alzheimer's disease

Alzheimer's disease (AD) is a neurodegenerative disorder featured by declines of judgement, cognition, memory, and behavior (Zhou et al., 2018). AD is the leading cause of dementia, becoming one of the largest public health concerns. Currently, 30 million people suffer from AD, and the World Health Organization has reported that the number of patients will triple over the next 20 years (Tangaro et al., 2017). Owing to the steady growth of the aging population, an increasing prevalence of dementia is expected in both developing and developed countries. Accumulation of Aβ peptide into senile plaques has been considered one of the major causes of AD (Singh et al., 2018). Two types of Aβ peptides, Aβ_{40} and Aβ_{42}, can exist outside as well as inside nerve cells. Aβ has been found to be a normal metabolite of amyloid precursor protein (APP), produced by the cleavage of APP by β-secretase and γ-secretase (Habib et al., 2017). The senile plaque mainly consists of Aβ_{40} and Aβ_{42}, which can produce several types of oligomeric structures such as protofibrils, fibrils and plaques according their extent of oligomerization (Palop et al., 2010). Several Aβs linked through hydrogen bonds form a protofibril, and aggregation of several protofibrils generates a fibril. Further aggregation of fibrils form plaques that are highly toxic to neurons (Takahashi et al., 2017). In AD, Aβ deposits as diffuse and compact plaques, and the latter consisting of Aβ fibrils are associated with a change of pathology in the brain and surrounding parenchyma, while diffuse plaques are not involved in degenerative changes (Baltes et al., 2011). Aβ aggregate-induced neurotoxicity, oxidative stress, and inflammatory reactions are related to the etiology of AD. Several studies have reported that the cytotoxic effect of Aβ is attributed to

its aggregation. Human amyloid precursor protein (hAPP) was transferred to mice and increased levels of Aβ altered the neuronal expression of synaptic activity-regulated genes (Palop et al., 2007), and an Aβ-induced model of AD in rodents showed deficits in learning and memory abilities (Zhang et al., 2015). To date, the U.S. Food and Drug Administration (FDA) has approved only five drugs for AD: donepezil, galantamine, rivastigmine, tacrine, and memantine. However, these medications only temporarily improve cognition and delay the disease progression for a short period (Chopra et al., 2011).

1.2. *Ambrosia artemisiifolia*

The genus *Ambrosia* consists of approximately 50 species worldwide (The Plant List). *A. artemisiifolia*, native to the United States, spreads with competitive seeds and can grow rapidly; it is now recognized as an invasive species in Korea. Previous chemical studies of this plant have reported several sesquiterpenes, triterpenes, and caffeic acid derivatives (Tamura et al., 2004; Jakupovic et al., 1988).

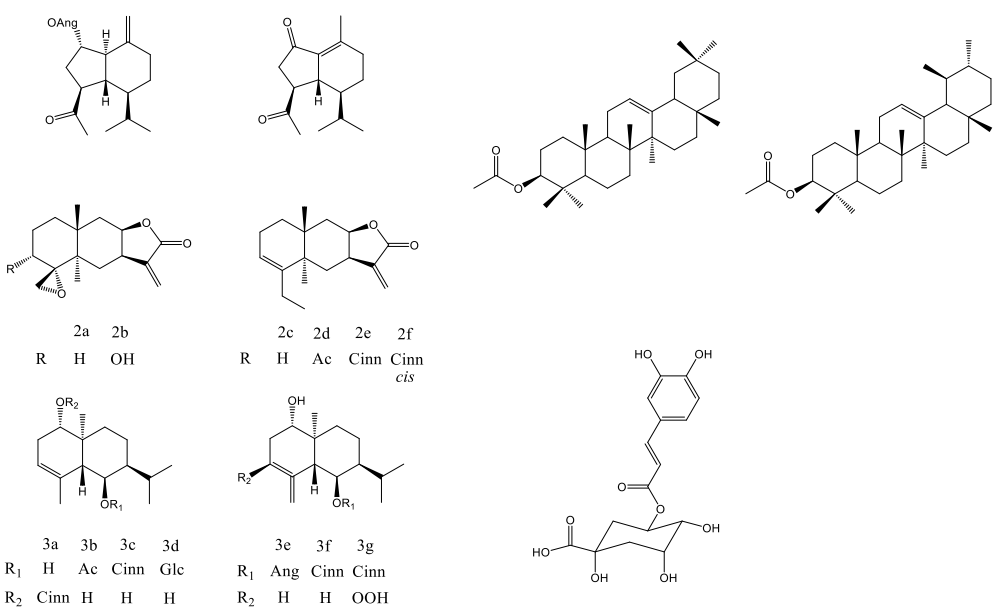

Figure 48. Structures of chemical constituents reported in *A. artemisiifolia.*

1.3. Mass defect filtering

Discovery of previously undescribed compounds in natural products is becoming a challenge since large amount of known compounds have been already reported. Thus, the demands of developing strong analysis tool was increased and mass defect filtering was introduced in natural product field recently. Mass defect filtering was first developed as a metabolite analysis tool in pharmacokinetics field (Zhu et al., 2006). Drug metabolite profiling using liquid chromatography/mass spectrometry is essential in pharmaceutical research. Metabolites can be anticipated using mass spectrometry since they are formed via well-known biotransformation such as hydroxylation or methylation. The concept of algorithm was that the difference of mass defect value between phase 1 and phase 2 metabolite fall within 50 mDa in pharmacokinetics field. The change in mass defect ranges from – 43 mDa (sulfation) to + 32 mDa (glucuronidation). For example, demethylation changes the mass defect by -23 mDA and hydroxylation affects +16 mDa. Thus, defining the mass defect ranging from – 23 m DA to + 16 mDa allows rapid detection of demethylated or hydroxylated metabolites from parent drug. The advantage and reproducibility of this method was proved in biological samples such as plasma, feces, bile and liver microsomes (Bateman et al., 2007).

Mass defect filtering was applied to natural products field recently and facilitate to discover previously undescribed compounds. In the natural product field, the classification of natural products covers almost all types of organic molecules and each family possess different range of mass defect. Therefore, mass defect present strong evidence to classify compounds according to their family and this concept is also related to relative mass defect. The mass defect value of ^{1}H is 0.0078 and that

of ^{16}O is – 0.0051 (Table 6). Therefore, the higher the ratio of proton to oxygen, the higher the mass defect value and vice versa. Phenolic compounds such as flavonoid contain several benzene rings, thus the ratio of proton to oxygen tend to be low. However, at the same time, the ratio of proton to oxygen is high in terpenes resulting in high value of mass defect. For example, as shown in figure 49, compound **1** is terpene and its nominal mass is 442 and compound **2** is flavonoid glycoside and its nominal mass is 448. The difference of nominal mass between the former and the latter is only 6 Da. However, they display significant different mass defect value. Mass defect of compound **1** is 3810, whereas, that of compound **2** is 1005.

Table 6. Mass defect and abundance of elements

Element	Symbol	Exact mass	Abundance	Mass defect
Hydrogen	^{1}H	1.0078	99.19	0.0078
Deuterium	^{2}H	2.0141	0.015	0.0141
Carbon 12	^{12}C	12	98.90	0.0000
Carbon 13	^{13}C	13.0034	1.10	0.0034
Nitrogen 14	^{14}N	14.0030	99.63	0.0030
Nitrogen 15	^{15}N	15.0001	0.37	0.0001
Oxygen 16	^{16}O	15.9949	99.76	− 0.0051
Oxygen 17	^{17}O	16.9991	0.038	0.0001
Oxygen 18	^{18}O	17.9992	0.20	− 0.0008
Fluorine	^{19}F	18.9984	100.00	0.0016
Sulfur 32	^{32}S	31.9720	95.02	− 0.0280
Sulfur 33	^{33}S	32.9707	0.75	− 0.0293
Sulfur 34	^{34}S	33.9694	4.21	− 0.0306

This is because they contain significantly different ratio of proton to oxygen. Thus, limited range of nominal mass in combination with limited range of ratio of proton to oxygen allows to rapidly find certain derivatives.

In this study, the chemical constituents of *A. artemisiifolia* were analyzed by high-resolution mass spectrometry to list up its chemical constituents. The RMD value (505) of some peaks (nominal mass:560) were determined as a terpene. This was well matched with previous studies that sesquiterpene lactones or eudesmane sesquiterpene glycosides were obtained from this plant (Jakupovic et al., 1988). To confirm their chemical structures in detail, NMR screening was performed to sub-fractions. First, five fractions were prepared by column chromatography from 70% ethanol extract according to their polarity. Then, each five fractions were chromatographed by Sephadex-LH20 to remove phenolic compounds and finally terpene-rich sub-fractions were yielded. Five terpene rich fractions were analyzed by ^{1}H NMR spectrum. As shown in figure 50, two fractions presented HMG specific methylene peaks around δ_{H} 2.60 with overlapped resonances. Based on Scifinder database, only few sesquiterpene glycosides with HMG group was reported from nature. Using MDF method with well-designed parameter, the interferences were removed and only targeted peaks were presented.

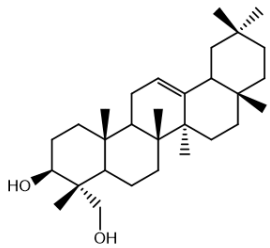

1

1	2
$C_{30}H_{50}O_2$	$C_{21}H_{20}O_{11}$
442.3810	448.1005

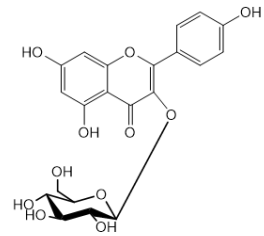

2

Figure 49. Chemical formula and exact mass of two different classes of compounds

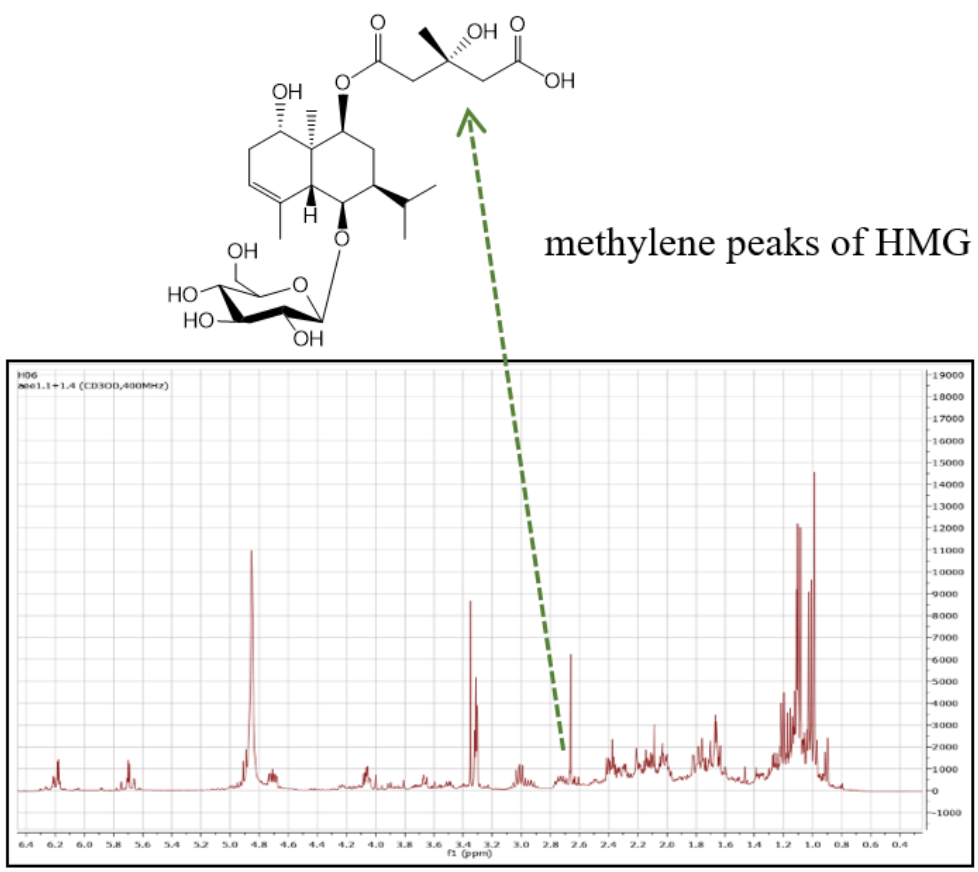

Figure 50.[1]H NMR spectrum of terpene-rich fraction

1.4. Purpose of research

Three hundred extracts were selected from the KBNMB (Korea Bioactive Natural Material Bank) and screened for their inhibitory activities against Aβ-induced NO production. As a result, 10 μg/mL of the ethyl acetate extract of *A. artemisiifolia* L. (Asteraceae) inhibited around 50% of Aβ-induced NO production. Thus, the purification of bioactive compounds from *A. artemisiifolia* was performed by bio-guided isolation (Scheme 3).

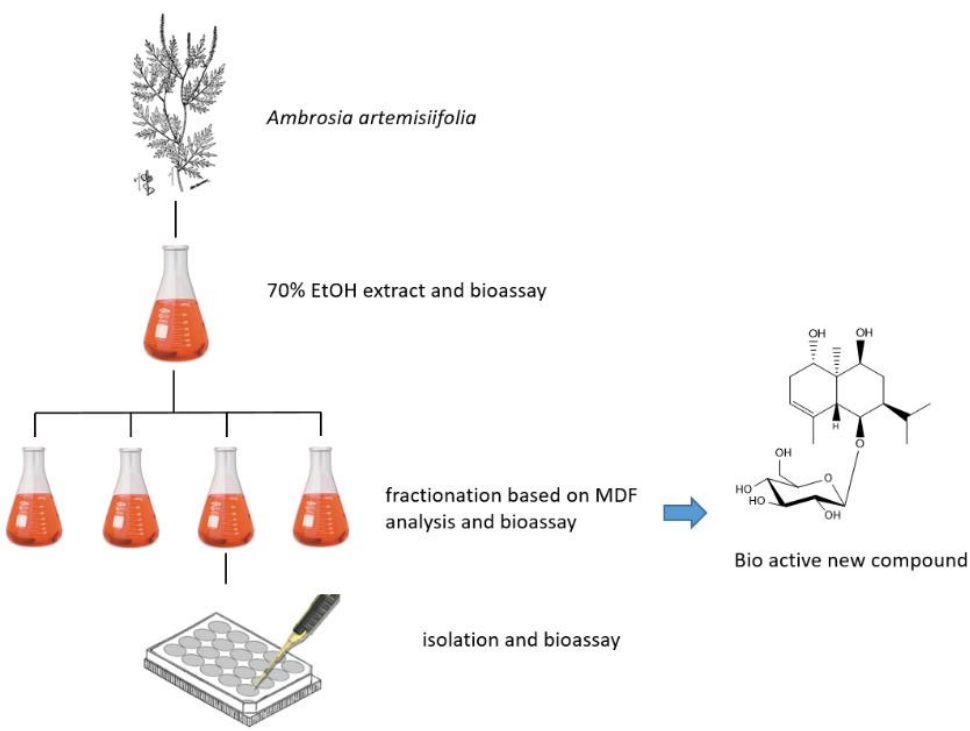

Scheme 3. The bio-guided isolation strategy of *A. artemisiifolia*.

2. Materials and methods

2.1. Plant materials

The whole plants of *A. artemisiifolia* was collected in September 2015 in Wonju, Gangwon Province, Korea. The sample was identified botanically by W. K. Oh. A voucher specimen (SNU2015-10) was deposited at the Medicinal Plant Garden of Seoul National University, Seoul, Korea.

2.2. Chemicals, reagents, and chromatography

Almost chemical and bioassay reagents, and experimental instruments in Part 2 were used similarly to Part 1. However, there have other chemicals and equipment in this part, including:

- MPLC (Biotage-Isolera One, Biotage, Charlotte, NC, USA)
- C_{18} SNAP cartridges (KP-C18-HS; 120 g, Biotage)
- L-cystein (Tokyo chemical industry Co.Ltd, Tokyo, Japan)
- phenyl isothiocyanate (Tokyo chemical industry Co.Ltd, Tokyo, Japan)
- anhydrous pyridine (99.8%, Sigma-Aldrich, Missouri, USA)
- Sep-pak plus long (Waters Associates, Milford, USA)

2.3. Mass defect filtering

Based on library dataset (Scifinder), eudesmane glycoside with HMG moiety or eudesmane glycoside containing two sugar groups may have a high possibility to be

a novel compound. To find certain derivatives, limited range of nominal mass and mass defect value were set. The difference of mass defect between HMG group and glucose was 10 mDa and the difference of mass defect among the sugar group is less than 10 mDa. (Figure 50). Thus, parameters were optimized according to these conditions. Nominal mass ranged from 520 to 610 and mass defect tolerance of ±10 mDa was set.

2.4. Extraction and isolation schemes

The air-dried and powdered whole plants of *A. artemisiifolia* (4 kg) were extracted with 70% EtOH (20 L) three times (each 1 day) at room temperature. The extract (405 g) was partitioned with *n*-hexane (3 × 3 L), EtOAc (3 × 3 L), *n*-BuOH (3 × 3 L), and H_2O. The EtOAc-soluble partition (96 g) was loaded onto a silica gel column (9.5 × 60 cm), eluted with *n*-hexane/acetone (1:0 to 0:1), to obtain seven fractions (A-G). Fraction A (21 g) was chromatographed via an open RP-18 column (2.5 × 40 cm) with MeOH/H_2O (4:6 to 10:0) as solvents to give six sub-fractions. Fraction A.3 (100 mg) was crystallized from MeOH/H_2O (6:4) to yield compound **11** (24 mg). Fraction A.4 (90 mg) was crystallized from MeOH/H_2O (6:4) to yield compound **12** (10 mg). Fraction A.6 (320 mg) was purified by semi-preparative HPLC (43% aqueous CH_3CN, flow rate 3 mL/min) to isolate compounds **9** (6.0 mg; t_R = 48.5 min) and **10** (5.5 mg; t_R = 54.0 min). Fraction C (15 g) was subjected to passage over an open RP-18 column (4.5 × 40 cm) with MeOH/H_2O (7:13 to 20:0) as solvents to give seven sub-fractions. Further purification of fraction C.5 (450 mg) using semi-preparative HPLC (26% aqueous CH_3CN, flow rate 3 mL/min) yielded compound **8** (8.0 mg; t_R = 28.2 min). Fraction D (10 g) was subjected to the open

RP-18 column (4.5 × 40 cm) separation using a CH_3CN/H_2O gradient (7:13 to 20:0), to give eight sub-fractions. Faction D.4 (800 mg) was subjected to Sephadex LH-20 column chromatography with a $MeOH/H_2O$ system (17:3) to yield two sub-fractions. Compounds **2** (7.0 mg; t_R = 42.0 min) and **7** (3.6 mg; t_R = 17.0 min) were isolated from fraction D.4.1 using semi-preparative HPLC (26% aqueous CH_3CN, flow rate 3 mL/min). Fraction D.5 (430 mg) was purified using semi-preparative HPLC (26% aqueous CH_3CN, flow rate 3 mL/min) to afford compound **3** (6.8 mg; t_R = 35.5 min). After fraction D.6 (1.3 g) was separated by MPLC with a gradient system (5% CH_3CN/H_2O; 10 min/ 60% CH_3CN/H_2O; 60 min) to yield three fractions, subfraction D.6.1 (360 mg) was purified by semi-preparative HPLC (26% aqueous CH_3CN, flow rate 3 mL/min) to furnish compound **4** (2.3 mg; t_R = 65.2 min). Compounds **5** (2.4 mg; t_R = 44.8 min) and **6** (2.1 mg; t_R = 52.0 min) were obtained by semi-preparative HPLC (26% aqueous CH_3CN, flow rate 3 mL/min) from fraction D.6.2 (460 mg). Fraction D.6.3 (490 mg) was purified by semi-preparative HPLC with a gradient system (30% CH_3CN/H_2O; 8 min/ 45% CH_3CN/H_2O; 33 min) to provide compounds **13** (6.0 mg; t_R = 27.0 min) and **14** (5.0 mg; t_R = 25.0 min). Fraction E (9 g) was separated using an open RP-18 column (4.5 × 40 cm; 150 μm particle size), with a $MeOH/H_2O$ (4:6 to 10:0) solvent system to produce ten sub-fractions. Fraction E.6 (300 mg) was further purified by semi-preparative HPLC (26% aqueous CH_3CN, flow rate 3 mL/min) to obtain compound **1** (2.0 mg; t_R = 28.0 min).

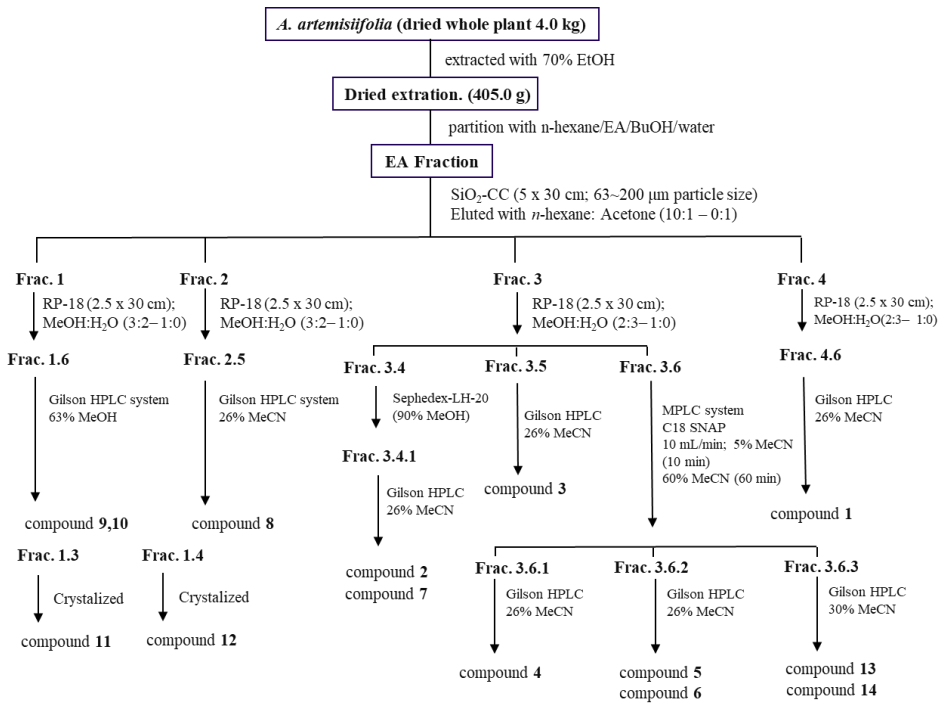

Scheme 4. Isolation scheme of *A. artemisiifolia*..

2.5. Chemical and spectral properties of isolated compounds

1*α*,6*β*,9*β*-Trihydroxy-5,10-bis-*epi*-eudesm-3-ene-9-*O*-[(*S*)-3″-hydroxy-3″-methylglutaryl]-6-*O*-*β*-D-glucopyranoside (**1**)

Amorphous powder

$C_{27}H_{44}O_{12}$

$[\alpha]_D^{25}$ 6.1 (*c* 0.5, MeOH)

HRESIMS *m/z* 559.2773 $[M - H]^-$ (calcd for 559.2760)

UV (MeOH) λ_{max} (log ε) 217 (3.16) nm

IR (KBr) ν_{max} 3395, 2925, 1725, 1625 cm^{-1}

^1H NMR data (400 MHz, DMSO-d_6): See table 7

^{13}C NMR data (100 MHz, DMSO-d_6): See table 8

1*α*,6*β*,9*β*-Trihydroxy-5,10-bis-*epi*-eudesm-3-ene-1-*O*-[(*S*)-3″-hydroxy-3″-methylglutaryl]-6-*O*-*β*-D-glucopyranoside (***2***)

Amorphous powder

$C_{27}H_{44}O_{12}$

$[\alpha]_D^{25}$ 13.8 (*c*, 0.5, MeOH)

HRESIMS *m/z* 559.2794 $[M - H]^-$ (calcd for 559.2760)

UV (MeOH) λ_{max} (log ε) 217 (3.16) nm

IR (KBr) ν_{max} 3399, 2926, 1720, 1455, 1083 cm^{-1}

^1H NMR data (600 MHz, DMSO-d_6): See table 7

^{13}C NMR data (150 MHz, DMSO-d_6): See table 8

1*β*,6*α*-Dihydroxy-7-*epi*-eudesm-3-ene-1-*O*-[(*S*)-3″-hydroxy-3″-methylglutaryl]-6-*O*-*β*-D-glucopyranoside (**3**)

Amorphous powder

$C_{27}H_{44}O_{11}$

$[\alpha]_D^{25}$ 1.7 (c 0.5, MeOH)

HRESIMS *m*/*z* 543.2820 $[M - H]^-$ (calcd for 543.2811).

UV (MeOH) λ_{max} (log ε) 216 (3.17) nm

IR (KBr) ν_{max} 3403, 2920, 1720, 1620 cm^{-1}

^1H NMR data (600 MHz, DMSO-d_6): See table 7

^{13}C NMR data (150 MHz, DMSO-d_6): See table 8

1*α*,6*β*,9*β*-Trihydroxy-5,10-bis-*epi*-eudesm-3-ene-9-*O*-[(*S*)-3″-hydroxy-3″-methylglutaryl]-6-*O*-(6′-*O*-acetyl)-*β*-D-glucopyranoside (**4**)

Amorphous powder

$C_{29}H_{46}O_{13}$

$[\alpha]_D^{25}$ 31.8 (*c* 0.3, MeOH)

HRESIMS *m/z* 601.2876 $[M - H]^-$ (calcd for 601.2866).

UV (MeOH) λ_{max} (log ε) 217 (3.20) nm

IR (KBr) ν_{max} 3389, 2913, 1731, 1615, 1435, 1085 cm^{-1}

^1H NMR data (800 MHz, DMSO-d_6): See table 7

^{13}C NMR data (200 MHz, DMSO-d_6): See table 8

1*α,*6*β,*9*β*-Trihydroxy-5,10-bis-*epi*-eudesm-3-ene-1-*O*-α-L-arabinopyranosyl-6-*O*-*β*-D-glucopyranoside (**5**)

Colorless gum

$C_{26}H_{44}O_{12}$

$[\alpha]_D^{25}$ −2.0 (*c* 0.5, MeOH)

HRESIMS *m*/*z* 593.2812 $[M + HCOO]^-$ (calcd for 593.2815).

UV (MeOH) λ_{max} (log ε) 217 (2.72) nm

IR (KBr) ν_{max}: 3410, 2910, 1620 cm^{-1}

^1H NMR data (800 MHz, DMSO-d_6): See table 9

^{13}C NMR data (200 MHz, DMSO-d_6): See table 10

1*α,*6*β,*9*β*-Trihydroxy-5,10-bis-*epi*-eudesm-3-ene-6-*O*-*β*-D-glucopyranoside (**6**)

Amorphous powder

$C_{21}H_{36}O_8$

$[\alpha]_D^{25}$ 1.7 (*c* 0.2, MeOH)

HRESIMS *m*/*z* 461.2382 $[M + HCOO]^-$ (calcd for, 461.2392).

UV (MeOH); λ_{max} (log ε) 217 (2.78) nm

IR (KBr) ν_{max} 3413, 2909, 1615 cm^{-1}

^1H NMR data (600 MHz, DMSO-d_6): See table 9

^{13}C NMR data (150 MHz, DMSO-d_6): See table 10

1*β*,6*α*-Dihydroxy-7-*epi*-eudesm-3-ene-6-*O*-*β*-D-apiofuranosyl-(1→6)-*β*-D-glucopyranoside (**7**)

Colorless gum

$C_{26}H_{44}O_{11}$

$[\alpha]_D^{25}$ −1.6 (*c* 0.5, MeOH)

HRESIMS *m*/*z* 577.2850 $[M + HCOO]^-$ (calcd for 577.2866).

UV (MeOH); λ_{max} (log ε) 217 (2.68) nm

IR (KBr) ν_{max} 3403, 2911, 1630 cm^{-1}

^1H NMR data (800 MHz, DMSO-d_6): See table 9

^{13}C NMR data (200 MHz, DMSO-d_6): See table 10

1*β*,6*α*-Dihydroxyeudesman-4(15)-ene-1-*O*-*β*-D-glucopyranoside (**8**)

White amorphous powder

$C_{21}H_{36}O_7$

$[\alpha]_D^{25}$ -10.5 (*c* 0.1, MeOH)

HRESIMS *m*/*z* 399.2360 $[M - H]^-$ (calcd for 399.2382).

UV (MeOH): λ_{max} (log ε) 215 (3.0) nm

IR (KBr) ν_{max} 3440, 2984, 1715, 1160, 1490 cm^{-1}

^1H NMR (400 MHz, $CDCl_3$): δ_H 4.95 (1H, s, H-15a), 4.74 (1H, s, H-15b), 4.29 (1H, d, *J* = 7.7 Hz, H-1'), 3.86 (1H, dd, *J* = 11.7, 1.8 Hz, H-6'a), 3.67 (1H, dd, *J* = 11.6, 5.4 Hz, H-6'b), 3.63 (1H, m, H-6), 3.51 (1H, dd, *J* = 11.5, 4.4 Hz, H-1), 2.31 (1H, m,

H-11), 2.24 (1H, m, H-3a), 2.05 (1H, m, H-8a), 2.01 (1H, m, H-2a), 1.98 (1H, m, H-3b), 1.76 (1H, d, *J* = 10.1 Hz, H-5), 1.54 (1H, m, H-2b), 1.50 (1H, m, H-9a), 1.23 (1H, m, H-9b), 1.22 (1H, m, H-8b), 0.94 (3H, d, *J* = 7.1 Hz, H-12), 0.85 (3H, d, *J* = 6.9 Hz, H-13), 0.74 (3H, s, H-14).

3-Deacetoxylhymenolane (**9**)

White amorphous powder

$C_{19}H_{28}O_6$

$[\alpha]_D^{25}$ -40.2 (*c* 0.2, MeOH)

HRESIMS *m/z* 351.1800 $[M - H]^-$ (calcd for 351.1807)

UV (MeOH): λ_{max} (log ε) 212 (3.7) nm

IR (KBr) ν_{max} 1730, 1380, 1053 cm^{-1}

^1H NMR (600 MHz, $CDCl_3$): δ_H 5.21 (1H, ddd, *J* = 8.0, 8.0, 4.8 Hz, H-3), 4.64 (1H, ddd, *J* = 11.7, 6.4, 4.3 Hz, H-8), 4.60 (1H, d, *J* = 7.5 Hz, H-4), 2.90 (1H, dq, *J* = 14.9, 7.4 Hz, H-11), 2.68 (1H, m, H-7), 2.22 (1H, dt, *J* = 13.7, 4.7 Hz, H-2a), 2.15 (1H, m, H-9a), 2.06 (3H, s, AcO), 2.04 (3H, s, AcO), 2.04 (1H, m, H-10), 1.80 (1H, td, *J* = 13.5, 4.7 Hz, H-2b), 1.72 (1H, m, H-9), 1.71 (1H, m, H-1), 1.56 (1H, dd, *J* = 14.7, 2.1 Hz, H-6a), 1.09 (3H, d, *J* = 7.5 Hz, H-13), 1.09 (3H, s, H-15), 1.03 (3H, d, *J* = 7.5 Hz, H-14).

3*α*,4*β*-Diacetylhymenoratin (**10**)

White amorphous powder

$C_{19}H_{26}O_6$

$[\alpha]_D^{25}$ 34.8 (*c* 0.2, MeOH)

HRESIMS *m*/*z* 349.1642 $[M - H]^-$ (calcd for 349.1651)

UV (MeOH): λ_{max} (log ε) 209 (3.3) nm

IR (KBr) ν_{max} 1735, 1640, 1452, 1053 cm^{-1};

^1H NMR (400 MHz, $CDCl_3$): δ_H 6.25 (1H, d, *J* = 2.5 Hz, H-13a), 5.50 (1H, d, *J* = 2.5 Hz, H-13b), 5.25 (1H, ddd, *J* = 7.9, 7.9, 4.8 Hz, H-3), 4.77 (1H, d, *J* = 7.5 Hz, H-4), 4.68 (1H, ddd, *J* = 12.0, 7.8, 3.3 Hz, H-8), 3.21 (1H, m, H-7), 2.23 (1H, m, H-9a), 2.18 (1H, m, H-2a), 2.12 (1H, m, H-10), 2.08 (3H, s, AcO), 2.05 (3H, s, AcO), 1.84 (1H, m, H-2b), 1.78 (1H, m, H-9b), 1.71 (1H, m, H-1), 1.60 (1H, m, H-6a), 1.55 (1H, m, H-6b), 1.08 (3H, s, H-15), 1.06 (3H, d, *J* = 7.5 Hz, H-14).

Ambrosic acid (**11**)

White amorphous powder

$C_{15}H_{20}O_4$

$[\alpha]_D^{25}$ 55.8 (*c* 0.1, MeOH)

HRESIMS *m*/*z* 263.1289 $[M - H]^-$ (calcd for 263.1283).

UV (MeOH): λ_{max} (log ε) 209 (3.0) nm

IR (KBr) ν_{max} 3150, 3118, 1720, 1690 cm^{-1}

^1H NMR (400 MHz, $CDCl_3$): δ_H 6.41 (1H, br s, H-13a), 5.65 (1H, br s, H-13b), 4.37 (1H, m, H-8), 2.94 (1H, br d, *J* = 11.9 Hz, H-7), 2.49 (1H, m, H-3a), 2.40 (1H, m, H-2b), 2.28 (1H, m, H-3b), 2.22 (1H, m, H-9a), 2.22 (1H, m, H-10), 2.13 (1H, m, H-6b), 1.74 (1H, m, H-2b), 1.51 (1H, t, *J* = 13.0 Hz, H-6b), 1.22 (3H, d, *J* = 7.0 Hz, H-14), 1.01 (3H, s, H-15).

Cumambrin B (**12**)

White amorphous powder

$C_{15}H_{20}O_4$

$[\alpha]_D^{25}$ -30.4 (*c* 0.1, MeOH)

HRESIMS *m*/*z* 263.1273 $[M - H]^-$ (calcd for 263.1283).

UV (MeOH): λ_{max} (log ε) 214 (3.4) nm

IR (KBr) ν_{max} 1760, 1635, 1435 cm^{-1}

^1H NMR (400 MHz, CD_3OD): δ_H 6.13 (1H, dd, *J* = 3.6, 0.9 Hz, H-13a), 6.01 (1H, dd, *J* = 3.3, 0.9 Hz, H-13b), 5.52 (1H, d, *J* = 1.6 Hz, H-3), 4.09 (1H, dd, *J* = 10.7, 9.4 Hz, H-6), 3.89 (1H, m, H-8), 3.51 (1H, m, H-7), 2.72 (1H, dd, *J* = 10.6, 7.9 Hz, H-1), 2.53 (1H, m, H-5), 2.26 (1H, dd, *J* = 15.7, 5.2 Hz, H-10), 2.21 (2H, m, H-2), 1.88 (3H, d, *J* = 1.8 Hz, H-15), 1.79 (1H, d, *J* = 15.7, 1.6 Hz, H-9b), 1.23 (3H, s, H-14).

^{13}C NMR (100 MHz, CD_3OD): δ_C 172.2 (C-12), 144.5 (C-4), 141.7 (C-11), 126.9 (C-3), 121.5 (C-13), 82.7 (C-6), 75.1 (C-10), 72.7 (C-8), 56.1 (C-1,5), 52.2 (C-7), 42.5 (C-9), 34.6 (C-2), 32.9 (C-14), 18.1 (C-15).

N^1,*N*^{5},*N*^{10}-Tri-*p*-coumaroylspermidine (**13**)

Yellow amorphous powder

$C_{34}H_{37}N_3O_6$

$[\alpha]_D^{25}$ 80.5 (*c* 0.2, MeOH)

HRESIMS *m*/*z* 582.2616 $[M - H]^-$ (calcd for 582.2604).

UV (MeOH): λ_{max} (log ε) 228 (2.5), 295 (3.4) nm

IR (KBr) ν_{max} 3394, 2960, 1650, 1448, 1210 cm^{-1}

^{1}H NMR (600 MHz, CD_3OD): δ_H 7.53/7.50 (1H, m, H-7''), 7.48/7.47 (1H, m, H-7'''), 7.47/7.43 (1H, m, H-2'',6''), 7.44/7.43 (1H, m, H-7'), 7.39 (1H, m, H-2''',6'''), 7.39/7.35 (1H, d, *J* = 8.5 Hz, H-2',6'), 6.85/6.81 (1H, d, *J* = 15.0 Hz, H-8''), 6.79 (1H, m, H-3''',5'''), 6.78/6.77 (1H, m, H-3',5'), 6.76/6.71 (2H, m, H-3'',5''), 6.42 (1H, d, *J* = 15.0 Hz, H-8'''), 6.40/6.37 (1H, d, *J* = 15.0 Hz, H-8'), 3.52 (4H, m, H-4, 6), 3.33 (4H, m, H-2, 9), 1.92/1.85 (2H, quin, *J* = 6.0 Hz, H-3), 1.67 (2H, m, H-7), 1.60 (2H, m, H-8).

^{13}C NMR (150 MHz, CD_3OD): δ_C 169.3 (C-9'''), 169.4/169.2 (C-9''), 169.3 (C-9'), 160.7/160.5 (C-4',4'',4'''), 144.4 (C-7''), 142.2/141.9/141.8 (C-7',7'''), 130.9 (C-2'',6''), 130.6 (C-2',6',2''',6'''), 127.9 (C-1''), 127.7 (C-1',1'''), 118.5 (C-8'''), 118.3/118.2 (C-

8'), 116.8 (C-3',3",3"',5',5",5"'), 114.9 (C-8"), 49.0/47.6 (C-6), 47.0/45.7 (C-4), 40.1/39.9 (C-9), 38.2/37.9 (C-2), 30.6/28.9 (C-3), 27.9/27.8 (C-8), 27.9/26.3 (C-7).

N^1,N^5-Di-*p*-coumaroyl-N^{10}-caffeoyl spermidine (**14**)

Yellow amorphous powder

$C_{34}H_{37}N_3O_7$

$[\alpha]_D^{25}$ 67.9 (*c* 0.2, MeOH)

HRESIMS *m/z* 598.2540 $[M - H]^-$ (calcd for $C_{34}H_{36}N_3O_7$, 598.2553).

UV (MeOH): λ_{max} (log ε) 228 (2.1), 295 (3.7) nm

IR (KBr) ν_{max} 3398, 2955, 1647, 1440, 1208 cm^{-1};

^{1}H NMR (500 MHz, CD_3OD): δ_H 7.47/7.44 (2H, m, H-5",9"), 7.46 (1H, m, H-3"), 7.40/7.39 (2H, m, H-5',9' or H-5",9"'), 7.38 (1H, m, H-3',3"'), 7.06 (1H, d, *J* = 15.0 Hz, H-2"), 6.97 (1H, m, H-5',5"'), 6.82-6.70 (1H, m, H-5'or 5"'/6' or 6"'/8'/8"'/9' or 9"'/6"/8"), 6.43/6.40/6.38/6.37 (1H, m, H-2',2"'), 3.55 (2H, m, H-2, 9), 1.86 (2H, m, H-3), 1.65 (4H, m, H-7, 8).

Table 7. ^{1}H NMR spectroscopic data for compounds **1-4** (in DMSO-d_6).

position	**1**[a]	**2**[b]	**3**[b]	**4**[c]
1	3.93, dd (9.8, 7.0)	5.17, dd (8.8, 7.6)	4.78, d (9.5, 7.3)	3.91, dd (10.0, 6.9)
2	2.25, m 1.91, m	2.61, m 1.97, m	2.37, d (15.9) 1.93, m	2.28, m 1.94, ddd, (10.1, 7.1, 2.2)
3	5.28, br s	5.28, br s	5.25, br s	5.28, br s
4	-	-	-	-
5	3.01, br s	3.09, br s	2.57, m	3.03, br s
6	4.43, m	4.46, m	4.41, dd (11.8, 4.8)	4.40, m
7	1.59, m	1.47, m	1.90, m	1.54, m
8	2.25, m 2.12, m	2.27, dt (14.6, 7.1) 1.65, dd (14.9, 9.7)	1.77, d (14.4) 1.65, m	2.20, dt (15.2, 6.4) 1.79, ddd (16.0, 8.0, 0.8)
9	4.95, br d (5.9)	3.82, m	1.44, d (12.2) 1.30, m	4.99, dd (6.7, 1.4)
10	-	-	-	-
11	2.07, m	2.03, m	2.24, m	2.08, m
12	1.04, d (6.5)	1.01, d (6.5)	1.05, d (6.0)	1.03, d (6.6)
13	0.90, d (6.5)	0.93, d (6.5)	0.97, d (6.0)	0.91, d (6.6)
14	0.92, s	0.97, s	0.99, s	0.92, s
15	1.91, br s	1.88, br s	1.93, br s	1.89, br s
glucose				
1’	4.44, d (7.6)	4.43, d (7.7)	4.43, d (7.7)	4.43, d (7.8)
2’	3.20, m	3.20, m	3.22, m	3.24, m
3’	3.34, m	3.35, m	3.35, m	3.36, m
4’	3.31, m	3.33, m	3.23, m	3.41, dd (10.0, 6.9)
5’	3.22, m	3.24, m	3.21, m	3.21, m
6’	3.80, dd (11.0, 2.2) 3.70, dd (10.8, 4.5)	3.79, m 3.70, dd (11.8, 4.9)	3.65, dd (11.8, 5.7) 3.87, dd (11.9, 1.7)	4.41, dd (11.8, 2.1) 4.12, dd (11.8, 7.0)
HMG				
2’’	2.63, m	2.65, m	2.64, m	2.67, m
4’’	2.61, m	2.63, m	2.61, m	2.63, m
6’’	1.38, s	1.37, s	1.35, s	1.42, s
AcO				2.04, s

[a] NMR 400 MHz; [b] NMR 600 MHz; [c] NMR 800 MHz

Table 8. ^{13}C NMR spectroscopic data for compounds **1**-**4** (in DMSO-d_6).

position	**1**[a]	**2**[b]	**3**[b]	**4**[c]
1	71.5	75.7	80.0	70.9
2	33.4	31.1	30.6	33.4
3	122.0	120.8	121.7	121.8
4	137.0	136.4	138.1	136.8
5	46.6	46.4	47.1	46.6
6	77.6	77.9	75.2	78.0
7	43.2	43.5	41.2	43.5
8	29.1	32.0	22.1	29.4
9	74.1	69.9	32.1	73.9
10	42.7	42.0	40.1	42.6
11	29.2	30.1	26.3	29.4
12	22.7	22.2	24.1	22.6
13	22.2	21.7	22.8	22.2
14	12.7	13.9	12.7	12.8
15	24.1	22.7	25.8	23.9
glucose				
1’	104.1	104.9	100.0	104.4
2’	75.4	75.6	75.7	75.1
3’	78.2	78.1	78.2	78.1
4’	71.7	71.5	72.2	71.9
5’	77.4	77.8	78.0	75.1
6’	62.8	62.6	63.1	65.2
HMG				
1’’	172.3	172.6	172.5	172.8
2’’	46.6	46.7	46.5	46.9
3’’	70.9	70.8	70.7	70.9
4’’	46.3	46.4	46.1	46.6
5’’	172.3	175.2	175.5	175.0
6’’	27.9	27.8	27.8	28.0
AcO				172.7
				20.8

[a] NMR 100 MHz; [b] NMR 150 MHz; [c] NMR 200 MHz

Table 9. ^{1}H NMR spectroscopic data for compounds **5-7** (in DMSO-d_6).

position	**5**[c]	**6**[b]	**7**[c]
1	4.01, dd (9.6, 7.2)	4.07, dd (9.4, 7.4)	3.49, dd (9.8, 6.7)
2	2.42, m 2.05, m	2.35, m 1.89, m	2.25, m 1.95, m
3	5.27, br s	5.27, br s	5.25, br s
5	2.97, br s	2.99, br s	2.45,br d (10.2)
6	4.43, m	4.44, m	4.38, dd (11.1, 4.6)
7	1.46, m	1.42, m	1.89, m
8	2.25, m 1.68, ddd (15.1, 9.7, 2.0)	2.28, m 1.62, ddd (15.0, 9.8, 1.5)	1.68, m 1.80, m
9	4.07, dd (7.3, 2.0)	3.93, d (6.5)	1.57, m, 1.31, td (13.6, 4.8)
11	2.04, m	1.99, m	2.21, m
12	0.94, d (6.7)	0.93, d (6.5)	0.99, d (6.8)
13	1.02, d (6.6)	1.01, d (6.5)	1.07, d (6.8)
14	0.91, s	0.83, s	0.87, s
15	1.86, br s	1.85, br s	1.91, br s
	arabinose	glucose	glucose
1’	4.37, d (7.6)	4.43, d (7.8)	4.43, d (7.7)
2’	3.81, m	3.17, m	3.21, m
3’	3.45, m	3.32, m	3.31, m
4’	3.32, m	3.32, m	3.27, m
5’	3.22, m 3.15, m	3.23, m	3.31, m
6’		3.79, dd (11.8, 2.5) 3.68, dd (11.8, 5.1)	3.93, dd (11.1, 1.7) 3.60, dd (11.1, 5.9)
	glucose		apiofuranose
1’’	4.45, d (7.6)		4.99, d (1.9)
2’’	3.17, m		3.88, d (1.8)
3’’	3.32, m		-
4’’	3.54, m		3.90, d (9.6) 3.74, d (9.6)
5’’	3.24, m		3.58, s
6’’	3.81, m 3.68, dd (11.9, 5.3)		

[b] NMR 600 MHz; [c] NMR 800 MHZ

Table 10. ^{13}C NMR spectroscopic data for compounds **5-7** (in DMSO-d_6).

position	**5**[c]	**6**[b]	**7**[c]
1	82.1	71.6	77.3
2	33.0	33.9	33.5
3	121,7	121.5	122.5
4	136.4	136.1	137.8
5	46.2	46.6	47.3
6	77.8	78.4	75.7
7	43.6	43.7	41.6
8	31.8	32.4	22.7
9	70.2	70.3	32.1
10	43.0	42.9	41.3
11	29.9	30.2	26.5
12	21.9	21.6	22.9
13	22.3	22.1	24.1
14	13.7	12.7	11.6
15	26.1	22.6	26.1
	arabinose	glucose	glucose
1’	105.9	104.9	100.0
2’	77.9	75.6	75.7
3’	75.5	78.1	78.2
4’	71.2	71.4	71.9
5’	70.0	77.8	76.8
6’		62.6	68.2
	glucose		apiofuranose
1’’	104.1		110.7
2’’	75.7		78.1
3’’	78.2		80.6
4’’	71.6		75.0
5’’	78.1		66.0
6’’	62.7		

[b] NMR 150 MHz; [c] NMR 200 MHz

2.6. Determination of the absolute configuration of sugars in compounds **5** and **7**.

Compound **5** (0.9 mg) was hydrolyzed with 1 N HCl (1.0 mL) for 8 h at room temperature and compound **7** (0.9 mg) was hydrolyzed by 2 N HCl (1.0 mL) at 60 ℃ for 3 h. For each, after neutralization with Na_2CO_3 and concentration under reduced pressure, L-cysteine methyl ester hydrochloride in anhydrous pyridine (0.5 mg) was added, followed by heating for 1 h at 60 ℃. Then, phenyl isothiocyanate (0.1 mL) was added, and the mixture was heated at 60 ℃ for 1 h. The final solution was analyzed by LC-MS (column: an INNO C_{18} column, 5 μm, 120 Å , 4.6 × 250 mm; 10-80% CH_3CN/H_2O, 0-30 min; detection wavelength: 203 nm; flow rate: 1.0 mL/min). The retention times of the sugar derivatives were established by comparison with those of the derivatives of commercial L-arabinose (t_R = 7.21 min), D-glucose (t_R = 6.95 min), and D-apiose (t_R = 7.90 min), respectively. Thus, it was determined to be the D-configuration of the glucose and apiose and the L-configuration of arabinose moieties in compounds **5** and **7**.

2.7. Absolute configuration of HMG (3-hydroxy-3-methylglutaryl) in compound **1**.

(*S*)-1-Phenylethylamine (1.52 μL, 12.0 μmol), benzotriazol-1-yl-oxytripyrrolidinophosphonium hexafluorophosphate (PyBOP, Sigma-Aldrich) (4.6 mg, 9.2 μmol), Et_3N (2.28 μL, 18.0 μmol), and hydroxybenzotriazole (HOBt, Sigma-Aldrich) (1.6 mg, 12.0 μmol) were mixed with a solution containing compound **1** (3.9 mg, 6.0 μmol) and then cooled in ice bath. The mixture was stirred at 25 °C for 9 h, and dilute aqueous HCl was added to quench the reaction. The mixture was partitioned with EtOAc and consequently separated over a silica gel ($CHCl_3$/MeOH,

19:1, 10:1, and 1:1) to yield **1a** (3.0 mg). The ESIMS analysis showed a [M + HCOO]$^-$ peak at *m/z* 708. $LiBH_4$ (2.2 mg, 67.5 μmol) was mixed with a **1a**-containing solution (3.0 mg, 4.5 μmol) and THF (0.3 mL). After 24 h of stirring at 25 ℃, the solution was mixed with 10 μL of HCl (0.2 N) and then partitioned with EtOAc. The resulting extract was separated over silica gel ($CHCl_3$/MeOH, 19:1, 10:1, and 1:1) and yielded a colorless oil. For acetylation, the sample was stirred at 25 ℃ for 24 h with Ac_2O (2.1 μL, 22.5 μmol) in pyridine (30 μL), and diluted using H_2O. The mixture was partitioned with EtOAc to yield **1b** (0.5 mg).

*3(R)-5-O-Acetyl-1-[(S)-phenylethyl]-mevalonamide (**1b**)*: colorless oil; ^{1}H NMR ($CDCl_3$, 600 MHz) δ_H 7.26-7.36 (5H, m, Ph), 5.15 (1H, q, J = 7.1 Hz, H-1'), 4.23 (2H, m, H-5), 2.41, 2.29 (each 1H, d, J = 14.8 Hz, H-2), 2.04 (3H, s, Ac), 1.85-1.87 (2H, m, H-4), 1.51 (3H, d, J = 6.9 Hz, H-2'), 1.24 (3H, s, H-6); ESIMS *m/z* 294.2 [M + H]$^+$.

2.8. Computational chemistry for ECD calculation.

Conformational analysis was performed by means of the CONFLEX software using the MMFF94 force field. Geometry optimization [B3LYP/6-31G(d) in vacuo] and TDDFT calculations were carried out with Turbomole (Yang et al., 2015). Boltzman distributions were calculated from the B3LYP/6-31g(d) energy and the ECD spectra were generated as the sum of Gaussian. R_i and ΔE_i represented the strengths of rotation, and the value of σ in the equation was 0.10 eV.

$$\Delta\varepsilon(E) = \frac{1}{2.297 \times 10^{-39}} \frac{1}{\sqrt{2\pi}\sigma} \sum_{i}^{A} \Delta E_i R_i e^{\left[-(E-\Delta E_i)^2/(2\sigma)^2\right]}$$

Each major conformer of **1**-**4** occupied 99% of the Boltzmann population and the spectra of each simulation matched well to the corresponding experimental one. This suggested that the absolute configurations for the aglycones were 1*S*,5*R*,6*R*,7*S*,9*S*,10*S* (**1** and **4**), 1*S*,5*R*,6*R*,7*S*,9*S*,10*R* (**2**), and 1*R*,5*S*,6*S*,7*R*,10*R* (**3**), respectively.

2.9. Hydrolysis of **1-3**, **5**, and **7**.

Hydrolysis of compounds **1-3** and **5** were performed to confirm the configuration of C-1. Acid hydrolysis of **1** by stirring at room temperature for 4 h in 3 mL of 1 N HCl yielded **1c**. Acid hydrolysis of compounds **2**, **5**, and **7** by stirring for 8 h in 3 mL of 1 N HCl yielded **2a, 5a**, and **7a**, respectively. Alkaline hydrolysis of compound **3** by stirring for 24 h in 3 mL of 3 N KOH yielded **3a**

1β,6α-Dihydroxy-7-epi-eudesm-3-ene-6-O-β-D-*glucopyranoside* (***3a***). ^{1}H NMR (CD_3OD, 800 MHz) δ_H 5.25 (m, H-3), 4.45 (d, J = 7.6 Hz, H-1'), 4.39 (dd, J = 11.2, 4.5 Hz, H-6), 3.77 (m, H-6a'), 3.68 (dd, J = 11.9, 4.1 Hz, H-6b'), 3.49 (dd, J = 9.8, 6.7 Hz, H-1), 3.33 (m, H-3'), 3.30 (m, H-5'), 3.26 (m, H-4'), 3.22 (m, H-2'), 2.45 (m, H-5), 2.24 (m, H-2a), 2.21 (m, H-11), 1.94 (m, H-2b), 1.91 (br s, H_3-15), 1.86 (m, H-7), 1.80 (m, H-8a), 1.68 (m, H-8b), 1.57 (m, H-9a), 1.31 (td, J = 13.6, 4.8 Hz, H-9b), 1.07 (d, J = 6.8 Hz, H_3-13), 0.99 (d, J = 6.8 Hz, H_3-12), 0.87 (s, H_3-14); ^{13}C NMR (CD_3OD, 200 MHz) δ_C 137.8 (C-4), 122.5 (C-3), 100.0 (C-1'), 78.2 (C-3'), 77.9 (C-5'), 77.3 (C-1), 75.7 (C-6), 75.7 (C-2'), 72.1 (C-4'), 63.0 (C-6'), 47.3 (C-5),

41.6 (C-7), 41.3 (C-10), 33.5 (C-2), 32.1 (C-9), 26.4 (C-11), 26.0 (C-15), 24.1 (C-13), 22.9 (C-12), 22.7 (C-8), 11.4 (C-14); ESIMS *m*/*z* 445 $[M + HCOO]^-$.

2.10. Measurement of cell viability.

The cell cytotoxicity was evaluated using the 3-[4,5-dimethylthiazol-2-yl]-2,5-diphenyl tetrazolium bromide (MTT) reagent (Sigma). Briefly, HT22 cells, immortalized mouse hippocampal neuronal cells, were maintained in Dulbecco's modified Eagle's medium (DMEM) (HyClone, Logan, UT, USA) containing 10% fetal bovine serum (FBS) (HyClone), 100 U/mL penicillin and 100 μg/mL streptomycin. Then, 96-well plates were used to seed cells (4000 cells/well) and incubated for 24 h. Test compounds were dissolved in dimethyl sulfoxide (DMSO) (Junsei, Japan) and diluted in serum-free medium [final DMSO concentration 0.1-0.2 % (v/v)]. After 24 h of incubation, a 2 mg/mL MTT solution (20 μL) was added to each well and incubation was continued for 4 h in the dark. The supernatants were removed and formazan crystals were dissolved in DMSO. The absorbance was recorded with a microplate reader (VersaMax, PA, USA) at 550 nm.

2.11. Cytotoxicity assay and fluorescence images of Aβ_{42}-transfected HT22 cells.

HT22 cells were seeded into 96-well plates at 4000 cells/well and incubated for 2-3 h at 37 ℃ under a 5% CO_2 atmosphere. The cells in each well were transfected with 0.2 μg of pEGFP-C1/Aβ_{42} plasmid (a gift from Professor Junsoo Park, Yonsei University, Korea) with Lipofectamine 2000 reagent (Invitrogen, Carlsbad, CA,

USA). After 10 h of transfection, the compounds dissolved in the medium and used to treat the cells. Afterwards, the cells were continually incubated for 24 h and 20 μL of MTT solution (2 mg/mL) were added. Similarly, HT22 cells were grown on sterilized glass coverslips and transfected with Aβ_{42} plasmid for 10 h. The cells were replaced with fresh medium containing 2% FBS with or without test compounds. After 24 h of incubation, the cells were washed once with phosphate-buffered saline (PBS) (Takara, Japan). Fluorescence microscopy was applied to capture both fluorescence and bright-field images (Olympus IX70, Olympus Corporation, Tokyo, Japan).

2.12. Flow cytometry analysis of fluorescence intensity.

For flow-cytometry analysis, the HT22 cells were seeded into 6-well plates for 2-3 h. After being transfected with the Aβ_{42} plasmid for 10 h, the cells were exposed to the test compounds using medium supplemented with 2% FBS. The cells were then incubated for 24 h at 37 ℃ under a 5% CO_2 atmosphere. Afterwards, all cells (both dead and live) were collected by a trypsinization method. The cells were resuspended in PBS and a flow cytometer (BD, FACS Calibur, San Jose, CA, USA) was used for analysis. For each test compound, at least 10,000 events were counted and data were calculated using gates.

2.13. Statistical analysis.

Data was processed through variance analysis (ANOVA) to determine the significance of differences between each group followed by Tukey's or Duncan's post hoc test. A p-value < 0.05 was taken as a significant difference (* $p < 0.05$, ** $p < 0.01$, and *** $p < 0.001$).

3. Results and discussion

3.1. Mass defect filtering

The chemical identification of 70% ethanol extracted *A. artemisiifolia* was carried out using ultra-high-pressure liquid chromatography-quadrupole time-of-flight tandem mass spectrometry (UHPLC-qTOF-MS/MS). As mentioned above, only few eudesmane glycosides possessing either HMG group or two sugar groups were reported from nature. Thus, MDF was performed to find targeted peaks. In the process of setting the mass defect parameter, it was discovered that the chemical formula of HMG ($C_6H_8O_4$) was similar with that of glucose ($C_6H_{10}O_5$). Thus the mass defect value of HMG and glucose is similar (Figure 51).

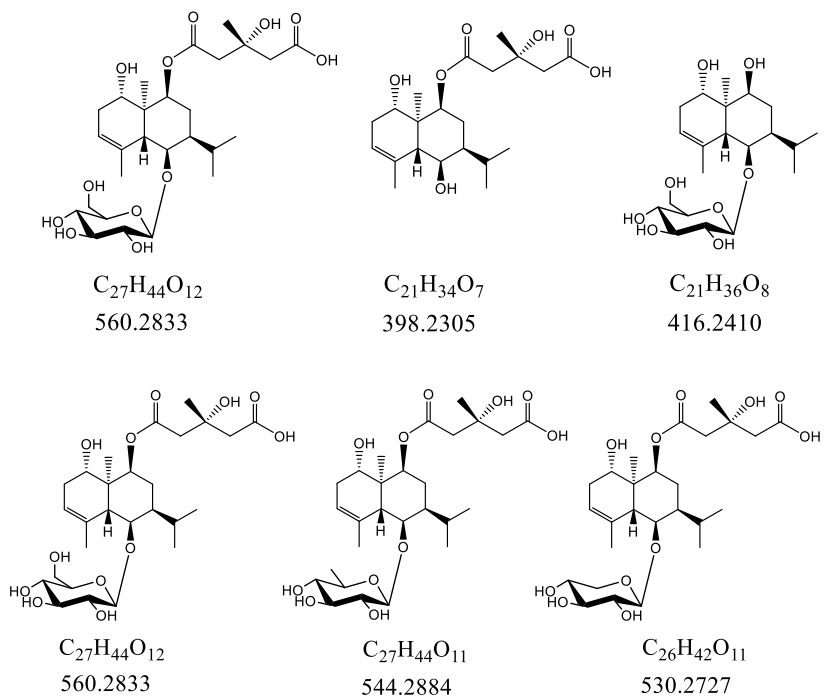

Figure 51. Chemical formula and exact mass of targeted compounds

This tendency also applies to sugar groups. Each sugar shares similar chemical formula (glucose: $C_6H_{10}O_5$, rhamnose: $C_6H_{10}O_4$, arabinose: $C_5H_8O_4$) resulting in similar mass defect value. Therefore, in a range from 520 to 610 with the mass defect tolerance of ±10 mDa, eudesmane glycosides possessing either HMG group or two sugar groups were selected.

As a result, targeted peaks (compounds **1**-**5** and **7**) were shown and their exact mass suggested their novelty. (Figure 52 and Tables 7-10). The targeted peaks were difficult to identify in total extraction, however, they were shown clearly after mass defect filtering. This work demonstrated the feasibility of the mass defect filtering method for picking new compounds in complex chromatography. It eliminated the background noise as well as presenting certain targeted derivatives.

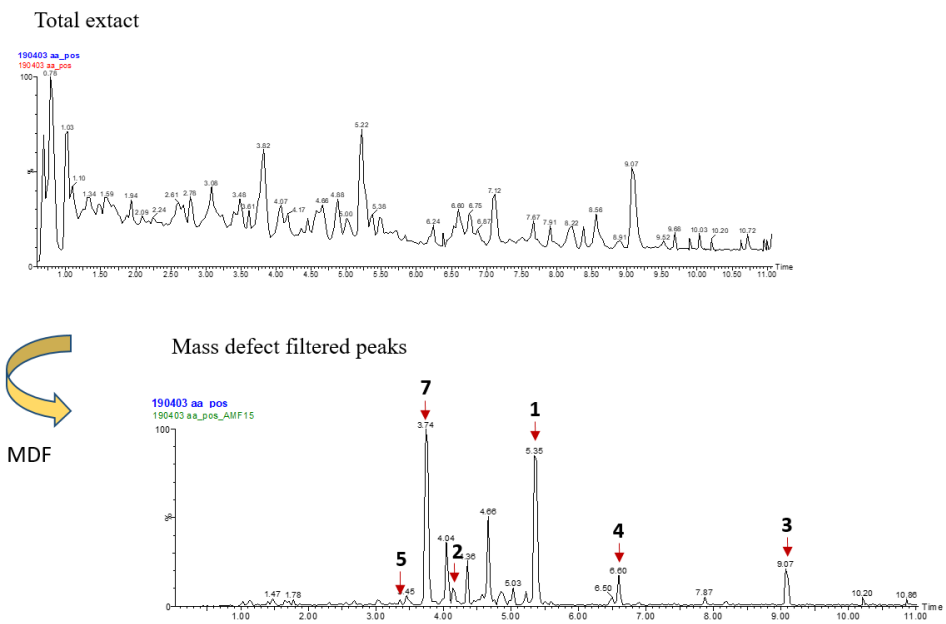

Figure 52. Mass defect filtered chromatogram of *A. artemissifolia*.

3.2. Structural elucidation of isolated compounds (**1-14**)

3.2.1. Compound **1**

Compound **1** was isolated as an amorphous powder with $[\alpha]_D^{25}$ 6.1 (*c* 0.5, MeOH). The HRESIMS data (*m/z* 559.2773 $[M - H]^-$, calcd for $C_{27}H_{43}O_{12}$, 559.2760) established the molecular formula as $C_{27}H_{44}O_{12}$. The IR bands at 3395, 1725, and 1625 cm^{-1} were indicative of hydroxy, carbonyl, and olefinic groups. The ^1H NMR data showed an olefinic proton at δ_H 5.28 (1H, br s), an allylic methyl group at δ_H 1.91 (3H, br s), a singlet methyl group at δ_H 0.92 (3H, s), and two doublet methyl moieties [δ_H 1.04 (3H, d, J = 6.5 Hz) and 0.90 (3H, d, J = 6.5 Hz)], suggesting the occurrence of an eudesmane-type sesquiterpene, with the corresponding carbon signals at C-3 (δ_C 122.0), C-4 (δ_C 137.0), C-12 (δ_C 22.7), C-13 (δ_C 22.2), C-14 (δ_C 12.7), and C-15 (δ_C 24.1) (Figure 53). The COSY correlations between H-1/H-2, H-2/H-3, H-3/H-5, H-5/H-6, H-6/H-7, H-7/H-8, H-8/H-9, and H-9/H-14 together with HMBC correlation between H-1/C-14 confirmed the A/B ring system of an eudesmane sesquiterpene (Figures 56-57). The HMBC correlations from two doublet methyl groups to one tertiary carbon (H_3-12/C-11 and H_3-13/C-11) indicated an isopropyl group, and its position was confirmed by the HMBC correlation from H-11 (δ_H 2.07) to C-7 (δ_C 43.2). Other proton signals of two pairs of methylene protons [δ_H 2.63 (2H, m) and 2.61 (2H, m)] and a singlet methyl group at δ_H 1.38 (3H, s) were predicted to be from a 3"-hydroxy-3"-methylglutaryl (HMG) moiety, with corresponding carbon signals at C-2" (δ_C 46.6), C-4" (δ_C 46.3), and C-6" (δ_C 27.9). The chemical structure of compound **1** is similar to 1α-cinnamolyoxy-6β-hydroxy-5,10-bis-*epi*-eudesm-3-ene isolated from *A. artemisioides* but additionally showed

the presence of a HMG moiety and a glucopyranosyl group along with the absence of a cinnamoyl group (Jakupovic et al., 1988). The linkage of a HMG moiety was determined at C-9 by the HMBC correlation from H-9 (δ_H 4.95) to C-1" (δ_C 172.3) (Figure 54). The glycosylation position was established by HMBC cross-peaks between H-1' (δ_H 4.44) and C-6 (δ_C 77.6) (Figure 55). A concerted method that consists of the process of amination, reduction, and acetylation revealed the absolute configuration of the HMG group (Eom et al., 2016). (*S*)-1-Phenylethylamine was used to obtain the aminated compound **1a**. Subsequently, compound **1a** was reduced with $LiBH_4$, and then acetylated with Ac_2O to give 5-*O*-acetyl-1-[(*S*)-phenylethyl]mevalonamide (**1b**) (Figure 60). The proton NMR information of **1b** was consistent with (3*R*)-5-*O*-acetyl-1-[(*S*)-phenylethyl]mevalonamide, but not (3*S*)-5-*O*-acetyl-1-[(*S*)-phenylethyl]mevalonamide (Kamo et al., 2004) (Figure 61). The relative configuration of the aglycone of **1** was determined by interpretation of its NOESY data. In the NOESY spectrum, H-1 (δ_H 3.93) correlated with H-5 (δ_H 3.01), whereas H-14 (δ_H 0.92) was correlated to H-6 (δ_H 4.43), H-7 (δ_H 1.59), and H-9 (δ_H 4.95), as shown in Figure 58. With respect to the ^{13}C NMR chemical shifts, a significant difference was suggested for C-1 according to the configuration of the hydroxy group found in previous research for eudesmane-type sesquiterpenes (Hu et al., 2001; Chernenko et al., 1994; Zhang et al., 2003; Mahmoud et al., 1997). The chemical shift of C-1 (δ_C 72.1) with an α-oriented hydroxy group is relatively upfield compared to C-1 (δ_C 79.4) with a β-oriented hydroxy group (Hu et al., 2001; Chernenko et al., 1994). The HMG moiety of **1** was removed by acid hydrolysis to yield **1c** and the similar carbon chemical shift of C-1 (δ_C 71.7) with that of previous reported compounds (δ_C 72.1) with an α-oriented hydroxy group confirmed the

configuration at C-1. To define the absolute configuration of **1**, ECD calculations were performed for (1*S*,5*R*,6*R*,7*S*,9*S*,10*S*)-1 and (1*R*,5*S*,6*S*,7*R*,9*R*,10*R*)-1 by TDDFT at the B3LYP/def-SV(P) level (Table 11). Conformers for (1*S*,5*R*,6*R*,7*S*,9*S*,10*S*)-**1** were searched using the molecular mechanics force field, and four major conformers occupied 99% of the Boltzmann population (Table 11). The absolute configuration of compound **1** was established based on the good agreement between the calculated ECD spectrum of (1*S*,5*R*,6*R*,7*S*,9*S*,10*S*)-**1** and the experimental ECD spectrum (Figure 59). Therefore, compound **1** was defined as 1*α*,6*β,*9*β*-trihydroxy-5,10-bis-*epi*-eudesm-3-ene-9-*O*-[(*S*)-3"-hydroxy-3"-methylglutaryl]-6-*O*-*β*-D-glucopyranoside.

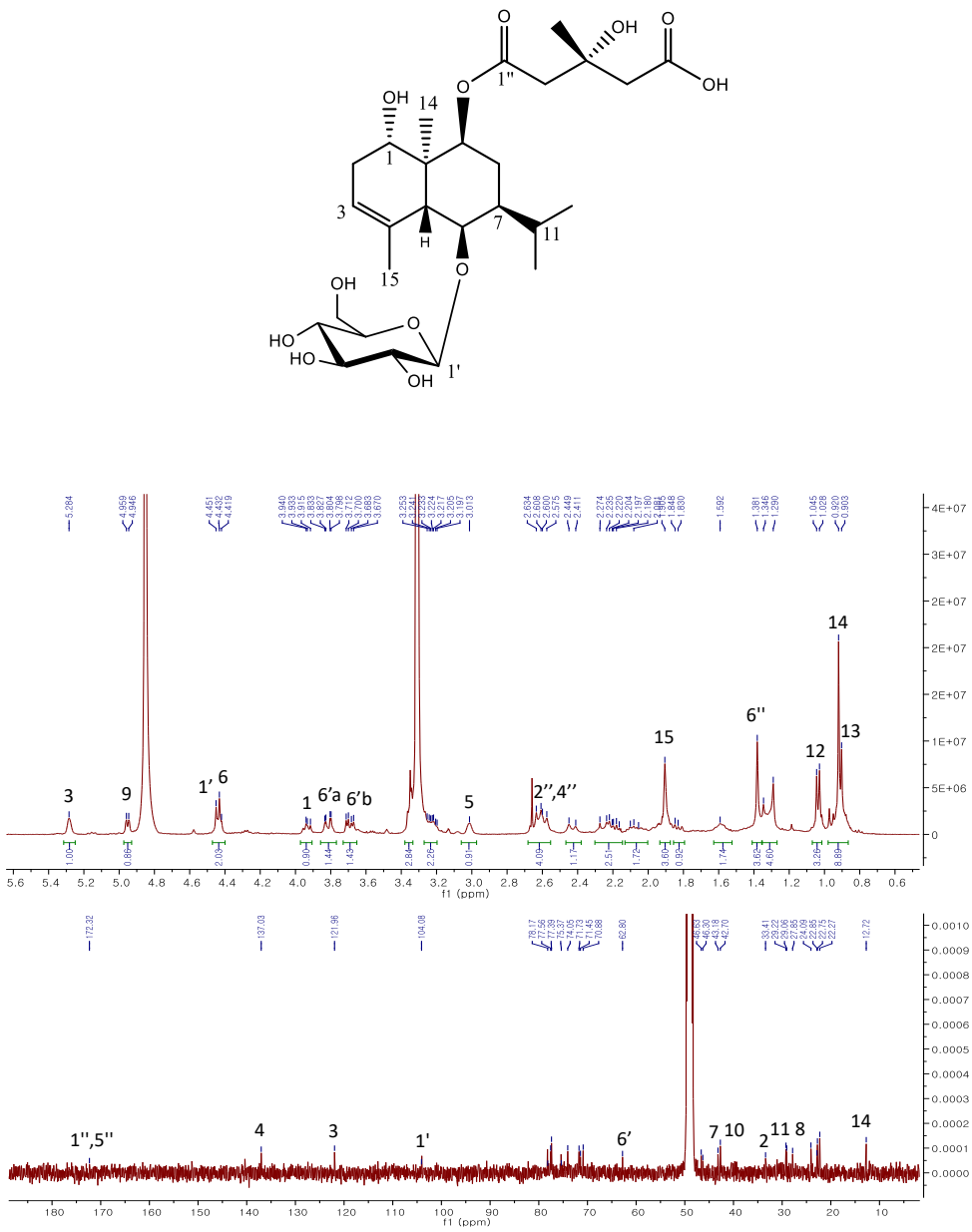

Figure 53. ^{1}H and ^{13}C NMR spectra (CD_3OD, 400/100 MHz) of compound **1**

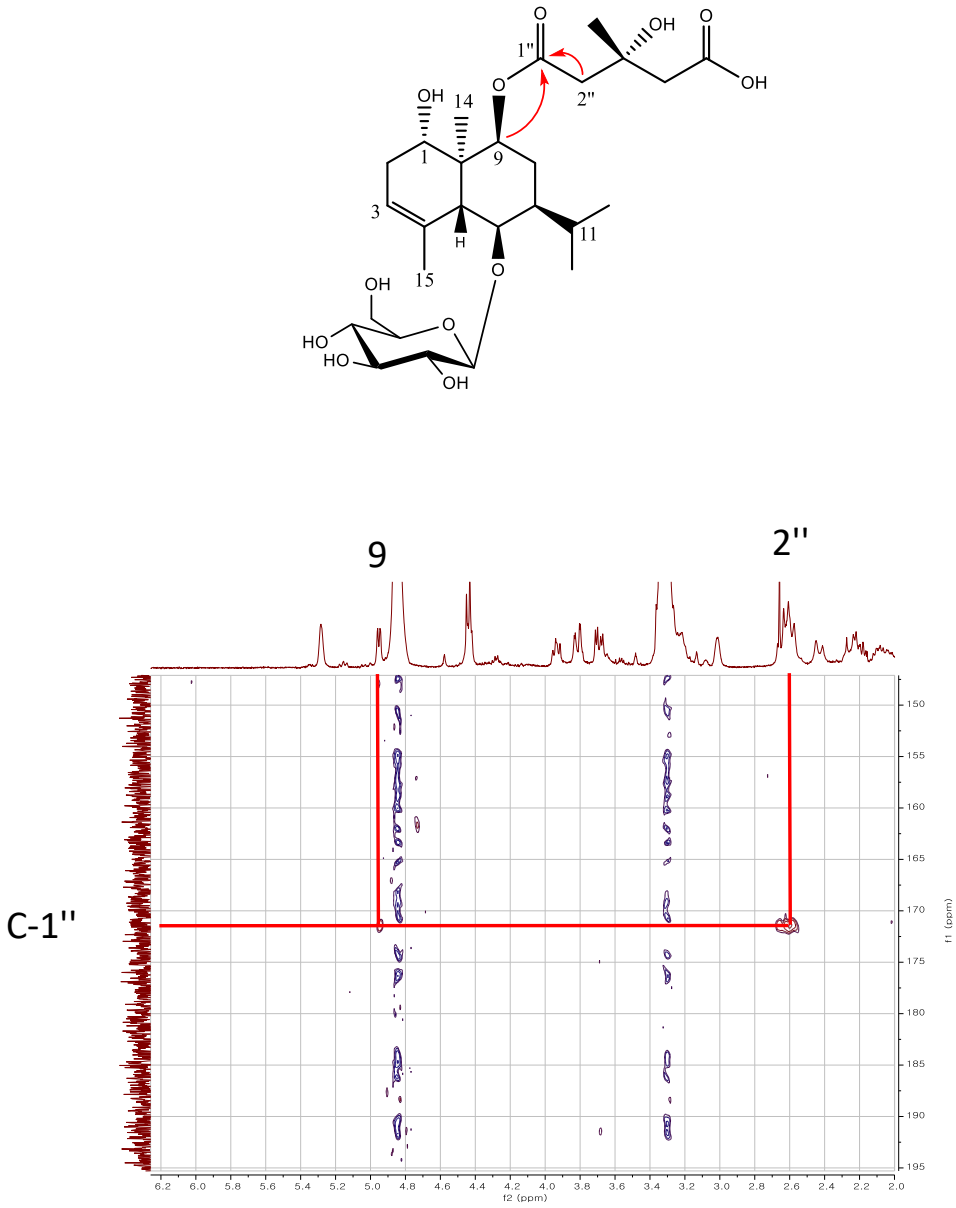

Figure 54. Key HMBC correlations (CD_3OD, 400 MHz) of compound **1**

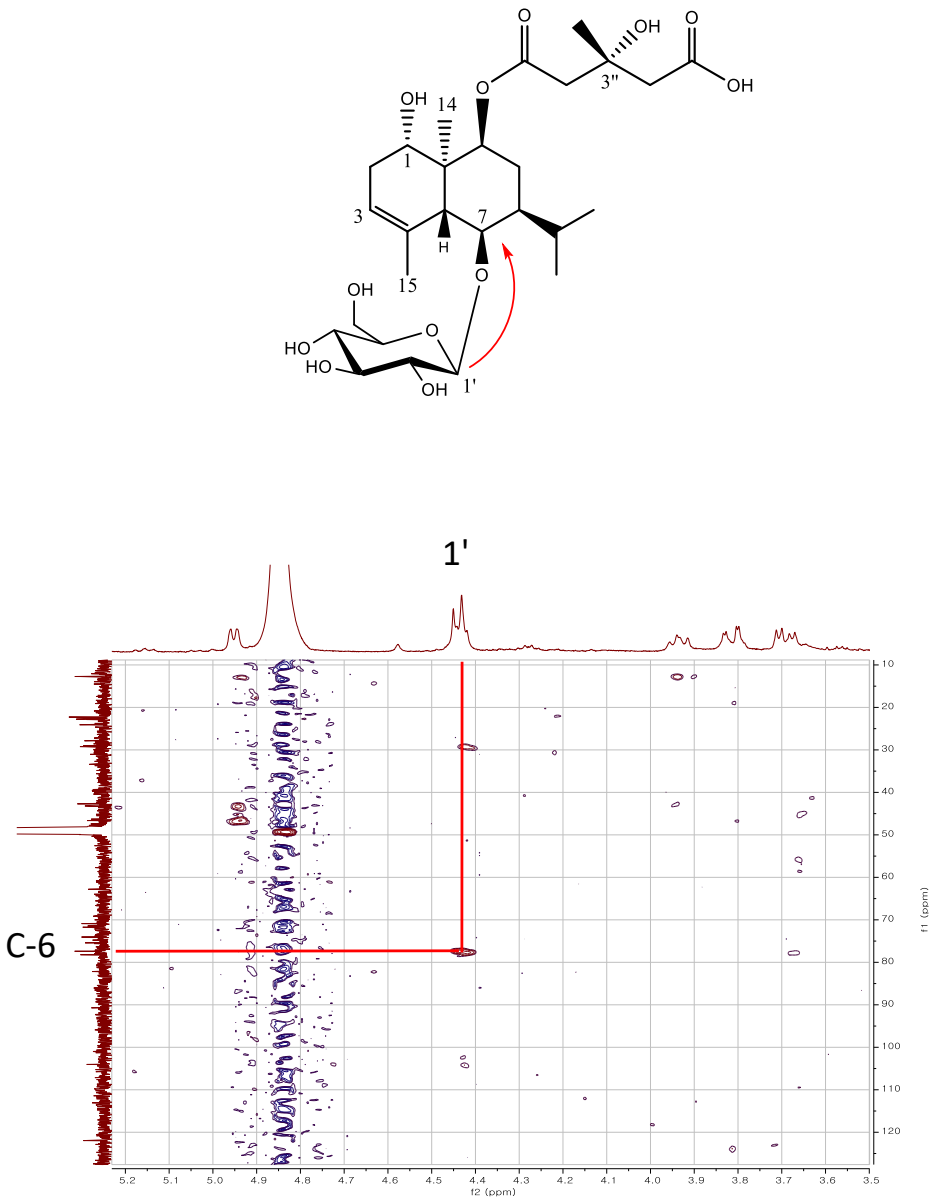

Figure 55. Key HMBC correlations (CD_3OD, 400 MHz) of compound **1**

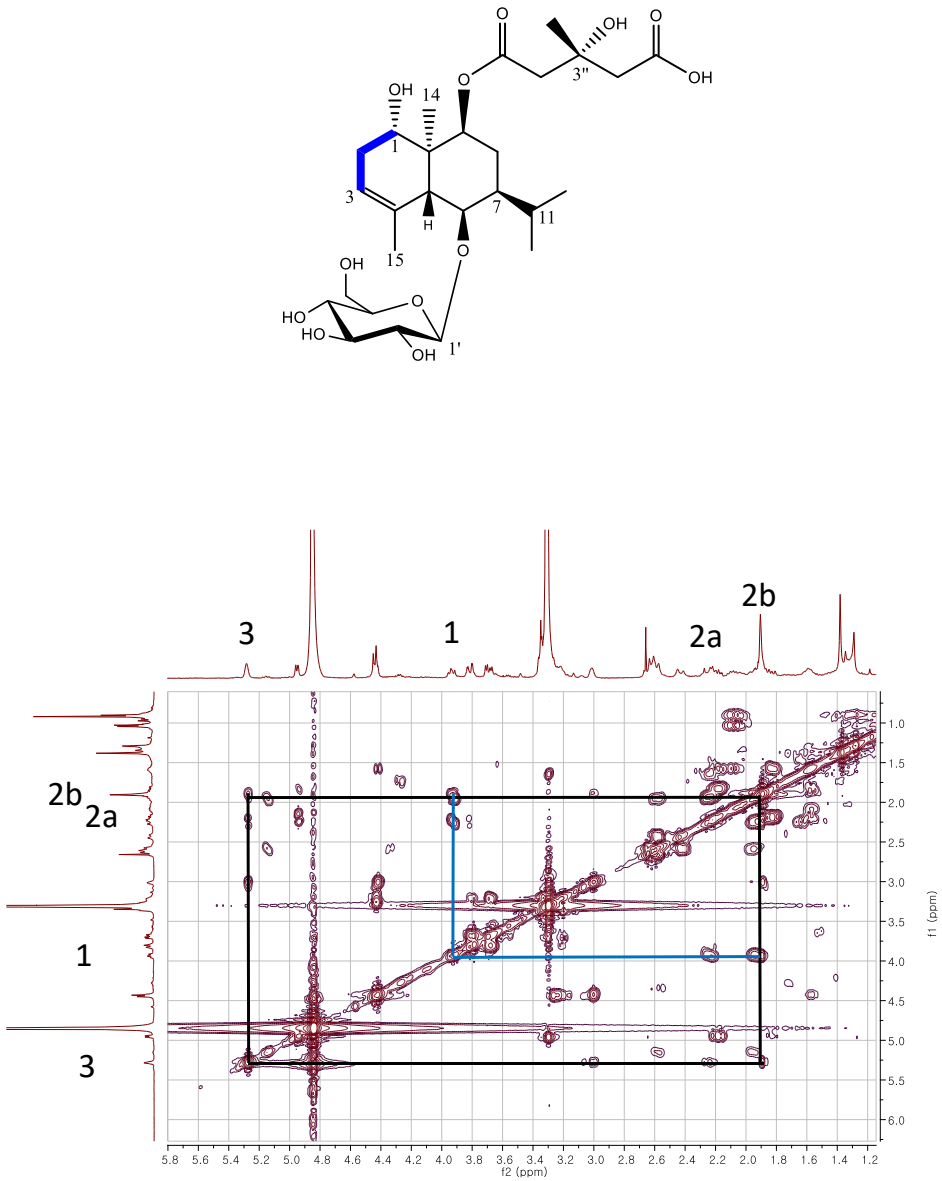

Figure 56. Key COSY correlations (CD_3OD, 400 MHz) of compound **1**

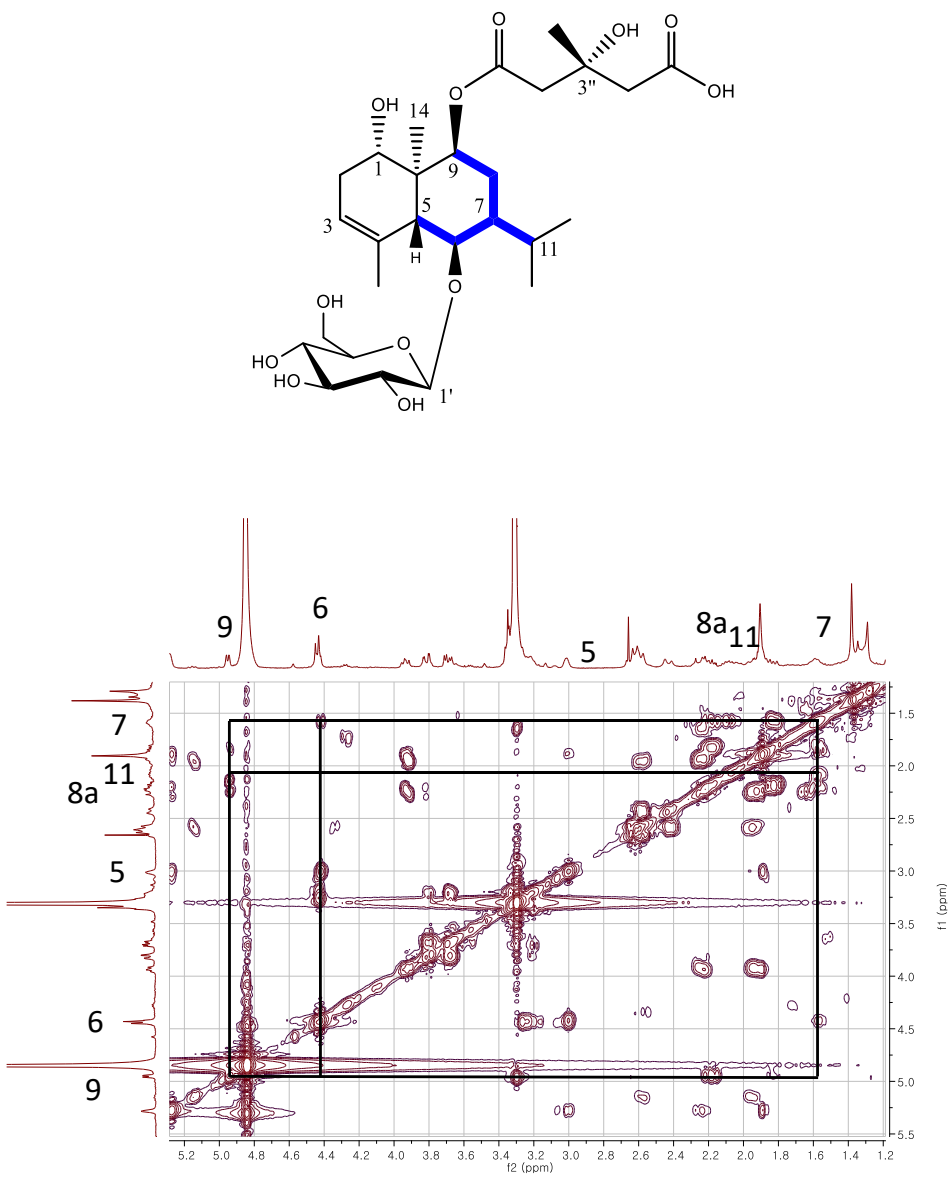

Figure 57. Key COSY correlations (CD_3OD, 400 MHz) of compound **1**

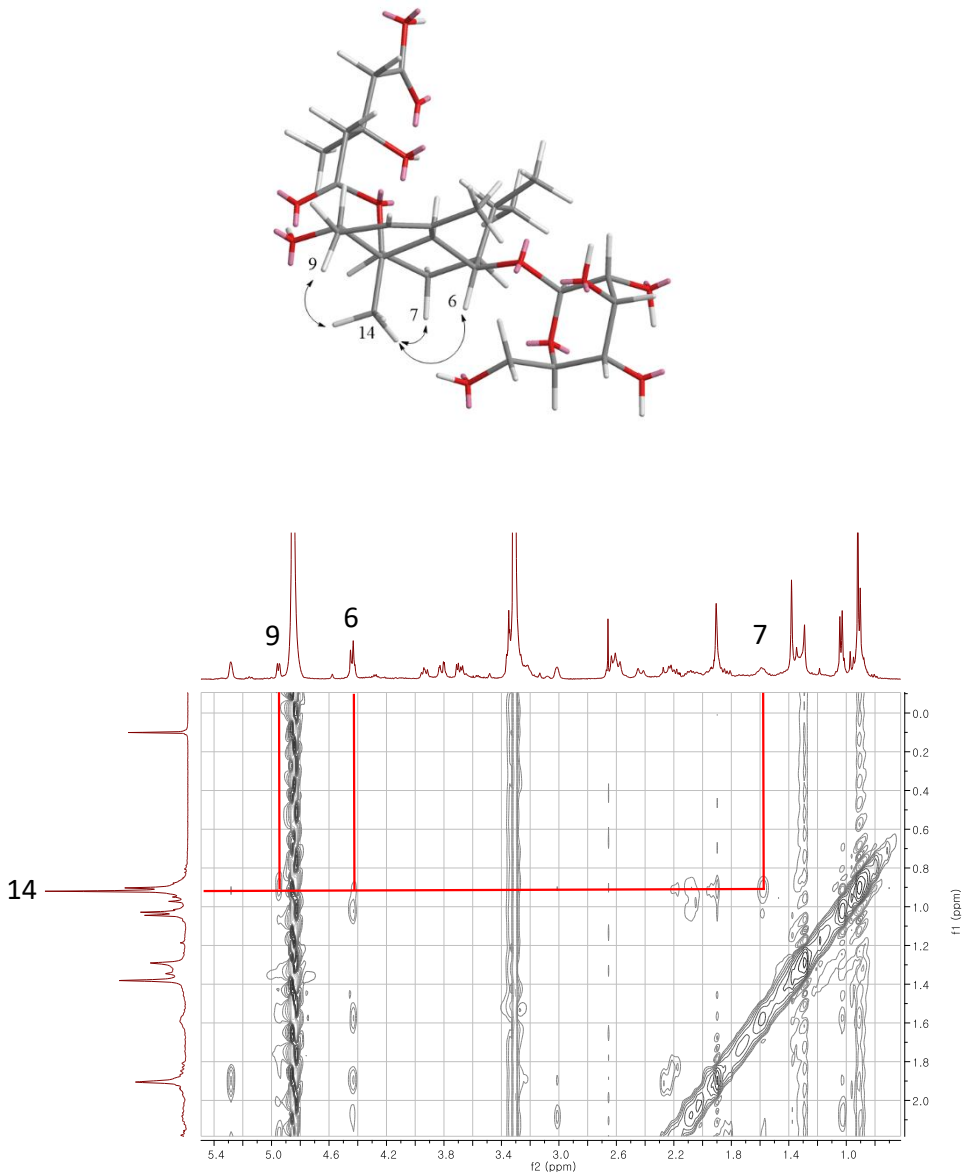

Figure 58. Key NOESY correlations (CD_3OD, 400 MHz) of compound **1**

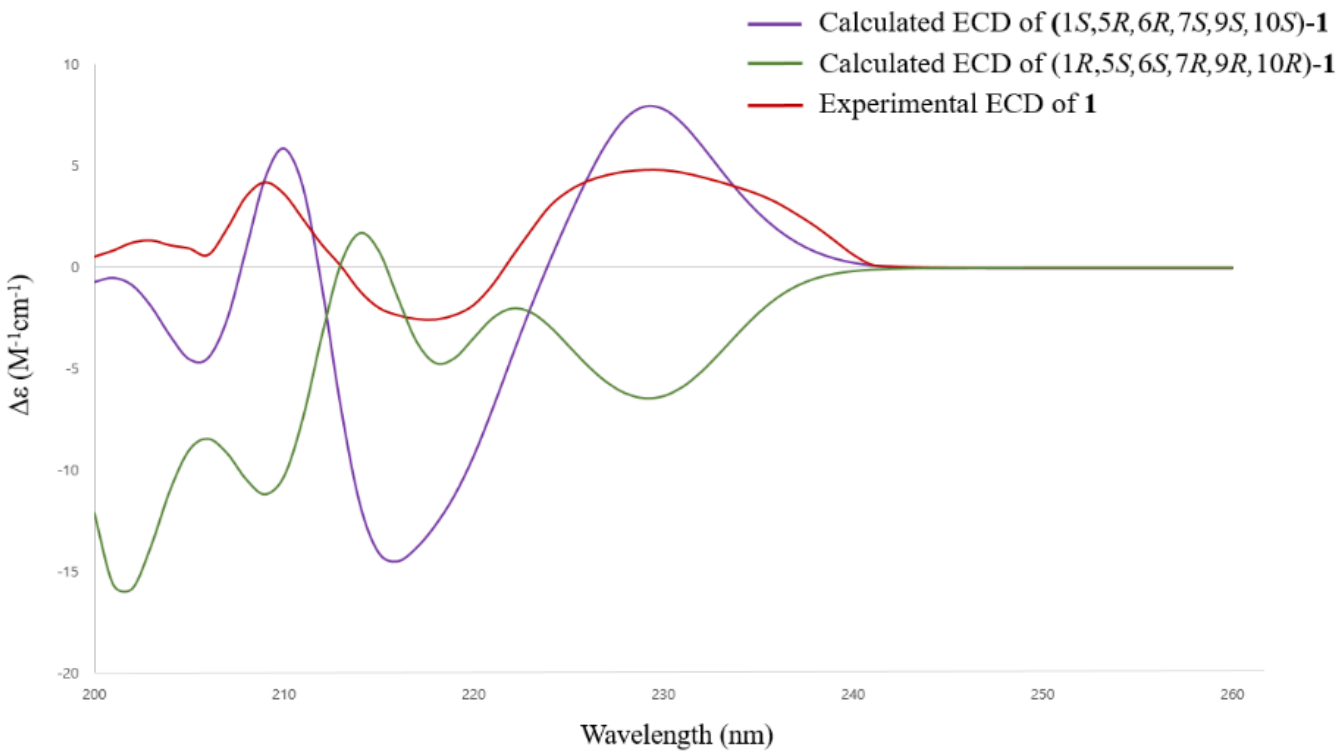

Figure 59. Comparison of experimental and calculated ECD spectra of compound **1**

Table 11. Calculated DFT B3LYP/def-SV(P) free energies, population and theoretical averaged rotary strength values for the major conformers of (1*S*,5*R*,6*R*,7*S*,9*S*,10*S*) of compound **1**

conformer	ΔG[a]	p_i[b]	*n* states[c]											
			1	**2**	**3**	**4**	**5**	**6**	**7**	**8**	**9**	**10**	**11**	**12**
1	0.000	41.5	10.8	6.8	7.0	0.8	-0.1	2.0	0.2	6.4	-9.6	5.9	-3.6	3.2
2	0.031	39.4	-10.3	32	-12.4	-2.2	0.1	-0.4	0.3	-8.4	9.2	-4.7	-4.6	3.1
3	0.506	17.7	-0.1	-1.9	-3.7	-9.8	0.8	-9.6	4.0	6.6	-5.2	-4.8	0.1	3.0
4	2.026	1.3	1.0	-0.2	0.5	0.4	-0.2	0.6	-5.0	7.0	-2.4	-3.4	3.1	2.8
Weighted value			0.4	15.1	-2.6	-2.3	0.1	-1.0	0.8	0.6	-1.3	-0.3	-3.2	3.1
Average wavelength (nm)			186	191	193	194	196	198	202	210	213	216	217	228

[a]DFT B3LYP/def-SV(P) Gibbs free energies in kcal/mol relative to the absolute G value for the global minimum -1880.2327 kcal/mol. [b]In percent from ΔG values at 298 K and 1 atm. $p_i = \frac{e^{-\varepsilon_i/kT}}{\sum_{i=1}^{M} e^{-\varepsilon_i/kT}}$ (K=Boltzmann constant, T = temperature, ε = Energy). [c]DFT B3LYP/def-TZVP rotary strength values.

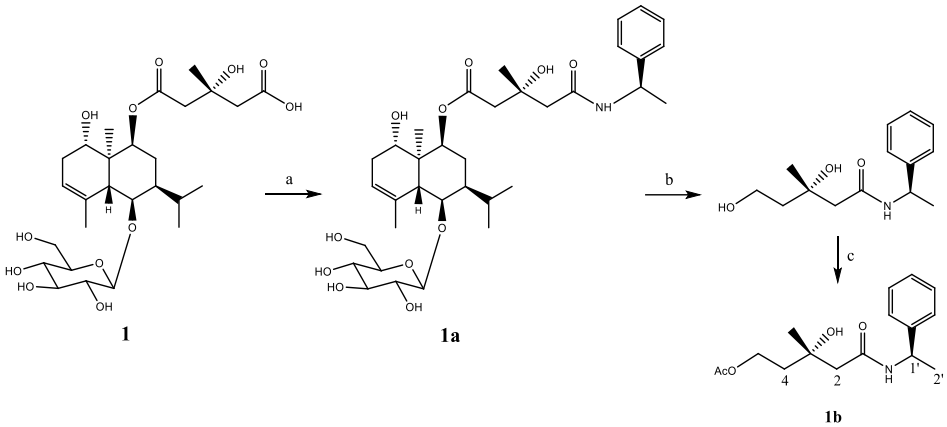

Figure 60. Absolute configuration of the HMG moiety in compound **1**. Steps applied were of amination (a), reduction (b), and acetylation (c). Synthesis of key intermediate **1b**: (a) (*S*)-1-phenylethylamine, PyBOP, Et_3N, HOBt, DMF of 9 h; (b) $LiBH_4$, THF of 24 h; (c) Ac_2O, pyridine of 24 h.

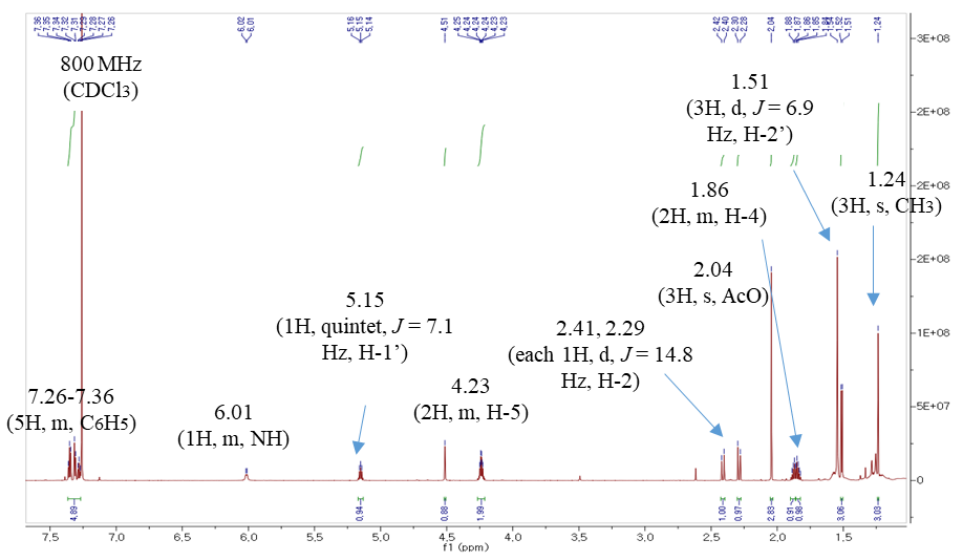

Figure 61. ^{1}H NMR spectrum (chloroform-*d*, 600 MHz) of **1b**

3.2.2. Compound **2**

Compound **2** was isolated as an amorphous powder with $[\alpha]_D^{25}$ 13.8 (*c* 0.3, MeOH) and its molecular formula of $C_{27}H_{44}O_{12}$ was analyzed based on the HRESIMS (*m*/*z* 559.2794 $[M - H]^-$, calcd for $C_{27}H_{43}O_{12}$, 559.2760). Its ^1H and ^{13}C NMR data revealed that compound **2** possesses a similar structure to compound **1** (Figure 62). The major difference found for compound **2** was in the attachment of HMG to C-1 (δ_C 75.7), which was confirmed by a HMBC correlation from H-1 (δ_H 5.17) to C-1" (δ_C 172.6). The HMBC correlation from the anomeric proton (δ_H 4.43) to C-6 (δ_C 77.9) was used to establish the glycosylation position (Figure 63). NOESY correlations peaks of H-1/H-5, H-14/H-6, H-14/H-7, and H-14/H-9 revealed the relative configuration of **2** (Figure 64). To compare the chemical shift of C-1 with those of other analogues, compound **2** was hydrolyzed to remove the HMG moiety from C-1, and yielded **2a**. The chemical shift of C-1 in **2a** proved to be similar to that of previously reported compounds that possess an α-oriented hydroxy group (Hu et al., 2001; Zhang et al., 2003). To determine the absolute configuration of **2**, ECD calculations were applied in which the calculated ECD spectrum of (1*S*,5*R*,6*R*,7*S*,9*S*,10*R*)-**2** and the experimental ECD spectrum were well matched (Table 12 and Figure 65). Therefore, compound **2** was determined structurally as 1α,6β,9β-trihydroxy-5,10-bis-*epi*-eudesm-3-ene-1-*O*-[(*S*)-3"-hydroxy -3"-methylglutaryl]-6-*O*-β-D-glucopyranoside.

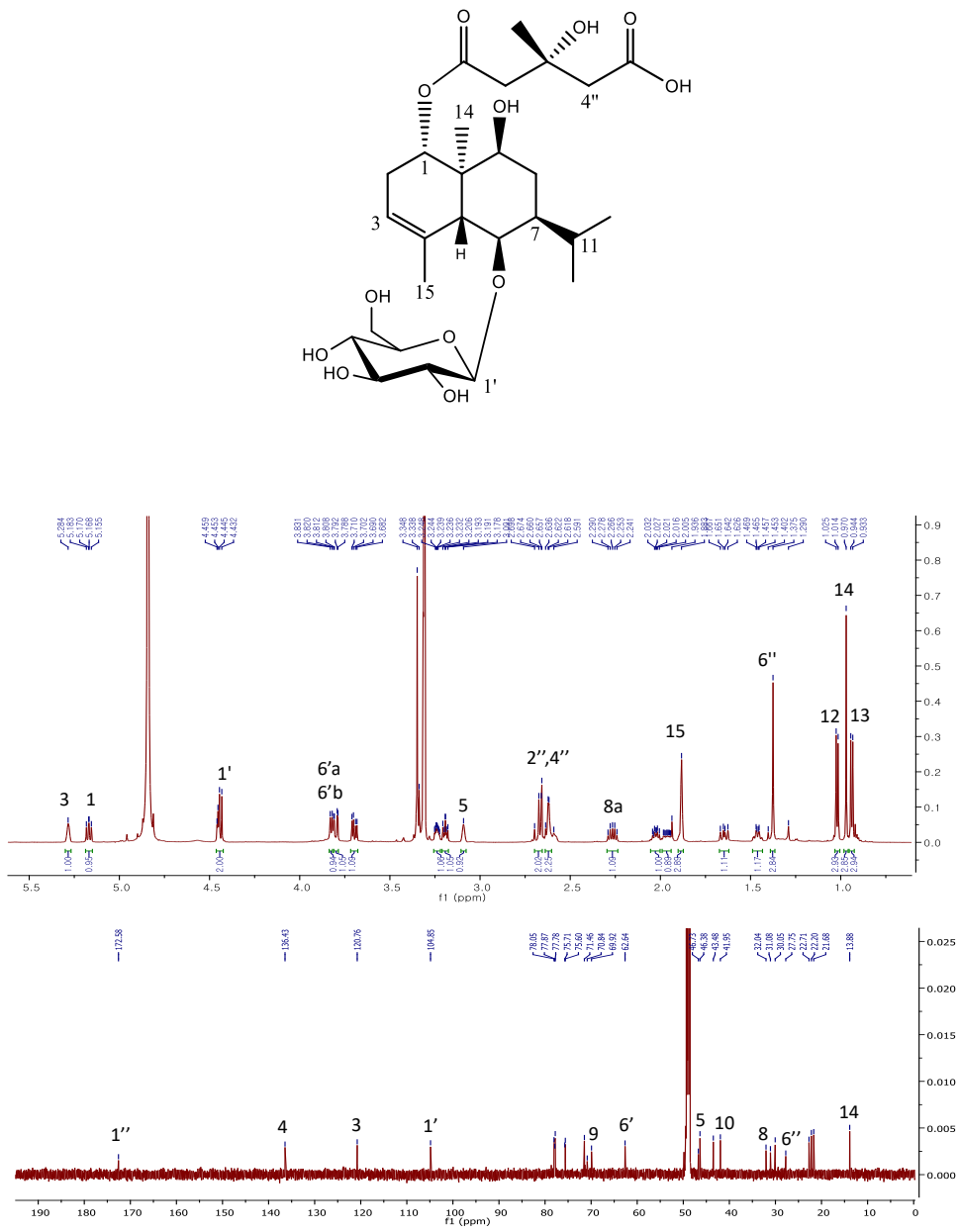

Figure 62. ^{1}H and ^{13}C NMR spectra (CD_3OD, 600/150 MHz) of compound **2**

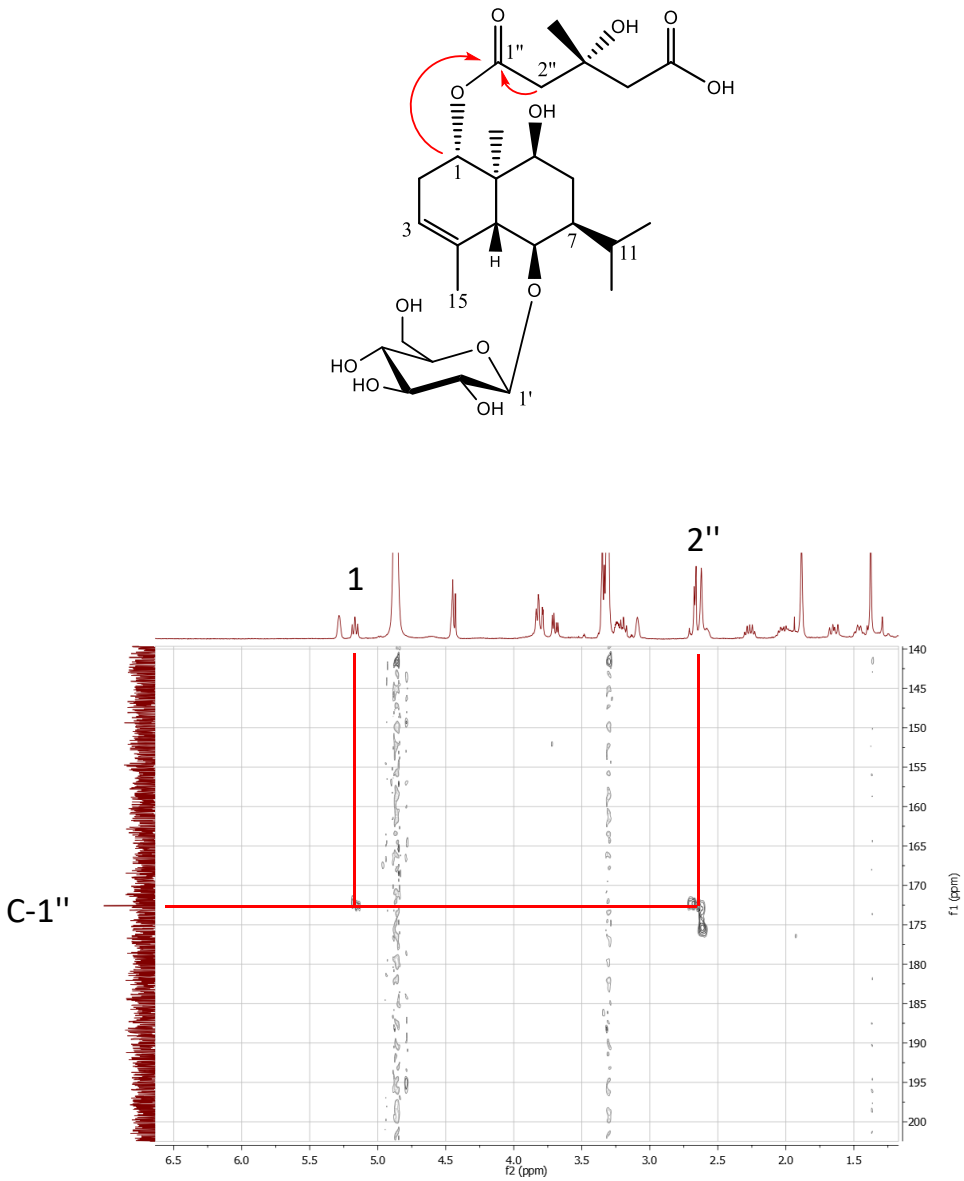

Figure 63. Key HMBC correlations (CD_3OD, 600 MHz) of compound **2**

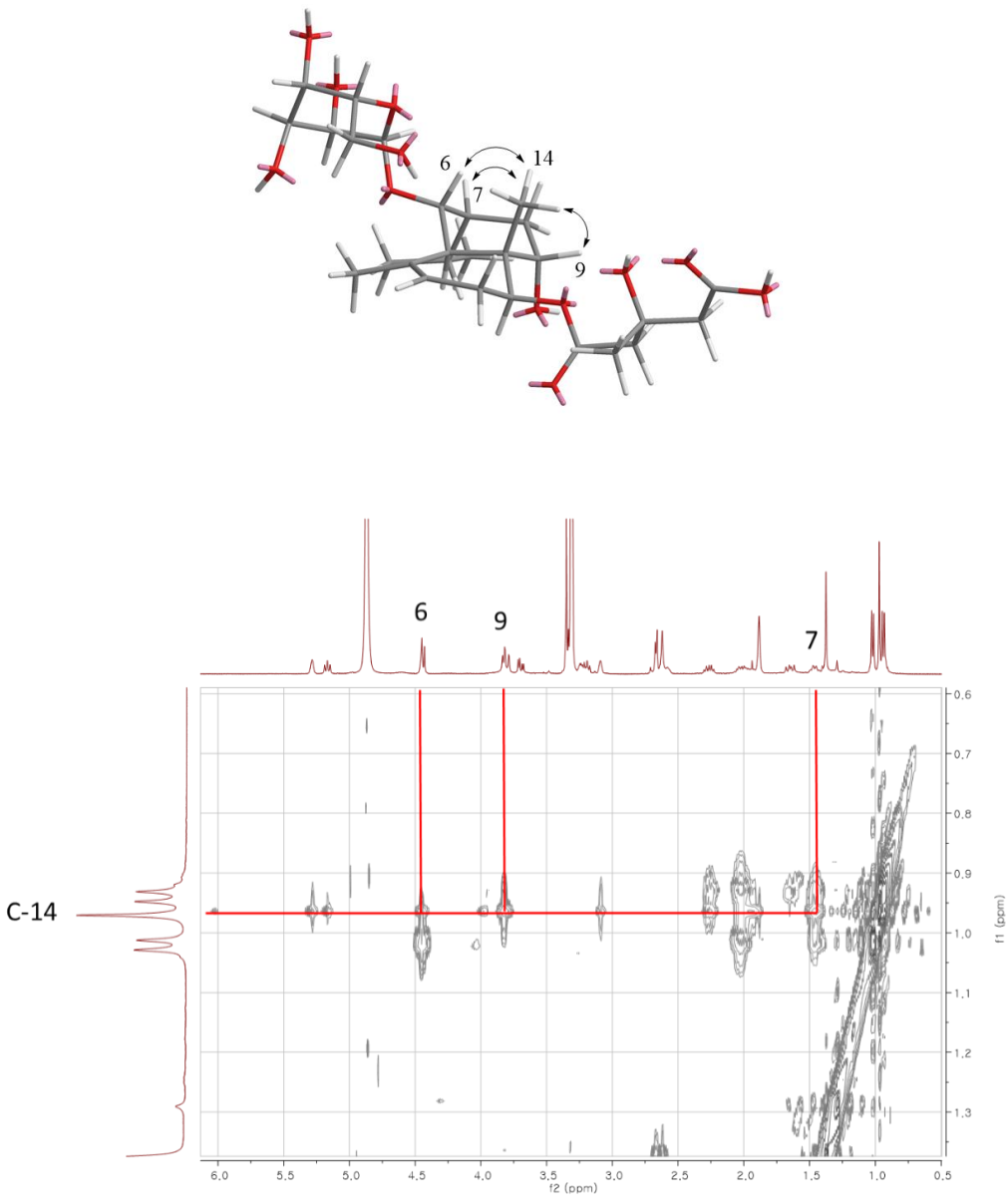

Figure 64. Key NOESY correlations (CD_3OD, 600 MHz) of compound **2**

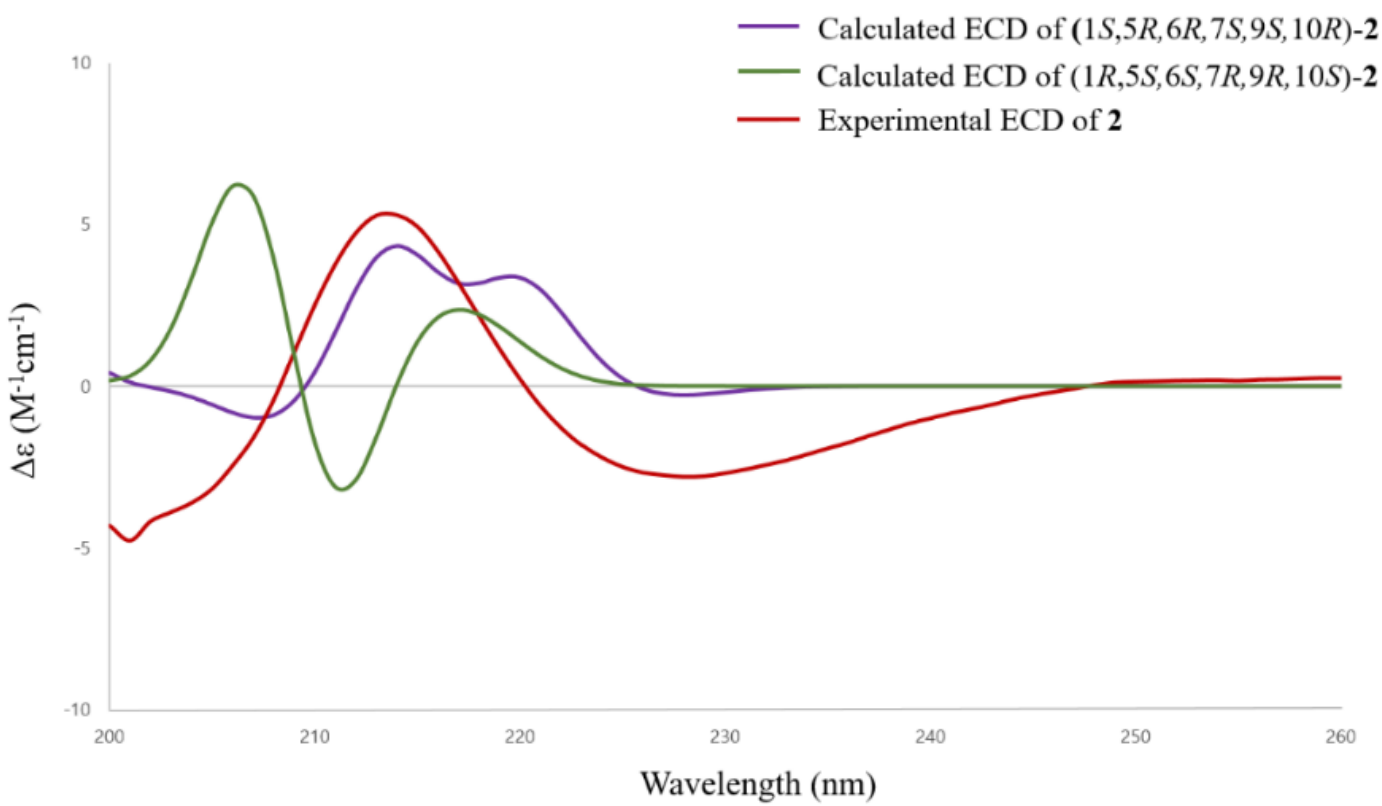

Figure 65. Comparison of experimental and calculated ECD spectra of compound **2**

Table 12. Calculated DFT B3LYP/def-SV(P) free energies, population and theoretical averaged rotary strength values for the major conformers of (1*S*,5*R*,6*R*,7*S*,9*S*,10*R*) of compound **2**

conformer	ΔG[a]	p_i[b]	*n* states[c]											
			1	**2**	**3**	**4**	**5**	**6**	**7**	**8**	**9**	**10**	**11**	**12**
1	0	62.22	0.4	-0.7	3.5	0.6	0.1	-0.4	-0.7	0.3	3.6	-3.8	3.8	-0.2
2	0.378	32.88	-0.2	4.4	-0.2	-0.3	-0.6	-0.1	-0.3	-0.1	2.8	-3.4	4.2	-0.1
3	1.632	3.96	-0.1	2.0	1.1	0.4	-0.2	-0.2	-0.6	0.2	2.7	-2.7	3.5	-0.3
4	2.485	0.94	0.1	-0.1	0.5	0.2	-0.1	-0.1	-0.2	0.1	2.1	-2.1	2.7	1.0
Weighted value			0.2	1.1	2.2	0.3	-0.1	-0.3	-0.6	0.2	3.3	-3.6	3.9	-0.2
Average wavelength (nm)			190.1	192.4	195.0	196.8	197.0	204.3	208.2	213.2	214.8	217.1	219.0	226.8

[a]DFT B3LYP/def-SV(P) Gibbs free energies in kcal/mol relative to the absolute G value for the global minimum -1987.2041 kcal/mol. [b]In percent from ΔG values at 298 K and 1 atm. $p_i = \frac{\varepsilon_i^{-\varepsilon_i/kT}}{\sum_{i=1}^{M} \varepsilon_i^{-\varepsilon_i/kT}}$ (K=Boltzmann constant, T = temperature, ε = Energy). [c]DFT B3LYP/def-TZVP rotary strength values.

3.2.3. Compound **3**

Compound **3**, an amorphous powder with $[\alpha]_D^{25}$ 1.7 (*c* 0.5, MeOH) gave a molecular formula of $C_{27}H_{44}O_{11}$ from the HRESIMS ion peak at *m*/*z* 543.2820 $[M - H]^-$ (calcd for $C_{27}H_{43}O_{11}$, 543.2811). The NMR data of compound **3** showed similar patterns to those of 9*β*-*O*-(*E*-*p*-hydroxycinnamoyl)-1*β*,6*β*-dihydroxy-*trans*-eudesm-3-en-6-*O*-*β*-D-glucopyranoside isolated from *Aster koraiensis*, except for the presence of the HMG moiety and the absence of a hydroxycinnamoyl group (Lee et al., 2012) (Figure 66). The HMBC correlations from H-1 (δ_H 4.78) to C-1" (δ_C 172.5) and from an anomeric proton (δ_H 4.43) to C-6 (δ_C 75.2) suggested that the HMG unit and the glucopyranosyl group are located at C-1 and C-6, respectively (Figure 67). The relative configuration of compound **3** was suggested based on the NOESY cross-peaks (Figure 68). In the NOESY spectrum, H-1 (δ_H 4.78) showed a correlation with H-5 (δ_H 2.57), whereas H-14 (δ_H 0.99) gave correlations with H-6 (δ_H 4.41) and H-7 (δ_H 1.90). Acid hydrolysis of **3** yielded **3a.** The chemical shift at C-1 (δ_C 77.3) of compound **3a** was well matched with previous studies for compounds in which C-1 (δ_C 79.4) with a *β*-oriented hydroxy group is shifted downfield compared to C-1 (δ_C 72.1) in analogues with an *α*-oriented hydroxy group (Hu et al., 2001; Chernenko et al., 1994). Thus, H-1 was deduced to be *α*-oriented, while H-6 and H-7 were found to have a *β*-orientation. Furthermore, the *β*-oriented hydroxy group at C-1 showed a *γ*-gauche shielding effect over H_3-14, which, in turn, resulted in an upfield chemical shift of C-14. The absolute configuration of compound **3** was determined by ECD calculations. The experimental ECD spectrum of compound **3** was in good agreement with the calculated spectrum of 1*R*,5*S*,6*S*,7*R*,10*R* of **3** (Table 13 and

Figure 69). Therefore, compound **3** was assigned as 1*β*,6*α*-dihydroxy-7-*epi*-eudesm-3-ene-1-*O*-[(*S*)-3"-hydroxy-3"-methylglutaryl]-6-*O*-*β*-D-glucopyranoside.

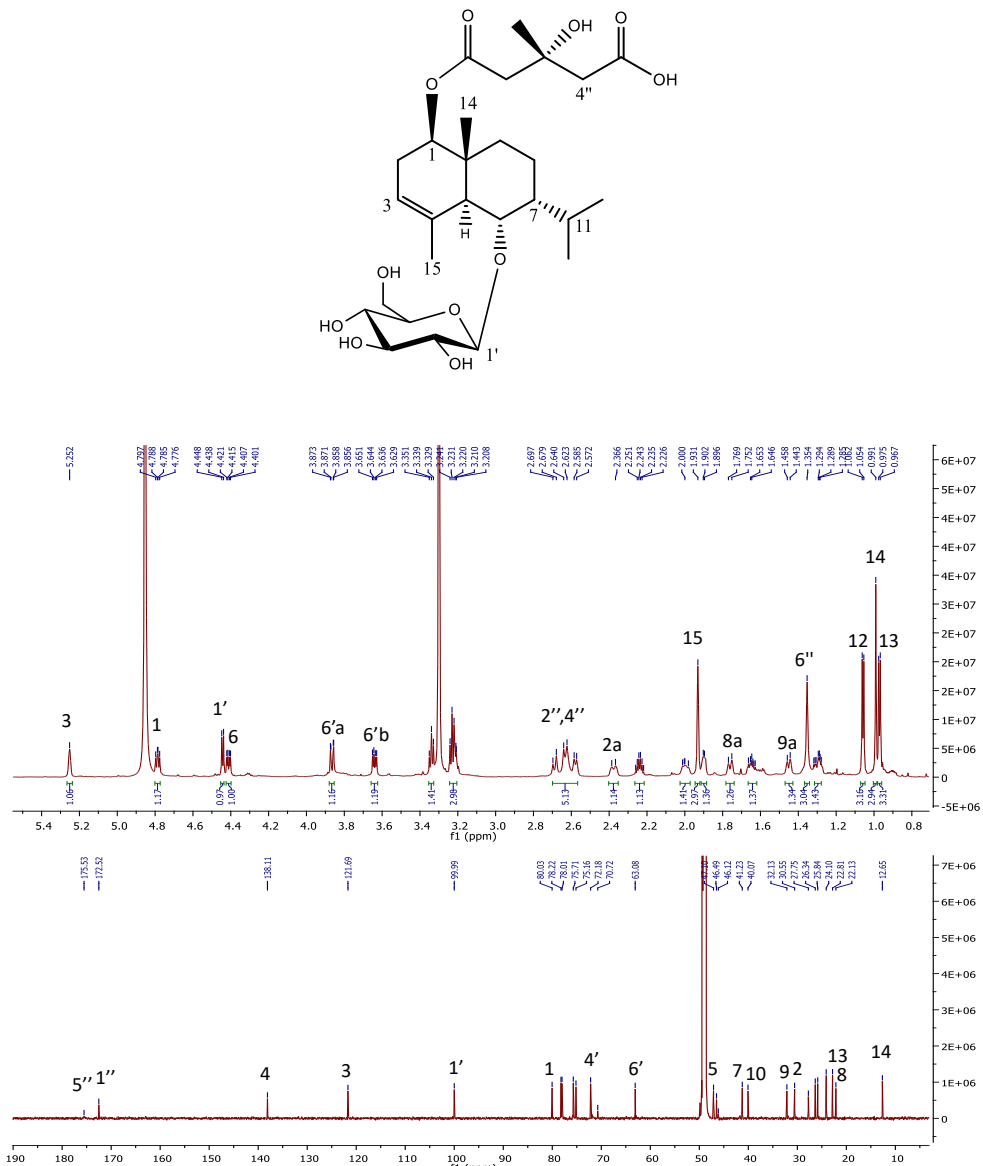

Figure 66. ^{1}H and ^{13}C NMR spectra (CD_3OD, 600/150 MHz) of compound **3**

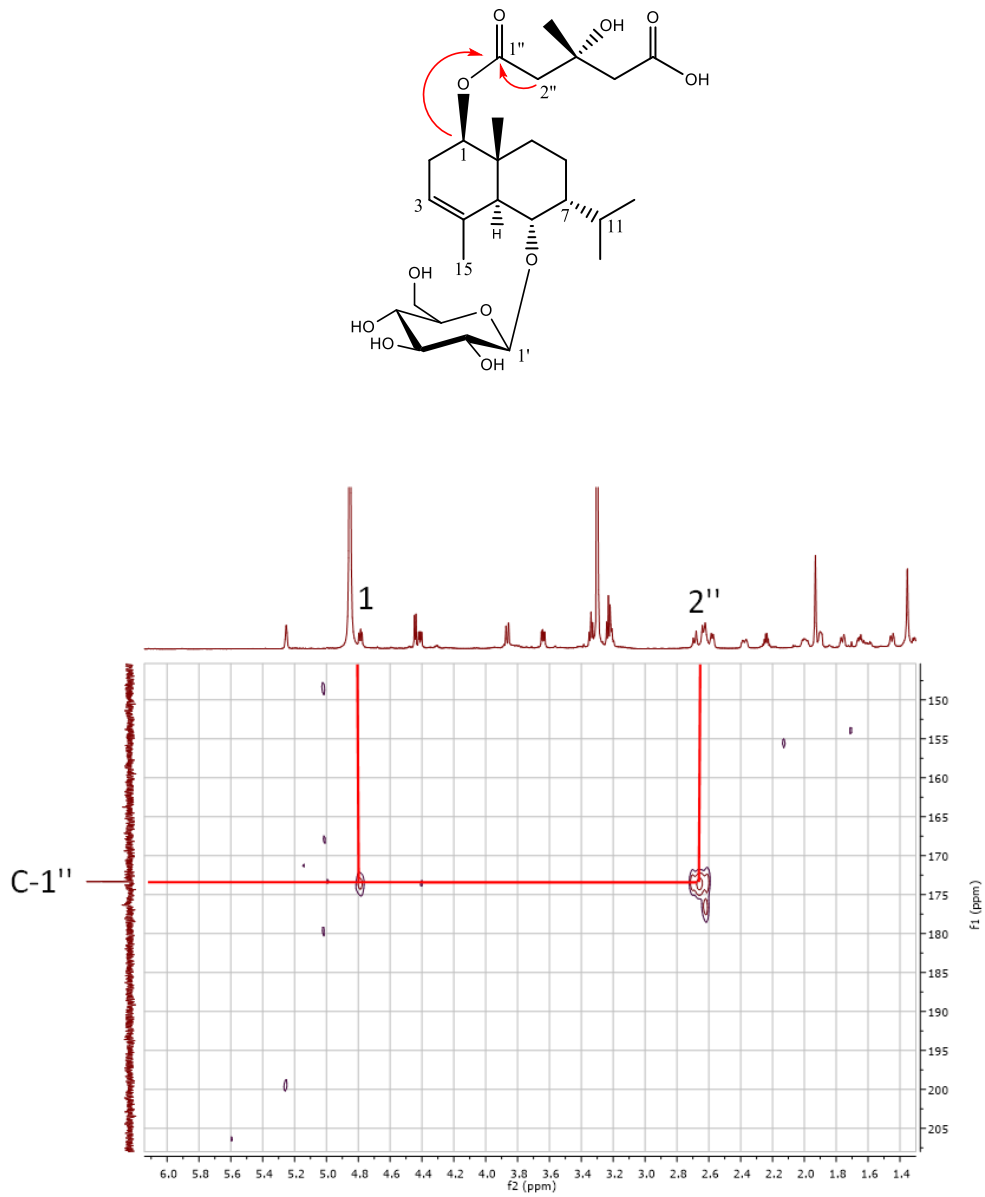

Figure 67. Key HMBC correlations (CD_3OD, 600 MHz) of compound **3**

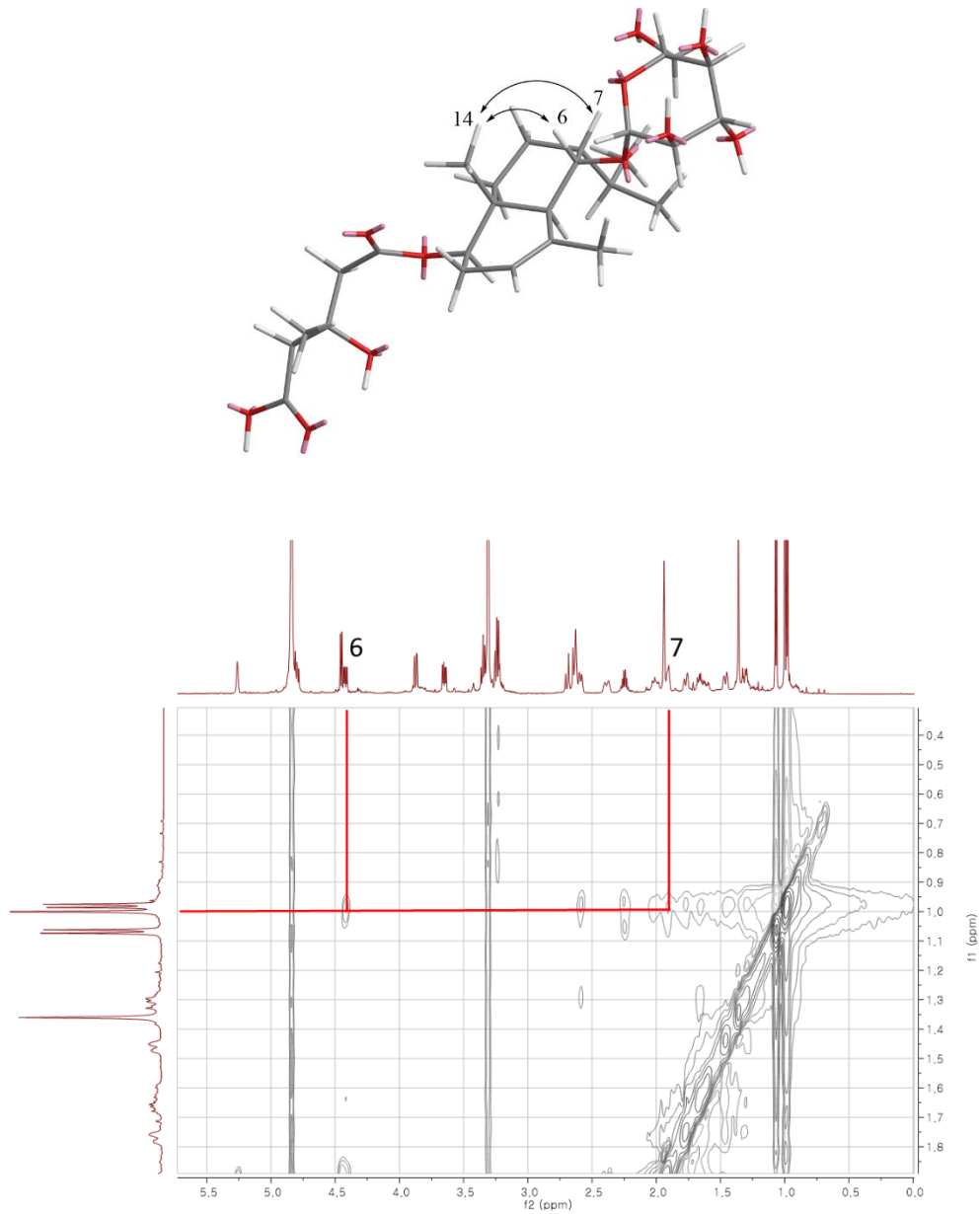

Figure 68. Key ROESY correlations (CD_3OD, 600 MHz) of compound **3**

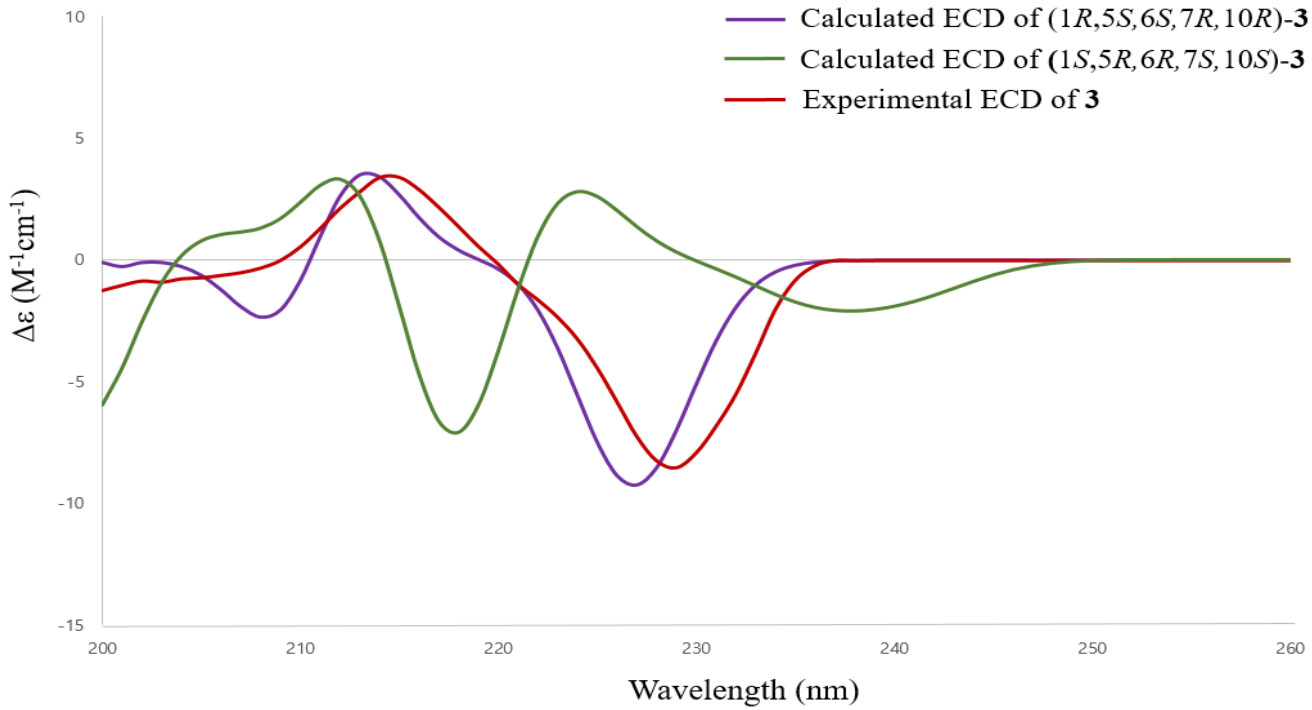

Figure 69. Comparison of experimental and calculated ECD spectra of compound **3**

Table 13. Calculated DFT B3LYP/def-SV(P) free energies, population and theoretical averaged rotary strength values for the major conformers of (1*R*,5*S*,6*S*,7*R*,10*R*) of compound **3**

conformer	ΔG[a]	p_i[b]	*n* states[c]											
			1	**2**	**3**	**4**	**5**	**6**	**7**	**8**	**9**	**10**	**11**	**12**
1	0	47.00	-0.4	-1.4	-10.5	-3.9	1.5	-0.7	-0.6	0.9	-2.5	3.5	-0.9	-5.3
2	0.195	33.84	0.4	0.1	-9.8	-1.4	-1.3	1.7	0.1	0.2	-3.0	3.4	0.3	-6.1
3	0.969	9.17	-1.9	-0.5	-4.7	-9.4	2.4	0.4	0.1	-0.4	-2.4	3.3	-0.6	-6.1
4	1.008	8.57	-1.0	0.2	-5.0	-2.4	1.2	0.5	0.2	0.4	-2.1	3.0	-0.1	-4.9
Weighted value			-0.3	-0.7	-9.1	-3.4	0.6	0.3	-0.2	0.5	-2.6	3.4	-0.4	-5.5
Average wavelength (nm)			183.6	184.5	187.2	184.5	188.8	192.4	198.2	204.4	206.5	209.3	223.5	223.7

[a]DFT B3LYP/def-SV(P) Gibbs free energies in kcal/mol relative to the absolute G value for the global minimum -1880.2327 kcal/mol. [b]In percent from ΔG values at 298 K and 1 atm. $p_i = \frac{e^{-\varepsilon_i/kT}}{\sum_{i=1}^{M} e^{-\varepsilon_i/kT}}$ (K=Boltzmann constant, T = temperature, ε = Energy). [c]DFT B3LYP/def-TZVP rotary strength values.

3.2.4. Compound **4**

Compound **4**, an amorphous powder with $[\alpha]_D^{25}$ 31.8 (*c* 0.3, MeOH), was determined to have a molecular formula of $C_{29}H_{46}O_{13}$, as suggested by the HRESIMS peaks at *m/z* 601.2876 $[M - H]^-$ (calcd for $C_{29}H_{45}O_{13}$, 601.2866). The IR absorption of compound **4** indicated the presence of hydroxy (3389 cm^{-1}), carbonyl (1731 cm^{-1}), and olefinic (1615 cm^{-1}) groups. NMR pattern of **4** was similar to that of **1**, and compound **4** was found to possess an acetyl group linked to the glucopyranoside moiety (Figures 70-71). The HMBC correlations from the signals of H-6a' (δ_H 4.41) and the acetyl group (δ_H 2.04) to the acetate carbonyl carbon (δ_C 172.7) suggested that this acetyl group is attached to C-6' of the glucose (Figure 72). The 6-*O*-acetyl-*β*-D-glucopyranosyl unit was determined to be at C-6 of the aglycone by the HMBC correlation from the anomeric proton (δ_H 4.43) to C-6 (δ_C 78.0). In addition, the position of the HMG moiety was deduced by the HMBC correlation from H-9 (δ_H 4.99) to C-1" (δ_C 172.8). The relative configuration of **4** was assigned based on the NOESY cross-peaks from H-1 (δ_H 3.91) to H-5 (δ_H 3.03) and from H-14 (δ_H 0.92) to H-6 (δ_H 4.40), H-7 (δ_H 1.54), and H-9 (δ_H 4.99) (Figure 73). Experimental ECD and calculated spectra gave the absolute configuration of compound **4** as 1*S*,5*R*,6*R*,7*S*,9*S*,10*S* (Table 14 and Figure 74). Thus, compound **4** was characterized as 1*α*,6*β*,9*β*-trihydroxy-5,10-bis-*epi*-eudesm-3-ene-9-*O*-[(*S*)-3"-hydroxy-3"-methylglutaryl]-6-*O*-(6′-*O*-acetyl)-*β*-D-glucopyranoside.

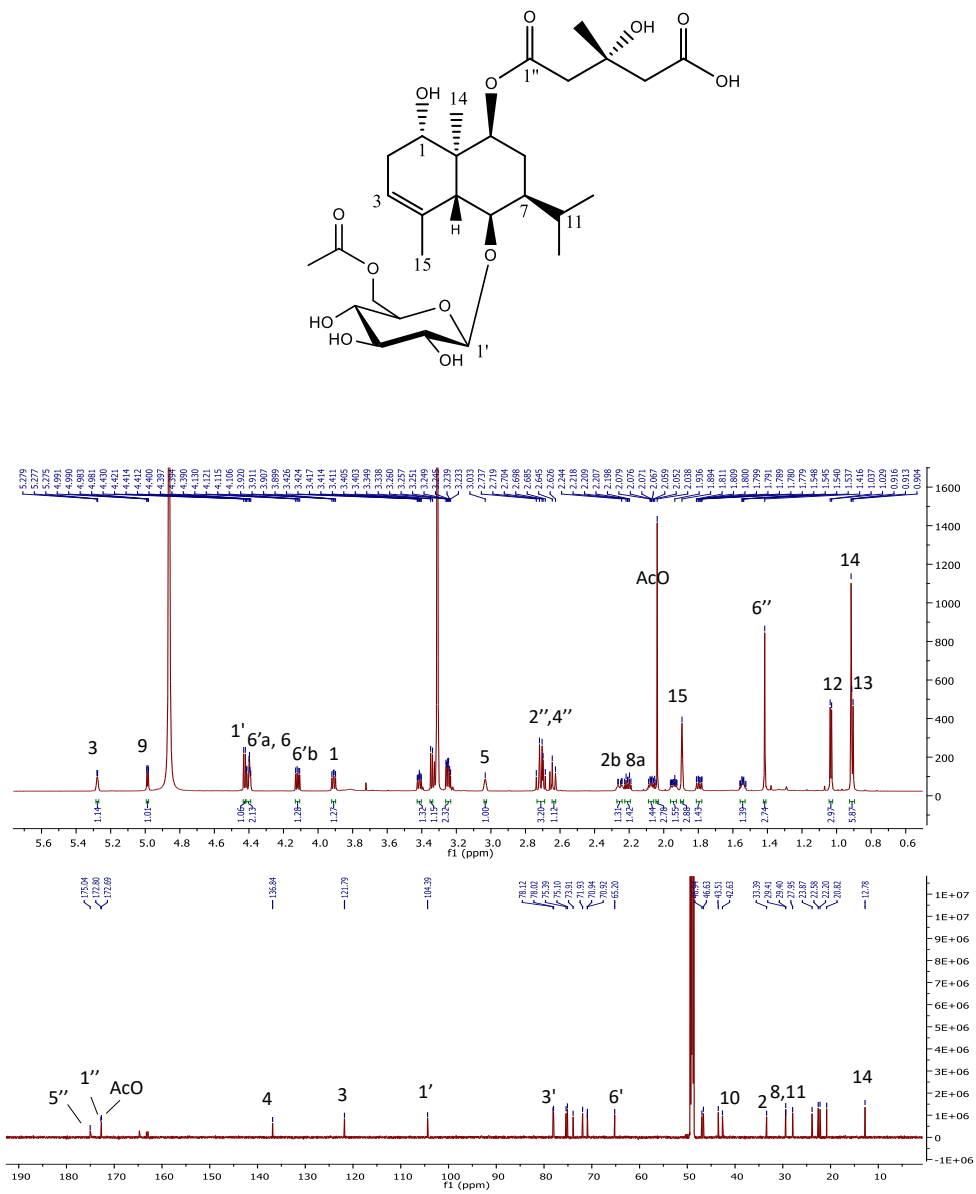

Figure 70. ^{1}H and ^{13}C NMR spectra (CD_3OD, 800/200 MHz) of compound **4**

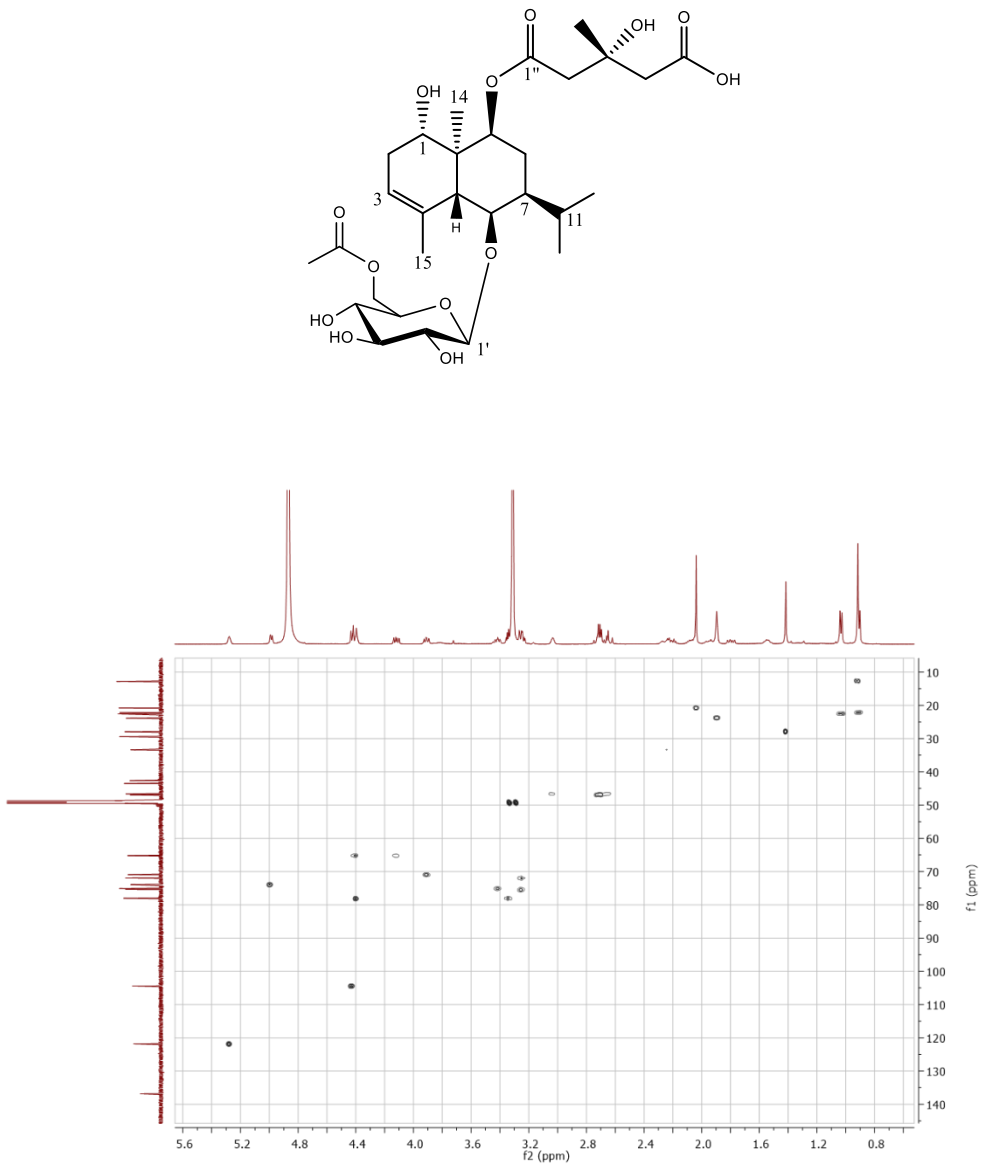

Figure 71. HSQC spectrum (CD_3OD, 800 MHz) of compound **4**

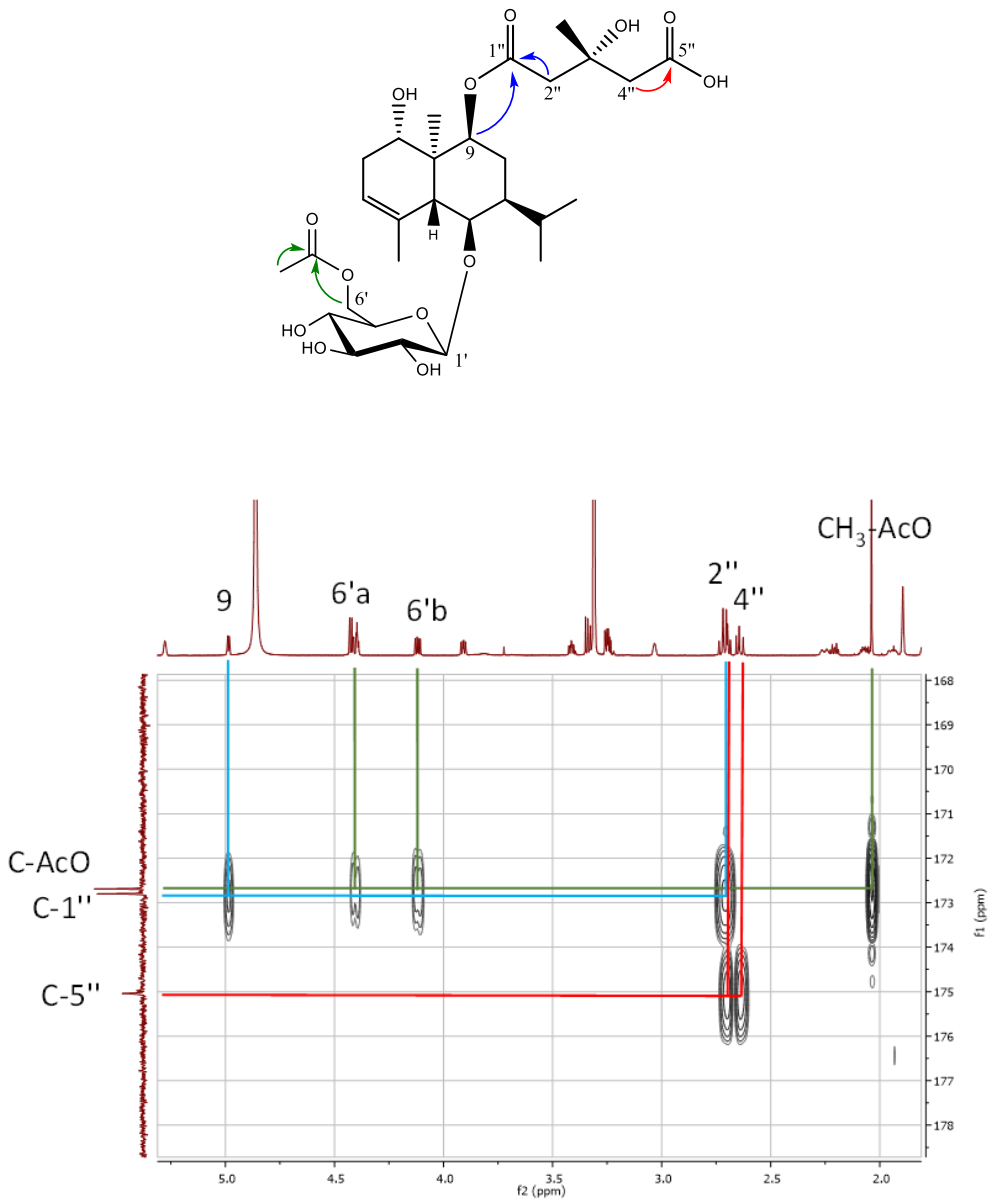

Figure 72. Key HMBC correlations (CD_3OD, 800 MHz) of compound **4**

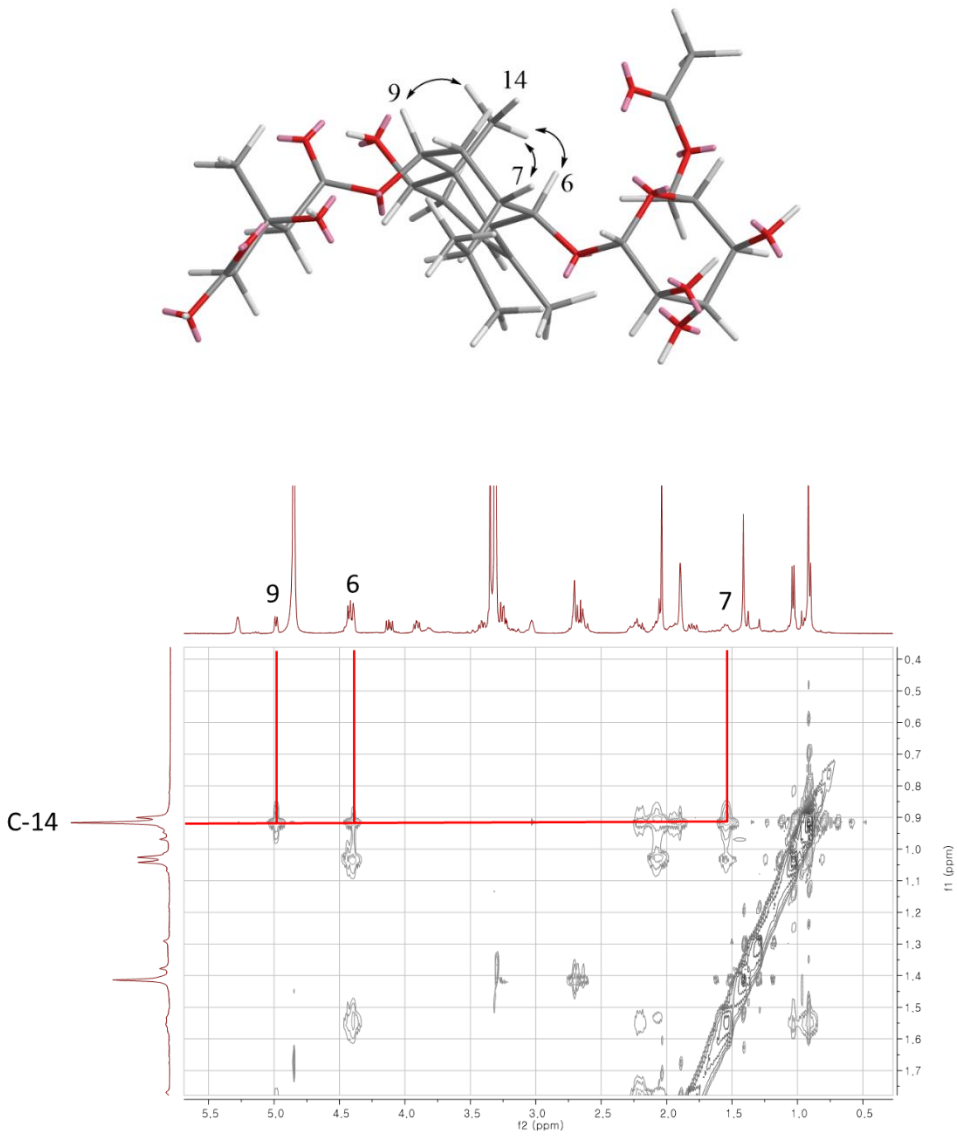

Figure 73. Key ROESY correlations (CD_3OD, 800 MHz) of compound **4**

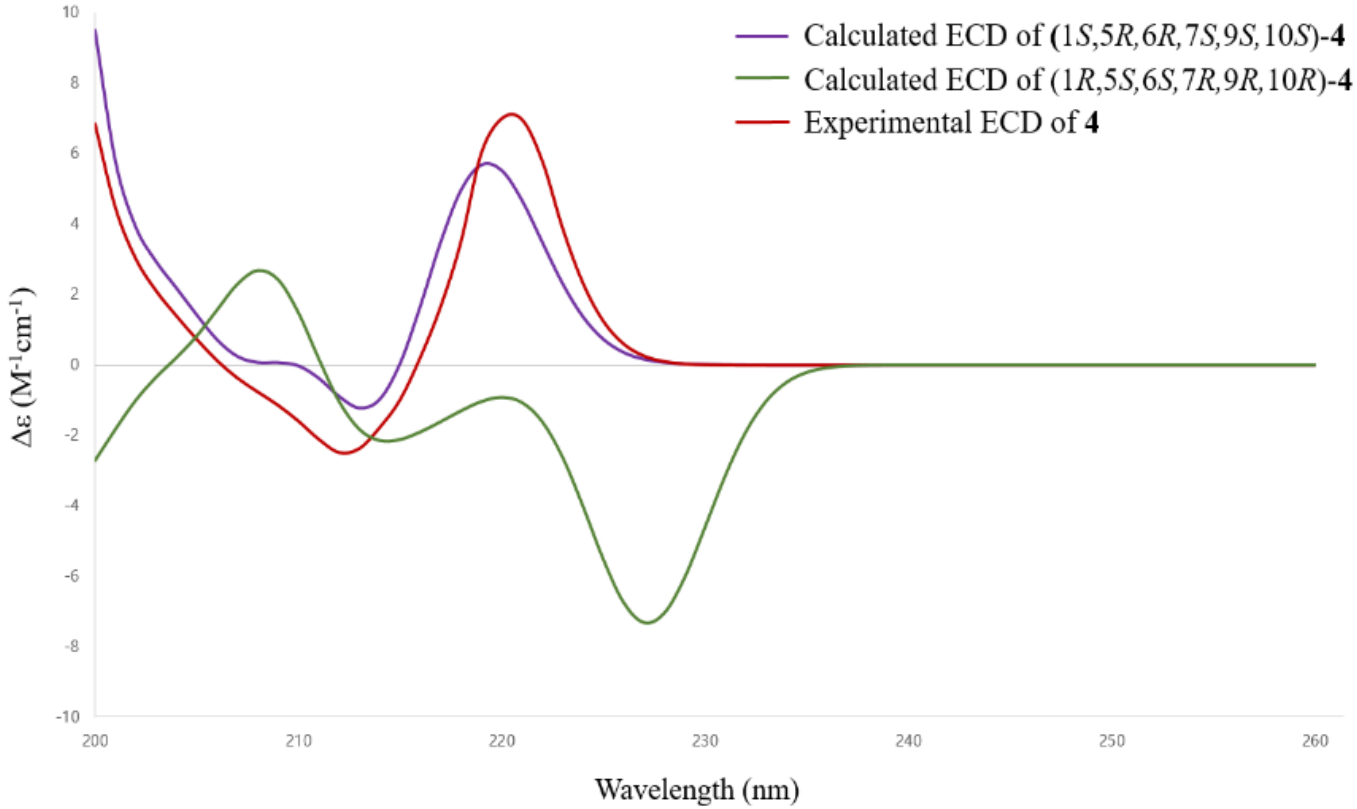

Figure 74. Comparison of experimental and calculated ECD spectra of compound **4**

Table 14. Calculated DFT B3LYP/def-SV(P) free energies, population and theoretical averaged rotary strength values for the major conformers of (1*S*,5*R*,6*R*,7*S*,9*S*,10*S*) of compound **4**

conformer	ΔG[a]	p_i[b]	*n* states[c]											
			1	**2**	**3**	**4**	**5**	**6**	**7**	**8**	**9**	**10**	**11**	**12**
1	0.000	31.2	0.1	-1.4	35.7	3.7	5.2	0.9	0.2	-0.4	0.6	-2.9	4.9	2.7
2	0.011	30.7	0.5	-1.5	32.5	3.5	5.3	1.3	0.1	-0.4	-2.6	0.5	5.1	2.5
3	0.065	28.0	-0.1	12.3	18.9	4.1	0.8	-1.7	2.2	0.3	-0.2	0.3	-2.0	-0.6
4	0.960	6.2	2.9	-1.6	-0.6	4.2	0.7	0.7	1.4	6.1	0.4	-15.2	0.2	-0.3
Weighted value			0.3	2.4	26.4	3.6	3.5	0.2	0.8	0.2	-0.6	-1.6	2.5	1.4
Average wavelength (nm)			190	191	193	195	197	202	202	208	213	213	218	220

[a]DFT B3LYP/def-SV(P) Gibbs free energies in kcal/mol relative to the absolute G value for the global minimum -1880.2327 kcal/mol. [b]In percent from ΔG values at 298 K and 1 atm. $p_i = \frac{e^{-\varepsilon_i/kT}}{\sum_{i=1}^{M} e^{-\varepsilon_i/kT}}$ (K=Boltzmann constant, T = temperature, ε = Energy). [c]DFT B3LYP/def-TZVP rotary strength values.

3.2.5. Compound **5**

Compound **5** was obtained as a colorless gum with $[\alpha]_D^{25}$ −2.0 (*c* 0.5, MeOH), and analyzed for the molecular formula of $C_{26}H_{44}O_{12}$ based on the HRESIMS ion peak at *m*/*z* 593.2812 $[M + HCOO]^-$ (calcd for $C_{27}H_{45}O_{14}$, 593.2815). The IR absorption of compound **5** indicated the presence of hydroxy (3410 cm^{-1}) and olefinic (1620 cm^{-1}) groups. The chemical structure of **5** proved to be similar to that of compound **2** except for the attachment of the arabinopyranosyl unit at C-1 (Figures 75-76). This was confirmed by the HMBC correlations from H-1' (δ_H 4.37) to C-1 (δ_C 82.1) and from H-1 (δ_H 4.01) to C-1' (δ_C 105.9) (Figure 77). The ROESY spectrum showed the correlations between H-1 (δ_H 4.01) and H-5 (δ_H 2.97), and between H-6 (δ_H 4.43), H-7 (δ_H 1.46), and H-14 (δ_H 0.91) (Figure 78). Acid hydrolysis of **5** gave **5a** for which the ^{13}C NMR data were identical with those of **1c** (Table 15). Reversed-phase HPLC analysis (co-injection) also demonstrated that **5a** is the same as **1c** (Figure 79). Therefore, compound **5** was defined as 1*α*,6*β*,9*β*-trihydroxy-5,10-bis-*epi*-eudesm-3-ene-1-*O*-α-L-arabinopyranosyl-6-*O*-*β*-D-glucopyranoside.

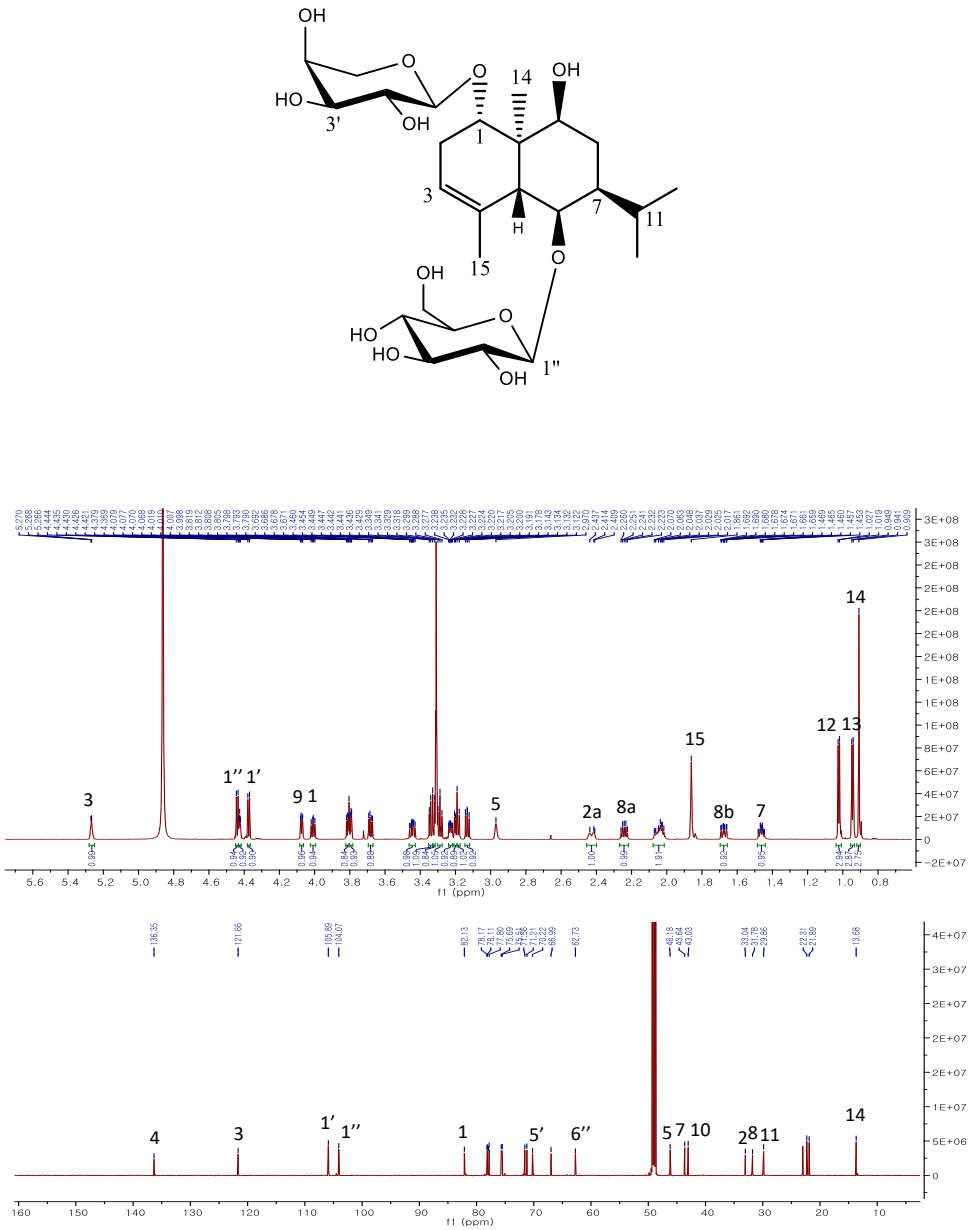

Figure 75. ^{1}H and ^{13}C NMR spectra (CD_3OD, 800/200 MHz) of compound **5**

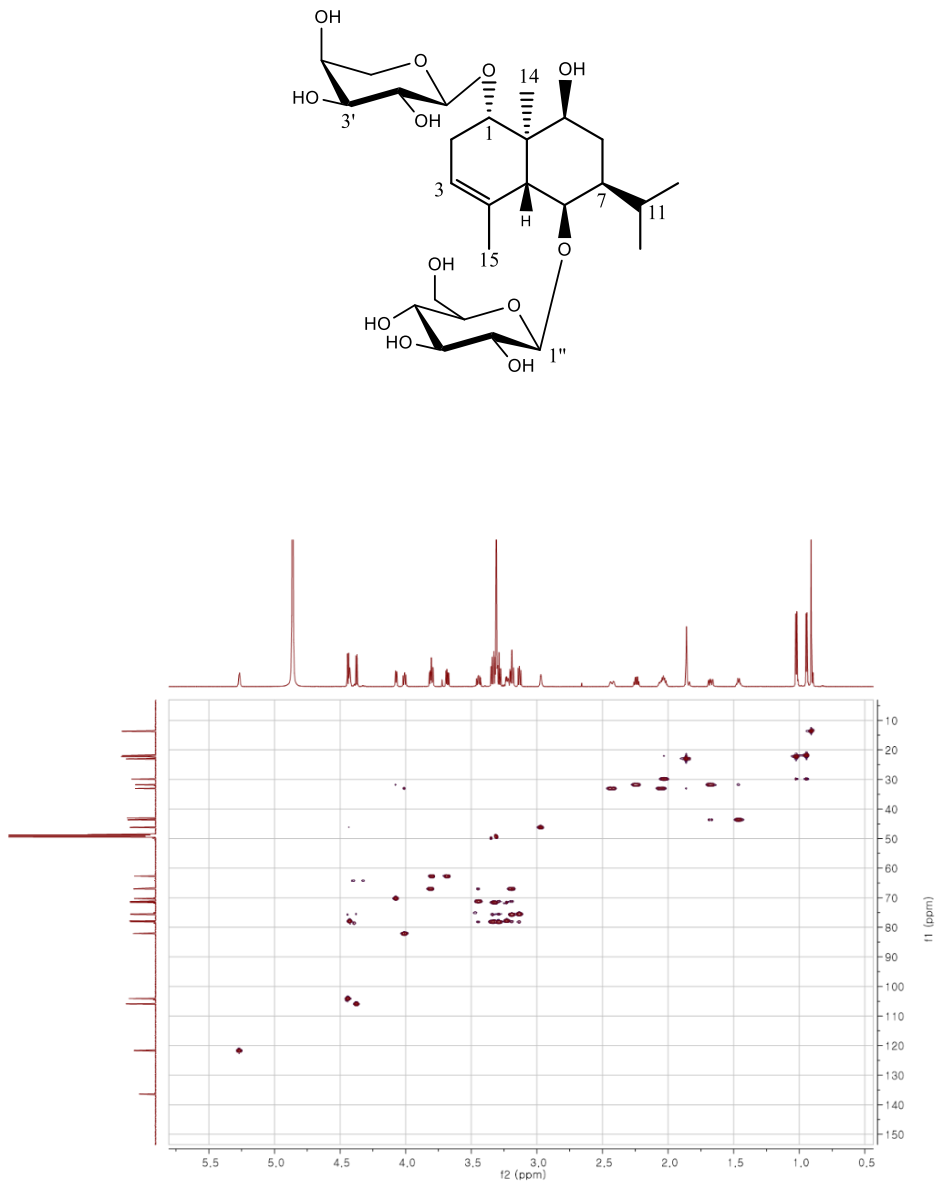

Figure 76. HSQC spectrum (CD_3OD, 800 MHz) of compound **5**

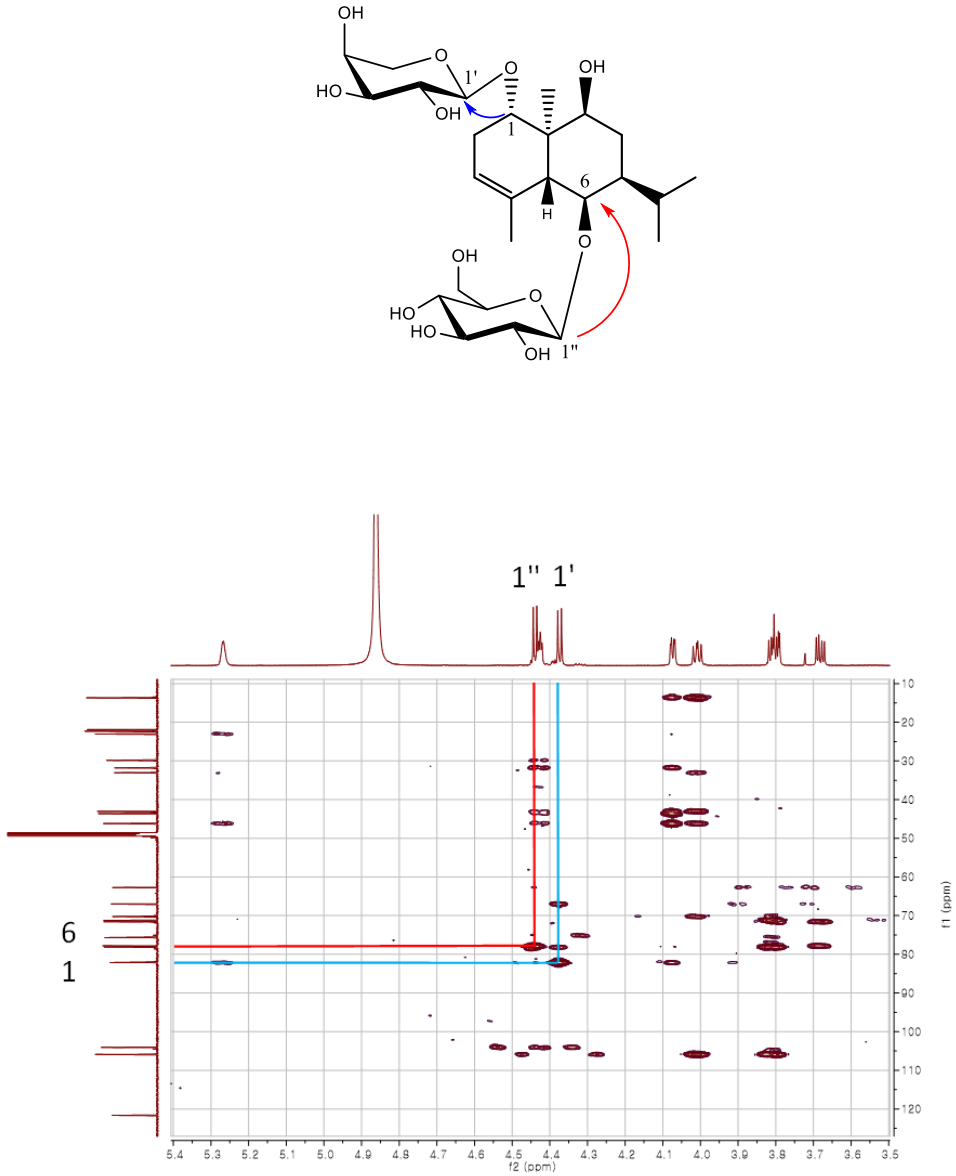

Figure 77. Key HMBC correlations (CD_3OD, 800 MHz) of compound **5**

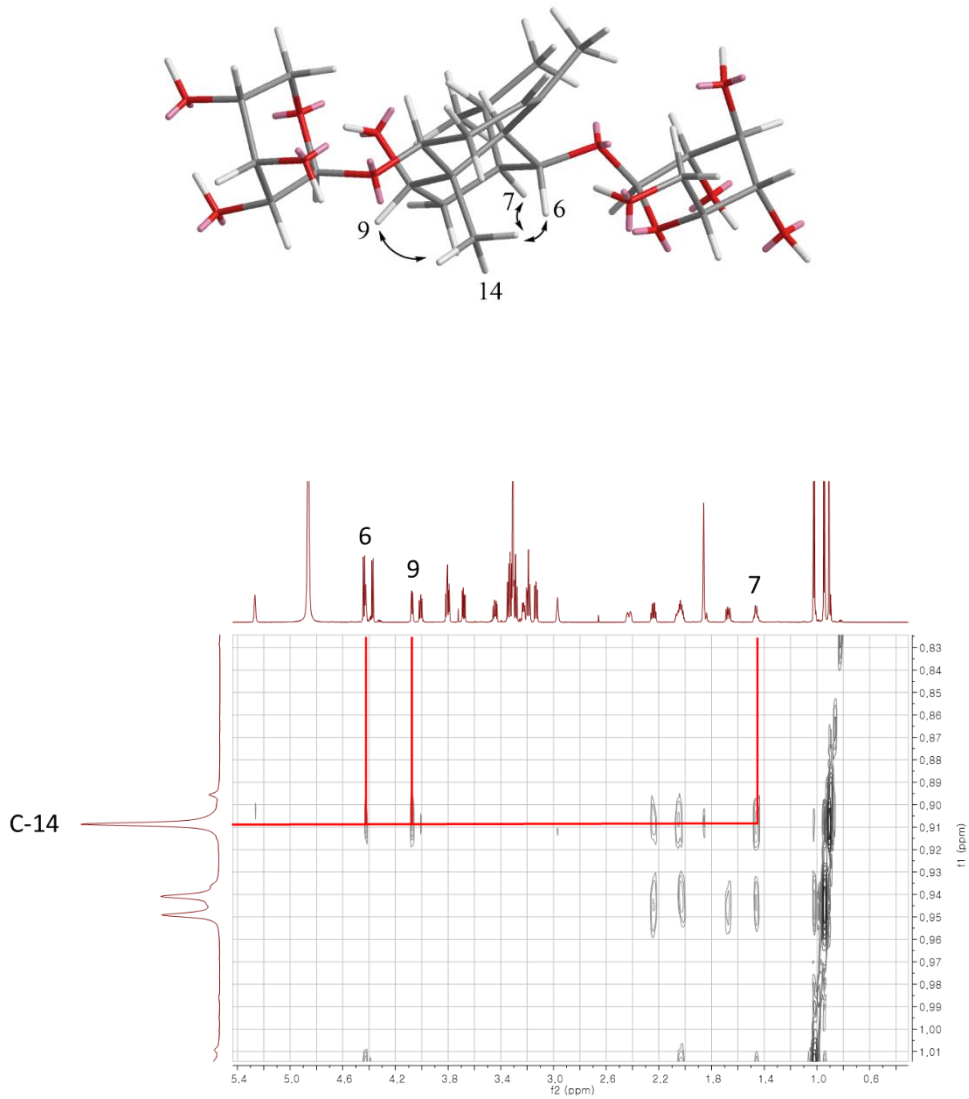

Figure 78. Key ROESY correlations (CD_3OD, 800 MHz) of compound **5**

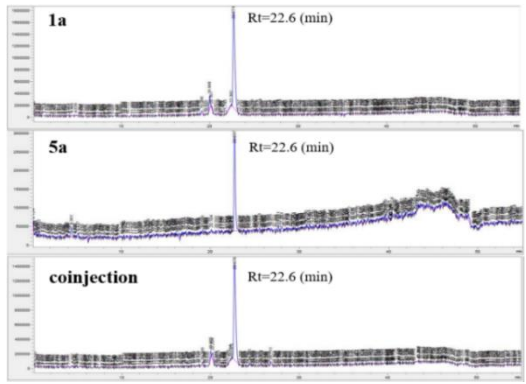

Figure 79. Reversed-phase HPLC analysis of **1c** (a)**, 5a** (b), and co-injection (c)

No	Compound 1c	Compound 5a
1	71.7, CH	71.7, CH
2	34.0, CH_2	33.9, CH_2
3	121.6, C	121.6, C
4	136.1, C	136.1, C
5	46.7, C	46.7, C
6	78.4, CH	78.4, CH
7	43.7, CH	43.7, CH
8	32.4, CH_2	32.4, CH_2
9	70.4, CH	70.4, CH
10	42.9, C	42.9, C
11	30.2, CH	30.2, CH
12	21.6, CH_3	21.6, CH_3
13	22.1, CH_3	22.1, CH_3
14	12.7, CH_3	12.7, CH_3
15	22.6, CH_3	22.6, CH_3
1′	104.9, CH	104.9, CH
2′	75.7, CH	75.7, CH
3′	78.1, CH	78.4, CH
4′	71.5, CH	71.5, CH
5′	77.8, CH	77.8, CH
6′	62.7, CH_2	62.7, CH_2

Table 15.^{13}C NMR data (methanol-d_4, 125 MHz) of compound **1c** and **5a**

3.2.6. Compound **6**

Compound **6** was isolated as an amorphous powder with $[\alpha]_D^{25}$ 1.7 (*c* 0.2, MeOH). HRESIMS analysis suggested a molecular formula of $C_{21}H_{36}O_8$, based on the $[M + HCOO]^-$ peak at *m*/*z* 461.2382, calcd for $C_{22}H_{37}O_{10}$, (*m*/*z* 461.2392). All the NMR data suggested that compound **6** was similar with compound **1** except for the absence of HMG (Figures 80-82). The ^{13}C NMR data of **6** were identical with those of **1c** and co-injection by reversed-phase HPLC analysis confirmed that compound **6** is identical to **1c**. Furthermore, same optical rotation value of compounds **1c** (1.7) and **6** (1.7) confirmed the identical of these two compounds. Therefore, compound **6** was determined as 1*α*,6*β*,9*β*-trihydroxy-5,10-bis-*epi*-eudesm-3-ene-6-*O*-*β*-D-glucopyranoside.

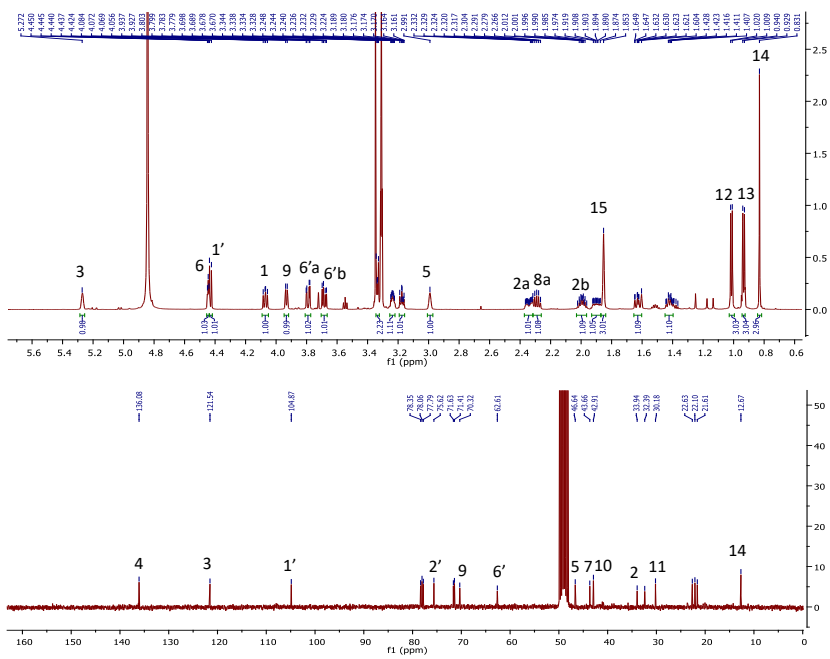

Figure 80. ^1H and ^{13}C NMR spectra (CD_3OD, 600/150 MHz) of compound **6**

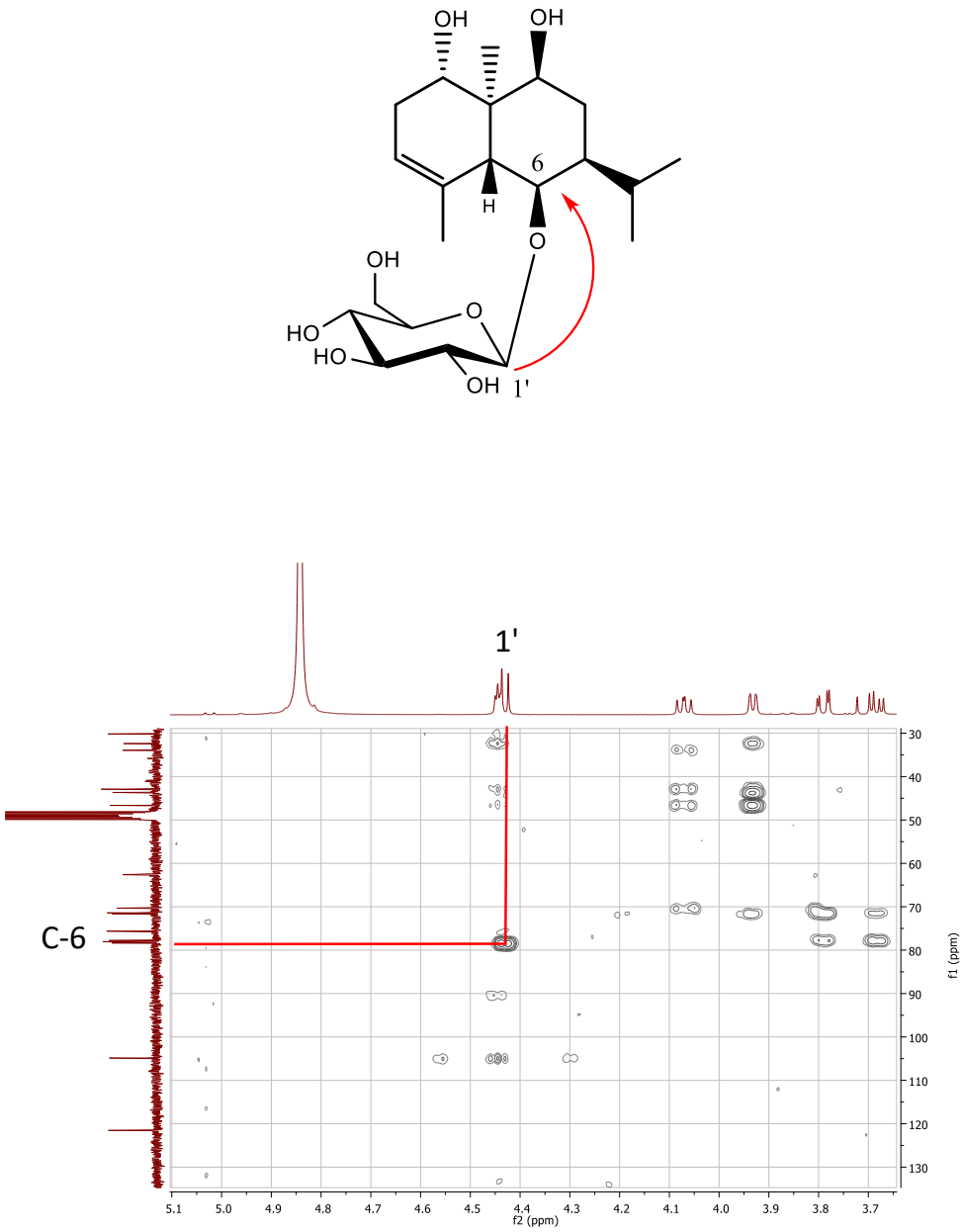

Figure 81. Key HMBC correlations (CD_3OD, 600 MHz) of compound **6**

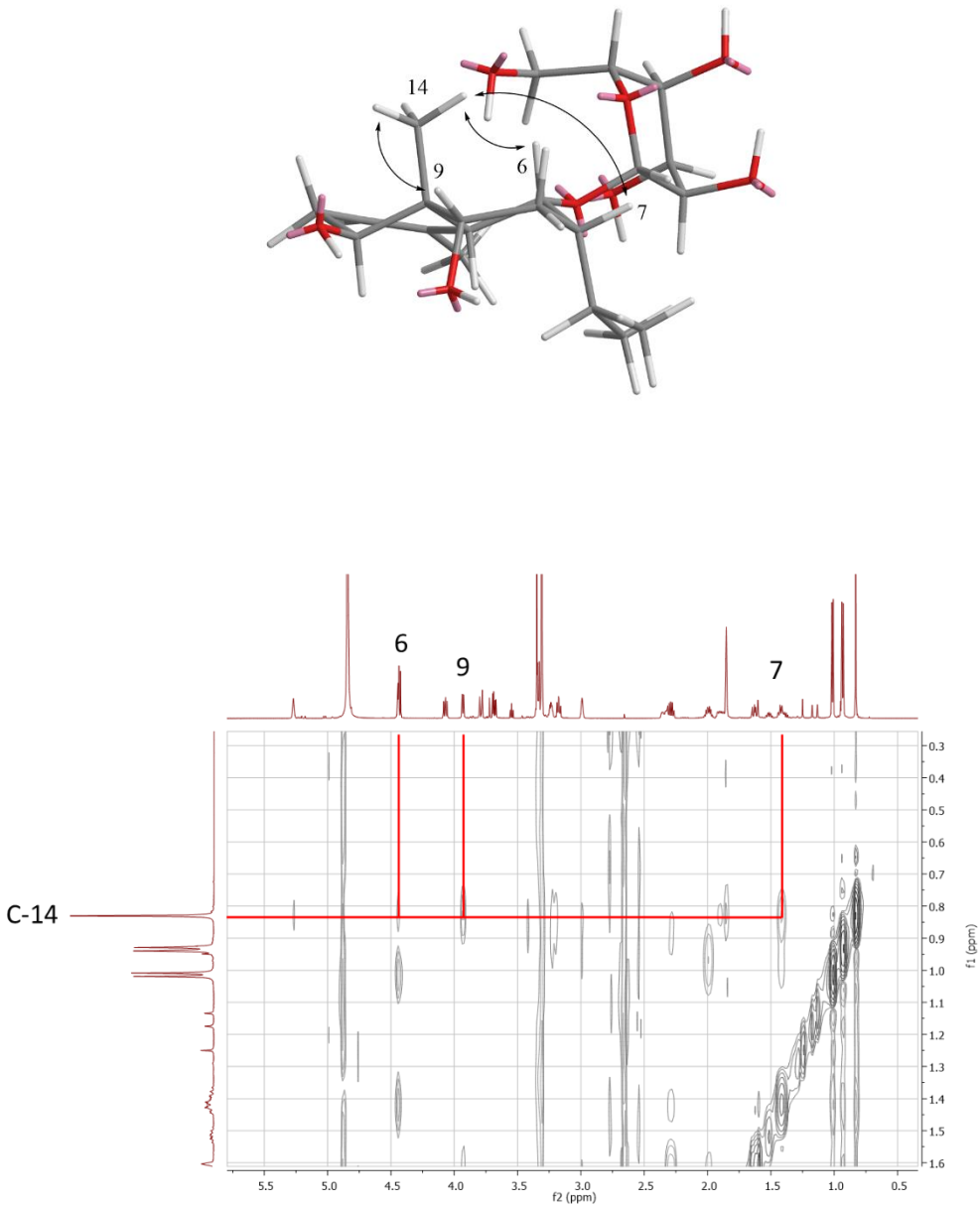

Figure 82. Key ROESY correlations (CD_3OD, 600 MHz) of compound **6**

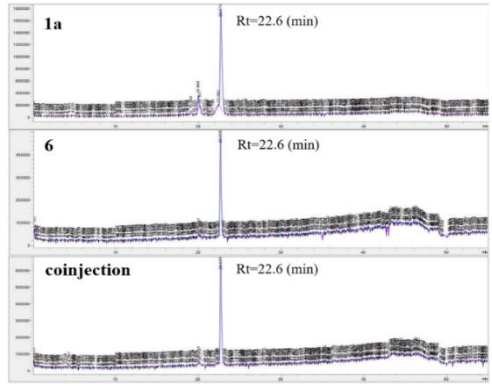

Figure 83. Reversed-phase HPLC analysis of **1c** (a)**, 6** (b), and co-injection (c)

No	Compound 1c	Compound 6
1	71.7, CH	71.6, CH
2	34.0, CH_2	33.9, CH_2
3	121.6, C	121.5, C
4	136.1, C	136.1, C
5	46.7, C	46.6, C
6	78.4, CH	78.4, CH
7	43.7, CH	43.7, CH
8	32.4, CH_2	32.4, CH_2
9	70.4, CH	70.3, CH
10	42.9, C	42.9, C
11	30.2, CH	30.2, CH
12	21.6, CH_3	21.6, CH_3
13	22.1, CH_3	22.1, CH_3
14	12.7, CH_3	12.7, CH_3
15	22.6, CH_3	22.6, CH_3
1′	104.9, CH	104.9, CH
2′	75.7, CH	75.6, CH
3′	78.1, CH	78.1, CH
4′	71.5, CH	71.4, CH
5′	77.8, CH	77.8, CH
6′	62.7, CH_2	62.6, CH_2

Table 16.^{13}C NMR data (methanol-d_4, 125 MHz) of compound **1c** and **6**

3.2.7. Compound **7**

Compound **7** was purified as a colorless gum with $[\alpha]_D^{25}$ –1.6 (*c* 0.5, MeOH) and gave a molecular formula of $C_{26}H_{44}O_{11}$ from the HRESIMS ion at *m*/*z* 577.2850 [M + HCOO]$^-$ (calcd for $C_{27}H_{45}O_{13}$, 577.2866). The broad IR peak at 3403 cm^{-1} and 1630 cm^{-1} indicated hydroxy and olefinic groups, respectively. The NMR of compound **7** resembled compound **3** except for the presence of an apiofuranosyl group and the absence of a HMG moiety in **7** (Figures 84-85). The anomeric proton at δ_H 4.99 (d, *J* = 1.9 Hz) was shown to belong to an apiose moiety from a series of pentose proton signals [(δ_H 3.88, d, *J* = 1.8 Hz; δ_C 78.1), (δ_H 3.90, d, *J* = 9.6 Hz and δ_H 3.74, d, *J* = 9.6 Hz; δ_C 75.0) and (δ_H 3.58, s; δ_C 66.0)] that included two methylene groups based on the COSY spectrum. HMBC cross-peaks between H-1′ (δ_H 4.43) and C-6 (δ_C 75.7), and between H-6' (δ_H 3.93) of the glucose and C-1″ (δ_C 110.7) of the apiose suggested the relative positions of the two sugar units (Figures 85-86). The NOESY spectrum exhibited cross-peaks from H-1 (δ_H 3.49) to H-5 (δ_H 2.45) and from H-14 (δ_H 0.87) to H-6 (δ_H 4.38) and H-7 (δ_H 1.86) (Figure 87). The sugars were confirmed as D-glucose and D-apiose using the method of Tanaka et al. The arabinofuranosyl moiety was removed by acid hydrolysis to afford **7a**, and reversed-phase HPLC on co-injection proved that **7a** is identical with **3a** (Figure 88). Accordingly, compound **7** was determined structurally as 1*β*,6*α*-dihydroxy-7-*epi*-eudesm-3-ene-6-*O*-*β*-D-apiofuranosyl-(1→6)-*β*-D-glucopyranoside.

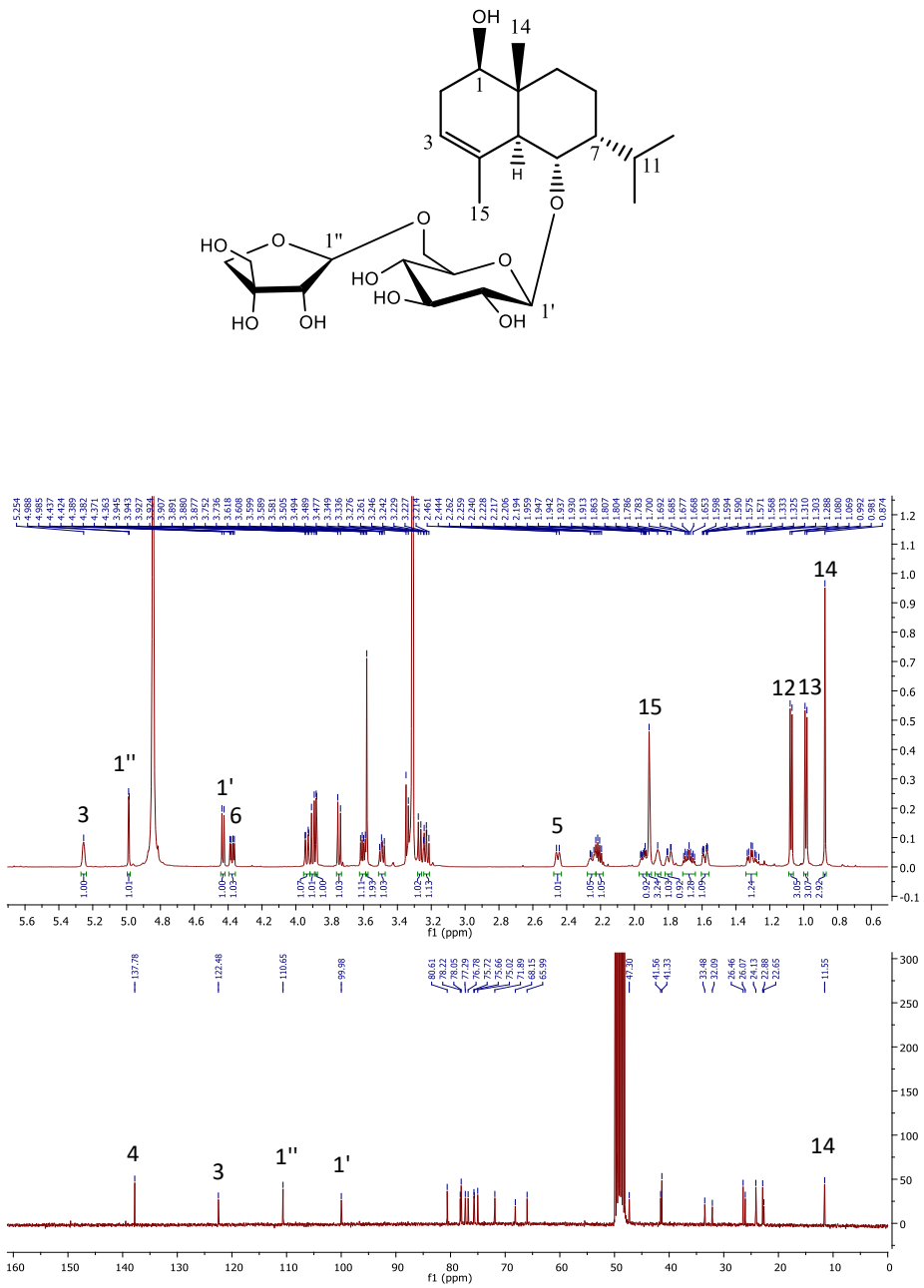

Figure 84. ^{1}H and ^{13}C NMR spectra (CD_3OD, 800/200 MHz) of compound **7**

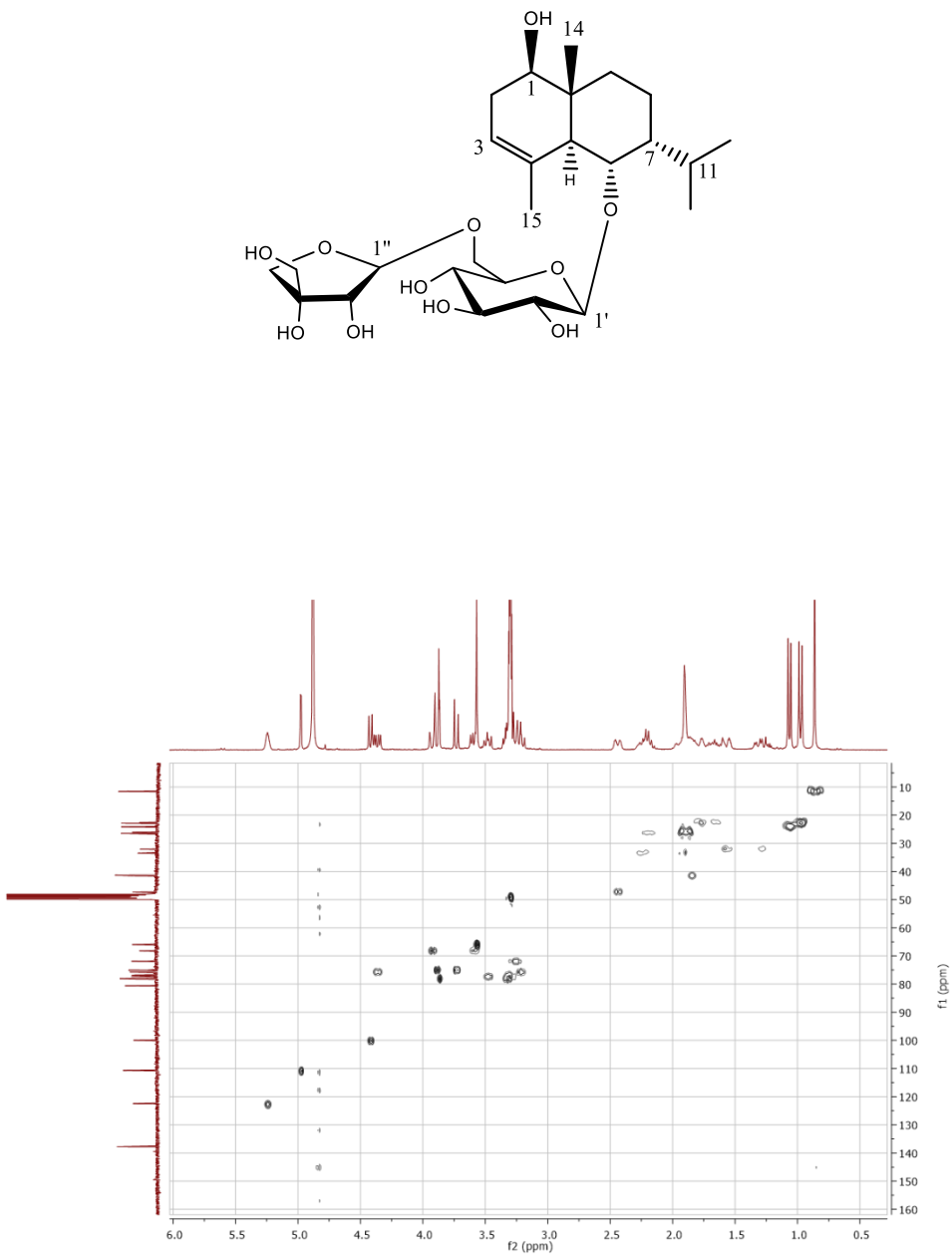

Figure 85. HSQC spectrum (CD_3OD, 800 MHz) of compound **7**

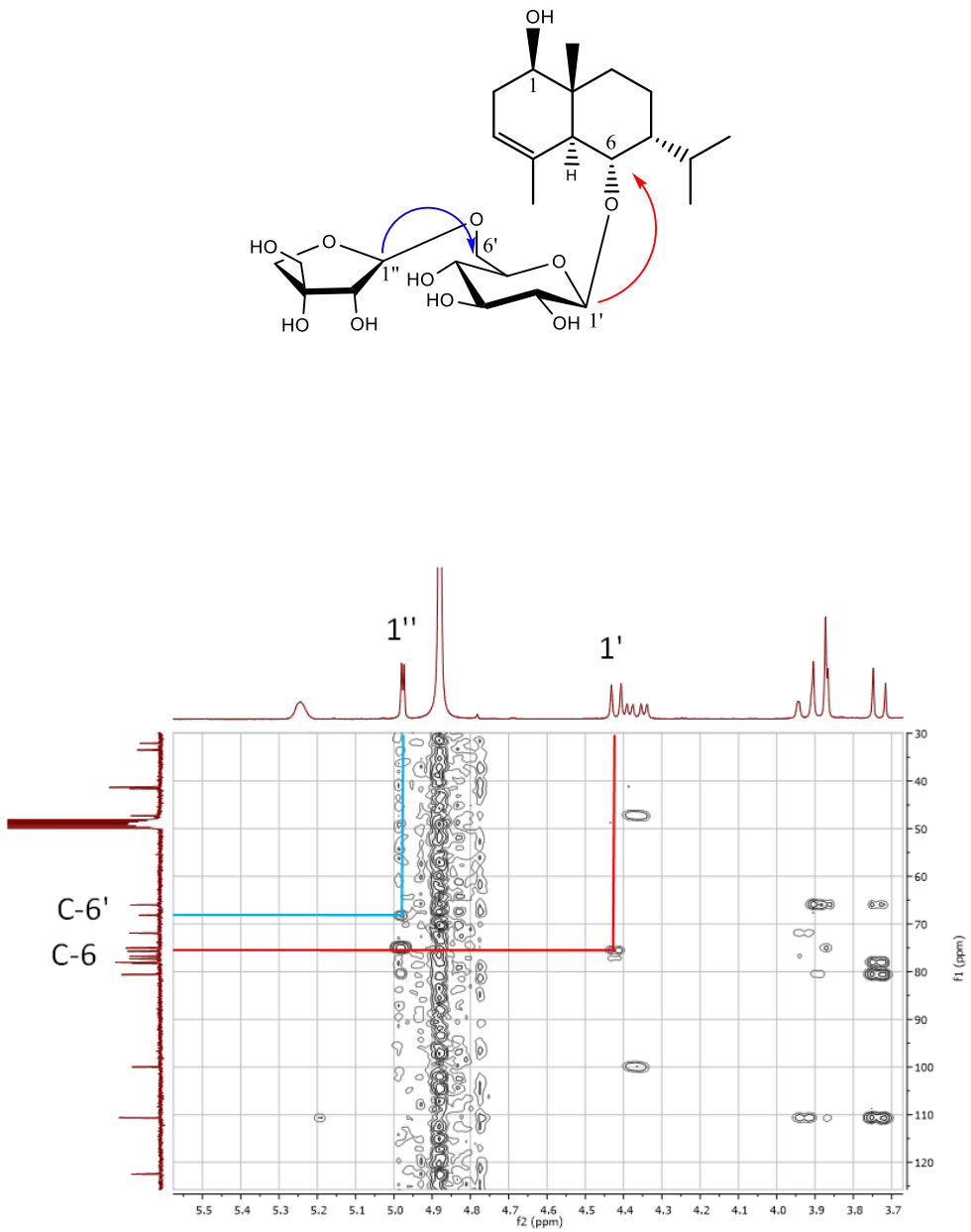

Figure 86. Key HMBC correlations (CD_3OD, 800 MHz) of compound **7**

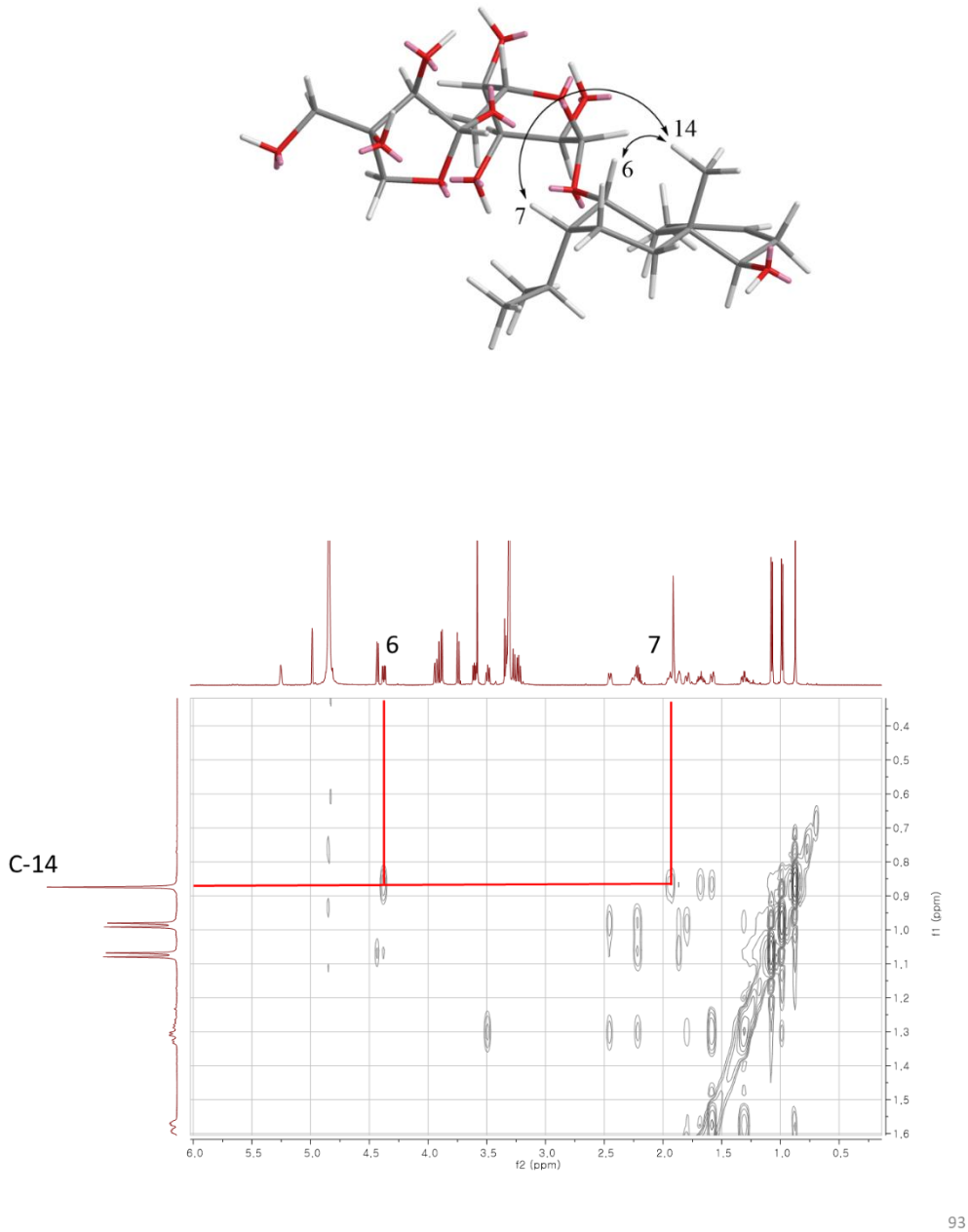

Figure 87. Key ROESY correlations (CD_3OD, 800 MHz) of compound **7**

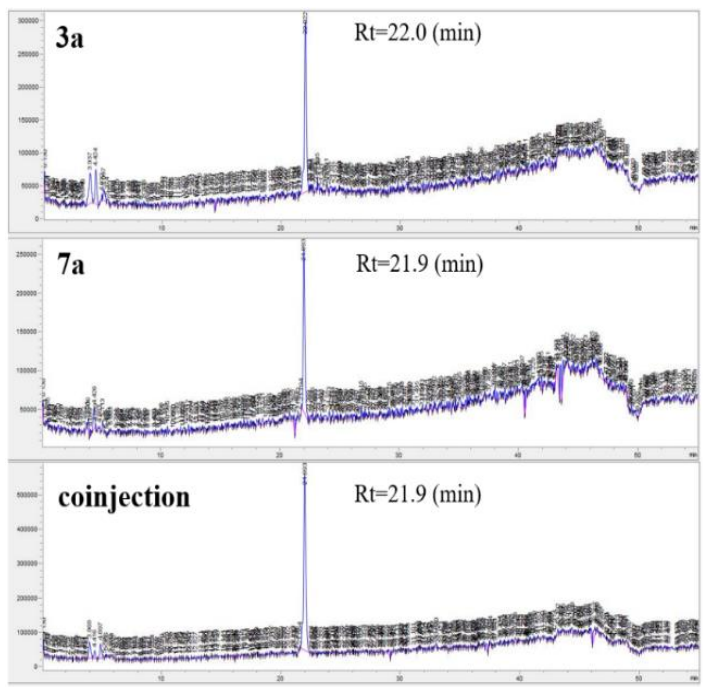

Figure 88. Reversed-phase HPLC analysis of **3a** (a)**, 7a** (b), and co-injection (c)

3.2.8. Compound **8**

Compound **8** was isolated as an amorphous powder with $[\alpha]_D^{25}$ -10.5 (*c* 0.1, MeOH). HRESIMS analysis suggested a molecular formula of $C_{21}H_{36}O_7$, based on the $[M-H]^-$ peak at *m*/*z* 399.2390, calcd for $C_{21}H_{35}O_7$, (*m*/*z* 399.2382). The ^{1}H NMR spectrum exhibited the presence of an exo-methylene protons [δ_H 4.95 and 1.74 (each 1H, s)], one pair of methyl group of isopropyl [δ_H 0.95 (3H, d, *J* = 7.0 Hz) and 0.85 (3H, d, *J* = 7.0 Hz) and one singlet methyl group [δ_H 0.74 (3H, s)] (Figure 89). The anomeric proton was shown at δ_H 4.29 (1H, d, 7.7) suggesting the presence of *β*-glucopyranose. Oxygenated methylene of glucopyranose moiety was presented at δ_H 3.87 (1H, dd, *J* = 11.7, 1.8 Hz) and 3.67 (1H, dd, *J* = 11.6, 5.4 Hz). With above spectroscopic data, compound **8** was characterized as 1*β*,6*α*-dihydroxyeudesman-4(15)-ene-1-*O*-*β*-D-glucopyranoside (Huong et al., 2014).

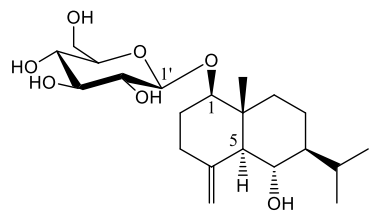

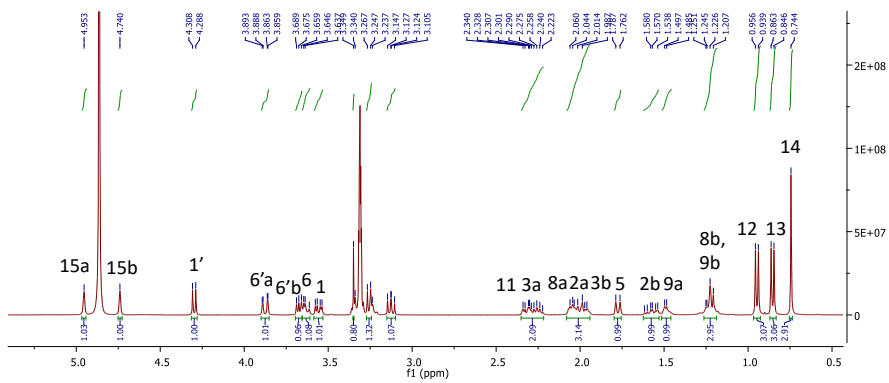

Figure 89. ^{1}H NMR spectrum (CD_3OD, 400 MHz) of compound **8**

3.2.9. Compound **9**

Compound **9**, an amorphous powder with $[\alpha]_D^{25}$ -40.2 (*c* 0.2, MeOH), was determined to have a molecular formula of $C_{19}H_{28}O_6$, as suggested by the HRESIMS peaks at *m/z* 351.1801 $[M - H]^-$ (calcd for $C_{19}H_{27}O_6$, 351.1807). The ^{1}H NMR data revealed the presence of three oxygenated protons [δ_H 5.21 (1H, ddd, *J* = 8.0, 8.0, 4.8 Hz), 4.64 (1H, ddd, *J* = 11.7, 6.4, 4.3 Hz), and 4.60 (1H, d, *J* = 7.5 Hz)], two acetoxy groups [δ_H 2.06 (3H, s), 2.04 (3H, s)], two doublet methyl groups [δ_H 1.09 (3H, d, *J* = 7.5 Hz), 1.03 (3H, d, *J* = 7.5 Hz)] and one singlet methyl group [δ_H 1.09 (3H, s)]. Based on above spectroscopic data, compound **9** was confirmed as 3-deacetoxylhymenolane (Gao et al., 1990).

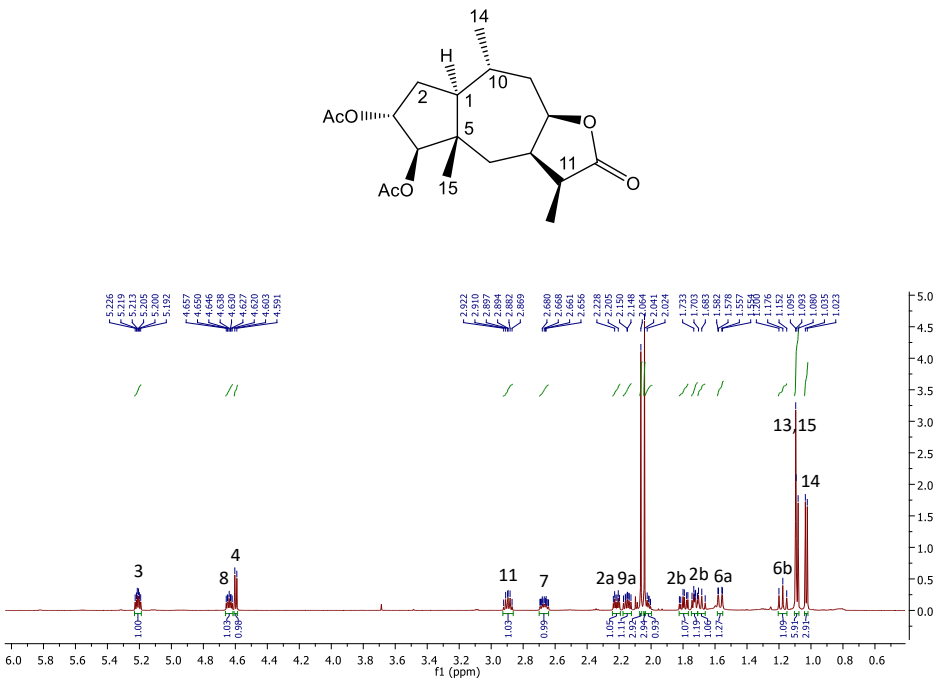

Figure 90. ^{1}H NMR spectrum (chloroform-*d*, 600 MHz) of compound **9**

3.2.10. Compound **10**

Compound **10** was purified as a colorless gum with $[\alpha]_D^{25}$ 34.8 (*c* 0.2, MeOH) and gave a molecular formula of $C_{19}H_{26}O_6$ from the HRESIMS ion at *m*/*z* 349.1658 [M – H]$^-$ (calcd for $C_{19}H_{25}O_6$, 349.1651). The ^{1}H NMR spectrum showed the similar signals with compound **9**. Three oxygenated protons [δ_H 5.25 (1H, ddd, *J* = 7.9, 7.9, 4.8 Hz), 4.77 (1H, d, *J* = 7.5 Hz), and 4.68 (1H, ddd, *J* = 12.0, 7.8, 3.3 Hz)], one doublet methyl group [δ_H 1.06 (3H, d, *J* = 6.0 Hz)] and one singlet methyl group [δ_H 1.08 (3H, s)] were shown (Figure 91). Two acetoxy protons were shown at [δ_H 2.02, 2.08 (each 3H, s)]. The major difference was the presence of terminal methylene moiety [δ_H 6.20 (1H, d, *J* = 2.5 Hz) and 5.50 (1H, d, *J* = 2.5 Hz)] suggesting that the replacement of the methyl group at C-11 by exo-methylene. With above observed spectroscopic data, compound **10** was confirmed as 3α,4β-diacetylhymenoratin. (Ahmed et al., 1995)

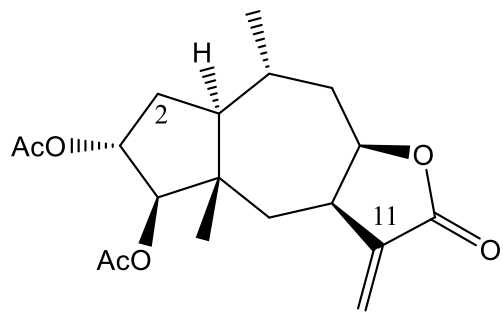

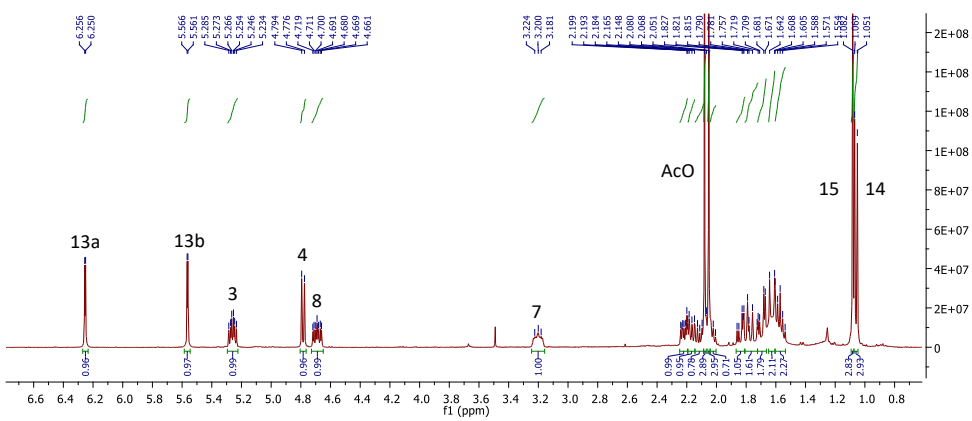

Figure 91. ^{1}H NMR spectrum (chloroform-*d*, 400 MHz) of compound **10**

3.2.11. Compound **11**

Compound **11** was isolated as an amorphous powder with $[\alpha]_D^{25}$ 55.8 (*c* 0.1, MeOH). HRESIMS analysis suggested a molecular formula of $C_{15}H_{20}O_4$, based on the $[M-H]^-$ peak at *m*/*z* 263.1288, calcd for $C_{15}H_{19}O_4$, (*m*/*z* 263.1283). The ^1H NMR data revealed the presence of terminal methylene group [δ_H 6.41 (1H, s) and 5.65 (1H, s)], one oxygenated proton [δ_H 4.37 (1H, m)], one doublet methyl [δ_H 1.22 (3H, d, *J* = 7.0 Hz)] and one singlet methyl [δ_H 1.01 (3H, s)]. In comparison with the spectroscopic data with literature, the structure of compound **11** was identified as ambrosic acid (Ahmed et al., 1995).

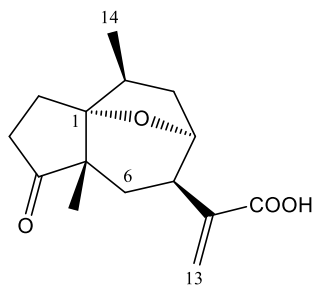

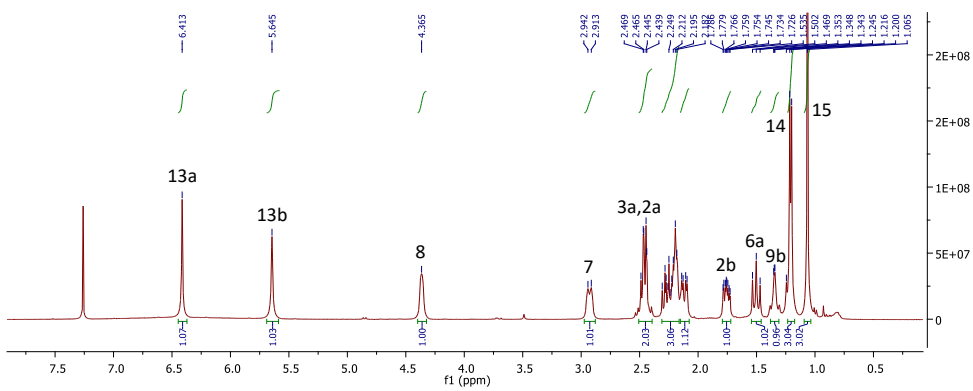

Figure 92. ^1H NMR spectrum (chloroform-*d*, 400 MHz) of compound **11**

3.2.12. Compound **12**

Compound **12** was purified as a colorless gum with $[\alpha]_D^{25}$ -30.4 (*c* 0.1, MeOH) and gave a molecular formula of $C_{15}H_{20}O_4$ from the HRESIMS ion at *m*/*z* 263.1278 $[M - H]^-$ (calcd for $C_{15}H_{19}O_4$, 263.1283). The ^1H NMR spectrum showed the terminal methylene group at 6.13 (1H, dd, *J* = 3.6, 0.9 Hz) and 6.01 (1H, dd, J = 3.3, 0.9 Hz), one olefinic proton at δ_H 5.52 (1H, d, *J* = 1.6 Hz), one allylic methyl at δ_H 1.88 (3H, d, *J* = 1.8 Hz) and one singlet methyl group [δ_H 1.23 (3H, s)]. The ^{13}C NMR spectrum presented 15 carbons including carbonyl group of lactone ring at δ_C 170.1, terminal methylene group at δ_C 121.3, double bond in pentacyclic ring at δ_C 143.8 and 125.2 and allylic methyl at δ_C 17.9 (Figure 93). Taken together, compound **12** was determined as cumambrin B (Vajs et al., 2000).

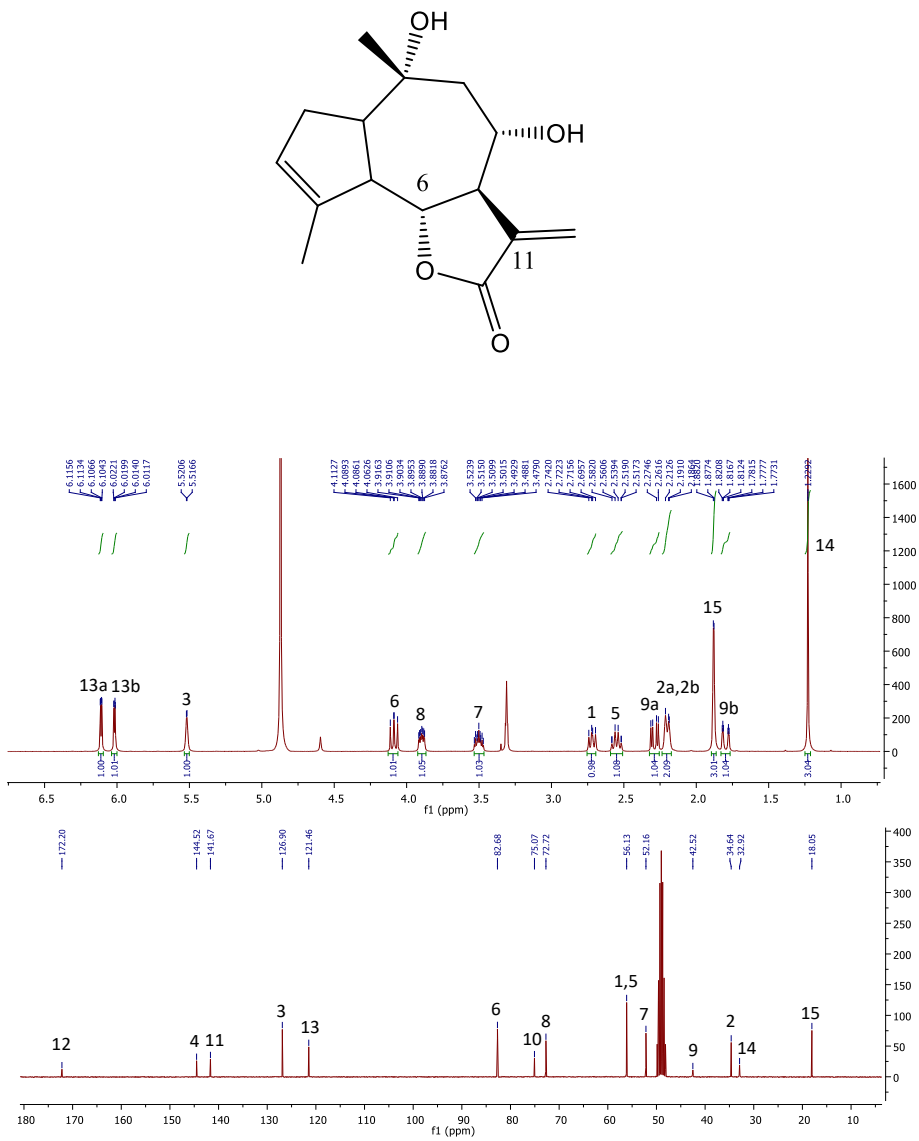

Figure 93. ^{1}H and ^{13}C NMR spectra (CD_3OD, 400/100 MHz) of compound **12**

3.2.13. Compound **13**

Compound **13** was obtained as a colorless gum with $[\alpha]_D^{25}$ 80.5 (*c* 0.2, MeOH), and analyzed for the molecular formula of $C_{34}H_{37}N_3O_6$ based on the HRESIMS ion peak at *m*/*z* 582.2610 $[M - H]^-$ (calcd for $C_{34}H_{36}N_3O_6$, 582.2604). The ^{1}H NMR spectrum suggested the existence of trans double bond [δ_H 6.85/6.81 (1H, d, *J* = 15.0 Hz), 6.42 (1H, d, *J* = 15.0 Hz) and 6.40/6.37 (1H, d, *J* = 15.0 Hz)] (Figure 94). Since compound **13** exists as two conformational isomers, the splitting phenomenon was presented. The ^{13}C NMR spectrum showed carbonyl groups at δ_C 169.3 and 169.2/169.4. Methylene carbons at C-3,7,8 [δ_C 30.6/28.9, 27.9/26.3, 27.9/27.8] showed relatively upfielded chemical shift than those of methylene carbons at C-2,4,6,9 [δ_C 38.2/37.9, 45.7/47.0, 49.0/47.6, 40.1/39.9] next to nitrogen. Thus, compound **13** was characterized as N^1,N^5,N^{10}-tri-*p*-coumaroylspermidine (Ma et al., 2001).

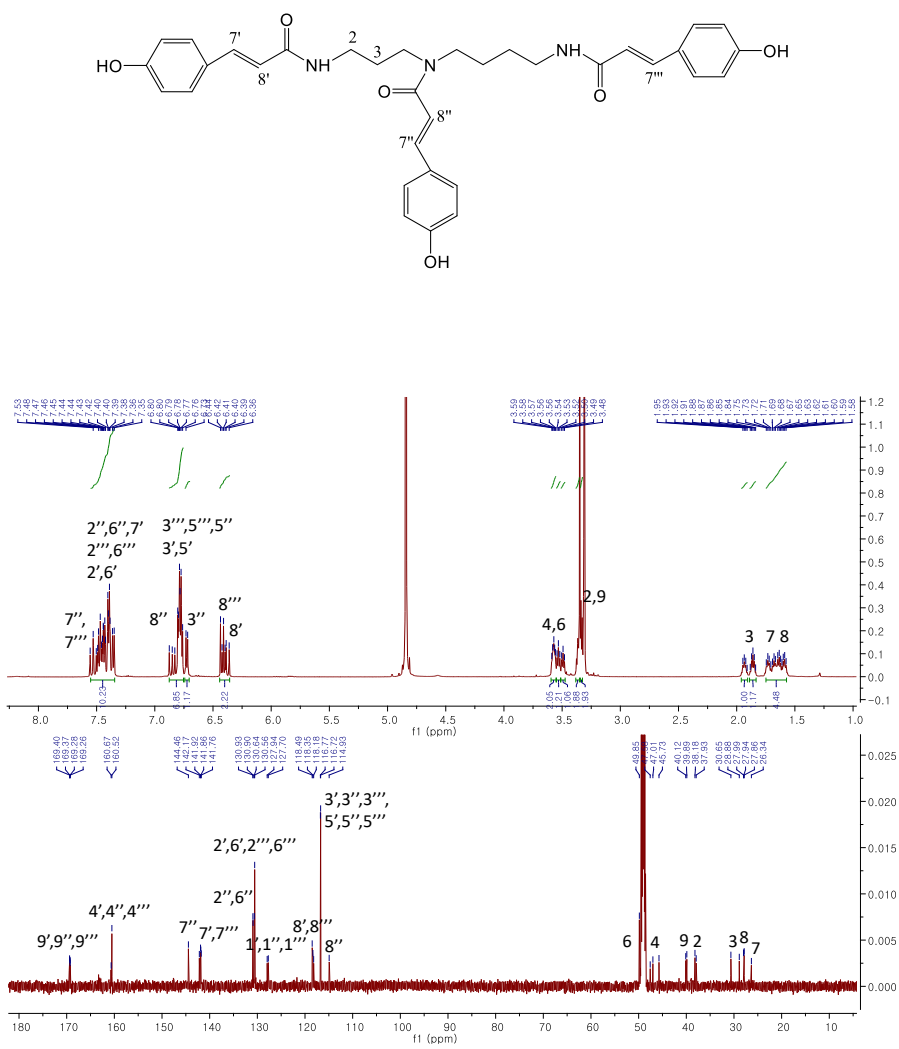

Figure 94. ^{1}H and ^{13}C NMR spectra (CD_3OD, 600/150 MHz) of compound **13**

3.2.14. Compound **14**

Compound **14** was isolated as an amorphous powder with $[\alpha]_D^{25}$ 67.9 (*c* 0.2, MeOH). HRESIMS analysis suggested a molecular formula of $C_{34}H_{37}N_3O_7$, based on the $[M-H]^-$ peak at *m*/*z* 598.2545, calcd for $C_{34}H_{36}N_3O_7$, (*m*/*z* 598.2553). Based on chemical formula, one hydroxyl group was deduced to be attached to compound **13**. The ^{1}H NMR spectrum of compound **14** showed similar pattern with that of compound **13** except the cinnamoyl moiety connected to center N atom (Figure 95). The proton signal of 7" was shifted upfield suggesting the presence of caffeoyl group to the center N atom. With above mentioned spectroscopic data and comparison to literature, compound **14** was determined as N^1,N^5-di-*p*-coumaroyl-N^{10}-caffeoyl spermidine (Walters et al., 2001).

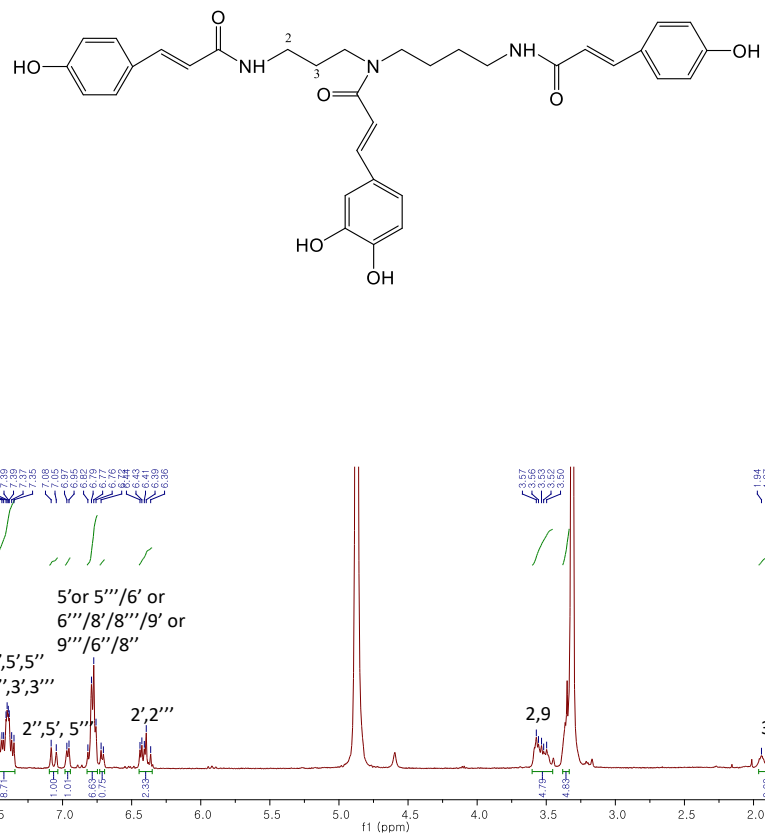

Figure 95. ^{1}H NMR spectrum (CD_3OD, 500 MHz) of compound **14**

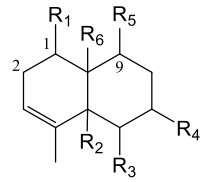

	R_1	R_2	R_3	R_4	R_5	R_6
1	α–OH	β–H	β–(*O*–β–D–glc)	β–Isopropyl	β–*O*–HMG	α–Me
2	α–*O*–HMG	β–H	β–(*O*–β–D–glc)	β–Isopropyl	α–OH	α–Me
3	β–*O*–HMG	α–H	α–(*O*–β–D–glc)	α–Isopropyl	H	β–Me
4	α–OH	β–H	β–(6–*O*–acetyl–β–D–glc)	β–Isopropyl	β–*O*–HMG	α–Me
5	α–(*O*–α–L–ara)	β–H	β–(*O*–β–D–glc)	β–Isopropyl	β–OH	α–Me
6	α–OH	β–H	β–(*O*–β–D–glc)	β–Isopropyl	β–OH	α–Me
7	β–OH	α–H	α–(*O*–β–D–apio–(1–6)–β–D–glc)	α–Isopropyl	H	β–Me

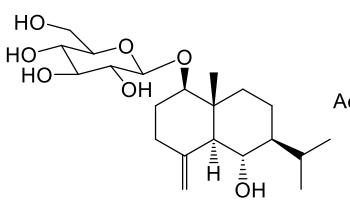

8

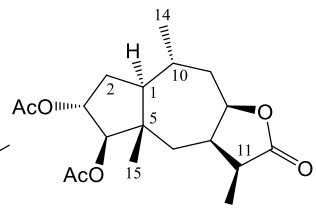

9

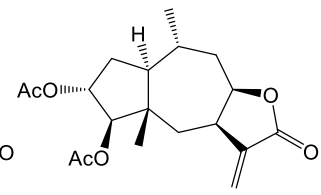

10

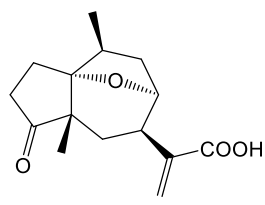

11

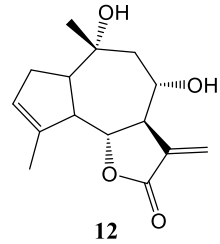

12

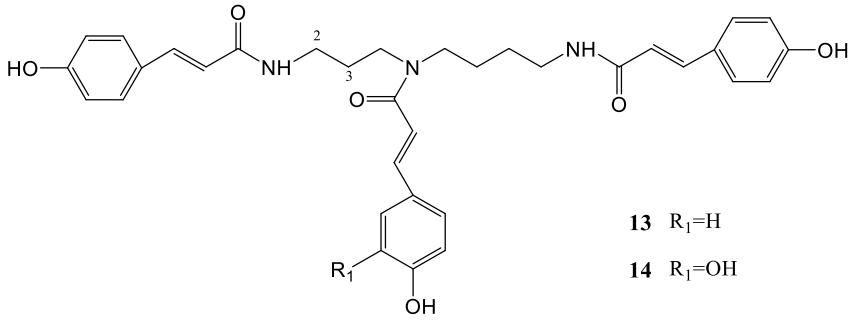

13 R_1=H

14 R_1=OH

Figure 96. Structures of isolated compounds from *A. artemisiifolia*.

3.3. Neuroprotective effects of isolated compounds from *A. artemisiifolia*

AD is a fatal degenerative brain disorder that affects the elderly, and approximately 60-80% of AD patients progress to dementia (Femminella et al., 2018). Many studies have demonstrated that the amyloid beta peptide is the major protein composition of neuritic plaques (Hong et al., 2016). Thus, many attempts have been made to find new chemical entities to protect the brain from Aβ-induced cytotoxicity. In the present study, bioassay-guided fractionation with a 70% EtOH extract of *A. artemisiifolia* led to the isolation of a total of 14 compounds from the EtOAc-soluble partition, which showed neuroprotective activity. To investigate the protective effect against the cytotoxicity induced by Aβ, HT22 cells were used, and were transfected with Aβ_{42} plasmids using Lipofectamine 2000 reagent. After 10 h of transfection, 40 μM of compounds **1**-**9**, **11**, **13**-**14**, and 5 μM of compounds **10** and **12** were added since compounds **10** and **12** showed significant cytotoxicity at 40 μM (Figure 97). Compounds **10** and **12** were marked with different color.

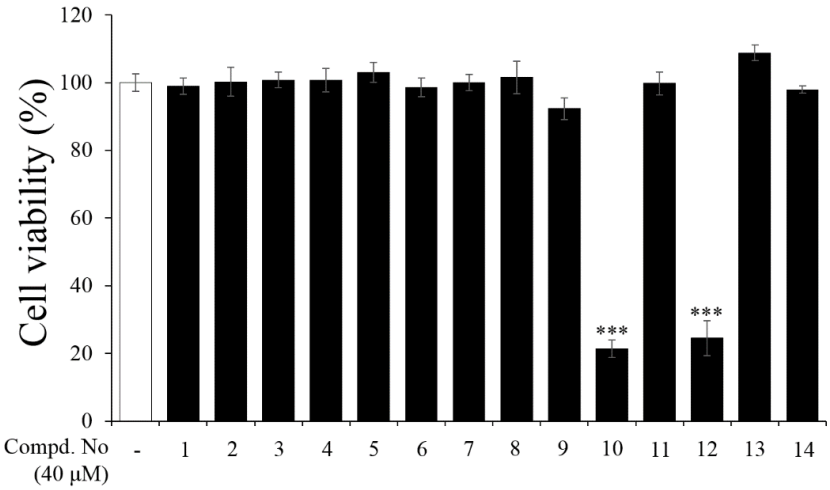

Figure 97. Cytotoxic effects of compounds **1-14** (40 μM) on HT22 cells

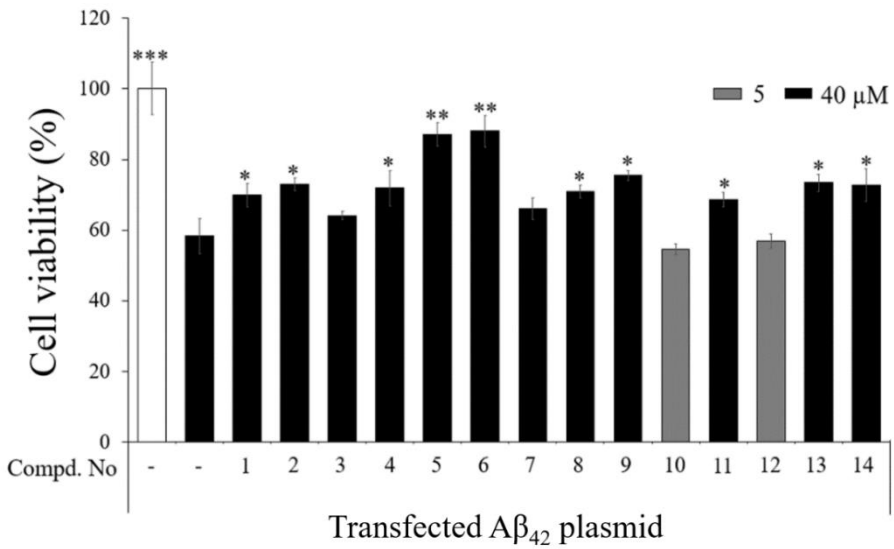

Figure 98. Neuroprotective effects of isolated compounds from *A. artemisiifolia* against cytotoxicity induced by Aβ_{42} plasmid transfection into HT22 cells. After 10 h of transfection, the transfected cells were exposed to the test compounds at a concentration of 40 μM, except for compounds **10** and **12** at 5 μM.

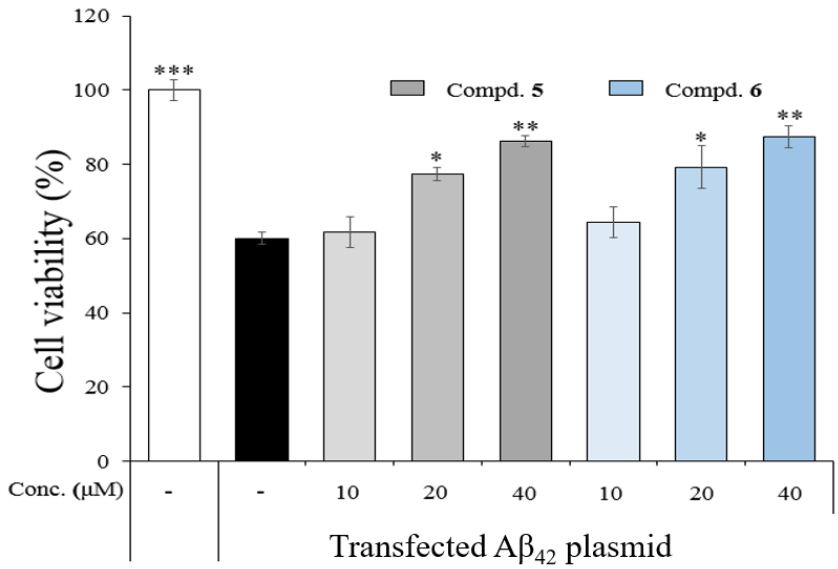

Figure 99. Compounds **5** and **6** at various concentrations. The cultures were incubated continuously for 24 h, and cell viability was measured using the MTT method.

Cell viability was measured by a MTT assay. Compounds **1**, **2**, **4**-**6**, **8**-**9**, **11**, and **13**-**14** showed protective effects against Aβ-induced cytotoxicity (Figure 98), and the activity of compound **5** was comparable to that of andrographolide as a positive control (Figure 99). In addition, compounds **5** and **6** presented dose-dependent activity (10, 20, and 40 μM) in Aβ_{42}-transfected cells. Thus, flow cytometry analysis was performed with the selected isolates, **5** and **6**. As shown in Figure 100, compounds **5** and **6** showed moderate decreases in fluorescence intensity in Aβ_{42}-transfected HT22 cells at a concentration of 40 μM, when compared to a vehicle. Structure-activity relationship (SAR) analysis revealed that the neuroprotective effects can be attributed to the 5,10-bis-*epi*-eudesm-3-ene-6-*O*-β-D-glucopyranosyl moiety in Aβ_{42}-transfected cells. Among all isolates, compounds possessing the 5,10-bis-*epi*-eudesm-3-ene-6-*O*-β-D-glucopyranosyl moiety increased cell viability against Aβ-induced cytotoxicity.

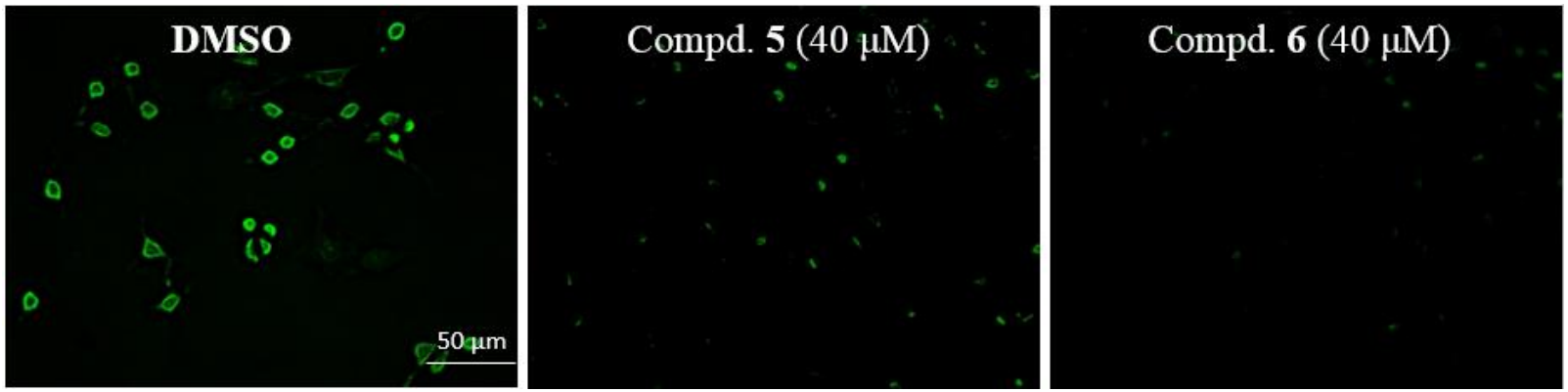

Figure 100. Effects of compounds **5** and **6** (40 µM) on the condensation of green fluorescence in Aβ_{42}-transfected cells.

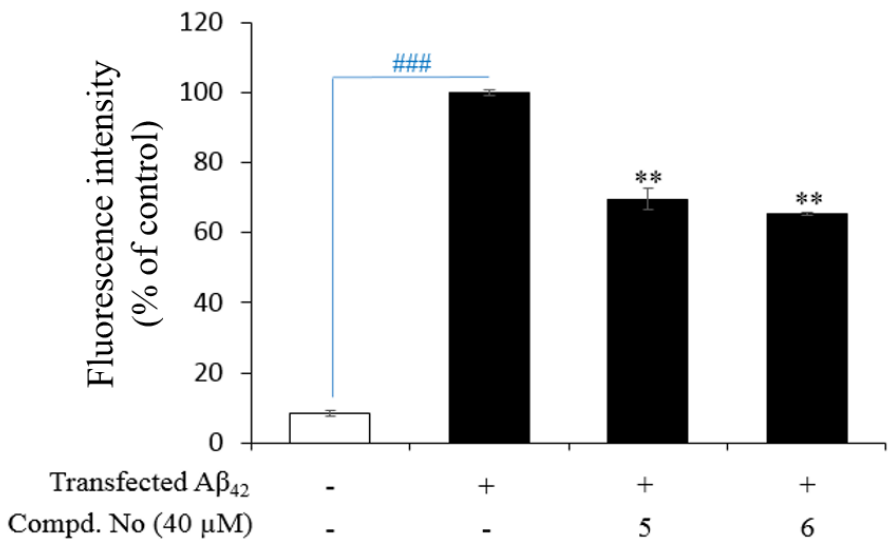

Figure 101. HT22 cells were transfected with pEGFP-C1/$A\beta_{42}$ plasmid using Lipofectamine 2000 reagent for 10 h. The transfected cells were then incubated with test compounds for 24 h, and fluorescence images were captured using a fluorescence microscope. Fluorescence intensity of the transfected cells was successfully analyzed using flow cytometry. After the $A\beta_{42}$-transfected cells were exposed to the test compounds for 24 h, the cells were collected and investigated by flow cytometry

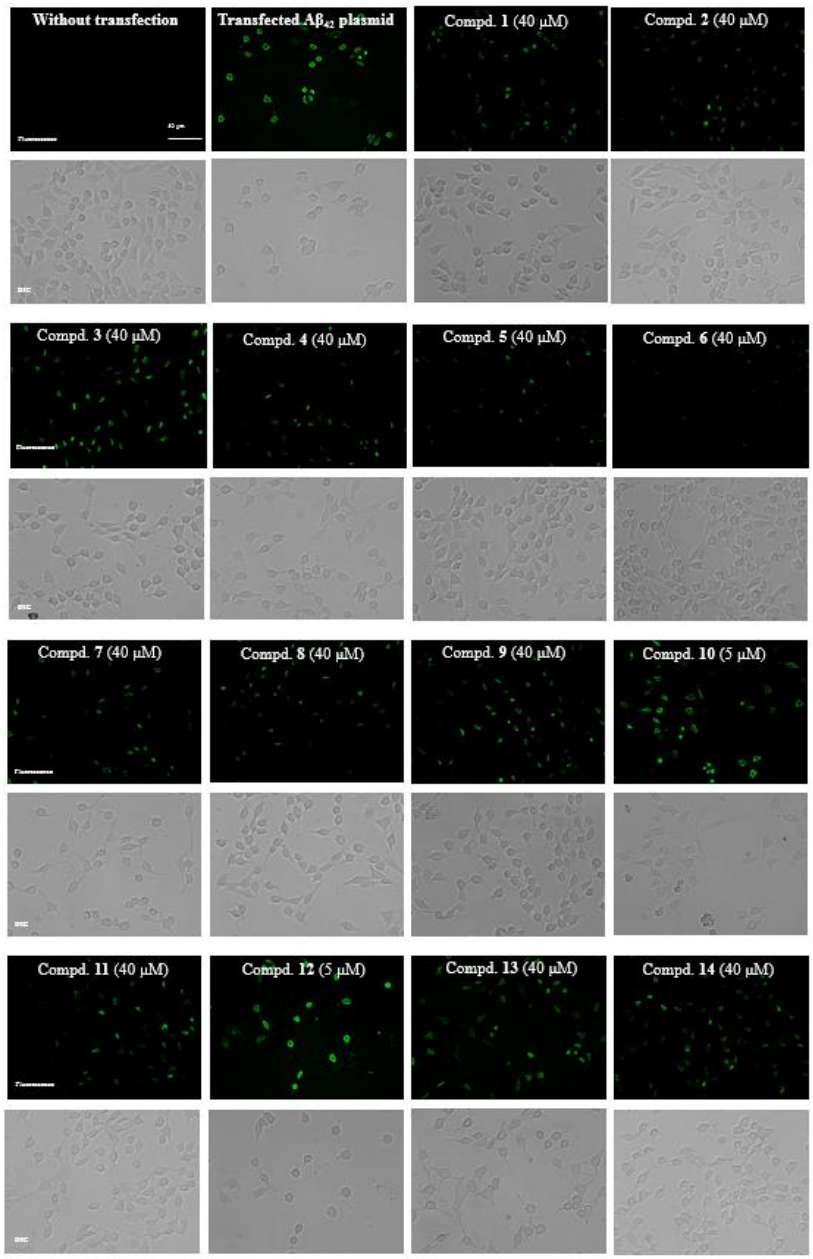

Figure 102**.** Effects of compounds **1-14** on the fluorescent signal induced by pEGFP-C1/Aβ_{42} plasmid transfection into HT22 cells. After 24 h of incubation with test compounds, the fluorescence and bright-field images were visualized using a fluorescence microscope.

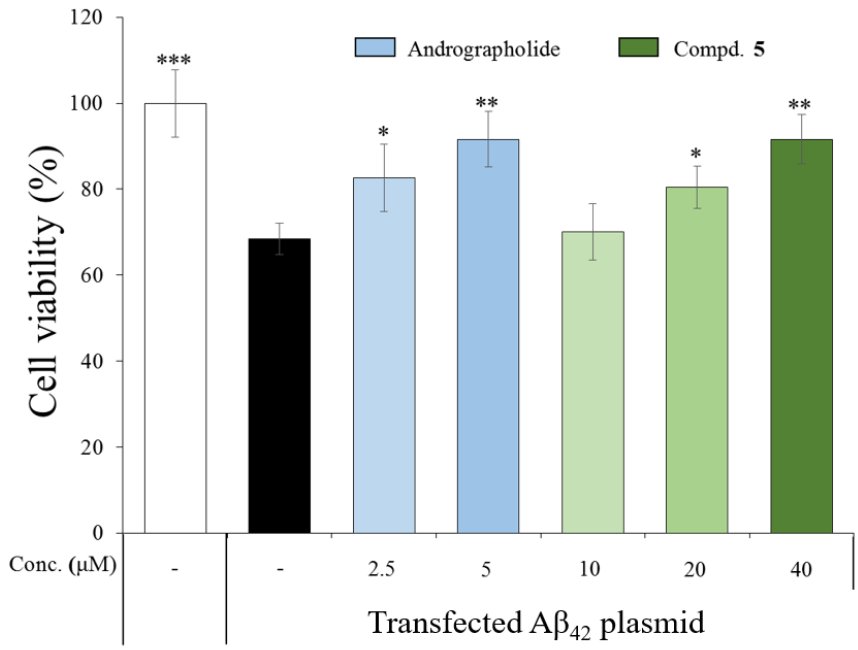

Figure 103. Neuroprotective effects of Andrographolide and compound **5** against cytotoxicity in the Aβ42-transfected cell model. The transfected-cells were treated with Andrographolide (2.5 and 5 μM) and compound 5 (10, 20, and 40 μM). The cultures were then incubated for 24 hours and the cell proliferation was evaluated using the MTT method. Result was calculated as means ± SD (n = 3); *p < 0.05, **p < 0.01, ***p < 0.001, compared with the Aβ42 transfection without treatment group

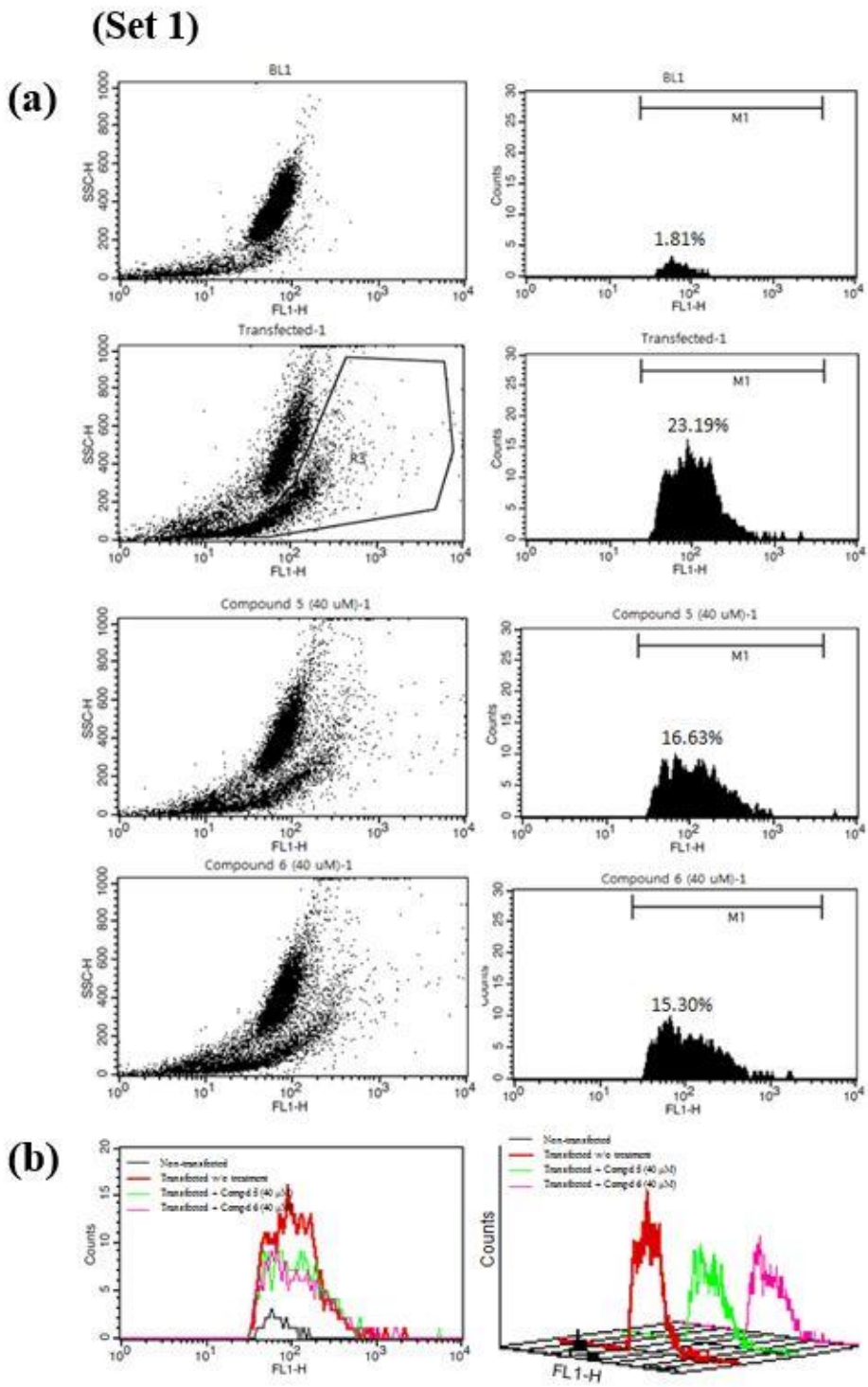

Figure 104. Flow cytometry profiles of three independent experiments

(Set 2)

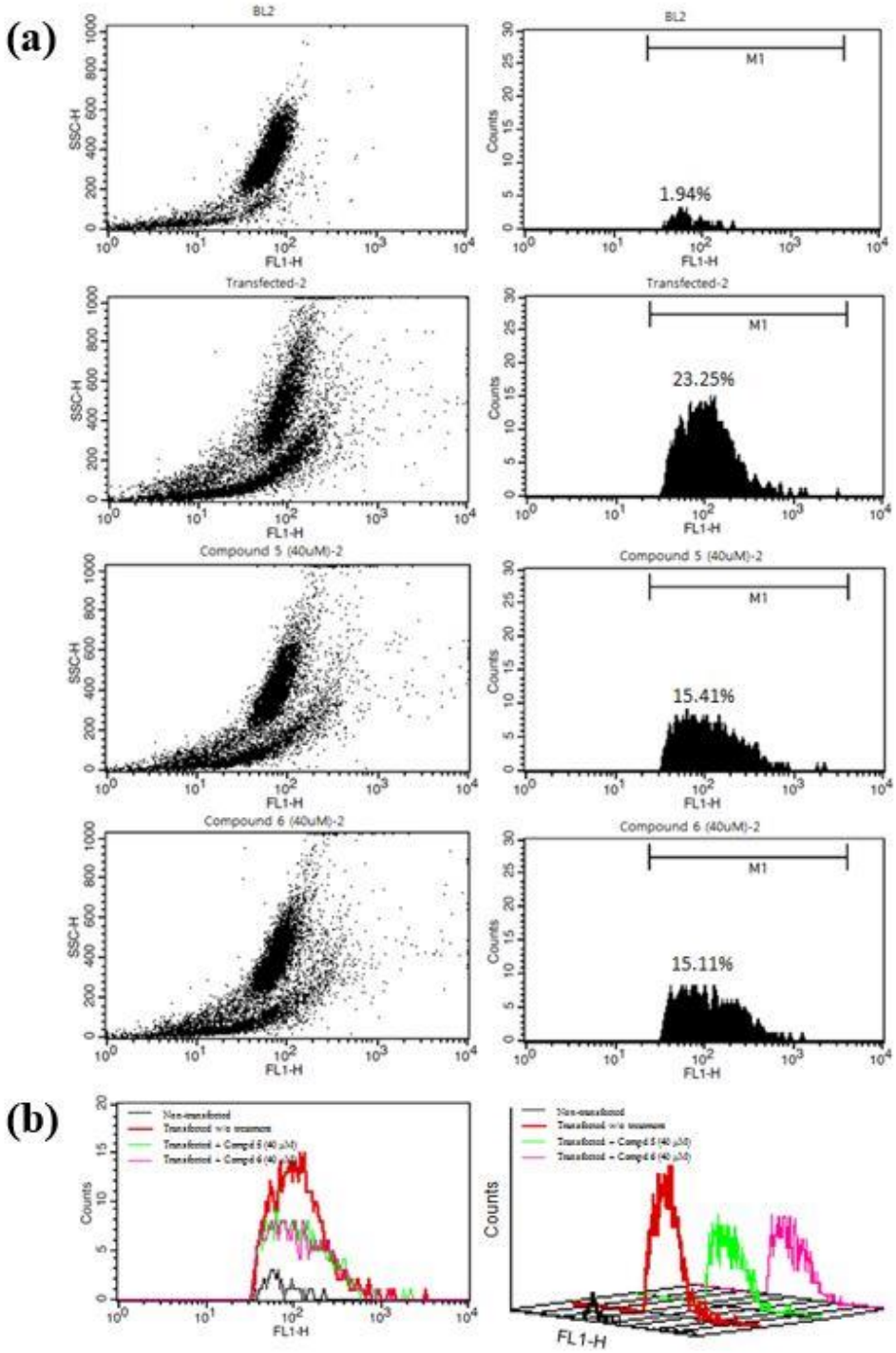
(a)
BL2
SSC-H
FL1-H
Counts
M1
1.94%
Transfected-2
23.25%
Compound 5 (40uM)-2
15.41%
Compound 6 (40uM)-2
15.11%
(b)
Non-transfected
Transfected w/o treatment
Transfected + Compd 5 (40 μM)
Transfected + Compd 6 (40 μM)

(Set 3)

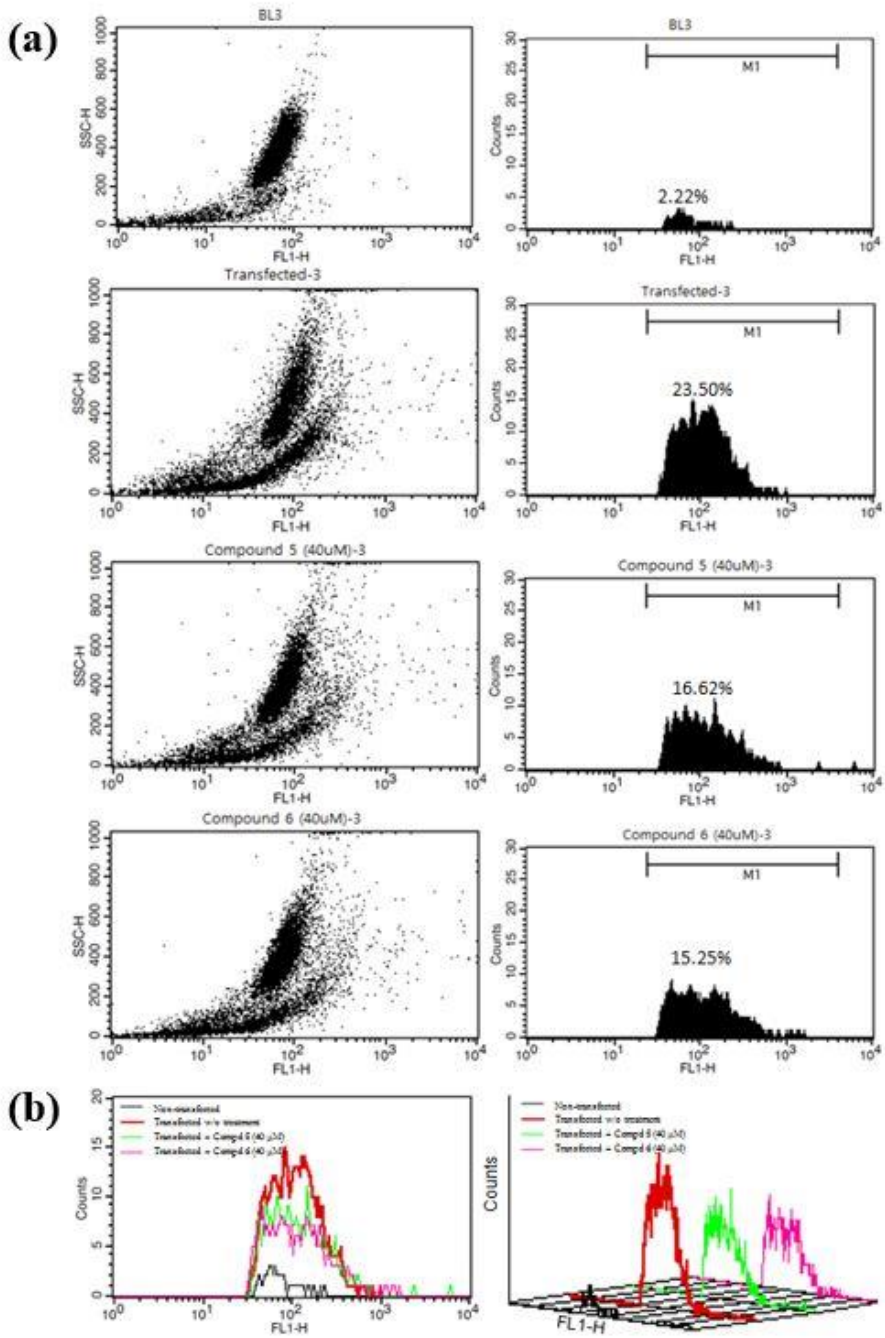
(a)
BL3
SSC-H
FL1-H
Counts
M1
2.22%
Transfected-3
23.50%
Compound 5 (40uM)-3
16.62%
Compound 6 (40uM)-3
15.25%
(b)
Counts
FL1-H

4. Conclusion

Bio-guided isolation allowed to isolate neuroprotective novel compounds. In the course of screening neuroprotective plants in KBNMB (Korea Bioactive Natural Material Bank), 70% ethanol extracted *A. artemisiifolia* showed strong activity. The total extract was analyzed by mass defect filtering method to find novel eudesmane sesquiterpene containing HMG group or sugar moiety. Limited mass range and well defined mass defect parameter enabled to filter the chromatogram. Herein, seven new eudesmane glycoside were isolated along with 7 known compounds. Compounds **1**-**4** were eudesmane glycosides with HMG moiety and compounds **5** and **7** were eudesmane glycosides containing two sugar moieties. Compounds **1**, **2**, **4**-**6**, **8**-**9**, **11**, and **13**-**14** showed protective effects against Aβ-induced cytotoxicity in Aβ_{42}-transfected HT22 cells. Compounds **5** and **6** showed most strong activity among the isolates. These results suggest that 70% ethanol extract *A. artemissifolia* and eudesmane glycosides (**5** and **6**) from this plant have neuroprotective effect.

References

Ahmed, A. A., Spring, O., Razek, M. H., Hussein, N. S., Mabry, T. J. Sesquiterpene lactones and other constituents from *Hymenoxys richardsonii* and *H. subintegra*. *Phytochemistry* 39, 1127-1131.

Ahmed, M. H., Byrne, C. D., 2007. Modulation of sterol regulatory element binding proteins (SREBPs) as potential treatments for non-alcoholic fatty liver disease (NAFLD). *Drug Discov Today* 12, 740-747.

Akihisa, T., Tamura, T., Matsumoto, T., 1987. 24-Methylene-25-methyllathosterol: a sterol from *Sicyos angulatus*. *Phytochemistry* 26, 575-577.

Allard, P. M., Péresse, T., Bisson, J., Gindro, K., Marcourt, L., Pham, V. C., Roussi, F., Litaudon, M., Wolfender, J. L. 2016. Integration of molecular networking and in-silico MS/MS fragmentation for natural products dereplication. *Anal Chem* 88. 3317-3323.

Ambrosia — The Plant List. http://www.theplantlist.org/1.1/browse/A/Compositae/Ambrosia/ (accessed Dec 13, 2018).

Assy, N., Nassar, F., Nasser, G., Grosovski, M., 2009. Olive oil consumption and non-alcoholic fatty liver disease. *World J Gastroenterol* 15, 1809-1815.

Baltes, C., Princz-Kranz, F., Rudin, M., Mueggler, T. 2011. Detecting amyloid-β plaques in Alzheimer's disease. *Methods Mol Biol* 711, 511-533.

Bateman, K. P., Castro-Perez, J., Wrona, M., Shockcor, J. P., Yu, K., Oballa, R., Nicoll-Griffith, D. A. 2007. MSE with mass defect filtering for in vitro and in vivo metabolite identification. *Rapid Commun. Mass Spectrom* 21,1485-96.

Chang, C. J., Tzeng, T. F., Liou, S. S., Chang, Y. S., Liu, I. M., 2011. Kaempferol regulates the lipid-profile in high-fat diet-fed rats through an increase in hepatic PPARα levels. *Planta Med* 77, 1876-1882.

Chernenko, G. F., Gamilov, Y. V., Shmidt, É. N. 1994. Diols from the oleoresin of *Picea ajanensis*. *Chem Nat Compd* 30, 328–331.

Chopra, K.; Misra, S.; Kuhad, A. 2011. Current perspectives on pharmacotherapy of Alzheimer's disease. *Expert Opin Pharmacother* 12, 335-350.

Collier, J., 2007. Non-alcoholic fatty liver disease. *Medicine* 35, 86-88.

Cui, C. X., Deng, J. N., Yan, L., Liu, Y. Y., Fan, J. Y., Mu, H. N., Sun, H. Y., Wang, Y. H., Han, J. Y., 2017. Silibinin Capsules improves high fat diet-induced nonalcoholic fatty liver disease in hamsters through modifying hepatic de novo lipogenesis and fatty acid oxidation. *J Ethnopharmacol* 208, 24-35.

Ding, L., Liu, J. L., Hassan, W., Wang, L. L., Yan, F. R., Shang, J., 2014. Lipid modulatory activities of *Cichorium glandulosum* Boiss et Huet are mediated by multiple components within hepatocytes. *Sci Rep* 4, 4715.

Eom, H. G., Lee, D., Lee, S., Noh, H. J., Hyun, J. W., Yi, P. H., Kang, K. S., Kim, K. H. 2016. Flavonoids and a limonoid from the fruits of citrus unshiu and their biological activity. *J Agric Food Chem* 64, 7171–7178.

Femminella, G. D., Thayanandan, T., Calsolaro, V., Komici, K., Rengo, G., Corbi, G., Ferrara, N. 2018. Imaging and Molecular Mechanisms of Alzheimer's Disease: A Review. *Int J Mol Sci* 19, E3702.

Fernie, A. R., Tohge, T., Wendenburg, R., Ishihara, H., Sulpice, R., Stitt, M., 2016. UV-B absorbing phenylacylated flavonol glycosides from *Ararbidopsis*

thaliana novel flavonol phenylacetransferase FPT2. *Eur Pat Appl* EP 3103806 A1 20161214.

Fox Ramos A. E., Evanno, L., Poupon, E., Champy, P., Beniddir, M. A. 2019. Natural products targeting strategies involving molecular networking: different manners, one goal. *Nat Prod Rep* doi: 10.1039/c9np00006b.

Gao, F., Wang, H., Mabry, T. J., Watson, W. H., Kashyap, R. P. 1990. Sesquiterpene lactones and a C_{20} aliphatic lactone from texas bitterweed, *Hymenoxys odorata*. *Phytochemistry* 29, 551-560.

Grauso, L., Yegdaneh, A., Sharifi, M., Mangoni, A., Zolfaghari, B., Lanzotti, V. 2019. Molecular Networking-Based Analysis of Cytotoxic Saponins from Sea Cucumber *Holothuria atra*. *Mar Drugs* 17. E86.

Garcia-Compean, D., Jaquez-Quintana, J. O., Gonzalez-Gonzalez, J. A., Maldonado-Garza, H., 2009. Liver cirrhosis and diabetes: Risk factors, pathophysiology, clinical implications and management. *World J Gastroenterol* 21, 280-288.

Gohar, A. A, Maatooq, G. T., Niwa, M., 2000. Two flavonoid glycosides from *Chenopodium murale*. *Phytochemistry* 53, 299-303.

Habib, A., Sawmiller, D., Tan, J. 2017. Restoring Soluble Amyloid Precursor Protein α Functions as a Potential Treatment for Alzheimer's Disease. *J Neurosci Res* 95, 973-991.

Hong, S., Dissing-Olesen, L., Stevens, B. 2016. New insights on the role of microglia in synaptic pruning in health and disease. *Curr Opin Neurobiol* 36, 128-34.

Huh, J., Ha, T. K. Q., Kang, K. B., Kim, K. H., Oh, W. K., Kim, J., Sung, S. H. 2017. C-Methylated Flavonoid Glycosides from *Pentarhizidium orientale*

Rhizomes and Their Inhibitory Effects on the H1N1 Influenza Virus. *J. Nat. Prod* 80, 2818-2824.

Hu, J. F., Lu, Y., Zhao, B., Feng, X. Z., Hamann, M. T. 2001. New eudesmenoic acid methyl ester from *Artemisia selengensis. Spectrosc Lett* 34, 75–81.

Huang, R., Ding, W., Zhou, Z., Li, Y. 2014. A novel eudesmane sesquiterpene glycoside from *Ambrosia artemisiifolia* L. *Biochem Syst Ecol* 57, 363-366.

Ikechukwu, O. J., Ifeanyi, O. S., 2016. The antidiabetic effects of the bioactive flavonoid (kaempferol-3-*O*-*β*-D-6-(*p*-coumaroyl) glucopyranoside) isolated from *Allium cepa*. *Recent Pat Anti infect Drug Discov* 11, 44-52.

Jakupovic, J., Jaensch, M., Bohlmann, F., Dillon, M. O. 1988. Eudesmanolides, 5,10-bis-*epi*-eudesmanes and oplopanone derivatives from Ambrosia artemisioides *Phytochemistry* 27, 3551-3556.

Kamo, T., Hirai, N., Matsumoto, C., Ohigashi, H., Hirota, M. 2004. Revised chirality of the acyl group of 8'-*O*-(3-hydroxy-3-methylglutaryl)-8'-hydroxyabscisic acid. *Phytochemistry* 65, 2517–2520.

Kang, W., Wang, J., Cao, N., 2012. Inhibitory activity of *Euphorbia humifusa* for *α*-glucosidase in vitro and in vivo. *Chem Nat Compd* 48, 886-888.

Kim, Y. H., Noh, J. R., Hwang, J. H., Kim, K. S., Choi, D. H., An, J. P., Oh, W. K., Lee, C. H., 2017. *Sicyos angulatus* ameliorates atherosclerosis through downregulation of aortic inflammatory responses in apolipoprotein E-deficient mice. *Exp Ther Med* 14, 5863-5870.

Kuo, Y. T., Lin, T. H., Chen, W. L., Lee, H. M., 2012. Alpha-lipoic acid induces adipose triglyceride lipase expression and decreases intracellular lipid accumulation in HepG2 cells. *Eur J Pharmacol* 692, 10-18.

Lara-Núñez, A., Sánchez-Nieto, S., Luisa Anaya, A., Cruz-Ortega, R., 2009. Phytotoxic effects of *Sicyos deppei* (Cucurbitaceae) in germinating tomato seeds. *Physiol Plant* 136, 180-192.

Lee, H. E., Kim, J. A., Whang, W. K., 2017. Chemical constituents of *Smilax china* L. stems and their inhibitory activities against glycation, aldose reductase, α-glucosidase, and lipase. *Molecules* 22, 451-469.

Lee, S. S., Baek, N. I., Baek, Y. S., Chung, D. K., Song, M. C., Bang, M. H., 2015. New flavonolignan glycosides from the aerial parts of *Zizania latifolia*. *Molecules* 20, 5616-5624.

Lee, J., Lee, Y. M., Lee, B. W., Kim, J. H., Kim, J. S. 2012. Chemical constituents from the aerial parts of *Aster koraiensis* with protein glycation and aldose reductase inhibitory activities. *J Nat Prod* 75, 267-270.

Ma, C. M., Nakamura, N., Hattori, M. 2001. Inhibitory Effects on HIV-1 Protease of tri-p-coumaroylspermidine from *Artemisia caruifolia* and related amides. *Chem Pharm Bull* 49, 915-917.

Mahmoud, A. A. 1997. 7-*epi*-eudesmanes, eudesmanoic acids, eudesmanolides and other sesquiterpenes from *Pluchea dioscoridis*. *Phytochemistry* 45, 1633-1638.

MFDS, 2018. Korean food standards codex. http://www.foodsafetykorea.go.kr/portal/safefoodlife/foodMeterial/foodMeterialDB.do (accessed 24 May 2018).

Na, C. S., Lee, Y. H., Murai, Y., Iwashina, T., Kim, T. W., Hong, S. H., 2013. Flavonol 3.7-diglycosides from the aerial part of *Sicyos angulatus* (Cucurbitaceae) in Korea and Japan. *Biochem Syst Ecol* 48, 235- 237.

Nothias L. F., Nothias-Esposito, M., da Silva, R., Wang, M., Protsyuk, I., Zhang, Z., Sarvepalli, A., Leyssen, P., Touboul, D., Costa, J., Paolini, J., Alexandrov, T., Litaudon, M., Dorrestein, P. C. 2018. Bioactivity-based molecular networking for the discovery of drug leads in natural product bioassay-guided fractionation. *J Nat Prod* 81, 758-767.

Oberti, J. C., Silva, G. L., Sosa, V. E., Kulanthaivel, P., Herz, W. 1986. Ambrosanolides and secoambrosanolides from *Ambrosia tenuifolia*. *Phytochemistry* 25, 1355-1358.

Palop, J. J., Chin, J., Roberson, E. D., Wang, J., Thwin, M. T., Bien-Ly, N., Yoo, J., Ho, K. O., Yu, G. Q., Kreitzer, A., Finkbeiner, S., Noebels, J. L., Mucke, L. 2007. Aberrant excitatory neuronal activity and compensatory remodeling of inhibitory hippocampal circuits in mouse models of Alzheimer's disease. *Neuron* 55, 697-711.

Palop, J. J., Mucke, L. 2010. Amyloid-β–induced neuronal dysfunction in Alzheimer's disease: from synapses toward neural networks. *Nat Neurosci* 13, 812-818.

Reddy, J. K., Rao, M. S., 2006. Lipid metabolism and liver inflammation. II. Fatty liver disease and fatty acid oxidation. *Am J Physiol Gastrointest Liver Physiol* 290, 852-858.

Refaat, J., Samy, M. N., Desoukey, S. Y., Ramadan, M. A., Sugimoto, S., Matsunami, K., Kamel, M. S., 2015. Chemical constituents from *Chorisia chodatii* flowers and their biological activities. *Med Chem Res* 24, 2939-2949.

Singh, A., Hasan, A., Tiwari, S., Pandey, L. M. 2018. Therapeutic Advancement in Alzheimer Disease: New Hopes on the Horizon? *CNS Neurol Disord*: *Drug Targets* 17, 571-589.

Spanou, C., Bourou, G., Dervishi, A., Aligiannis, N., Angelis, A., Komiotis, D., Skaltsounis, A. L., Kouretas, D., 2008. Antioxidant and chemopreventive properties of polyphenolic compounds derived from *Greek Legume* plant extracts. *J Agric Food Chem* 56, 6967-6976.

Takahashi, R. H., Nagao, T., Gouras, G. K. 2017. Plaque formation and the intraneuronal accumulation of β-amyloid in Alzheimer's disease. *Pathol Int* 67, 185-193.

Tamura, Y., Hattori, M., Konno, K., Kono, Y., Honda, H., Ono, H., Yoshida, M. 2004. Triterpenoid and caffeic acid derivatives in the leaves of ragweed, *Ambrosia artemisiifolia* L. (Asterales: Asteraceae), as feeding stimulants of *Ophraella communa LeSage* (Coleoptera: Chrysomelidae). *Chemoecology* 14, 113-118.

Tanaka, T., Nakashima, T., Ueda, T., Tomii, K., Kouno, I. 2007. Facile discrimination of aldose enantiomers by reversed-phase HPLC. *Chem Pharm Bull* 55, 899-901.

Tangaro, S., Fanizzi, A., Amoroso, N., Bellotti, R. 2017. A fuzzy-based system reveals Alzheimer's Disease onset in subjects with Mild Cognitive Impairment. *Phys Med* 38, 36-44.

Tilg, H., Moschen, A. R., 2008. Insulin resistance, inflammation, and non-alcoholic fatty liver disease. *Trends Endocrinol Metab* 19, 371-379.

Trauner, M., Arrese, M., Wagner, M., 2010. Fatty liver and lipotoxicity. *Biochimica et Biophysica Acta* 1801, 299-310.

Vajs, V., Todorović, N., Bulatović, V., Menković, N., Macura, S., Juranić, N., Milosavljević, S. 2000. Further sesquiterpene lactones from *Anthemis carpatica*. *Phytochemistry* 54, 625-633.

Vansco, M. F., Marchetti, B., Lester, M. I. 2018. Electronic spectroscopy of methyl vinyl ketone oxide: A four-carbon unsaturated *Criegee* intermediate from isoprene ozonolysis. *J Chem Phys* 149, 244309.

Walters, D., Meurer-Grimes, B., Rovira, I. 2001. Antifungal activity of three spermidine conjugates. *FEMS Microbiol Lett* 201, 255-258.

Xu, L., Wei, Y., Dong, D., Yin, L., Qi, Y., Han, X., Xu, Y., Zhao, Y., Liu, K., Peng, J., 2014. iTRAQ-based proteomics for studying the effects of dioscin against nonalcoholic fatty liver disease in rats. *RSC Adv* 4, 30704-30711.

Xu, S., Duan, W., Fang, L., Sun, Y., Dong, H., 2012. Isolation and characterization of chemical constituents from the petals of *Nelumbo nucifera*. *Asian J Chem* 24, 4619-4622.

Yang, J. L., Dhodary, B., Ha, T. K. Q., Kim, J., Kim, E., Oh, W. K. 2015. Three new coumarins from *Saposhnikovia divaricata* and their porcine epidemic diarrhea virus (PEDV) inhibitory activity. *Tetrahedron* 71, 4651-4658.

Yang, J. Y., Sanchez, L. M., Rath, C. M., Liu, X., Boudreau, P. D., Bruns, N., Glukhov, E., Wodtke, A., de Felicio, R., Fenner, A., Wong, W. R., Linington, R. G., Zhang, L., Debonsi, H. M., Gerwick, W. H., Dorrestein, P. C. 2013. Molecular networking as a dereplication strategy. *J Nat Prod* 76, 1686-1699.

Younossi, Z. M., Blissett, D., Blissett, R., Henry, L., Stepanova, M., Younossi, Y., Racila, A., Hunt, S., Beckerman, R., 2016. The economic and clinical burden of nonalcoholic fatty liver disease in the United States and Europe. *Hepatology* 64, 1577-1586.

Zhang, L., Fang, Y., Lian, Y., Chen, Y., Wu, T., Zheng, Y., Zong, H., Sun, L., Zhang, R., Wang, Z., Xu, Y. 2015. Brain-derived neurotrophic factor ameliorates learning deficits in a rat model of alzheimer's disease induced by Aβ1-42. *PLoS One* 10, e0122415.

Zhang, L., Gao, H. Y., Baba, M., Okada, Y., Okuyama, T., Wu, L. J., Zhan, L. B., 2014. Extracts and compounds with anti-diabetic complications and anti-cancer activity from *Castanea mollissina* Blume (Chinese chestnut). *BMC Complement Altern Med* 14, 422-431.

Zhang, H. J., Tan, G. T., Santarsiero, B. D., Mesecar, A. D., Hung, N. V., Cuong, N. M., Soejarto, D, D., Pezzuto, J. M., Fong, H. H. S. 2003. New Sesquiterpenes from *Litsea verticillata*. *J Nat Prod* 66, 609-615.

Zhang, S., Zheng, L., Dong, D., Xu, L., Yin, L., Qi, Y., Han, X., Lin, Y., Liu, K., Peng, J., 2013. Effects of flavonoids from *Rosa laevigata* Michx fruit against high-fat diet-induced non-alcoholic fatty liver disease in rats. *Food Chem* 141, 2108-2116.

Zang, Y., Zhang, L., Igarashi, K., Yu, C., 2015. The anti-obesity and anti-diabetic effects of kaempferol glycosides from unripe soybean leaves in high-fat-diet mice. *Food Funct* 6, 834-841.

Zhou, Y., Wang, Z. F., Li, W., Hong, H., Chen, J., Tian, Y., Liu, Z.Y. 2018. Protective effects of microRNA-330 on amyloid β-protein production, oxidative stress, and mitochondrial dysfunction in Alzheimer's disease by targeting VAV1 via the MAPK signaling pathway. *J Cell Biochem* 119, 5437-5448.

Zhu, M., Ma, L., Zhang, D., Ray, K., Zhao, W., Humphreys, W. G., Skiles, G., Sanders, M., Zhang, H. 2006. Detection and characterization of metabolites in biological matrices using mass defect filtering of liquid chromatography/high resolution mass spectrometry data. *Drug Metab Dispos* 34, 1722-1733.

국문초록

Part 1

가시박 (*Sicyos angulatus* L.)는 박과 (Cucurbitaceae) 식물로써 북미가 원산인 1 년생 덩굴식물이다. 가시박은 burcumber, one-seeded burcucumer, star-burcucumer 등의 영문명 또는 '안동오이'라는 한글명으로 불리운다. 가시박은 6~9 월에 개화하며 3 개에서 10 개의 열매가 뭉쳐서 나는데 가시가 위협적이고 날카롭다. 주로 강변에 많이 분포하나 장소를 가리지 않고 번식하여 주위 생태계를 교란시켜 환경부 지정 "생태계교란 야생식물"로 분류되지만 잎과 열매는 식품으로 지정되어 그 효과나 성분이 확인될 경우 건강기능식품으로서의 발전가능성이 있는 식물이다. 본 식물에서는 flavonoids glycoside, steroid 등이 분리 보고된 2 편의 논문이 있으며, 최근 본 연구팀에 의하여 가시박 70% 에탄올 추출물의 간경화 효과가 규명되었다. 가시박에 관하여 많은 연구가 보고되었지만 대부분이 생육, 생태에 관한 연구들이며 화학성분이나 생리활성에 관한 연구는 많지 않은 실정이다.

본 연구팀은 식물 추출 라이브러리 은행에서 선정된 식물 추출물 300 개를 대상으로 간지방 억제 활성 스크리닝 시험을 진행하였으며 그 결과 가시박 추출물이 유의미한 효과를 나타내었으며 이에 단일 화합물을 분리 및 동정하였으며 활성 평가를 시험하였다.

비알콜성 지방간질환 (nonalcoholic fatty liver disease; NAFLD)는 지방간, 비알콜성 지방간염, 섬유화증 및 간경변을 포함한다. 간세포 내에 중성지질

함량이 전체 간 무게의 5% 이상을 초과하는 상태를 말하며 인슐린 저항성 및 간 내 염증 반응을 유도하여 지방간염을 유도하기도 한다. 비알콜성 지방간이나 지방간염이 있는 환자의 20-40%가 결과적으로 섬유증이나 간경변을 가지게 된다고 보고된다. 또한 비만 인구가 증가함에 따라 점차 유병률이 증가하고 있으며 간기능 장애의 가장 흔한 원인이다. 비알콜성 지방간은 대사증후군과도 관련되는데 이는 탄수화물의 대사에 있어서 간이 중요한 역할을 하기 때문이다. 간은 글리코겐합성과 글리코겐분해를 통하여 혈당을 안정적으로 유지시키는데 간의 대사에 이상이 생길 시 혈당 조절이 실패하게 되며 이는 대사증후군을 일으키는 요인이 된다. 간경변을 가진 환자의 약 96%가 당내성을 가지며 30%의 환자는 당뇨를 가진다고 보고된다.

가시박 70% 에탄올 추출물은 그 구성성분이 분자네트워크 (molecular network)을 통하여 비슷한 화학적 구조별로 클러스터를 생성하였으며 GNPS 라이브러리를 통하여 화학적 구조가 제시되었다. 분자네트워크 (molecular network) 방법은 수 많은 분자간 조각이온 패턴의 유사도를 확인함으로써 그 유사성의 정도에 따라 서로 다른 그룹으로 구분 한다. 추출물 혹은 분획물의 샘플은 고해상도 질량분석기를 통하여 극성별로 피크가 나뉘어 지며 이때 각각의 피크는 조각이온 정보를 가지게 된다. 그 후 MZmine 등의 프로그램을 통하여 이 정보들이 보정되며 재가공된 정보는 GNPS 라이브러리 (https://gnps.ucsd.edu/)를 통하여 유사한 화학적 구조별로 cluster 를 형성하며 각각의 화학구조 또한 제시 된다. 그 결과 가시박의 flavonoid 배당체 그룹은 크게 두개의 소그룹으로 구분 되었으며, 그 중 하나의 소그룹은 flavonoid 를 비배당체로 하여 당이 연결된

구조를 가지며 다른 하나의 소그룹은 flavonoid 를 비배당체로 하여 당과 cinnamoyl 모획을 포함하는 구조인 것이 확인되었다.

가시박 추출물은 총 추출물 및 n-hexane, Ethyl acetate, n-BuOH 등으로 나뉘었으며 활성이 가장 좋은 Ethyl acetate 분획을 순상 및 역상 컬럼크로마토그래피, HPLC 등을 을 이용하여 단일화합물을 분리하였다. 총 13 종의 화합물을 분리하였으며 이 중 kaempferol 3-*O*-(6-*O*-*E*-feruloyl)-*β*-D-glucopyranosyl-7-*O*-*α*-L-rhamnopyranoside (**1**), kaempferol 3-*O*-*β*-D-apiofuranosyl-7-*O*-*β*-D-glucopyranosyl-(1→3)-*α*-L-rhamnopyranoside (**8**), quercetin 3-*O*-(6-*O*-*E*-feruloyl)-*β*-D-glucopyranosyl-7-*O*-*α*-L-rhamnopyranoside (**9**), kaempferol 3-*O*-(6-*O*-*E*-feruloyl)-*β*-D-glucopyranosyl-7-*O*-*α*-L-rhamnopyranosyl-(1→6)-*β*-D-glucopyranosyl-(1→3)-*α*-L-rhamnopyranoside (**11**), kaempferol 3-*O*-(6-*O*-*E*-feruloyl)-*β*-D-glucopyranosyl-7-*O*-*β*-D-glucopyranosyl-(1→3)-*α*-L-rhamnopyranoside (**12**), tricin 4'-*O*-(7''*R*,8''*R*-guaiacylglyceryl)ether-7-*O*-*α*-L-rhamnopyranosyl-(1→4)-*O*-*β*-D-glucopyranoside (**13**)의 6 종의 신규화합물을 분리할 수 있었다. 화합물 **13** 의 경우 flavonolignan glycoside 로써 ECD 계산을 통하여 입체구조가 결정되었다.

분리된 13 종의 화합물을 대상으로 간세포에서의 지방축적감소 효과를 확인하고자 하였다. 글루코스, 유리지방산, 인슐린을 처치하여 인슐린 저항성이 유도된 HepG2 세포에 13 종의 화합물 각각을 처치하였으며 감소된 중성지방의 양은 형광키트 (Cell Biolabs, Inc, CA, USA)를 통하여 확인되었다. 중정지방 억제

활성을 평가한 결과 화합물 (**1**-**4**, **6**, **11**-**13**)에서 모두 억제활성이 확인되었고 그 중 화합물 4 번이 가장 뛰어난 활성을 보였다. 또한 화합물 **1**, **3**, **4** 과 **13** 번은 10, 20, 40 μM 에서 농도의존적으로 지방의 양을 감소 시킴이 확인되었다. 화합물 **3** 번과 **4** 번은 정량 시험 결과 각각 추출물 대비 15.35 ± 0.01 mg/g, 1.35 ± 0.01 mg/g 의 양을 가지는 것으로 확인되었다.

구조적 특징에 따른 활성을 살펴보면, 분리된 화합물 중 cinnamoyl 작용기를 가지는 kaempferol 3-*O*-*β*-D-glucoside 유도체의 경우 모두 간 중성지방의 억제효과를 보였고 이는 기존 연구 결과들과 일치하였다. 또한 화합물 **13** 번의 경우 간보호 효과로 널리 알려진 실리마린의 성분들과 유사한 구조를 가지고 있다.

본 연구는 가시박 70% 에탄올 추출물과 이로부터 분리된 단일 화합물이 지방간 감소에 효과가 있다는 것을 제시하였다.

Part 2

돼지풀 (*Ambrosia artemisiifolia* L)은 국화과 (Asteraceae) 식물로써 북미가 원산인 1 년생 초본 식물이다. 돼지풀이란 이름은 영국의 hogweed 에서 유래하였으며 들이나 밭에 자라는 특징을 가진다. 또한 돼지풀은 가시박과 함께 대표적인 생태계 교란식물로써 높은 번식력과 타 식물과의 경쟁에서 우위를 점하는 특성으로 인해 전국에 걸쳐 분포하는 잡초이다. 전체에 굳센 털이 많으며 가지가 많이 갈라지고 줄기는 1.5m 까지 곧추서며 8-9 월에 개화한다. '단풍잎돼지풀'과 달리 잎이 손바닥 모양이 아닌 깃꼴로 갈라진다. 돼지풀에서는

sesquiterpene, triterpene 과 caffeic acid 유사체가 분리, 동정되었으며 항산화효과 항균효과등이 보고되어 있다.

본 연구팀은 식물 추출 라이브러리 은행에서 선정된 식물 추출물 300 개를 대상으로 뇌 신경보호 활성 스크리닝 시험을 진행하였으며 그 결과 돼지풀 추출물이 유의미한 활성 효과를 나타내어 추가적으로 추출물 중 활성분획에 관한 화합물 분리, 동정을 진행하였다.

알츠하이머 질환에서는 대뇌피질 속 신경세포의 손실로 인하여 뇌회의 위축이 발생하며 신경반과 신경원섬유농축을 보이는 특징을 가진다. 신경반은 독성물질인 베타아밀로이드(Aβ)가 응결되어 뇌신경세포를 둘러싸며 그 주변을 염증 세포가 둘러싸고 있는 형태를 나타낸다. 이는 강한 신경 독성을 유발하여 세포 사멸을 일으키고 신경퇴행을 유도하여 알츠하이머질환을 유발한다. 현재 전세계적으로 약 3 천만명의 인구가 알츠하이머 병으로 고통받고 있으며 세계보건기구 (WHO)는 향후 20 년간 이 숫자가 3 배 증가할 것이라 예측하고 있다.

질량결손필터링 (mass defect filtering)은 2 차 대사산물의 종류별로 기본골격을 이루는 수소, 산소, 질소 등의 원자의 비율이 다름을 이용하여 표적하는 특정 종류의 생리활성 물질을 분류하는데 정보를 제공한다. 탄소의 경우 12.0000 의 원자량을 가지며 수소, 산소의 경우에는 각각 1.0078, 15.9949 의 값을 가지게 되므로 수소 대비 산소의 비율이 높아질수록 낮은 질량결손 값을 가지며 이와 같은 원리를 이용해 표적 물질을 분류할 수 있다. 본 연구를 진행하는 중 eudesmane 배당체가 뇌신경 보호에 활성을 나타내는 것이 확인되었으며 또한

HMG (3′′-hydroxy-3′′-methylglutaryl) 기가 존재하는 eudesmane 배당체 혹은 2 개 이상의 당분자를 포함한 eudesmane 의 경우 신규화합물로 판별되었기에 질량결손필터링을 통하여 eudesmane 배당체 혹은 HMG 기를 포함하는 eudesmane 배당체를 분리 및 동정하였다. 또한 질량결손필터링을 하는 과정에서 이를 보완하는 방법으로 분획물단계에서의 NMR 스크리닝을 실시하였다. Silicagel 를 통하여 극성별로 5 개의 분획을 얻은 다음 Sephadex-LH20 컬럼을 이용하여 5 개분획 각각에 대하여 페놀성화합물과 terpene 을 구분 하였다. 각각의 terpene 분획을 ^{1}H-NMR 로 스크리닝하여 HMG 에서 특징적으로 나타나는 메틸렌 프로톤의 존재를 확인하였다.

돼지풀 추출물은 총 추출물 및, n-hexane, Ethyl acetate, n-BuOH 등으로 나뉘었으며 활성이 가장 뛰어난 Ethyl acetate 분획을 순상 및 역상 컬럼크로마토그래피, Sephadex-LH20, HPLC 등을 이용하여 단일화합물을 분리하였다. 총 14 종의 (**1-14**) 화합물이 분리되었으며 eudesmane 배당체 (**1-8**), sesquiterpene lactone (**11-12**), spermidine (**13-14**)로 분류된다. 이 중 eudesmane 배당체인 1*α*,6*β*,9*β*-trihydroxy-5,10-bis-*epi*-eudesm-3-ene-9-*O*-[(*S*)-3′′-hydroxy-3′′-methylglutaryl]-6-*O*-*β*-D-glucopyranoside (**1**), 1*α*,6*β*,9*β*-trihydroxy-5,10-bis-*epi*-eudesm-3-ene-1-*O*-[(*S*)-3′′-hydroxy-3′′-methylglutaryl]-6-*O*-*β*-D-glucopyranoside (**2**), 1*β*,6*α*-dihydroxy-7-*epi*-eudesm-3-ene-1-*O*-[(*S*)-3′′-hydroxy-3′′-methylglutaryl]-6-*O*-*β*-D-glucopyranoside (**3**), 1*α*,6*β*,9*β*-trihydroxy-5,10-bis-*epi*-eudesm-3-ene-9-*O*-[(*S*)-3′′-hydroxy-3′′-methylglutaryl]-6-*O*-(6′-*O*-acetyl)-*β*-D-

glucopyranoside (4), 1*α*,6*β*,9*β*-trihydroxy-5,10-bis-*epi*-eudesm-3-ene-1-*O*-*α*-L-arabinopyranosyl-6-*O*-*β*-D-glucopyranoside (5), 1*α*,6*β*,9*β*-trihydroxy-5,10-bis-*epi*-eudesm-3-ene-6-*O*-*β*-D-glucopyranoside (6), 1*β*,6*α*-dihydroxy-7-*epi*-eudesm-3-ene-6-*O*-*β*-D-apiofuranosyl-(1→6)-*β*-D-glucopyranoside (7)의 7 종의 신규화합물을 분리하였다. 화합물 1-4 의 경우 ECD 계산을 통하여 비당체의 절대구조를 정하였으며 화합물 1 의 HMG 의 경우 기존의 연구결과를 참고하여 amination, reduction, acetylation 등의 과정을 거쳐 절대구조를 결정하였다. 가수분해 과정을 통하여 화합물 1 에서 HMG 를 제거하였으며 이 화합물은 ^{13}C-NMR, HPLC 등을 통하여 화합물 6 과 동일함을 확인하여 화합물 6 의 절대 구조를 규명하였다. 화합물 5 번과 7 번의 경우도 동일하게 가수분해를 통하여 특정 당이 제거되었으며 이는 각각 HMG 기가 제거된 1 번과 3 번과 동일한 반응생성물임을 확인함으로써 절대구조를 결정하였다.

분리된 14 종의 화합물을 대상으로 뇌신경보호 효과를 확인하고자 하였다. pEGFP-C1/Aβ_{42} 플라스미드를 Lipofectamine 2000 regent 와 함께 HT-22 cell 로 도입하여 10 시간 반응시킨 후 14 종의 화합물을 각각 처치하여 화합물의 세포보호 효과를 관찰하였다. 화합물 1, 2, 4-6, 8-9, 11 그리고 13-14 번 화합물에서 뇌신경 보호효과가 나타났으며 화합물 5 번과 6 번은 10, 20, 40μM 에서 농도의존적으로 효과를 보였다.

본 연구는 돼지풀 70% 에탄올 추출물과 이로부터 분리된 단일 화합물이 뇌신경보호에 효과가 있다는 것을 제시하였다.

주요어: 가시박, 돼지풀, molecular networking, mass defect filtering, 비알콜성 지방간, 뇌신경보호.

학번: 2014-31251.

Scientific Publication

No.	Name of paper	Name of journal	Year published	Author
1	**Eudesmane Glycosides from *Ambrosia artemisiifolia* (Common Ragweed) as Potential Neuroprotective Agents**	***J. Nat. Prod.***	**2019**	**First author**
2	**Flavone glycosides from *Sicyos angulatus* and their inhibitory effects on hepatic lipid accumulation**	***Phytochemistry***	**2019**	**First author**
3	**Protein Tyrosine Phosphatase 1B Inhibitors from the Stems of *Akebia quinata***	***Molecules***	**2016**	**First author**
4	**Anti-hepatic steatosis activity of *Sicyos angulatus* extract in high-fat diet-fed mice and chemical profiling study using UHPLC-qTOF-MS/MS spectrometry**	***Phytomedicine***	**2019**	**Co-First author**
5	Oligostilbenes from the leaves of *Gnetum latifolium* and their biological potential to inhibit neuroinflammation	*Phytochemistry*	2019	Co-author
6	Prenylated Phenolic Compounds from the Leaves of *Sabia limoniacea* and Their Antiviral Activities against Porcine Epidemic Diarrhea Virus	*J. Nat. Prod.*	2019	Co-author
7	Dereplication of Components Coupled with HPLC-qTOF-MS in the Active Fraction of *Humulus japonicus* and It's Protective Effects against Parkinson's Disease Mouse Model	*Molecules*	2019	Co-author
8	Insulin Mimetic Activity of 3,4-Seco and Hexanordammarane Triterpenoids Isolated from *Gynostemma longipes*	*J. Nat. Prod.*	2018	Co-author
9	*Sicyos angulatus* ameliorates acute liver injury by inhibiting oxidative stress via upregulation of anti-oxidant enzymes	*Redox Rep.*	2018	Co-author
10	Andrographolide activates Keap1/Nrf2/ARE/HO-1 pathway in HT22 cells and suppresses microglial activation by Aβ42 through Nrf2-related inflammatory response	*Mediators Inflamm.*	2017	Co-author
11	*Sicyos angulatus* ameliorates atherosclerosis through downregulation of aortic inflammatory responses in apolipoprotein E-deficient mice	*Exp. Ther. Med.*	2017	Co-author